Behaviour of Particles in Closed Timelike Orbits and Massive Gravity Wormholes

by

AYANENDU DUTTA

This thesis is submitted in partial fulfillment of the requirements for the award of the degree of Doctor of Philosophy (Science) of Jadavpur University

Department of Mathematics
Jadavpur University
Kolkata 700032, West Bengal, India

2024

JADAVPUR UNIVERSITY
FACULTY OF SCIENCE
DEPARTMENT OF MATHEMATICS
KOLKATA-700032, WEST BENGAL, INDIA

CERTIFICATE FROM THE SUPERVISOR

This is to certify that the thesis entitled **"Behaviour of Particles in Closed Time-like Orbits and Massive Gravity Wormholes"** submitted by **Sri Ayanendu Dutta** who got his name registered on 17.02.2022 (Registration No. SOPHY1104822, Index No. 48/22/PHYS/27) for the award of Ph.D. (Science) Degree of Jadavpur University, is absolutely based upon his own work under the supervision of Subenoy Chakraborty and that neither this thesis nor any part of it has been submitted for either any degree/diploma or any other academic award anywhere before.

Subenoy Chakraborty 18/07/24

Subenoy Chakraborty
(Supervisor)
Department of Mathematics
Jadavpur University
Kolkata-700032, West Bengal, India

Professor
DEPARTMENT OF MATHEMATICS
Jadavpur University
Kolkata - 700 032, West Bengal

DECLARATION BY THE AUTHOR

I hereby declare that the thesis is based upon the research work carried out at the Department of Mathematics, Jadavpur University, Kolkata - 700032, India. Additionally, I declare that any part of it has not been submitted for any degree/diploma/fellowship or some other qualification at any other university or academic institution.

The author has produced all the figures presented in this thesis using Mathematica and Python software. The thesis has been checked multiple times with extreme care to free it from all discrepancies and typos. Even then vigilant readers may find some mistakes, and several portions of this thesis may seem unwarranted, mistaken, or incorrect. The author takes the sole responsibility for these unwanted errors which have resulted from his inadequate knowledge of the subject, or escaped his notice.

Finally, I state that, to the best of my knowledge, all the assistance taken to prepare this thesis has been properly cited and acknowledged.

Ayanendu Dutta, 18/07/2024

Ayanendu Dutta

To my parents

Jagannath Dutta

and

Karabi Dutta

ACKNOWLEDGMENTS

Amidst the ebbs and flows of the doctoral odyssey, I have traversed the realms of knowledge, delving deeper into the mysteries of my field with each passing day. This journey has been as much about scholarly inquiry as it has been about personal growth, resilience, and perseverance. It is a testament to the profound transformative power of dedication, curiosity, and the unwavering pursuit of excellence.

Before I begin thanking everyone who played a big role in my academic journey, I want to take a moment to talk about gratitude. Looking back, I'm truly amazed by all the support, encouragement, and guidance I've received along the way. As the pages of this thesis unfold, I can't help but think about all the people who have believed in me and helped me reach this point. So, here in the acknowledgments, I want to say a big thank you to those who have made my academic journey meaningful and purposeful.

First, I extend my deepest and heartfelt gratitude to my supervisor, Subenoy Chakraborty, for his immense support, invaluable guidance, and endless patience throughout my PhD journey. His expertise, encouragement, and mentorship have been instrumental in shaping this thesis. Without his constant push, I couldn't have reached this height. Apart from academic activities, he also guided me in nurturing faith in one's own principles. Moreover, his inspiration cannot be captured within a few sentences.

I am deeply indebted to my father, Jagannath Dutta, whose unwavering belief in me and steadfast support have been my pillars of strength. His encouragement and sacrifices have paved the way for my academic pursuits. Additionally, my father served as my first English teacher and showed me the true qualities of a noble human being. Despite being capable of changing the society with his brilliance, he struggled throughout his life, but always shielded me from the smallest shadows of difficulty.

To my mother, Karabi Dutta, whose unwavering faith, boundless love, and endless encouragement have been my guiding light. Most importantly, she is my first teacher of Mathematics. Her resilience and belief in my abilities have fueled my determination to pursue my dream of becoming a researcher. She always pushed me to be the one I

wanted to be. Without questioning any of my decisions, she always stood by my side, being an unshakable monument of faith.

I am grateful to the teacher, philosopher, and guide, Dr. Subhendu Rajbanshi, from my bachelor's studies, whose guidance and mentorship laid the foundation for my academic endeavors. His dedication to nurturing my academic growth and fostering a passion for learning has been invaluable. I always found him showing me the right path when I was struggling.

To my 'chotdada', Krishnendu Dutta, whose passion for astrophysics ignited my own curiosity and ambition to pursue a career in theoretical physics from my childhood. His guidance and encouragement from the earliest stages of my journey have been the foundation of my academics. Additionally, I thank all my other family members for their support and encouragement.

I am grateful to the Research Advisory Committee, comprising Prof. Arindam Bhattacharyya, Prof. Nabin Baran Manik (Head of Physics), and Prof. Kalyan K. Chattopadhyay (former Head of Physics), for their invaluable suggestions and encouragement in enhancing the quality of my research. Additionally, I express my sincere appreciation to Dr. Sourav Bhattacharya, Dr. Kanan K. Datta, and Dr. Saiyad Ali for generously sharing their time and expertise during the coursework sessions. Their informative and engaging classes were greatly beneficial. I also extend my thanks to all the members of the Department of Physics and Department of Mathematics at Jadavpur University for their assistance during this expedition.

Throughout my journey from childhood, I've had the privilege of encountering brilliant minds and exceptional personalities as my teachers. Hence, I extend my respect and gratitude to the teachers of my schools: Baliadanga Boys' Primary School, Baliadanga High School (H.S.), and the professors of Dum Dum Motijheel College. However, special mention must be made of my tutors from my school years, namely Rabindranath Halder, Biswajit Biswas, Sanjib Biswas, Mithun da, and Hasan dada.

During my two valuable years as a Master's student in the Department of Instrumentation Science, when I first joined the Jadavpur University, I had the privilege of being guided by esteemed professors such as Anup sir, Arun sir, Arijit sir and Sankar sir. Their mentorship played a pivotal role in strengthening my motivation for research activities.

In the symphony of academia, my decade-old friend Dhritimalya, who shared the entire journey from B.Sc. to Ph.D. with me, strengthened all the decisions throughout this adventure. To Nabanita, whose strength, inspiration, support, and true motivation made my struggles easier. Together, we've navigated challenges and celebrated successes with synchronicity. To Apurba, Sayan and Riktesh, my cherished friends, whose steadfast friendship, appreciation, and support have been a beacon of light. Their presence in my life is a constant reminder of the beauty of true friendship and has been an asset in this journey.

I extend my appreciation to my senior and junior lab mates, Akash da, Bikram da, Roshni di, Gopal da, Dipankar da, Sritan da, Soumya da and Madhukrishna, for their support, and encouragement. Their presence has enriched my academic experience and made the challenges more manageable.

Further, I am also deeply thankful to the Inter University Centre for Astronomy and Astrophysics (IUCAA), Pune, for their warm hospitality during my academic visit in April 2023. Special mentions go to IISER Kolkata and IIT Guwahati for their financial support in participating in the IAGRG meeting 2022 and the ICGC 2023 conferences.

In closing, I extend my deepest gratitude to all who have contributed to this journey. Each of you has played a significant role in shaping my academic and personal growth, and for that, I am deeply grateful. As I embark on the next chapter of my career, I carry with me the invaluable lessons and cherished memories forged during this remarkable voyage. Thank you for being an integral part of this extraordinary adventure.

Ayanendu Dutta 18/07/2024.

Ayanendu Dutta

ABSTRACT

Einstein's General Relativity comes with a disturbing yet fascinating time reversal pathology in the form of closed timelike curves (CTCs), which create challenges for the initial value Cauchy problem. These paths violate chronology, disrupting determinism, distinct from curvature singularities which disrupt physical laws. Despite attempts to eliminate CTCs through quantum theories and modified spacetime models, their full resolution remains elusive. While research in this area is more than half a century old, there are still missing ingredients to accommodate a concise description to effectively address this phenomenon, such as the properties of particles that may traverse these curves, limitations of backward time jumps, and the effect of spacetime horizons, among others. In this thesis, a number of these properties are addressed, particularly the formation of closed timelike curves and closed timelike geodesics (CTGs) in terms of zero and non-zero angular momentum of particles are explored within axisymmetric spacetime solutions. These particles are mainly considered to be neutral; however, for the Kerr-Newman spacetime with a charged source, particles with varying charge are also taken into account. The constructive analysis of spacetime diagrams for geodesic motion provides the geodesic confinements, which are applied to estimate the nature of particles, the role of confinement radius and the effect of horizons in the CTCs, along with the expression of backward time jump in CTGs.

Wormhole, on the other hand, is another phenomenological outcome of GR that offers hypothetical shortcuts through spacetime, enabling travel between distant regions or even different universes. It is potentially capable of violating causality by acting as a CTC when the special relativistic Twin paradox is applied on it. To extensively connect the CTCs with wormholes, the geodesic motion of particles and their visualization in wormhole embedding are presented, which create the possibility of CTG formation in the asymptotic geometries of either side of wormhole's throat. Since the recent discovery of the supermassive black hole shadow and the direct detection of gravitational waves, considerable attention has been focused on detecting other exotic objects and objects that may mimic black holes, thereby enhancing the importance of wormholes. Simultaneously, investigations conducted by LIGO-VIRGO have placed potential limitations on the graviton mass, further increasing the significance of the massive gravity theory. Thus, the formation of static and evolving wormholes in dRGT massive gravity has been explored, revealing the presence of a repulsive gravity effect potentially induced by massive gravitons. Subsequently, under these circumstances, hydrostatic stability analysis of wormhole formation is also conducted. Moreover, traversable wormholes require the presence of exotic matter at the throat to keep them open for traversability. In recent times, several studies have delved into non-exotic matter wormholes. Therefore, a thorough examination has been proposed to investigate traversability and the nature of matter contents at the throat, suggesting a significant possibility of non-exotic matter wormholes in massive gravity, with some evolving from non-exotic to exotic matter.

LIST OF PUBLICATIONS

The thesis is based on the following articles -

• Chapter 3 has been published as *"The role of closed timelike curves in particle motion within van Stockum spacetime: A generalization"*, **A. Dutta**, D. Roy and S. Chakraborty, **Int. J. Mod. Phys. D 31**, no. 13, 2250096 (2022),
(**arXiv:** 2208.14768 [gr-qc]). DOI: 10.1142/S0218271822500961

• Chapter 4 has been published as *"On the role of closed timelike curves and confinement structure around Kerr-Newman singularity"*, **A. Dutta**, D. Roy and S. Chakraborty, **Int. J. Mod. Phys. D** (2024),
(**arXiv:** 2406.02697 [gr-qc]). DOI: 10.1142/S0218271824500342

• Chapter 5 has been published as *"Particle motion around traversable wormholes: Possibility of closed timelike geodesics"*, **A. Dutta**, D. Roy and S. Chakraborty, **New Astron. 111**, 102236 (2024),
(**arXiv:** 2404.11984 [gr-qc]). DOI: 10.1016/j.newast.2024.102236

• Chapter 6 has been published as *"Wormhole formation in massive gravity: an analytic description"*, **A. Dutta**, D. Roy, N. J. Pullisseri and S. Chakraborty, **Eur. Phys. J. C 83**, no. 6, 500 (2023),
(**arXiv:** 2306.06911 [gr-qc]). DOI: 10.1140/epjc/s10052-023-11681-x

• Chapter 7 has been communicated as *"Evolving wormhole in dRGT massive gravity"*, **A. Dutta**, D. Roy and S. Chakraborty,

CONTENTS

LIST OF FIGURES

LIST OF TABLES

জীবনের কোনো লক্ষ্য নাই অথচ শিক্ষা আছে, ইহার কোনো অর্থই নাই।
— রবীন্দ্রনাথ ঠাকুর

CHAPTER 1

GENERAL RELATIVITY AND BEYOND

> "No matter how hard you try to teach your cat general relativity, you're going to fail."
>
> — Brian Greene

Albert Einstein's General Theory of Relativity (GR) [1] is undoubtedly one of the most brilliant achievements of scientific minds. Since the introduction of the theory, it has radically changed the view over natural phenomena, especially the prediction of black holes and gravitational singularity and the way the universe is imagined. Gravity is thought to arise from the interplay between space and time within the framework of differential geometry. General Relativity describes this phenomenon using a four-dimensional geometric structure called a manifold, along with a metric denoted as 'g' with a Lorentz signature. This metric, derived from a symmetric metric tensor $g_{\mu\nu}$ of rank 2, is determined by the "first fundamental form" of differential geometry, represented by the line element

$$ds^2 = g_{\mu\nu} dx^\mu dx^\nu \,, \tag{1.1}$$

where the four vector is $x^\mu = (ct, \vec{x})$. This equation is nothing but the generalized form of the flat space Minkowski line element as given by

$$ds^2 = \eta_{\mu\nu} dx^\mu dx^\nu \,, \tag{1.2}$$

in terms of Minkowski metric tensor $\eta_{\mu\nu}$.

Physically the metric g is significant in terms of local causality and the local conservation of energy-momentum. These two postulates are well established and are the building blocks of both the Special and General Theory of Relativity. However, most of the results of GR are solely dependent on a third postulate for the field equations of metric g that gravity is attractive for any matter with positive density. Nevertheless, the matter field on a manifold $\mathcal{M}$, that describes the spacetime matter content is primarily governed by the first two postulates as follows:

(a) **Local causality:** The equations that describe matter fields should ensure that within a convex normal neighborhood $\mathcal{U}$, if points p and q exist, a signal can be transmitted between them if and only if there is a continuously differentiable curve C^1 entirely within $\mathcal{U}$. This curve should have a non-zero tangent vector everywhere, being either timelike or null, and is referred to as non-spacelike. The direction of the signal transmission from p to q or vice versa, depends on the orientation of time within $\mathcal{U}$.

One may however formulate a much precise statement of the postulate with the help of Cauchy problem of matter field [2].

(b) **Local conservation of energy-momentum:** The equations that describe matter fields introduce a symmetric tensor T^{ab}, known as the energy-momentum tensor. This tensor is a function of the fields, their covariant derivatives, and the metric g_{ab}. It possesses two key properties:

(i) T^{ab} equals zero on an open set $\mathcal{U}$ if and only if all matter fields vanish on $\mathcal{U}$.

(ii) $T^{ab}{}_{;b} = 0$, where the semicolon denotes covariant differentiation.

Note that property (i) articulates the principle that every field possesses energy. This might trigger the possibility of negative energy, e.g. in a two non-zero fields system, where the energy-momentum tensor of one field exactly cancels the other.

1.1 The Field Equation

In Einstein's GR, tensor calculus formulates the mathematical foundation of the field equation. Tensor fields constitute a collection of geometric entities on a manifold, naturally derived from the manifold's structure. A tensor field is essentially tantamount to a tensor specified at every point on the manifold. To begin, tensors are initially defined at individual points of the manifold, commencing with the fundamental concept of a vector at a point. Thus, in terms of Einstein's *summation convention*, the coordinate transformation $x^\mu \to x'^\mu = x'^\mu(x^\nu)$ can be represented in tensor notations as

$$T'^{a_1 a_2 \ldots a_m}{}_{b_1 b_2 \ldots b_n} = \frac{\partial x'^{a_1}}{\partial x^{\rho_1}} \ldots \frac{\partial x'^{a_m}}{\partial x^{\rho_m}} \frac{\partial x^{\sigma_1}}{\partial x'^{b_1}} \ldots \frac{\partial x^{\sigma_n}}{\partial x'^{b_n}} T^{\rho_1 \rho_2 \ldots \rho_m}{}_{\sigma_1 \sigma_2 \ldots \sigma_n} \,. \tag{1.3}$$

In this framework, interest is now directed towards observing how the tensors transform under partial derivatives, i.e., $\partial_\mu = \frac{\partial}{\partial x^\mu}$,

$$\partial'_\mu A'^\nu = \frac{\partial x'^\nu}{\partial x^\alpha} \frac{\partial x^\beta}{\partial x'^\mu} \partial_\beta A^\alpha + \frac{\partial^2 x'^\nu}{\partial x^\alpha \partial x^\beta} \frac{\partial x^\beta}{\partial x'^\mu} A^\alpha \,. \tag{1.4}$$

Alongside, according to the definition, the generalized covariant derivative on a regular vector A^μ can be written as

$$\nabla_\mu A^\nu = \partial_\mu A^\nu + \Gamma^\nu_{\mu\lambda} A^\lambda \,, \tag{1.5}$$

where $\Gamma^{\rho}_{\mu\nu}$ is the metric connection, and it must be noted that this is clearly not a tensor since the transformation rule of the connection is different from that of the tensors. In GR, this metric connection is expressed as the Christoffel symbol given by

$$\Gamma^{\rho}_{\mu\nu} = \frac{1}{2} g^{\lambda\rho} \left(\partial_\mu g_{\lambda\nu} + \partial_\nu g_{\lambda\mu} - \partial_\lambda g_{\mu\nu} \right) . \tag{1.6}$$

As previously noted, the geometry of general relativity extends beyond the flat Minkowski space to include curvatures of spacetimes. While all details regarding the curvature and geometry of spacetime are encompassed within the metric tensor, it proves beneficial to introduce a curvature tensor. This tensor, referred to as Riemann curvature tensor, is formally defined as follows:

$$R^{\rho}_{\sigma\mu\nu} = \partial_\mu \Gamma^{\rho}_{\nu\sigma} - \partial_\nu \Gamma^{\rho}_{\mu\sigma} + \Gamma^{\rho}_{\mu\lambda} \Gamma^{\lambda}_{\nu\sigma} - \Gamma^{\rho}_{\nu\lambda} \Gamma^{\lambda}_{\mu\sigma} . \tag{1.7}$$

Note that there are a number of different techniques commonly used to derive Einstein's field equation. Here the Bianchi identity relation is adopted for a smooth construction of the equation. This approach primarily revolves around deriving a generalization of Poisson's equation, the field equation governing Newtonian gravity. Poisson's equation establishes a connection between the Newtonian gravitational potential (Φ) and the mass or energy density (ρ):

$$\nabla^2 \Phi = 4\pi G \rho . \tag{1.8}$$

On the other hand, the gravitational force in this framework is written as

$$\vec{F}_g = -m_g \vec{\nabla} \Phi . \tag{1.9}$$

In the given equation, m_g is referred to as the gravitational mass and can be conceptualized as the gravitational charge associated with the test particle. By substituting Eq. (1.9) into Newtonian mechanics' second law, one obtains $m_I \vec{a} = -m_g \vec{\nabla} \Phi$, where m_I represents the inertial mass. In Aristotelian physics, these two masses could, in general, differ significantly. Nevertheless, Galileo's experiments demonstrated that, for freely falling objects, the gravitational mass equals the inertial mass, i.e., $m_g = m_I$. This equality, known as the equivalence principle, allows to express the gravitational field as

$$\vec{a} = -\vec{\nabla} \Phi . \tag{1.10}$$

The trajectory and movement of test particles in free fall are consistent and independent of their masses. The Equivalence Principle's credibility was initially examined through experiments conducted by Eötvös [3] and confirmed by subsequent contemporary experiments [4–11]. Thus, the Equivalence Principle, governing the universality of massive particle dynamics, can be summarized as follows:

• Weak Equivalence Principle:
The Weak Equivalence Principle asserts that within sufficiently small regions of spacetime, a freely falling observer can not distinguish between the effects of a gravitational field and those of uniform acceleration.
This principle extends to a specific category of trajectories known as inertial trajectories, where unaccelerated particles move. Unaccelerated, in this context, implies that

a particle undergoing the influence of a gravitational field (i.e., freely falling) does not sense its acceleration. This conclusion led to the idea that gravity should not be considered a force, as a force typically induces acceleration.
However, with the advent of special relativity, a re-evaluation of the mass concept now tied to energy and momentum. Einstein proposed a generalization of the Equivalence Principle. This broader concept, termed the Strong Equivalence Principle, posits that:

• **Strong Equivalence Principle:**
This principle states that the outcome of any local experiment within a freely falling laboratory remains independent of its velocity or location in spacetime. Local experiments can not detect the presence of a gravitational field.
Laws of Physics exhibit an independence from the choice of coordinate systems and, within sufficiently small spacetime regions, reduce to the principles of Special Relativity. Einstein, observing this peculiar universality of the gravitational field, proposed that gravitational interaction is not a true force but is intricately connected to the curvature of spacetime.
While not universally applicable, in many cases, the laws of physics can be extended to a curved background using a straightforward approach. Initially, expressing equations in a coordinate-independent manner through tensors, one can subsequently replace partial derivatives with covariant derivatives. This method, known as the minimal coupling principle, facilitates the derivation of equations governing the motion of a test particle in General Relativity.

In Newtonian physics, a freely falling particle follows a straight-line path, whereas in curved spacetime, its trajectory is described by geodesics. In GR, these geodesics depict the motion of a particle influenced solely by gravitational interaction. In a curved spacetime background, geodesic curves serve as the analog of straight-lines; they represent paths of minimum length connecting two distinct points. For a parametric equation $x^\mu(\xi)$, a geodesic equation is written as follows:

$$\frac{d^2x^\mu}{d\xi^2} + \Gamma^\mu_{\rho\sigma}\frac{dx^\rho}{d\xi}\frac{dx^\sigma}{d\xi} = 0\,, \tag{1.11}$$

where ξ is called the affine parameter which has a particular point of interest, and it will be discussed in due course.

If the geodesic equation is intended to characterize the gravitational field, it should replicate Newtonian gravity (1.10) in the regime of weak field limit [12–15]. To achieve this, the weak field approximation is employed. In this approach, the metric tensor can be decomposed as

$$g_{\mu\nu}(x^\mu) = \eta_{\mu\nu} + h_{\mu\nu}(x^\mu)\,, \tag{1.12}$$

where $h_{\mu\nu}$ represents small perturbations over Minkowski spacetime. In the realm of GR, these metric perturbations ($h_{\mu\nu}$) arise from gravitating bodies and adhere to the condition $|h_{\mu\nu}| \leq 1$. This permits a linear-approximation analysis, and one may briefly outline the corresponding formalism and present the linear-order approximation equations of General Relativity. For a comprehensive examination, see [12–18].

Finally, by utilizing Eq. (1.12) and retaining only terms linear in the perturbation $h_{\mu\nu}$, under the condition of the Newtonian limit where velocities are significantly smaller

than the speed of light ($v << c$), and accounting for the static nature of the Newtonian gravitational field, the following relation is derived from Eq. (1.10):

$$h_{00} = -\frac{2\Phi}{c^2}\,. \tag{1.13}$$

In terms of the metric, this equation takes the form

$$g_{00} = -\left(1 + \frac{2\Phi}{c^2}\right)\,. \tag{1.14}$$

Now, the generalization of Poisson's equation (1.8) requires the introduction of energy-momentum tensor ($T_{\mu\nu}$) in the right hand side, since it enables to represent the interaction of energy and matter in General Relativity. Subsequently, given that the gravitational potential is generalized as the metric tensor $g_{\mu\nu}$, a second-rank symmetric tensor, it follows that the matter distribution density ρ should similarly be extended to a second-rank symmetric tensor $T_{\mu\nu}$. Alongside, it is recognized that the majority of equations involve derivations up to the second order. Consequently, one may seek an equation in the following form:

$$A_{\mu\nu}(g_{\mu\nu}, \partial g_{\mu\nu}, \partial^2 g_{\mu\nu}) = \kappa T_{\mu\nu}\,. \tag{1.15}$$

where κ is a proportionality constant. According to the local energy-momentum conservation (i.e., postulate (b)), one obtains

$$\nabla^\mu T_{\mu\nu} = 0\,. \tag{1.16}$$

Thus, one may find that the covariant derivative on $A_{\mu\nu}$ should also vanish, i.e., $\nabla^\mu A_{\mu\nu} = 0$. On the other hand, the left hand side of Eq. (1.8) demands something that produces the effect of the curvature of spacetime that denotes gravity. A suitable choice for a two-index tensor, constructed from the Riemann tensor and its contractions, would be the Ricci tensor. It is formulated as

$$R_{\mu\nu} = R^{\lambda}_{\mu\lambda\nu} = g^{\lambda\alpha} R_{\alpha\mu\lambda\nu}\,. \tag{1.17}$$

Considering that the Riemann tensor $R_{\mu\nu\rho\sigma}$ involves first and second derivatives of the metric tensor, it is acknowledged from differential geometry that any tensor containing up to second-order derivatives of the metric tensor can be expressed using the Riemann tensor and its constructions. However, the left hand side of the field equation can not be merely the Ricci tensor, as its divergence is generally non-zero.
To address this, it is proposed that the left hand side of the field equation should take the form of a two-index, divergence-free curvature tensor, denoted as the Einstein tensor $G_{\mu\nu}$. This tensor is then postulated to be proportional to the energy-momentum tensor, i.e.,

$$G_{\mu\nu} = \kappa T_{\mu\nu} \qquad \text{with} \qquad \nabla^\mu G_{\mu\nu} = 0\,. \tag{1.18}$$

The next step requires to find the actual form of the divergence-free tensor, and this can be formulated by adapting a very important property of the Riemann tensor, i.e.,

Bianchi identity which is the expression of covariant derivatives of Riemann tensor with different index combinations:

$$\nabla_\lambda R_{\rho\sigma\mu\nu} + \nabla_\rho R_{\sigma\lambda\mu\nu} + \nabla_\sigma R_{\lambda\rho\mu\nu} = 0\,. \tag{1.19}$$

By performing two contractions on this identity, the following result is arrived at:

$$\nabla^\mu \left(R_{\mu\nu} - \frac{1}{2} R g_{\mu\nu} \right) = 0\,, \tag{1.20}$$

where $R = g^{\mu\nu} R_{\mu\nu}$ is the Ricci scalar. Therefore, one may write, $G_{\mu\nu} = R_{\mu\nu} - \frac{1}{2} R g_{\mu\nu}$, and Eq. (1.18) takes the form

$$R_{\mu\nu} - \frac{1}{2} R g_{\mu\nu} = \kappa T_{\mu\nu}\,. \tag{1.21}$$

At this point, the next step is to compute the proportionality factor κ, and for that, the Newtonian weak field limit is adapted, as formulated during the derivation of Eq. (1.14). Hence, using the expression in (1.14), one may show that the Ricci scalar takes the form

$$R = \frac{2}{c^2} \nabla^2 \Phi\,, \tag{1.22}$$

and therefore the following 00-component of Ricci tensor is obtained:

$$R_{00} = \frac{1}{c^2} \nabla^2 \Phi\,. \tag{1.23}$$

Now, utilizing the expressions from equations (1.14), (1.22), and (1.23) with $T_{00} = \rho c^2$, they can be substituted into the 00-component of Eq. (1.21), and after some straightforward calculations, the following result is obtained:

$$\nabla^2 \Phi = \frac{1}{2} \kappa \rho c^4\,. \tag{1.24}$$

Upon comparing this equation with (1.8), it is simple to derive $\kappa = \frac{8\pi G}{c^4}$, such that the expression of the field equation is modified to

$$R_{\mu\nu} - \frac{1}{2} R g_{\mu\nu} = \frac{8\pi G}{c^4} T_{\mu\nu}\,. \tag{1.25}$$

The final step is to figure out how to introduce the cosmological constant into this equation. The inclusion of the cosmological constant (Λ) term in the Einstein field equation enables the accommodation of phenomena such as dark energy within the framework of gravity and cosmology. Importantly, the cosmological constant term can be effortlessly introduced into the field equation without additional complications. This is due to the fact that the (covariant) divergence of the metric tensor automatically equals zero ($\nabla^\mu g_{\mu\nu} = 0$), complying with the metric compatibility condition. Consequently, one may consistently introduce a term of the form of a constant multiplied by the

metric (i.e., $\Lambda g_{\mu\nu}$), and it would still satisfy all the underlying assumptions. Therefore, the final form of the field equation is given by

$$R_{\mu\nu} - \frac{1}{2}Rg_{\mu\nu} + \Lambda g_{\mu\nu} = \frac{8\pi G}{c^4}T_{\mu\nu}\,. \tag{1.26}$$

In the Newtonian limit, the cosmological constant is assumed to have a negligible impact on the Newtonian gravitational field, and thus, it can be disregarded (i.e., $\Lambda \approx 0$). Essentially, incorporating this term will not alter the value of the proportionality constant κ obtained from the Newtonian limit.

1.2 The Lagrangian formulation

Like any field theory, the general theory of relativity can be described using the Lagrangian formulation. By incorporating a kinetic term and a potential with the possible interactions, it is typically straightforward to formulate a Lagrangian for a given field. However, in general relativity, the field is represented by the metric tensor. As mentioned earlier, any tensor containing up to second-order derivatives of the metric tensor can be expressed using the Riemann tensor and its contractions. Consequently, the only nontrivial scalar suitable for use as a Lagrangian density is the Ricci scalar, such that

$$L = \int d^4x\sqrt{-g}R\,, \tag{1.27}$$

assuming g represents the determinant of the metric tensor. The action described above is commonly referred to as the Einstein-Hilbert action. To derive the field equations, one needs to perform a variation of the action with respect to the metric tensor ($g_{\mu\nu}$). By employing the relation $g_{\mu\alpha}g^{\nu\alpha} = \delta^{\nu}_{\mu}$ and the properties of the Kronecker delta, the variation can be expressed as $\delta_{\mu\nu} = -g_{\mu\rho}g_{\nu\sigma}\delta g^{\rho\sigma}$. Utilizing $R = g_{\mu\nu}R^{\mu\nu}$, the variation of the action can be written as:

$$\delta L = \delta L_1 + \delta L_2 + \delta L_3\,, \tag{1.28}$$

given that

$$\delta L_1 = \int d^4x\sqrt{-g}g^{\mu\nu}\delta R_{\mu\nu}\,, \tag{1.29}$$

$$\delta L_2 = \int d^4x\sqrt{-g}R_{\mu\nu}\delta g^{\mu\nu}\,, \tag{1.30}$$

$$\delta L_3 = \int d^4xR\delta\sqrt{-g}\,. \tag{1.31}$$

The second term δL_2 is already in the standard form, so the focus is on evaluating the other two terms. Referring to equations (1.7) and (1.17), it is observed that the Riemann (and the Ricci) tensor is expressed in terms of the Christoffel symbols. To

determine the variation of the Riemann tensor concerning the metric tensor, it is convenient to first find its variation with respect to the Christoffel symbols. The variation of the Christoffel symbols ($\delta\Gamma^{\rho}_{\mu\nu}$), defined as the difference between two Christoffel symbols, can be expressed as a tensor. Consequently, one may define its covariant derivative as:

$$\nabla_\lambda(\delta\Gamma^{\rho}_{\mu\nu}) = \partial_\lambda(\delta\Gamma^{\rho}_{\mu\nu}) + \Gamma^{\rho}_{\lambda\sigma}\delta\Gamma^{\sigma}_{\mu\nu} - \Gamma^{\sigma}_{\lambda\nu}\delta\Gamma^{\rho}_{\mu\sigma} - \Gamma^{\sigma}_{\lambda\mu}\delta\Gamma^{\rho}_{\nu\sigma}\,. \tag{1.32}$$

After algebraic manipulations, the variation of the Riemann tensor takes the form:

$$\delta R^{\rho}_{\mu\lambda\nu} = \nabla_\lambda(\delta\Gamma^{\rho}_{\mu\nu}) - \nabla_\nu(\delta\Gamma^{\rho}_{\lambda\mu})\,. \tag{1.33}$$

Substituting this equation into the first term of the action's variation, one gets

$$\delta L_1 = \int d^4x\sqrt{-g}\;\nabla_\sigma\left[g^{\mu\nu}\delta\Gamma^{\sigma}_{\mu\nu} - g^{\mu\sigma}\delta\Gamma^{\lambda}_{\lambda\mu}\right]\,. \tag{1.34}$$

The variation presented in the above equation takes the form of a total derivative, specifically $\nabla_\mu A^\mu$. Utilizing Stokes's theorem, the contribution of such a total derivative in the field equations is equivalent to a boundary contribution at infinity. By enforcing the variation to vanish at infinity, this boundary contribution can be eliminated. Therefore, a total derivative does not impact the field equations, allowing to set $\delta L_1 = 0$.

For the third term δL_3, the following relation is required, which is applicable to any square matrix M with a non-trivial determinant: $\ln(\det M) = \mathrm{Tr}(\ln M)$. The variation of the equation is then given by:

$$\frac{1}{\det M}\delta(\det M) = \mathrm{Tr}(M^{-1}\delta M)\,. \tag{1.35}$$

Applying this equation with $\det M = g$, it is found that $\delta g = -g g^{\mu\nu}\delta g_{\mu\nu}$. Consequently, the variation of the $\sqrt{-g}$ term appearing in δL_3 is easily determined as:

$$\delta\sqrt{-g} = -\frac{1}{2\sqrt{-g}}\delta g = -\frac{1}{2}\sqrt{-g}g^{\mu\nu}\delta g_{\mu\nu}\,. \tag{1.36}$$

By substituting into equation (1.8), the expression for δL is obtained as:

$$\delta L = \frac{\delta L}{\delta g^{\mu\nu}}\delta g^{\mu\nu} = \int d^4x\sqrt{-g}\left(R_{\mu\nu} - \frac{1}{2}Rg_{\mu\nu}\right)\delta g^{\mu\nu}\,. \tag{1.37}$$

From this equation, one can deduce the vacuum field equations of General Relativity i.e., $G_{\mu\nu} = 0$. The Lagrangian formulation's advantage becomes evident in later sections, showcasing its flexibility for modifications to General Relativity.

To derive the complete set of field equations, an additional term related to matter is added to the action:

$$L = \frac{1}{16\pi}\left(L_H + L_M\right)\,, \tag{1.38}$$

where L_H denotes the Einstein-Hilbert action, and L_M represents the matter Lagrangian. Utilizing the approximation of Newtonian limit ($d\tau = cdt$) on the spatial part of geodesic equation (1.11), the definition of the energy-momentum tensor is extracted as

$$T_{\mu\nu} = -\frac{2}{\sqrt{-g}}\frac{\delta L_M}{\delta g^{\mu\nu}}\,. \tag{1.39}$$

Consequently, the comprehensive field equations of General Relativity take the form:

$$R_{\mu\nu} - \frac{1}{2}Rg_{\mu\nu} = 8\pi T_{\mu\nu}\,. \tag{1.40}$$

Additionally, akin to the preceding section, one can introduce the cosmological constant into this equation through the metric compatibility approximation.

1.3 Modified Theories of Gravity

General Relativity, formulated by Einstein in 1915, stands as an immensely successful, extensively tested, and predictive theory. It has not only withstood all experimental validations but has also evolved into the fundamental framework for explaining nearly all gravitational phenomena known to date. Consequently, it has solidified its status as a true paradigm, especially in the domain of gravitation and physics at large. Recent strong field tests such as Binary pulsars [19–22], direct detection of gravitational waves from the binary black hole merger in LIGO and VIRGO [23, 24], direct observation of supermassive black hole shadow of M87 and Sagittarius A* in Event Horizon Telescope [25, 26], and others have precisely verified the validity of GR.

Cosmology on the other hand, is currently experiencing a flourishing era, marked by a pivotal focus on the intriguing observation that the universe is undergoing an accelerated expansion [27–33]. This phenomenon, posing one of the most significant and challenging problems in contemporary cosmology, introduces a new complexity to the governing gravitational equations. Historically, physics has addressed such complexities by either identifying previously unaccounted sources or by modifying the governing equations. The cause behind this acceleration remains an open and tantalizing question, giving rise to two major theoretical challenges in modern astrophysical and cosmological models, the dark matter and dark energy problems [34]. In the case of dark energy, observational data have compellingly confirmed the accelerated expansion of the universe. Notably, General Relativity struggles to provide a satisfactory explanation for these phenomena. A promising approach to address these challenges is to consider that, at large scales, GR may break down, and a more comprehensive action describes the gravitational field. This leads to questions about the nature of 'dark energy' driving the universe's acceleration— is it a vacuum energy, a dynamical field i.e., "quintessence" [35–38], or a result of infrared modifications to General Relativity [39]? Regarding dark matter, observations such as galactic rotation curves and mass discrepancies in galactic clusters suggest the existence of a non-interacting or weakly interacting form of dark matter at galactic and extra-galactic scales [40–43].

Some propose that modified gravity could explain galactic dynamics without introducing dark matter. For a more detailed review and references, see [44].

When dealing with a set of ideas constituting a loose and ad hoc definition of a theory, questions naturally arise. These questions might involve examining the fundamental principles underlying the theory, assessing their individual importance, and exploring the possibility of constructing an alternative, consistent theory by excluding some of these principles. There is also an interest in viewing the theory from a broader standpoint to determine if it can be classified within a more general category of theories. Whether one is eliminating principles from the theory or adopting a higher-level perspective, the overarching idea is centered around abstraction and generalization.

In the context of gravity, specifically within the field of GR, one can take its fundamental principles as a starting point. Analyzing simple theories that deviate from GR in a controlled manner becomes a valuable approach. These theories, often referred to as toy or straw-man theories, should be simple and easily manageable, each deviating from GR in only one aspect. By exploring the viability of such toy theories, researchers can gain a deeper understanding of the challenges involved in formulating modified theories of gravity. This approach involves a trial-and-error methodology in the quest for modified gravity theories.

1.3.1 Gravity's Evolution: Unraveling General Relativity and Beyond

Following the completion of the special theory of relativity by Einstein, the natural progression was to address the challenge of gravitation in a covariant manner, even though there was no unanimous agreement on this matter at that time. The observed displacement of the perihelion of Mercury had raised skepticism regarding the adequacy of the Newtonian approach to this gravitational problem in general. In this context, one may quote some of the finest lines about General Relativity by Paulo Crawford [45]:

> "Summarizing, Einstein's approach was embodied in heuristic principles that guided his search from the beginning in 1907. The first and more lasting one was the "Equivalence Principle" which states that gravitation and inertia are essentially the same. This insight implies that the class of global inertial frames singled out in special relativity can have no place in a relativistic theory of gravitation. In other words, Einstein was led to generalize the principle of relativity by requiring that the covariance group of his new theory of gravitation be larger than the Lorentz group. This will lead him through a long journey and in his first step, already in his review of 1907, Einstein formulated the assumption of complete physical equivalence between a uniformly accelerated reference frame and a constant homogeneous gravitational field. That is, the principle of equivalence extends the covariance of special relativity beyond Lorentz covariance but not as far as general covariance. Only later Einstein formulates a Generalized Principle of Relativity which would be satisfied if the field equation of the new theory could be shown to possess general covariance. But Einstein's story

> appealing to this mathematical property, general covariance, is full of ups and downs."

The initial efforts took the most logical path: integrating gravity into Special Relativity. However, it became evident, especially to Einstein, that gravity could not be adequately described using a scalar field alone. Einstein's attempt with a field 'c' corresponding to the speed of light proved unsuccessful, leading him to recognize the impracticality of a "scalar gravity" [45, 46]. Subsequently, Einstein shifted to a tensor formalism to tackle the gravitational problem. On the other hand, figures like Nordström, in his first theory, insisted on a scalar field (the field being denoted as m), while others like Abraham opposed the use of special relativity (Lorentz invariance) and formulated non-covariant theories [46, 47]. This somewhat chaotic state of affairs ultimately resolved in favor of Einstein's tensor approach and the formulation of the general theory of relativity. Nordström's two theories (and other scalar theories of gravity) became outdated remnants of the transition to the geometric understanding of space-time.

Despite this resolution, questions persisted about the generality of the principles of GR. As early as 1919, attempts were made to develop a higher-order theory of gravity, where the field equations differ from GR's with an order greater than second. A. Eddington [48] and H. Weyl [49] initiated these attempts, primarily driven by the pursuit of theoretical completeness. Around the same time (1920), discussions arose regarding whether the metric or the connection should be considered the principal field related to gravity. In 1924, Eddington introduced a purely affine version of GR in vacuum. Later, Schrödinger extended Eddington's theory to include a non-symmetric metric [50]. These theories are vacuum-based, and considerable challenges arise when attempting to incorporate matter into them.

It is noteworthy to mention another approach to this question, involving both a metric and a connection that are, to some extent, independent. The Einstein-Cartan theory serves as a notable example, utilizing a non-symmetric connection and Riemann-Cartan spaces [51]. This theory accommodates the existence of torsion and links it to the presence of spin.

Now in the following section, some of the most useful and relevant theories of modified gravity will be discussed.

1.3.2 $f(R)$ Gravity

An area of interest in modified gravity theory has gained considerable attention recently, focusing on $f(R)$ modifications. This is merely the simplest form of modification to Einstein's General Theory of Relativity in which the traditional Einstein-Hilbert action is replaced by an arbitrary function of the Ricci scalar R [52, 53]. Within this framework, various studies have explored the possibility of understanding galactic dynamics without invoking dark matter [54–58]. Some investigations have also

connected $f(R)$ gravity models with Modified Newtonian Dynamics (MOND) and the pioneer anomaly by introducing a coupling of R with the matter Lagrangian density [59, 60]. For a comprehensive overview, see [61]. Earlier interest in $f(R)$ theories stemmed from inflationary scenarios, such as the Starobinsky model, where they considered $f(R) = R - \Lambda + \alpha R^2$ [62]. Moreover, it has been demonstrated that late-time cosmic acceleration can be explained within this framework [63]. Consequently, $f(R)$ gravity has been explored for the criteria of viable cosmological models as referred in [64–69]. However, in the Solar system regime, stringent weak field constraints have narrowed down the proposed models [70–74], although some models have withstood scrutiny [75–80].

To describe the induced gravity, the metric formalism is employed, which involves varying the action with respect to $g_{\mu\nu}$. It is important to note that alternative approaches, such as the Palatini formalism and the metric-affine formalism, have also been explored [81–90].

The realization of $f(R)$ theory in static, spherically symmetric compact objects have been investigated in different scenarios. For instance, one may sum up the major studies regarding gravitational collapse and black holes in vacuum or electromagnetic background geometry [91–105], neutron stars [106–115], and wormholes [116–120].

The action for $f(R)$ gravity is written in the following way:

$$S = \frac{1}{2\kappa}\int d^4x\sqrt{-g}f(R) + S_M(g^{\mu\nu}, \psi)\,, \tag{1.41}$$

where $\kappa = 8\pi G$, $S_M(g^{\mu\nu}, \psi) = \int d^4x\sqrt{-g}\mathcal{L}_m(g^{\mu\nu}, \psi)$ is the matter action, and g is the determinant of the metric $g_{\mu\nu}$. The symbol $\mathcal{L}_m$ denotes the Lagrangian density of matter, where matter interacts minimally with the metric $g_{\mu\nu}$, and ψ denotes the collection of matter fields.

By varying the action with respect to $g_{\mu\nu}$, one finds

$$FR_{\mu\nu} - \frac{1}{2}fg_{\mu\nu} - \nabla_\mu\nabla_\nu F + g_{\mu\nu}\Box F = \kappa T^{(m)}_{\mu\nu}\,, \tag{1.42}$$

with $F \equiv \frac{df}{dR}$. When equation (1.42) is contracted, it yields the following relation:

$$fR - 2f + 3\Box F = T\,. \tag{1.43}$$

This equation demonstrates that the Ricci scalar serves as a complete dynamical degree of freedom, and here, $T = T^\mu_\mu = g^{\mu\nu}T_{\mu\nu}$ represents the trace of the stress-energy-momentum tensor.

The main results and features of the $f(R)$ gravity model can be summarized as follows:

• Certain choices of $f(R)$ models permit significant deviation from the ΛCDM in the later stages of cosmological evolution, while resembling the early cosmological dynamics of ΛCDM. This modification in gravity becomes evident in the evolution of cosmological perturbations due to alterations in the effective gravitational coupling. These alterations give rise to various intriguing observational implications, including modifications to galaxy and CMB power spectra, as well as effects on weak lensing.

• The instability proposed by Dolgov-Kawasaki [121] could be avoided in the metric $f(R)$ model only when $f''(R) \geq 0$.

• Metric $f(R)$ gravity might potentially satisfy the weak-field limit criteria and serve as an alternative to dark energy, but it must rely on the effectiveness of the chameleon mechanism. This imposes constraints on the permissible choices of $f(R)$ function, which cannot be straightforwardly delineated by simple forms.

1.3.3 $f(R,T)$ Gravity

In the $f(R,T)$ modified theory [122], gravitational Lagrangian depends on and is a function of R and T. The field equations derived from this theory rely on a source term determined by the variation of the Energy-Momentum Tensor (EMT). Thus, the specific form of these equations entirely depend on the type of matter content present in the universe. The relationship between geometry and matter are expressed through the function $f(R,T)$, involving both minimal and non-minimal curvature-matter coupling. Furthermore, in this theory, the EMT is non-conservative, leading to non-geodesic motion of timelike test particles. This deviation from geodesic motion results in additional acceleration experienced by particles due to the coupling of geometry-matter. This intriguing feature has attracted significant attention, leading to considerable advancements in the literature over the years.

Various aspects of $f(R,T)$ gravity have been explored in different scenarios, including thermodynamic investigations within the framework of $f(R,T)$ gravity [123], the cosmic coincidence problem [124], analysis of cosmological phase space [125], formulation of scalar perturbations [126], examination of Gravastars [127], $f(R,T)$ models as the source of dark matter effects [128], study of polar gravitational waves and their evolution [129], cosmic chronometers and parameters of standard distance measurement [130], analysis of cosmic censorship hypothesis together with gravitational collapse in Vaidya spacetime [131] and wormholes [132–138].

The action for $f(R,T)$ can be realized as

$$S = \frac{1}{16\pi}\int d^4x\sqrt{-g}\big[f(R,T) + \mathcal{L}_m\big]\,, \tag{1.44}$$

where $f(R,T)$ being any function of R and T. Here, the EM tensor of the matter field can be represented by the matter Lagrangian density $\mathcal{L}_m$ as

$$T_{\mu\nu} = -\frac{2}{\sqrt{-g}}\frac{\delta(\sqrt{-g}\mathcal{L}_m)}{\delta g^{\mu\nu}}\,. \tag{1.45}$$

Since, the matter Lagrangian solely depends on the metric $g_{\mu\nu}$, and not on its derivative, it is defined as

$$T_{\mu\nu} = g_{\mu\nu}\mathcal{L}_m - \frac{2\partial\mathcal{L}_m}{\partial g^{\mu\nu}}\,. \tag{1.46}$$

Finally, one may vary the action with respect to $g_{\mu\nu}$ and obtain the field equation as

given by

$$\delta S = \frac{1}{16\pi}\int d^4x\sqrt{-g}\Big[f_R(R,T)R_{\mu\nu}\delta g^{\mu\nu} + f_R(R,T)g_{\mu\nu}\Box\delta g^{\mu\nu} - f_R(R,T)\nabla_\mu\nabla_\nu\delta g^{\mu\nu} + f_T(R,T)\frac{\delta(g^{\alpha\beta}T_{\alpha\beta})}{\delta g^{\mu\nu}}\delta g^{\mu\nu} - \frac{1}{2}g_{\mu\nu}f(R,T)\delta g^{\mu\nu} + 16\pi\frac{1}{\sqrt{-g}}\frac{\delta(\sqrt{-g}\mathcal{L}_m)}{\delta g^{\mu\nu}}\Big], \quad (1.47)$$

where $f_R(R,T)$ and $f_T(R,T)$ are the differentiation of $f(R,T)$ with respect to R and T respectively. On the other hand, by varying the trace of EM tensor T with respect to $g_{\mu\nu}$, the expression is obtained as

$$\frac{\delta(g^{\alpha\beta}T_{\alpha\beta})}{\delta g^{\mu\nu}}\delta g^{\mu\nu} = T_{\mu\nu} + \Theta_{\mu\nu}\,. \quad (1.48)$$

Note that, the covariant derivative ∇_μ is associated with the Levi-Civita connection of the metric, and the D'Alembertian operator $\Box \equiv \nabla^\mu\nabla_\mu$ has the form $\Box \equiv \frac{\partial_\mu(\sqrt{-g}g^{\mu\nu}\partial_\nu)}{\sqrt{-g}}$. Similarly, it is necessary to define $\Theta_{\mu\nu} = g^{\alpha\beta}\frac{\delta T_{\alpha\beta}}{\delta g^{\mu\nu}}$, where for the perfect fluid, this tensor becomes

$$\Theta_{\mu\nu} = -2T_{\mu\nu} + pg_{\mu\nu}\,. \quad (1.49)$$

Now, employing by parts integration mechanism in Eq. (1.47), the final field equation in $f(R,T)$ gravity is arrived at:

$$(R_{\mu\nu} - \nabla_\mu\nabla_\nu)f_R(R,T)g_{\mu\nu} + \Box f_R(R,T)g_{\mu\nu} - \frac{1}{2}f(R,T)g_{\mu\nu} = 8\pi T_{\mu\nu} - f_T(R,T)(T_{\mu\nu} + \Theta_{\mu\nu})\,. \quad (1.50)$$

The $f(R,T)$ modification in the Einstein-Hilbert action can introduce significant deviations from the standard general relativity, or $f(R)$ gravity and impose major differences in the cosmology, gravitational collapse and others. In the recent past, cosmological models in $f(R,T)$ theory have been proposed in different functional forms of f, one of which attracted significant attention is $f(R,T) = f_1(R) + f_2(T)$. This model mimics the so called $f(R,T) = R + 2\lambda T$, and $f(R,T) = R - 2\chi T$ cosmology, where special limits on λ and χ has been applied from the observational data to model strange stars [139], white dwarfs [140], or the atmosphere around Earth [141] in particular.

1.3.4 dRGT massive Gravity

From the early twentieth century, after the introduction of GR, it was largely expected that it can describe the underlying force of gravity with ultimate precession agreeing with observations. In the point of view of modern particle physics, the uniqueness of GR has been investigated for massless spin-2 particles [142–146]. Nevertheless, introducing mass into a spin-1 and spin-2 particle dates back to 1939 when Fierz and Pauli came up with their mass term [147]. At the linear order, massless spin-2 particles are under linearized diffeomorphism symmetry similar to the U(1) gauge symmetry of photons. However, coupling of matter with this spin-2 field that describes graviton,

ultimately pushes this symmetry to be non-linear. This makes the massive gravity theory completely non-linear (unlike an isolated spin-2 field) due to the non-linear configuration of the field. Thus, the GR equivalent non-linear theory approach is highly challenging particularly due to the two major issues, first of which being the van Dam-Veltman-Zakharov (vDVZ) discontinuity. The propagator of a massive spin-2 field realizes five degrees of freedom independent of their value of mass, whereas the theory underlying massless spin-2 field i.e., GR, denotes propagation with two degrees of freedom. This issue defines the origin of vDVZ discontinuity [148, 149]. Vainshtein however resolved the subtlety couple of years later by describing the rest of the degrees of freedom that creates the discontinuity, to be adjusted by its own interactions [150]. See [151] for a recent review.

The most concerning second puzzle is the Boulware-Deser (BD) ghost instability [152] that comes hand in hand with the non-linearization of Fierz-Pauli massive gravity. This marked a significant attention in the past couple of decades to avoid BD ghost either in the Dvali-Gabadadze-Porrati (DGP) model of soft massive gravity [153–155], or in a three-dimensional 'new massive gravity' (NMG) [156], or in the ghost-free de Rham-Gabadadze-Tolley (dRGT) massive gravity [157, 158]. See [159] for a detailed review.

A massive gravity theory demands the introduction of a reference fiducial metric $f_{\mu\nu}$, which can be Minkowski type, in general at the linear order. Instead of the whole metric $g_{\mu\nu}$, the mass term for gravity is determined from the fluctuation $h_{\mu\nu}$ with respect to $f_{\mu\nu}$. This breaks the diffeomorphism invariance in the linearized level, where the Stückelberg trick supports the gauge symmetry by changing reference metric to $\eta_{\mu\nu} \to \left(\eta_{\mu\nu} - \frac{2}{M_{\rm Pl}}\partial_{(\mu}\chi_{\nu)}\right)$, and keeping $h_{\mu\nu} - 2\partial_{(\mu}\chi_{\nu)}$ invariant under linearized diffeomorphism. Similarly, the non-linear Stückelberg trick restores covariance by replacing $f_{\mu\nu}$ (which may not be Minkowski type) with $\tilde{f}_{\mu\nu}$ [160, 161] as $f_{\mu\nu} \to \tilde{f}_{\mu\nu} = \partial_\mu\phi^a\partial_\nu\phi^b f_{ab}$, where ϕ^a $(a = 0, 1, 2, 3)$ be the Stückelberg field. In this way, one may introduce the tensor

$$X^\mu_\nu = g^{\mu\alpha}\tilde{f}_{\alpha\nu} = \partial^\mu\phi^a\partial_\nu\phi^b f_{ab}\,, \tag{1.51}$$

where the unitary gauge, $\mathbb{X} = g^{-1}f$.

Now, prior to defining the BD ghost, the generic Fierz-Pauli mass term in spin-2 field $h_{\mu\nu}$ can be written in terms of possible mass notations $h_{\mu\nu}$ and h^2 as

$$\mathcal{L}_{\rm FP} = -\frac{1}{8}m^2\left(h^2_{\mu\nu} - Ah^2\right)\,, \tag{1.52}$$

with A being a dimensionless parameter. The non-linear extension of this mass term is non-linear coordinate transformation invariant, and is given by

$$\mathcal{L}^{\rm (nl)}_{\rm FP} = -m^2M^2_{\rm Pl}\sqrt{-g}\left([(\mathbb{I} - \mathbb{X})^2] - [\mathbb{I} - \mathbb{X}]^2\right)\,. \tag{1.53}$$

The BD ghost can be easily observed in the form of Ostrogradsky instability [162, 163] under the non-linear Stückelberg trick. In the helicity-0 mode π, Eq. (1.51) is given by

$$\mathbb{X}^\mu_\nu = \partial^\mu_\nu - \frac{2}{M_{\rm Pl}m^2}\Pi^\mu_\nu + \frac{1}{M^2_{\rm Pl}m^4}\Pi^\mu_\alpha\Pi^\alpha_\nu\,, \tag{1.54}$$

focusing on the flat reference metric $f_{\mu\nu} = \eta_{\mu\nu}$. Then, the mass term in (1.53) is expressed as

$$\mathcal{L}^{(\mathrm{nl})}_{\mathrm{FP},\pi} = -\frac{4}{m^2}\left([\Pi^2]-[\Pi]^2\right) + \frac{4}{M_{\mathrm{Pl}}m^4}\left([\Pi^3]-[\Pi][\Pi^2]\right) + \frac{1}{M^2_{\mathrm{Pl}}m^6}\left([\Pi^4]-[\Pi^2]^2\right), \tag{1.55}$$

where $([\Pi^3]-[\Pi][\Pi^2])$ and $([\Pi^4]-[\Pi^2]^2)$ operators incorporate the propagation of an extra degree of freedom which is a ghost by the Ostrogradsky theorem. This is solely a non-linear level proposition, that implies an appropriate background configuration $\pi = \pi_0 + \delta\pi$. In terms of non-linear Fierz-Pauli mass term, this extra degree of freedom defines the Boulware-Deser ghost having mass

$$m^2_{ghost} \sim \frac{M_{\mathrm{Pl}}m^4}{\partial^2\pi_0}\,, \tag{1.56}$$

under the background configuration π_0.

In massive gravity, the consistency of Fierz-Pauli mass term $(h^2 - h_{\mu\nu})$ depends on the total derivative Lagrangian

$$\mathcal{L}^{(2)}_{\mathrm{derivative}} = [\Pi]^2 - [\Pi^2]\,. \tag{1.57}$$

One may change $[\Pi]$ and $[\Pi^2]$ by $\langle\mathcal{K}\rangle$ and $\langle\mathcal{K}^2\rangle$, that sufficiently extend $\mathcal{L}^{(2)}_{\mathrm{derivative}}$ covariantly away from $h_{\mu\nu} = 0$. This may ensure the ghost-free decoupling limit, and the Lagrangian for massive gravity is modified to

$$\mathcal{L} = \frac{M^2_{\mathrm{Pl}}}{2}\sqrt{-g}\left(R - \frac{m^2}{4}\mathcal{U}(g,H)\right)\,, \tag{1.58}$$

with the potential

$$\mathcal{U}(g,H) = -4\left(\langle\mathcal{K}\rangle^2 - \langle\mathcal{K}^2\rangle\right)\,, \tag{1.59}$$

which can also be derived in quintic order

$$\begin{aligned}\mathcal{U}(g,H) = &\left(\langle H^2\rangle - \langle H\rangle^2\right) - \frac{1}{2}\left(\langle H\rangle\langle H^2\rangle - \langle H^3\rangle\right)\\ &- \frac{1}{16}\left(\langle H^2\rangle^2 + 4\langle H\rangle\langle H^3\rangle - 5\langle H^4\rangle\right)\\ &- \frac{1}{32}\left(2\langle H^2\rangle\langle H^3\rangle + 5\langle H\rangle\langle H^4\rangle - 7\langle H^5\rangle\right) + \cdots\,.\end{aligned} \tag{1.60}$$

These last two Lagrangians can be directly derived from

$$\mathcal{L}_\lambda = \frac{M^2_{\mathrm{Pl}}}{2}\sqrt{-g}\left[R - m^2\left(\mathcal{K}^2_{\mu\nu} - \mathcal{K}^2\right)\right] + \sqrt{-g}\lambda^{\mu\nu}\left(g^{\alpha\beta}\mathcal{K}_{\mu\alpha}\mathcal{K}_{\beta\nu} - 2\mathcal{K}_{\mu\nu} + H_{\mu\nu}\right), \tag{1.61}$$

where λ^μ_ν is Lagrange multiplier, and $\mathcal{K}^\mu_\nu = \delta^\mu_\nu - \sqrt{\partial^\mu\phi^a\partial_\nu\phi^b\eta_{ab}}$. This theory, in the general formalism, has a well-defined Cauchy problem in arbitrary background, and is ghost-free in the decoupling limit.

The dRGT massive gravity theory has been widely explored since its appearance in 2010. In a static, spherically symmetric model of dRGT, two extra characteristic scales

i.e., the effective cosmological constant and a constant potential for global monopole term arises [164, 165]. They impose significant deviations to the known results from Einstein's GR. For instance, investigations regarding black holes, black strings, their stability, greybody factor [166–196], Hawking evaporation [197], black hole with EHT M87* observational signature [198], galaxy rotation curve from observed data [199], inflationary scenario and cosmological aspects [200–203], wormhole solutions [204–207], and others [208–216] are among few of them.

The phenomenology, and the theoretical to observational perspectives of the dRGT massive gravity theory has a significant interest in research. The major progresses and further possibilities arising from the theory can be summarized as follows:

• The model independent graviton mass in terms of the Hubble parameter is bounded between $m \lesssim 10^{-30} - 10^{-33}$ eV. Notably, one may lose the relevant effect of this graviton in the observable universe when $m << 10^{-33}$ eV. However, it is expected that potentially new observational signatures may appear with interesting values of graviton mass.

• In this theory, the dynamics of the arbitrary reference metric [217] gives the consistent bi-gravity formalism [218], in which two interacting metrics support the mass spectrum of interactions between massless and massive spin-2 field, i.e., interaction of general relativistic field with massive spin-2 field. This is the theory of interacting metrics [219].

• The bi-gravity along with dRGT massive gravity is analytic and natural in the Vielbein formalism. This may lead to the multi-gravity of an arbitrary number of interacting spin-2 fields [220, 221].

• dRGT massive gravity successfully avoids the long standing BD ghost with definite proof. This may open up windows for newer theories that propagate a lesser number of degrees of freedom.

CHAPTER 2

THEORETICAL ASPECTS OF BACKWARD TIME ORIENTATION: CTC AND WORMHOLE

> "Time travel used to be thought of as just science fiction, but Einstein's general theory of relativity allows for the possibility that we could warp space-time so much that you could go off in a rocket and return before you set out."
>
> — Stephen Hawking

The qualitative and quantitative understanding of the concepts of "time" is an extremely difficult venture, yet it appears to be closely linked to change, as highlighted in Aristotle's renowned metaphor: *"Time is the moving image of Eternity"* [222]. Much of the confusion surrounding the notion of "time," akin to "space," stems from its multifaceted nature. One crucial distinction to address initially is the aspect of time pertaining to "When?" Typically, events are located in relation to one another temporally. In physics, events hold paramount significance. Aristotle delves into the intricacies of the concept of time, stating that *"Time is the number of changes with respect to the before and the after."* [223] In essence, time serves as a means of quantifying alterations, implying that if there is no change, there is no time.

Following this, Newton introduced his revolutionary concept of Newtonian time, wherein he acknowledges the existence of "common time" but also introduces a new variable, Newtonian time t, which progresses independently, regardless of whether other changes occur. Importantly, Newton emphasized that this t variable is not directly observable; contrary to popular belief, it does not align with our direct perception of time. Instead, Newton clarified that this time cannot be directly computed, perceived, or detected outside of movement. When calculating object movements relative to this time, elegant equations of motion, particularly in the Newtonian framework, can be

formulated. This underscores the significant point that clocks essentially represent "processes" designed to closely adhere to Newton's concept of time.

Einstein's introduction of special relativity in 1905 further revolutionized our understanding by unifying Newtonian concepts of space and time within Minkowski space. By 1915, with the advent of General Relativity, it was elucidated that space and time manifest as a field denoted by $g_{\mu\nu}(x)$, and a clock assumes the role of an object whose dynamics along the worldline γ, are intertwined with the gravitational field. A clock in spacetime moves alongside a small pendulum, measuring intervals of its own time, which essentially gauge aspects of the gravitational field $g_{\mu\nu}(x)$. Therefore, time by a clock during its motion along γ is manifested as

$$t_\gamma = \int_\gamma \sqrt{g_{\mu\nu} dx^\mu dx^\nu} \,. \tag{2.1}$$

This conceptually aligns with Newton's intuition, recognizing time as an entity inherent within the gravitational field. However, this entity is not positioned "above" other elements of the world; rather, it is just one component within the broader framework of the gravitational field. Consequently, Newtonian time is reduced to merely a variable within the universe's constituents. According to GR, time flows at varying speeds depending on the observer's perspective or location. This is however the fundamental ingredient for the direction of research in some quantum description of gravity, it is mostly the closest picture for an accurate conceptualization of time.

In the theory of Relativity, the empirical understanding of a series of events is replaced with a sequence of events. The concept of an event can thus be refined to represent a precise point in space and a specific moment in time. By adopting this perspective, a sequence of events naturally follows a defined temporal sequence. Through experimentation, it is confirmed that certain events precede others, establishing a clear notion of "causality" where some events (effects) are instigated by others (causes).

Therefore, grasping the conceptual definition and comprehension of time presents a formidable challenge yet holds immense significance. Special Relativity offers valuable quantitative insights into fundamental processes concerning time dilation effects. In contrast, the General Theory of Relativity delves deeply into analyzing the effects of time flow within both strong and weak gravitational fields. As time becomes intricately woven into the fabric of spacetime, GR introduces complex non-trivial geometries, including *closed timelike curves (CTCs)* [224], which enable the possibility of time travel. These curves permit an observer traveling along their trajectory to return to an event coinciding with their departure, thereby challenging the traditional notion of causality and introducing the Mystery box, namely the time travel paradoxes [225]. This phenomenon raises profound questions about the fundamental nature of time, casting a shadow over our understanding. Given the pivotal role of causality in constructing physical theories, the concept of time travel and its associated paradoxes necessitate careful consideration.

A wide array of solutions to Einstein's field equations (EFEs) exist, many of which allow CTCs. Among these solutions, two notable characteristics emerge prominently. First, there are solutions with "tipping over of light cones" due to rotation around a cylindrically symmetric axis. Second, there are solutions such as wormholes, that

violate the Energy Conditions of GR, which play a fundamental role in singularity theorems and classical black hole thermodynamics [2]. Significant attention has also been directed towards exploring the quantum aspects associated with closed timelike curves [226–228].

2.1 Closed Timelike Curves

A closed timelike curve is nothing but the intersection of the worldline of a body to its previous point. Closed timelike curves generically disrupt the chronological order of time, known as chronology, resulting in the loss of determinism. Unlike curvature singularities that cause the breakdown of physical laws, CTCs signify a breakdown in predictability. However, similar to the singularity problem, the region of spacetime that connects CTCs causally (referred to as the causality-violating region) presents challenges to defining the initial value Cauchy problem, leading to the concept of the "Cauchy horizon" [224, 229]. Despite efforts to mitigate the occurrence of CTCs by introducing modified spacetime models, such as [230], a comprehensive understanding remains elusive [231–234].

The generation of CTCs by the tipping over of light cones due to strong curvature effect, are a common feature in many stationary cylindrically symmetric (axisymmetric) rotating solutions of General Relativity. The long standing history of CTCs first came into existence when in 1949 Gödel discovered his exact cosmological solution of Einstein's field equation allows for closed timelike lines [235]. In his own words, he writes, *"it is theoretically possible in these worlds to travel into the past, or otherwise influence the past."* Since then, it has subsequently been found that other spacetime solutions, such as the van Stockum rotating dust [236], Kerr metric [237], modified van Stockum dust i.e., Tipler's cylinder [238], Bonnor's rotating dust cloud [239], and Gott's cosmic string [240] have been found to exhibit these curves.

The general metric describing a stationary, rotating, axisymmetric solution is expressed as [224, 238, 241]

$$ds^2 = -F(r)dt^2 + 2M(r)d\phi dt + L(r)d\phi^2 + H(r)dr^2 + H(r)dz^2\,, \tag{2.2}$$

where t, r, ϕ, z are the usual cylindrical coordinates. Notably, the metric components solely depend on the radial coordinate r, and the determinant, g, maintains a Lorentzian signature provided that $(FL+M^2) > 0$. Because the angular coordinate, ϕ, is periodic, an azimuthal curve described by the worldline $\gamma = \{t = r = z = \text{constant}\}$ defines an invariant length $\ell_\gamma^2 \equiv (2\pi)^2 L(r)$ for a closed curve. With $L(r)$ negative, a closed timelike curve can be obtained for fixed (t, r, z). Subsequently, for $L(r) = 0$, it is a closed null curve (CNC).
For the tipping over of light cones, consider $ds^2 = 0$ with $\dot{\phi} = \frac{d\phi}{dt}$, such that one gets

$$\frac{d\phi}{dt} = \frac{-M \pm \sqrt{M^2 + FL}}{L}\,, \tag{2.3}$$

where $(FL+M^2) > 0$ holds. Therefore, when $L(r) < 0$, the light cones tip over significantly away from the symmetry axis to allow for potential journeys into the past [224].

For an extensive review, see [242].
Now, in the following subsections, various well-known exact solutions of the EFE incorporating CTCs will be briefly summarized.

2.1.1 Gödel's cosmological solution

In 1949, Kurt Gödel in his new type of cosmological solution with rotation of matter, considered the line element [235]

$$ds^2 = a^2\left(dx_0^2 - dx_1^2 + \frac{1}{2}e^{2x_1}dx_2^2 - dx_3^2 + 2e^{x_1}dx_0dx_2\right), \tag{2.4}$$

with a being an arbitrary positive number. The solution encompasses a uniform rotating dust universe of non-zero cosmological constant, λ. The underlying Einstein field equation having total energy-momentum tensor $T_{ik} = \rho u_i u_k + \frac{\lambda}{8\pi}g_{ik}$, is satisfied when

$$1/a^2 = 8\pi\rho, \qquad \lambda = -1/2a^2 = -4\pi\rho\,, \tag{2.5}$$

corresponding to a positive pressure solution. Notice that, with proper rearrangement of energy-momentum tensor for a perfect fluid scenario with rotation, the energy density $\tilde{\rho}$ and pressure $\tilde{p}$ can be summed as

$$T_{ik} = (\tilde{\rho} + \tilde{p})u_i u_k + \tilde{p}g_{ik}\,, \tag{2.6}$$

in a zero cosmological constant universe. Now, one may find the modified energy-momentum components from Eq. (2.5) as:

$$\tilde{\rho} = \tilde{p} = \frac{1}{8\pi a^2} > 0\,. \tag{2.7}$$

Therefore, the usual classical energy conditions are satisfied.
To discuss the causal description of the system, it is effective to introduce an alternate set of coordinates (t, r, ϕ, y), in a cylindrical system. This has the rotational symmetry around the symmetry axis at $r = 0$, and with proper coordinate transformations, the line element reads

$$ds^2 = 4a^2\left(dt^2 - dr^2 - dy^2 + (\sinh^4 r - \sinh^2 r)d\phi^2 + 2\sqrt{2}\sinh^2 r d\phi dt\right). \tag{2.8}$$

This line element exhibits some special characteristics for the timelike lines. Consider a radial location c, such that $\sinh(c) = 1$, i.e., $c = \ln(1+\sqrt{2})$; then for all $R > c$, one obtains $(\sinh^4 R - \sinh^2 R) > 0$. Hence, for $(+,-,-,-)$ metric signature, any timelike curve defined by $r = R$ with $\{t = y = \text{constant}\}$ is closed; and, this may allow for the light cones to be tipped over after a certain radial distance from the symmetry axis. This is merely the first example of a closed timelike curve in literature.

Few years later of the Gödel's discovery, Chandrasekhar and Wright disarmed Gödel's claim for the possibility of time travel by proposing that geodesics in the spacetime are necessarily not closed [243]; yet Stein later demonstrated that CTCs in the metric are non-geodesic in nature [244]. One of the interesting features coming

out of these studies is that CTCs can also be non-geodesics. However, the generalized solution of Gödel spacetime as investigated by Novello and Reboucas, presented the successive causal and non-causal regions of CTGs (closed timelike geodesics i.e., closed timelike curves that are geodesics) [245].

Over the years, numerous studies have been conducted on geodesic and non-geodesic motions in Gödel's metric for a complete description of particle orbits within CTCs. For instance, one may refer to the analysis of Pfarr [246] and Malament [247, 248]. Subsequently, using the effective potential approach, Novello *et al.* discussed the complete structure of geodesic motion within the spacetime [249]. Finally, for the recent interests on Gödel universe, the following references can be considered [250–258].

2.1.2 van Stockum rotating dust

While Gödel first discovered that his solution contains CTCs, van Stockum dust is probably the first solution of EFE that allows for the CTCs. Willem Jacob van Stockum, while proposing his rotating dust cylinder in 1936 [236], was unaware about the presence of CTCs. It was discovered much later by Frank J. Tipler in 1974 [238]. In this subsection, the results of van Stockum cylinder as analyzed by Tipler, will be discussed in particular.

The stationary, axisymmetric van Stockum solution for a rapidly rotating dust cylinder of infinite length is sustained by the balancing forces of the centrifugal repulsion produced by the dust cylinder and the inward gravitational attraction. The cylinder is covered by a vacuum on the outside. There are two separate solutions for the interior and exterior geometry of the dust where the line element for the solutions are written in the cylindrical system (t, r, ϕ, z). [1]

• ***Interior solution:***
The interior solution of van Stockum metric for which $r < R$, where R is the radius of the dust cylinder, is given by

$$ds^2 = -dt^2 + 2ar^2 d\phi dt + r^2(1 - a^2r^2)d\phi^2 + e^{-a^2r^2}(dr^2 + dz^2)\,, \tag{2.9}$$

with a being the angular velocity of the cylinder. The Lorentzian signature is fulfilled as $(FL + M^2) = r^2 > 0$. From the Einstein field equation, one may obtain

$$\rho = \frac{a^2}{2\pi} e^{a^2r^2}\,, \tag{2.10}$$

where the four velocity is $u^i = (1, 0, 0, 0)$. Therefore, for the positive energy density dust source, all the classical energy conditions are satisfied.

For the closed timelike curves to appear, consider an azimuthal curve with $\{t = r = z = \text{constant}\}$, and a negative coefficient of $d\phi^2$. Therefore, the necessary condition for CTCs is $ar > 1$, which is the radial location of the CTCs having radius r. Hence, larger the angular velocity of the cylinder, smaller the radius of CTC.

[1] The cylindrical symmetric van Stockum line element is in accordance with the general metric (2.2). Therefore, results of the interior and exterior metric are summarized in the general metric coefficient forms $F(r)$, $M(r)$, $L(r)$, $H(r)$.

Notice that, causality violation can be avoided by requiring radius of the cylinder $R < 1/a$, for which the interior and exterior solution merges and a causally well-behaved solution can be constructed. So, the upper bound of the angular velocity is restricted to $aR = 1$, creating timelike particle trajectories for the whole r.

• ***Exterior solution:***
According to van Stockum, the exterior solution is given by $aR > 1$. The possibility for the region can be separated into three, as given by

(i) $0 < aR < 1/2$.

$$H(r) = e^{-a^2r^2}\,(r/R)^{-2a^2r^2}\,, \qquad L(r) = \frac{rR\sinh(3\beta+\alpha)}{2\sinh(2\beta)\cosh(\beta)}\,,$$
$$M(r) = \frac{r\sinh(\beta+\alpha)}{\sinh(2\beta)}\,, \qquad F(r) = \frac{r\sinh(\beta-\alpha)}{R\sinh(\beta)}\,, \tag{2.11}$$

where

$$\alpha = \alpha(r) = (1-4a^2R^2)^{1/2}\ln(r/R) \qquad \text{and} \qquad \beta = \beta(r) = \operatorname{arctanh}(1-4a^2R^2)^{1/2}\,.$$

(ii) $aR = 1/2$.

$$H(r) = e^{-1/4}\,(r/R)^{-1/2}\,, \qquad L(r) = (rR/4)\,[3+\ln(r/R)]\,,$$
$$M(r) = (r/2)\,[1+\ln(r/R)]\,, \qquad F(r) = (r/R)\,[1-\ln(r/R)]\,. \tag{2.12}$$

(iii) $aR > 1/2$.

$$H(r) = e^{-a^2r^2}\,(r/R)^{-2a^2r^2}\,, \qquad L(r) = \frac{rR\sin(3\sigma+\gamma)}{2\sin(2\sigma)\cos(\sigma)}\,,$$
$$M(r) = \frac{r\sin(\sigma+\gamma)}{\sin(2\sigma)}\,, \qquad F(r) = \frac{r\sin(\sigma-\gamma)}{R\sin(\sigma)}\,, \tag{2.13}$$

where

$$\gamma = \gamma(r) = (4a^2R^2-1)^{1/2}\ln(r/R) \qquad \text{and} \qquad \sigma = \sigma(r) = \arctan(4a^2R^2-1)^{1/2}\,.$$

For the merged interior-exterior geometry, the spacetime is Lorentzian for $R \leq r < \infty$, since the interior Lorentzian is fulfilled. The $aR \leq 1/2$ solution is causally well-behaved, but the $aR > 1/2$ solution contains causality violation in the whole spacetime. An interesting feature of the van Stockum metric is the presence of closed timelike geodesics (CTGs), as investigated by Steadman [259]. Further, the geodesic confinements in the solution was studied by Opher *et al.* [260].

The complete structure of van Stockum spacetime is not asymptotically flat, and as it defines an infinitely long dust cylinder, the solution is unphysical. However, the phenomenology is interesting. The metric reduces to a Kerr solution when a modification of the cylinder behaves as a "ring singularity" [237], yet the Kerr solution also contains CTCs.

2.1.3 Bonnor's dust cloud

Bonnor investigated a stationary, rotating, cylindrical symmetric exact solution of EFE that describes a rigidly rotating dust cloud about the symmetry axis [239]. The dust cylinder is finitely extended and the line element reads

$$ds^2 = -dt^2 + 2nd\phi dt + (r^2 - n^2)d\phi^2 + e^{\mu}(dr^2 + dz^2)\,, \tag{2.14}$$

where

$$n = \frac{2hr^2}{R^3}, \qquad \mu = \frac{h^2r^2(r^2 - 8z^2)}{2R^8}, \qquad R^2 = (r^2 + z^2)\,, \tag{2.15}$$

in the comoving coordinates. The rotation parameter is given by h. At the $z = 0$ slice of the spacetime, the causality violating region is easily obtained using $L(r, z) = r^2 - 4h^2r^4/(r^2 + z^2)^3 < 0$ condition, as given by

$$r^4 < 4h^2. \tag{2.16}$$

It was argued that portions of the timelike geodesics in the spacetime have access to the causality violating regions where coordinate time can possibly run backward [261]. However, as a whole, the geometry does not allow the presence of CTGs [261, 262].

2.1.4 Gott cosmic string

The pleasing model of time-machine constructed by J. Richard Gott describes an exact solution of EFE for two non-intersecting, simultaneously moving straight cosmic strings [240]. The spacetime that describes this geometry is static, axisymmetric, and the strings are located along the symmetry axis. The cylindrical symmetric interior metric of a uniform density string is flat and free of a cone singularity, and is given by

$$ds^2 = -dt^2 + d\rho^2 + \frac{1}{8\pi\varepsilon}\sin^2\left(\sqrt{8\pi\varepsilon}\rho\right)d\phi^2 + dz^2\,, \tag{2.17}$$

where ρ is the radial coordinate, ε is the uniform density of the strings for a cylindrical radius ρ_0, and is taken positive. The energy-momentum tensor components on the orthonormal frame for the strings is

$$T_{\hat{t}\hat{t}} = -T_{\hat{z}\hat{z}} = \varepsilon\,. \tag{2.18}$$

The exterior metric must be a static and cylindrical symmetric vacuum solution of Einstein's equations. The interior and exterior spacetimes should then be joined at the string surface at $\rho = \rho_0$, using the Darmois-Israel junction conditions. The exact exterior metric is given by

$$ds^2 = -dt^2 + dr^2 + (1 - 4\mu)^2r^2d\phi^2 + dz^2\,, \tag{2.19}$$

where $\mu = \frac{1}{4}\left(1 - \cos\left(\rho_0/\bar{\rho}\right)\right)$ is the linear energy density, or mass per unit length, having $\bar{\rho} = (8\pi\varepsilon)^{-1/2}$.

The CTCs appear in the Gott cosmic string by the effect of gravitational lensing and relativity of simultaneity. Importantly, the CTCs do not violate the weak or null energy

condition, whereas the solution does not contain any singularity. In view of Hawking's Chronology Protection Conjecture [263] (which will be briefly discussed later in this chapter), this solution has an additional importance. The conjecture states that the physical laws naturally disallow the creation of backward time flow, or even if objects like wormholes are created, the throat does not sustain for traversability. Researchers have delved into the investigation whether the CTCs pre-exist in the spacetime (i.e., intersect the spacelike hypersurface), or they create at some specific instant of time. Ori showed that CTCs necessarily coincide all t = constant hypersurface which is in accordance with the chronology protection [264]. Alongside, Cutler investigated the global structure of the hypersurface and concluded that the CTCs are confined at some specific locations of the spacetime where they emerge from the underlying spacelike and achronal hypersurfaces [265]. Further, the global two string hypersurface is identical to a generic Misner space, as discussed by Grant [266]. According to Laurence [267], the region of CTC in Gott two string space is identical to the generalized Misner space, and this result has been used to propose the vacuum polarization effect on the Grant space. Moreover, the construction of Gott time-machine is physically not realistic due to the unphysical acausal behaviour [268–272].

2.1.5 Infinite spinning cosmic string

The infinitely long cosmic string spinning about the z axis with a delta function source, can be denoted by the following metric in cylindrical coordinate:

$$ds^2 = -[d(t + 4J\phi)]^2 + dr^2 + (1 - 4\mu)^2 r^2 d\phi^2 + dz^2 \,, \tag{2.20}$$

where the mass per unit length μ, is equal to the tension τ; and J is the angular momentum per unit length. The system is analogous to the van Stockum, except the asymptotic structure [224, 273].
Following to a transformation $\tilde{t} = (t + 4J\phi)$, $\tilde{\phi} = (1 - 4\mu)\phi$, the range of $\tilde{\phi}$ is now restricted to $\{0 \leq \tilde{\phi} \leq 2\pi(1 - 4\mu)\}$, and one may get

$$ds^2 = -d\tilde{t}^2 + dr^2 + r^2 d\tilde{\phi}^2 + dz^2 \,, \tag{2.21}$$

with

$$\left(\tilde{t}, r, \tilde{\phi}, z\right) \equiv \left(\tilde{t} + 8\pi J, r, \tilde{\phi} + 2\pi(1 - 4\mu), z\right) \,. \tag{2.22}$$

Outside $r = 0$ interior core, the spacetime is locally flat, and the geometry is significantly identical to the flat Minkowski space. Moreover, peculiar phenomena can be observed while going once around the string. There is a deficit angle of $\Delta\theta = 8\pi\mu$, which may have been missed by the spatial slices from the traveler's point of view. Consequently, the traveler undergoes a backward time-jump while going once around, which is given by

$$\Delta\tilde{t} = 8\pi J \,. \tag{2.23}$$

This describes the azimuthal closed timelike curves, which may have been arranged to cover the whole spacetime. The chronology violating region is spread across the entire

manifold and the CTC is subject to the following condition:

$$r < \frac{4J}{1-4\mu}\,. \tag{2.24}$$

Now, for a concluding remark of this section, one may summarize that a number of other cylindrical and spherical symmetric spacetimes support the existence of CTCs, Kerr solution [237] being one of them. Another important solution is the Kerr-Newman spacetime [274], which is interesting in view of the gravitoelectric and gravitomagnetic components of matter. Back in the sixties, Brandon Carter performed the complete analytic extension of the Kerr and Kerr-family (e.g. Kerr-Newman) solutions including the causal and acausal structures [275, 276]. It is widely known as the Carter time-machine. Few years later Calvani and collaborators on the other hand, analyzed the causality violation around Kerr naked singularity and concluded that geodesic lines does not violate causality in particular [277]. This may bring forth the non-geodesic closed timelike curves. For instance, the geodesics that violate causality are commonly termed as closed timelike geodesics (CTGs), as discussed earlier. CTGs are a subclass of CTCs, and most importantly, very few exact solution of EFE permits the presence of CTGs. See for instance [278–284], for studies on CTGs. Further, for recent works on CTCs, refer to [285–301].

2.2 Wormholes

Wormholes serve as seamless connections between either separate universes or distant locations within the same universe. The physics of wormholes can be traced back to 1916, when Flamm investigated the Schwarzschild metric [302] immediately after its discovery. However, the first significant contribution in history was marked in 1935, when Einstein and Nathan Rosen analyzed the elementary particle problem in terms of a "bridge" connecting two identical geometries [303]. This mathematical representation, termed as the "Einstein-Rosen bridge", serves the first fundamental construction of wormholes. But for many years, this field was laid dormant, until in the fifties, when John Archibald Wheeler worked on the bridge geometries in Reissner-Nordström and Kerr, where he discussed the Planck scale quantum foam as connection between different locations of spacetime [304, 305]. This was later derived to be the Euclidean wormholes by Hawking [306]. The object Wheeler was working on, is not free of singularity [307], and is the gravitational and electromagnetic coupled entity called "Geons". However, apart from that, the introduction of the term "Wormhole" dates back to 1957, when Misner and Wheeler coined the name while investigating the gravitational and electromagnetic charge (unquantized) and mass as properties of curved empty space [308].

As referred to Geons, it possess peculiar properties like origin of gravitational mass from electromagnetic field ("mass without mass"), and it has no inherent charge ("charge without charge"). This created significant curiosity to the researchers, leading to exploration of the field in different contexts [309–317]; however, due to the lack of physical behaviour and experimental evidence, it soon faded away. Nevertheless, in

1960, Misner considered Geon representation to investigate wormhole model in vacuum EFE [318]. Due to the merging of two asymptotic geometries at the wormhole throat, the inevitable question of causality came forward, as to whether a light signal could actually traverse through the throat and make a shortcut. Wheeler and Fuller answered the question in terms of Schwarzschild solution, where it is observed that the throat does not survive to let a signal pass through, thus, the causality is preserved [319]. But, in contrast, the study of Graves and Brill on the wormhole-like solution in Reissner-Nordström emerged as a candidate that allowed electric flux to pass through the throat, while the throat survived the contraction (up to a minimum radius) and re-expansion with a finite proper time [320].

The modern renaissance of traversable wormhole dynamics was brought into light by Kip Thorne and his student Michael Morris, in their classic 1988 Morris-Thorne paper [321]. This wormhole, having two mouths and the throat (the minimum radius where two asymptotic geometries are glued), laid the foundation of a possible natural object, like stars and black holes. In this work, they considered a specific wormhole metric and then solved the EFE to derive the energy-momentum components in a reverse method. The most interesting feature of this model was that it is two-way traversable, subject to the peculiarity of stress-energy components, which must violate the classical null energy condition (NEC) for the throat to survive [321–324]. This matter having negative energy density and that violates the energy condition is named as "exotic matter". Note that, NEC is the weakest of all four classical energy conditions, owing to the fact that the violation of NEC consequently means the violation of all the energy conditions. Classical matters are believed to satisfy these pointwise energy conditions [2], although certain quantum fields like Casimir effect and Hawking evaporation necessarily violate them. One may refer to [325] for a review. Further, quantum systems in classical gravity background violate the null and weak energy conditions over a small scale. This may lead to the introduction of average energy conditions which will be discussed later in this section [326, 327].

The constraints on negative energy fluxes [328] comes from the new set of energy conditions as discussed by Ford in the seventies [329]. These constraints further led to the introduction of Quantum Inequality (QI) which was pioneered by Ford and Roman in 1995 [330]. This inequality eventually limits the magnitude and allows times for the negative energy density by extracting the distributional information [330–333]. In this context, the wormhole geometries in QI have significant interest [331, 334]. Having the application of QI, these analyses showed that the exotic matter is restricted to an extremely small scale, or there must present large redshift i.e., large tidal force leading to the question on traversability [331]. Thus, Ford and Roman confirmed that macroscopic traversable wormholes have a rare existence. Consider [335, 336] for reviews.

Recent findings in cosmology indicate a compelling deviation from the strong energy condition (SEC) within the cosmological fluid, alongside intriguing indications that the null energy condition (NEC) could potentially be infringed upon within classical settings [33, 38, 337]. Consequently, there is a gradual erosion of the traditional authority of the weak and null energy conditions, along with other associated energy conditions, as if they were immutable laws [338]. Undoubtedly, this shift bears implications for

the theoretical frameworks surrounding the conception and construction of wormholes. Referring to quantum effects, since it is a good candidate in energy condition violations, the wormhole solution in semiclassical regime, which is coupled to a quantum scalar field, is found to be self-consistent under the quantum inequalities [339, 340]. Further, upon recognizing that nonminimal scalar fields contravene the weak energy condition, a series of internally consistent classical wormholes were discovered [341]. Therefore, exotic geometries like wormholes may naturally arise in quantum fields. In this regard, multiple wormhole solutions certainly have been explored within the realm of semi-classical gravity in existing literature. For instance, refer to [342–348].

It is worth noting that prior to the surge in interest sparked by Morris-Thorne's seminal work [321], classical wormholes have already been explored by Homer Ellis in 1973 [349], followed by further investigations detailed in [350]. Additionally, related consistent solutions were independently discovered by Kirill Bronnikov in 1973 [351], Takeshi Kodama in 1978 [352], and Gérard Clément in 1981 [353]. These pioneering contributions, predating the wormhole resurgence, are discussed briefly in [354]. Furthermore, Harris [355] later rediscovered a self-consistent Ellis wormhole by employing an exotic scalar field. In a parallel direction, Matt Visser aimed to reduce the energy condition violations, thus, constructed a number of wormhole solutions, including cubic wormholes, surgically modified Schwarzschild space, Roman ring, self-dual solutions and others [356–361]. Alongside these major developments in wormhole physics, he was motivated to compile detailed findings on the topic. Thus, including a series of new ideas, he presented the book *"Lorentzian Wormholes: From Einstein to Hawking"* in 1995. Preceding Visser's book, notable applications of wormhole dynamics were explored by Frolov and Novikov, who connected wormholes with black hole physics [362]. Hochberg and Kephart investigated an intriguing cosmological application of wormholes concerning the horizon problem [363]. Within the context of cosmic strings, Clément [364], Aros and Zamorano [365] discovered wormhole solutions, while Schein and Aichelburg [366, 367] investigated wormholes supported by strings. Teo proposed the rotating traversable model [368], followed by a generalization in [369] by Kuhfittig. Hayward and Koyama extended the concept of wormholes utilizing a crossflow of null dust waves [370], employing a model involving pure phantom and impulsive radiation to analyze the analytic model of traversable wormholes from Schwarzschild black holes [371, 372]. Refer to [373–384], for related literature.

A primary focus in wormhole research involves minimizing the violation of the null energy condition whenever feasible. In the context of dynamic wormholes, specific regions can particularly avoid the averaged null energy condition [360, 385–389]. Visser *et al.* [390, 391] addressed the limitation of energy conditions in quantifying the overall extent of matter violating these conditions. They introduced a novel measure, termed the "volume integral quantifier," to precisely quantify this concept.

Certain studies have introduced a cosmological constant into their proposed wormhole construction. For instance, see [392–402]. Assessing an object's stability against various forms of perturbation is consistently a crucial concern. Particularly, the thin-shell wormhole stability for equation of state [392, 393, 396, 403–405], or the linear radial perturbation [358, 394, 406–408] have been studied. It is also found that Ellis drainhole [349, 350] is stable under linear perturbation [409], but unstable under

nonlinear perturbation [410]. In alternative theories beyond GR, researches have uncovered various wormhole solutions, like in higher dimensions [402, 411, 412], in non-symmetric theory [413], in Brans-Dicke [414–420], in Kaluza-Klein [421], in Einstein-Gauss-Bonnet [422], in 2d dilaton theory [423], in brane world scenario [424–427], in Randall-Sundrum model [428], in $f(R)$ gravity [116, 429], and in $f(R,T)$ gravity [135–138]. Alongside there are studies in higher derivative gravity that consistently captures the analysis of wormhole throats. For example, one may refer to [430–432].

Wormholes play a crucial role in the investigation of time machines as they offer a means for creating non-eternal time machines, using the twin paradox approach [322] or by utilizing the GR redshift method [433]. Such an outcome becomes feasible when CTCs emerge beyond a certain hypersurface, known as the chronology horizon, which represents a specific instance of a Cauchy horizon [229, 434]. However, it is necessary to realize whether classical or semiclassical impacts destroy the system. Although research indicates that the classical stabilization of the system is straightforward [224, 322], but, semiclassical calculations present conflicting results, with some favoring its destruction [226, 263, 435], which would enforce chronology protection [263], while others suggest the persistence of the time machine [359, 436, 437]. The debate surrounding Misner spacetime remains ongoing, with arguments both favoring [438] and disfavoring [439], and subsequently swinging back in favor [440] of chronology protection. Ultimately, it is emphasized that semiclassical calculations alone would not resolve the chronology protection issue [441]; instead, the resolution requires the framework of quantum gravity, as previously anticipated by Thorne [442].

In the context of cosmology, recent observations have validated the remarkable phenomenon of accelerated expansion of the universe attributed to the presence of "dark energy" characterized by negative pressure. The extensively examined possibilities include the "quintessence", where the parameter range falls within $-1 < \omega < -1/3$, or "phantom energy" exhibiting the property $\omega < -1$. The potential existence of phantom energy, which suggests a breach of the null energy condition, rekindles interest in wormhole physics. Extensive exploration has been conducted regarding this possibility within the realm of wormholes, as referred in [443–458].

Over the last decade, significant advancements in wormhole physics have ranged from theoretical models for observations to newer theoretical derivations. With the advancement of numerical programming, the geodesic trajectories on the wormhole embedding geometry are now easy to visualize. Olmo *et al.* conducted an extensive examination of the geodesic structure for three distinct types of wormholes: Reissner-Nordström-like, Schwarzschild-like, and Minkowski-like [459]. Their findings suggest the potential for geodesically complete trajectories within all three geometries. Chakraborty and Pradhan explored the geodesic structure within a non-static rotating "Teo" wormhole [460]. Mishra and Chakraborty proposed a comprehensive examination of null and timelike geodesics concerning rotating wormholes and the Morris-Thorne wormhole, with a particular focus on the Ellis drainhole [461]. Taylor examined the conditions for traversability of test particles and scalar fields along with the visualization of geodesic trajectories on the wormhole embedding diagram [462]. The geodesics may pass through the throat for escape orbits, be reflected by the potential of the wormhole, or become trapped in an unstable bound orbit. Similarly, Cataldo *et al.* investigated

the behaviour of test particles in Schwarzschild-like wormhole spacetime [463]; and recently, Willenborg *et al.* [464] studied the geodesic motion around a class of wormhole, constructed within Einstein gravity and involves a conformally coupled scalar field, as proposed by Barcelo and Visser [341]. They analytically solved the geodesic equations using Weierstraß functions and explored the potential for different orbits and parameter variations.

In the last decade, the milestone discovery of black hole photon sphere (shadow) [25, 26], and the gravitational wave from binary black hole mergers [23, 24] have increased enormous attention on the observation of possible presence for black hole mimickers like wormholes. In the context of shadow cast by wormhole throats, Amir *et al.* recently investigated the shadows of Kerr-like wormholes [465] and charged wormholes within the framework of Einstein-Maxwell-dilaton theory [466]. Wielgus *et al.* developed a Reissner-Nordström (RN) wormhole by connecting two distinct RN spaces with varying mass and charge, resulting in non-mirror-symmetric wormholes [467]. This alteration affects the photon sphere, potentially leading to two photon rings observable to a distant observer. The doubling of the photon rings was attributed to the doubling of the effective potential maximum. Nonetheless, mirror-symmetric wormholes possibly cast number of photon rings and intriguing strong lensing effects [468–470]. Consequently, for the shadows of rotating wormhole, one may consider [471–473]. Alongside references [474–480] combine similar literature on the subject.

Gravitational waves (GW) represent more than just a novel tool for exploring gravity's nature in high-speed dynamic settings [481–483]. They provide an avenue for investigating unusual astrophysical entities, including firewalls, boson stars, gravastars, and notably, wormholes. These exotic compact objects resemble black holes in that their radii closely match the Schwarzschild radii of black holes. However, they generate additional echoes following the ringdown phase [484]. Wormholes are distinct due to their double-peak potential, facilitating the oscillation of gravitational waves (GW) between these peaks while gradually escaping the wormhole, resulting in a sequence of echoes [485–488]. Alternative methods for detecting wormholes involve identifying the anti-chirp signal generated as a black hole passes through the wormhole [489]. Consequently, observation of echoes from electromagnetic signals [490], use of time-dependent scattering theory to distinguish that transmitted wave has isolated chirp, while reflected wave has anti-chirp behaviour [491], and measurement of the unusual movements of objects on one side of the throat influenced by charge and mass on the opposite side [492, 493], can also be addressed.

Modern approaches in wormhole theory using quantum fields and strings have already begun to be widely discussed in the community. In an attempt to resolve the "firewall paradox" in quantum black holes [494, 495], Juan Maldacena and Leonard Susskind apparently proposed a beautiful relationship between quantum entanglement and wormhole in 2013. Referring to the work of Einstein and Rosen on the Einstein-Rosen (ER) bridge [303], and Einstein, Podolsky and Rosen [496] (EPR) on entanglement states, they proposed highly entangled states of two black holes that create a EPR pair through ER=EPR [497]. Employing the AdS/CFT correspondence, which establishes a connection between quantum gravity in anti–de Sitter spacetime and conformal field theory on its boundary, they analyzed the maximally extended black

hole in asymptotically anti–de Sitter space. In the realm of general relativity, this creates an existing solution where two remote black holes are linked through a wormhole. In this line of approach, a number of other studies have came forward in the modern quantum realm, such as wormhole through a double trace deformation [498], wormhole in four dimensions [499], asymptotically flat wormhole with short transit times [500], perturbative analysis on self-supporting wormholes [501], and wormholes traversable to humans [502, 503]. This theoretical advancement led to the most interesting discovery in wormhole physics till date. In 2022, Jafferis *et al.* claimed to observe possible traversability of a wormhole in a quantum computation environment through teleportation of information [504]. The teleportation system utilizes a Hamiltonian comprising seven Majorana fermions with five fully-commuting terms. This has been produced through a machine-learning method aimed at mimicking the teleportation characteristics of the Sachdev-Ye-Kitaev (SYK) model [505, 506]. The acquired Hamiltonian accurately replicates the gravitational dynamics of the SYK model and showcases gravitational teleportation via an entangled wormhole.
Now, in the following subsections, mathematical foundations for some of the major wormhole solutions are examined in a form of review.

PRE-TRAVERSABLE ERA

2.2.1 Einstein-Rosen bridge

In [303], Einstein and Rosen explored the concept of an elementary particle theory of matter and electricity, aiming to avoid singularities by utilizing only the variables of general relativity $g_{\mu\nu}$ and Maxwell theory φ_μ. Their solutions entail representing physical space mathematically as two identical sheets, with a particle symbolized by a "bridge" joining these sheets.

Consider the static, spherically symmetric Schwarzschild metric

$$ds^2 = \left(1 - \frac{2m}{r}\right) dt^2 - \frac{dr^2}{\left(1 - \frac{2m}{r}\right)} - r^2(d\theta^2 + \sin^2\theta d\phi^2)\,, \tag{2.25}$$

in the $(+,-,-,-)$ signature. At $r = 2m$, g_{11} component becomes infinite, indicating singularity. In this point, Einstein and Rosen considered a new variable $u^2 = (r - 2m)$, that leads to the modification of Eq. (2.25) as

$$ds^2 = \left(\frac{u^2}{u^2 + 2m}\right) dt^2 - 4(u^2 + 2m)du^2 - (u^2 + 2m)^2(d\theta^2 + \sin^2\theta d\phi^2)\,, \tag{2.26}$$

where $g_{\mu\nu}$ is completely regular. Hence, it becomes possible to address this solution which remains devoid of singularities at all finite points. As the parameter u traverses from $-\infty$ to $+\infty$, the radial coordinate r varies from $+\infty$ to $2m$, and then from $2m$ to $+\infty$. Consequently, the four-dimensional space is delineated mathematically into two identical sections or "sheets," referring to $u > 0$ and $u < 0$, connected by a hyperplane where either $r = 2m$ or $u = 0$. They colloquially referred to this connection as a "bridge."

Subsequently, from the Maxwell field, the Reissner-Nordström metric is given by

$$ds^2 = \left(1 - \frac{2m}{r} - \frac{\varepsilon^2}{2r^2}\right) dt^2 - \frac{dr^2}{\left(1 - \frac{2m}{r} - \frac{\varepsilon^2}{2r^2}\right)} - r^2(d\theta^2 + \sin^2\theta d\phi^2)\,, \tag{2.27}$$

where ε is the electrical charge. Similar to the previous case, with $m = 0$, one may consider $u^2 = (r^2 - \varepsilon^2/2)$, for which (2.27) takes the form

$$ds^2 = \left(\frac{2u^2}{2u^2 + \varepsilon^2}\right) dt^2 - du^2 - (u^2 + \varepsilon^2/2)(d\theta^2 + \sin^2\theta d\phi^2)\,. \tag{2.28}$$

It is also singularity-free throughout the whole space of the finite points within the region of two sheets, with the charge symbolized by a bridge. It serves as a depiction of a fundamental massless, charged particle.

2.2.2 Ellis drainhole

In 1973, Homer Ellis constructed a particle model in terms of motion of ether through a "drainhole". This solution is significantly intriguing as it replicates a wormhole. The construction starts from the spherically symmetric general line element

$$ds^2 = dt^2 - [d\rho - f(\rho)dt]^2 - r(\rho)^2 d\Omega^2\,, \tag{2.29}$$

where $d\Omega^2 = d\theta^2 + \sin^2\theta d\phi^2$, and $f(\rho)$ is a non-negative function. The single cross term in the line element of $\mathcal{M}$ is $2f(\rho)d\rho dt$, thus, the vector $\partial/\partial t$ is not orthogonal to the hypersurfaces of constant t everywhere unless $f = 0$. In such a scenario, $\mathcal{M}$ becomes static.

Using the mathematical approaches involving solving Einstein's field equation, Ellis established that, $r(\rho)^2 = (\rho^2 + n^2)$, where n represents the radius of the drainhole. Now, the absence of ether flow indicates that $f = 0$, yet the drainhole persists in an open state due to the condition $r(\rho) = (\rho^2 + n^2)^{1/2} \geq n > 0$. The manifold exhibits symmetry concerning reflection across the drainhole. Therefore, the famous Ellis wormhole metric takes the form

$$ds^2 = dt^2 - d\rho^2 - (\rho^2 + n^2)d\Omega^2\,. \tag{2.30}$$

In terms of the Morris-Thorne model, the (n^2/r) term takes the form of a shape function, which has been extensively used in literature as Ellis wormhole shape function.

For a remark, one may add that, considering ether at rest, double-sided particles lack mass in both sides, yet the drainhole can still trap particles while staying open. It can hold the particles infinitely, or can release them without imparting any acceleration. These particles, devoid of mass, charge, and spin, possess the ability to transform, upon disturbance, into a scalar-field wave transmitting at the wave velocity depending upon the manifold.

Ellis also constructed a dynamic model for the evolving, flowless drainhole manifold [350], for which the metric is modified to

$$ds^2 = dt^2 - d\rho^2 - [(1 + a^2)\rho^2 + a^2 t^2]d\Omega^2\,. \tag{2.31}$$

He concluded that the evolving, flowless drainhole can be conceptualized as representing the cycle of birth and renewal of a scalar particle, which spans infinitely from infinite size in both the past and future. This particle lacks gravitational influence, as the "ether flow" identified as gravity in the static solution, is excluded in the evolving solution from the outset. What remains is solely space, dynamically evolving as field equations suggest.

TRAVERSABLE ERA

2.2.3 Traversable Morris-Thorne wormhole

An alternative approach to solving the Einstein field equation involves adopting a reverse philosophy: starting with a compelling and unusual spacetime metric and subsequently determining the corresponding matter source responsible for the geometry. For the traversable Lorentzian Morris-Thorne wormhole, this matter source is identified as "exotic matter," which contravenes the null energy condition. This geometry also permits the existence of closed timelike curves, leading to violations of causality.

One may start with the static, spherically symmetric line element ansatz

$$ds^2 = -e^{2\Phi(r)}dt^2 + \frac{dr^2}{(1-b(r)/r)} + r^2 d\Omega^2\,, \tag{2.32}$$

where $d\Omega^2 = (d\theta^2 + \sin^2\theta d\phi^2)$. The function $\Phi(r)$ is referred to as the redshift function because it is associated with gravitational redshift, while $b(r)$ is termed the shape function as it dictates the morphology of the wormhole [321]. Note that, the metric must follow the condition $\Phi(r) \to 0$ and $b(r)/r \to 0$ as $r \to \infty$, for the spacetime to be asymptotically flat. On the other hand, the traversability of the wormhole requires a horizon-free geometry, implying $g_{tt} = -e^{2\Phi(r)} \neq 0$, so that the redshift function must be finite everywhere. Now, the radial coordinate r is non-monotonic, decreasing from $+\infty$ to r_0 which is a minimum, denoting the position of the wormhole throat, where $b(r_0) = r_0$, and then increasing from r_0 to $+\infty$. The g_{rr} coefficient becomes infinite at the throat, indicating a coordinate singularity. Therefore, it is required to introduce the proper radial distance

$$l(r) = \pm \int_{r_0}^{r} \frac{dr}{\sqrt{1-b(r)/r}}\,, \tag{2.33}$$

which is finite everywhere. The metric (2.32) is now expressed in the proper radial distance as

$$ds^2 = -e^{2\Phi(l)}dt^2 + dl^2 + r^2(l)d\Omega^2\,. \tag{2.34}$$

Note that, $l = 0$ at the wormhole throat, whereas it covers $+\infty$ to 0, and 0 to $-\infty$ respectively in the upper and lower universe.

2.2.3.1 The embedding surface

To illustrate a wormhole using embedding diagram and draw out pertinent details for selecting the shape function, $b(r)$, one can start with the respective line element for a fixed moment of time, $t =$ constant, represented as:

$$ds^2 = \left(1 - \frac{b(r)}{r}\right)^{-1} dr^2 + r^2 d\Omega^2 \,. \tag{2.35}$$

For visualization, this metric is embedded into a metric of 3D Euclidean space of a 2-sphere, given by:

$$ds^2 = dz^2 + dr^2 + r^2 d\Omega^2 \,. \tag{2.36}$$

Now, comparing Eq. (2.35) with (2.36), the expression for the embedding surface is obtained as:

$$\frac{dz}{dr} = \pm \left(\frac{r}{b(r)} - 1\right)^{-\frac{1}{2}} \,. \tag{2.37}$$

This equation characterizes the embedding surface's relationship with respect to r, see Figure 2.1. The wormhole throat $r = r_0$ is the minimum radius of the surface, where $dz/dr \to \infty$. Consequently, the asymptotic flatness of the geometry requires $dz/dr \to 0$ as $r \to \infty$.

For a solution to qualify as a wormhole, it is necessary to enforce the condition that the throat flares out, as depicted in the figure. This *flaring-out condition* dictates that it must exhibit $d^2r/dz^2 > 0$ at or near the throat. By differentiating Eq. (2.37) with respect to z, one may obtain

$$\frac{d^2r}{dz^2} = \frac{-rb'(r) + b(r)}{2b(r)^2} > 0 \,. \tag{2.38}$$

At the throat r_0, it is confirmed that the function satisfies $b'(r_0) < 1$. Therefore, the extremely important flaring-out condition of the wormhole reads $-rb'(r) + b(r) > 0$. However, the flaring-out and embedding technique has a fundamental disadvantage of high coordinate dependence.

2.2.3.2 The field equation

The set of orthonormal basis vectors is important for the simplification of physical and mathematical analysis. These vectors can be understood as the proper reference frame of an observer who remains stationary with (r, θ, ϕ) held constant. In the coordinate system of (t, r, θ, ϕ), the orthonormal basis vectors are

$$\begin{cases} \mathbf{e}_{\hat{t}} = \mathbf{e}^{-\Phi} e_t \\ \mathbf{e}_{\hat{r}} = (1 - b/r)^{1/2} \mathbf{e}_r \\ \mathbf{e}_{\hat{\theta}} = r^{-1} \mathbf{e}_\theta \\ \mathbf{e}_{\hat{\phi}} = (r \sin\theta)^{-1} \mathbf{e}_\phi \,. \end{cases} \tag{2.39}$$

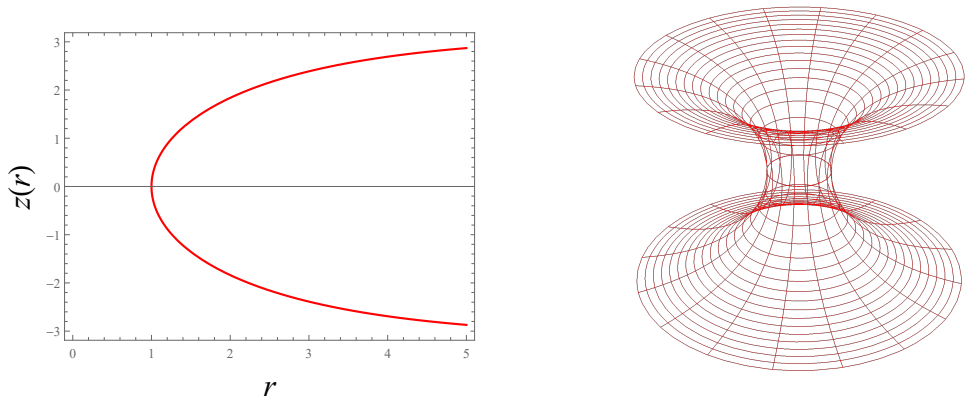

(a) (b)

Figure 2.1: (a) Two-dimensional, and (b) three-dimensional visualization of the traversable wormhole embedding surface along t = constant hypersurface.

For the line element (2.32), the non-zero components of Einstein tensor can be calculated from $G_{\hat{\mu}\hat{\nu}} = R_{\hat{\mu}\hat{\nu}} - \frac{1}{2}Rg_{\hat{\mu}\hat{\nu}}$, that yields:

$$G_{\hat{t}\hat{t}} = \frac{b'}{r^2}\,, \tag{2.40}$$

$$G_{\hat{r}\hat{r}} = -\frac{b}{r^3} + 2\left(1-\frac{b}{r}\right)\frac{\Phi'}{r}\,, \tag{2.41}$$

$$G_{\hat{\theta}\hat{\theta}} = G_{\hat{\phi}\hat{\phi}} = \left(1-\frac{b}{r}\right)\left[\Phi'' + \left(\Phi' + \frac{1}{r}\right)\left(\Phi' - \frac{rb'-b}{2r(r-b)}\right)\right]. \tag{2.42}$$

The EFE, $G_{\hat{\mu}\hat{\nu}} = 8\pi T_{\hat{\mu}\hat{\nu}}$, enforces that the energy-momentum tensor $T_{\hat{\mu}\hat{\nu}} = \mathrm{diag}(\rho(r), -\tau(r), p(r), p(r))$ is directly proportional to the Einstein tensor. Here, $\rho(r)$ is the total energy density of the matter. The radial tension $\tau(r)$, and the pressure $p(r)$ are respectively equivalent to the negative of radial pressure $p_r(r)$, and the tangential pressure $p_t(r)$. Therefore, from the Einstein field equation the energy-momentum components are obtained as

$$\rho(r) = \frac{1}{8\pi}\frac{b'}{r^2}\,, \tag{2.43}$$

$$p_r(r) = -\tau(r) = \frac{1}{8\pi}\left[-\frac{b}{r^3} + 2\left(1-\frac{b}{r}\right)\frac{\Phi'}{r}\right], \tag{2.44}$$

$$p_t(r) = p(r) = \frac{1}{8\pi}\left(1-\frac{b}{r}\right)\left[\Phi'' + \left(\Phi' + \frac{1}{r}\right)\left(\Phi' - \frac{rb'-b}{2r(r-b)}\right)\right]. \tag{2.45}$$

At the throat, these expressions are modified to

$$\rho(r_0) = \frac{1}{8\pi}\frac{b'(r_0)}{r_0^2}\,, \tag{2.46}$$

$$p_r(r_0) = -\tau(r_0) = -\frac{1}{8\pi r_0^2}\,, \tag{2.47}$$

$$p_t(r_0) = p(r_0) = \frac{1}{8\pi}\left(\frac{1-b'(r_0)}{2r_0}\right)\left(\Phi'(r_0)+\frac{1}{r_0}\right)\,. \tag{2.48}$$

Now, integrating (2.43), one may obtain

$$b(r) = b(r_0) + \int_{r_0}^{r} 8\pi\rho(r')r'^2dr' = 2m(r)\,, \tag{2.49}$$

which can be rewritten as

$$m(r) = \frac{r_0}{2} + \int_{r_0}^{r} 4\pi\rho(r')r'^2dr'\,. \tag{2.50}$$

This equation represents the effective mass within a sphere of radius r at the interior. At spatial infinity, it however provides the mass distribution of the wormhole geometry. Upon differentiation of Eq. (2.44) with respect to r, and substituting b' and Φ'' respectively from (2.43) and (2.45), the following expression is obtained

$$\tau' = (\rho-\tau)\Phi' - \frac{2}{r}(p+\tau)\,, \tag{2.51}$$

which denotes the hydrostatic equilibrium condition of the material balancing the wormhole, and can also be derived from the energy-momentum conservation, $T^{\hat{\mu}\hat{\nu}}{}_{;\hat{\nu}} = 0$. Equation (2.51) is used to analyze the stability of the static traversable wormholes.

2.2.3.3 Exotic matter

Before deducing the nature of matter content at the Morris-Thorne wormhole throat, it is customary to introduce the brief discussions of the energy conditions.

Pointwise energy conditions

It is well-known that traversable wormholes demand "exotic matter" at the throat that necessarily violates the energy conditions. It is believed that classical matters satisfy these conditions, however, some quantum fields, such as the Casimir effect do not. Here, the energy conditions are defined using a diagonal energy-momentum tensor [2], $T^{\mu\nu} = \text{diag}(\rho, p_1, p_2, p_3)$, where p_j are the principal pressures. Note that, for perfect fluid, $p_1 = p_2 = p_3$.

• **Null Energy Condition (NEC):** From the definition of NEC, for a null vector n^μ, $T_{\mu\nu}n^\mu n^\nu \geq 0$, in the principal pressure form, which takes the form

$$\rho + p_j \geq 0\,, \qquad \forall j\,. \tag{2.52}$$

• **Weak Energy Condition (WEC):** For a timelike vector u^μ, WEC defines $T_{\mu\nu}u^\mu u^\nu \geq$

0. Physically, $T_{\mu\nu}u^\mu u^\nu$ represents the energy density as computed by an observer moving along a timelike trajectory with four-velocity u^μ. Thus, in the principal pressure form, WEC gives

$$\rho \geq 0 \qquad \text{and} \qquad \rho + p_j \geq 0\,, \qquad \forall j\,. \tag{2.53}$$

Therefore, WEC entails the NEC.

• **Strong Energy Condition (SEC):** According to SEC, for any timelike vector u^μ, $\left(T_{\mu\nu} - \frac{T}{2}g_{\mu\nu}\right)u^\mu u^\nu \geq 0$, where T is the trace of $T_{\mu\nu}$. So, in the principal pressure form

$$\rho + p_j \geq 0 \qquad \text{and} \qquad \rho + \sum_j p_j \geq 0\,, \qquad \forall j\,. \tag{2.54}$$

This means, SEC entails the NEC, but it doesn't always imply the WEC.

• **Dominant Energy Condition (DEC):** The Dominant Energy Condition (DEC), expressed as $T_{\mu\nu}u^\mu u^\nu \geq 0$ for a timelike vector u^μ, ensures that the energy density is always locally positive and the flux is not spacelike but either null or timelike. In the principal pressure form, it reads

$$\rho \geq 0 \qquad \text{and} \qquad p_j \in [-\rho, +\rho]\,, \qquad \forall j\,. \tag{2.55}$$

Thus, DEC entails WEC and NEC, but it doesn't always imply the SEC.

Averaged energy conditions

Deviation from the pointwise energy conditions prompted the adoption of averaging energy conditions [326]. These averaged energy conditions are comparatively less stringent, and allows for localized breaches as long as the energy conditions are satisfied on average during integration over null or timelike geodesics.

• **Averaged Null Energy Condition (ANEC):** According to the definition, for a generalized affine parameter λ, ANEC holds for a null curve, $\mathcal{S}$, when

$$\int_{\mathcal{S}} T_{\mu\nu}n^\mu n^\nu d\lambda \geq 0\,. \tag{2.56}$$

If the trajectory $\mathcal{S}$ represents a null geodesic, then λ simplifies to a standard affine parameter.

• **Averaged Weak Energy Condition (AWEC):** According to the definition, if s parametrizes proper time, AWEC holds for a timelike curve, $\mathcal{S}$, when

$$\int_{\mathcal{S}} T_{\mu\nu}u^\mu u^\nu ds \geq 0\,. \tag{2.57}$$

For defining the matter content at the wormhole throat, Morris and Thorne defined the following function from Eq. (2.43), (2.44):

$$\xi = \frac{\tau - \rho}{|\rho|} = \frac{-b' + b/r - 2r(1 - b/r)\Phi'}{|b'|}\,. \tag{2.58}$$

By using the flaring-out condition from (2.38), this equation modifies to provide the exoticity function:

$$\xi = \frac{2b^2}{r|b'|}\frac{d^2r}{dz^2} - 2r\left(1 - \frac{b}{r}\right)\frac{\Phi'}{|b'|}\,. \tag{2.59}$$

Since, ρ and b' are finite, and $(1 - b/r)\Phi' \to 0$ at or near the throat, one may have

$$\xi(r_0) = \frac{\tau_0 - \rho_0}{|\rho_0|} > 0\,. \tag{2.60}$$

The requirement $\tau_0 > \rho_0$ poses significant challenges, indicating that the radial tension at the throat r_0 must surpass the energy density. Hence, Morris and Thorne termed matter constrained by this restriction as "exotic matter". Subsequent examination confirms that this matter violates NEC (and consequently all the energy conditions) [224, 321, 322, 360].

For example, consider a straightforward solution where $b = b(r)$ and $\Phi(r) = 0$ [2], such that equations (2.43)-(2.45) simplify to:

$$\begin{aligned}
\rho(r) &= \frac{b'(r)}{8\pi r^2}\,,\\
\tau(r) &= \frac{b(r)}{8\pi r^3}\,,\\
p(r) &= \frac{-rb'(r) + b(r)}{16\pi r^3}\,.
\end{aligned} \tag{2.61}$$

It is noteworthy that the nature of energy density hinges on the sign of $b'(r)$. For instance, suppose $b(r) = r_0^2/r$, corresponding to the embedding surface, $z(r) = r_0 \cosh^{-1}(r/r_0)$, which exhibits the following result:

$$\frac{dz}{dr} = \frac{r_0}{\sqrt{r^2 - r_0^2}}\,. \tag{2.62}$$

The wormhole matter is consistently exotic everywhere, with $\xi > 0$ throughout, while ρ, τ and p diminish as $r \to +\infty$.

Utilizing the Raychaudhuri equation for null geodesic congruence, it can also be demonstrated that this configuration contravene the ANEC at the wormhole throat [2, 224, 241].

2.2.3.4 Conditions of traversability

Consider that an advanced human civilization creates a space station at $l = -l_1$, at the lower universe, and makes a trip to the upper universe at $l = l_2$. The traveler has

[2] Note that when $\Phi(r) = 0$, it represents the well-studied ultrastatic wormhole geometry. It is most significant since it denotes zero-tidal force wormhole, where a stationary particle always remains stationary in a gravitational acceleration-free frame.

radial velocity $v(r)$, with respect to an observer at r. Therefore,

$$v = e^{-\Phi}\frac{dl}{dt} = \mp e^{-\Phi}\left(1-\frac{b}{r}\right)^{-1/2}\frac{dr}{dt}\,, \tag{2.63}$$

$$v\gamma = \frac{dl}{d\tau} = \mp\left(1-\frac{b}{r}\right)^{-1/2}\frac{dr}{d\tau}\,, \tag{2.64}$$

where, $dl, dr, dt, d\tau$ are the coordinate lapse corresponding to proper distance, radial distance, coordinate time, and proper time respectively, with respect to the observer. One may now impose the boundary conditions, such as, asymptotic flatness at the station, i.e., $b/r \ll 1$, small redshift of the signals at infinity, i.e., $\Delta\lambda/\lambda = e^{-\Phi}-1 \approx -\Phi$, or $|\Phi| \ll 1$, gravitational acceleration at the space station is smaller than or equal to that of the Earth, i.e., $g \leq g_{\oplus}$, so that $|\Phi'| \leq g_{\oplus}$ must hold.

Other desired conditions that must be met include, short journey time with respect to both the traveler and observer at the station, the gravitational acceleration and the tidal force must not exceed Earth's gravitational acceleration ($g_{\oplus}$) and tidal force.

• **Total traversal time:** Morris-Thorne considered a travel time of one year, as computed by the traveler and stationary observers at $l = -l_1$ and $l = l_2$, such that

$$\Delta\tau_{\text{traveler}} = \int_{-l_1}^{l_2}\frac{dl}{v\gamma} \leq 1 \text{ year}\,, \tag{2.65}$$

$$\Delta t_{\text{space station}} = \int_{-l_1}^{l_2}\frac{dl}{ve^{\Phi}} \leq 1 \text{ year}\,, \tag{2.66}$$

respectively.

• **Acceleration felt by a traveler:** Implementing a Lorentz transformation on the stationary observers' orthonormal basis as given by (2.39), the orthonormal basis vectors for traveler's proper frame, i.e., ($\mathbf{e}_{\hat{0}'}$, $\mathbf{e}_{\hat{1}'}$, $\mathbf{e}_{\hat{2}'}$, $\mathbf{e}_{\hat{3}'}$), is obtained as:

$$\begin{aligned}
\mathbf{e}_{\hat{0}'} &= \gamma\mathbf{e}_{\hat{t}} \mp \gamma v\mathbf{e}_{\hat{r}}\,,\\
\mathbf{e}_{\hat{1}'} &= \mp\gamma\mathbf{e}_{\hat{r}} + \gamma v\mathbf{e}_{\hat{t}}\,,\\
\mathbf{e}_{\hat{2}'} &= \mathbf{e}_{\hat{\theta}}\,,\\
\mathbf{e}_{\hat{3}'} &= \mathbf{e}_{\hat{\phi}}\,,
\end{aligned} \tag{2.67}$$

where $\gamma = (1-v^2)^{-1/2}$. Hence, the four-acceleration, i.e., $a^{\hat{\mu}'} = u^{\hat{\mu}'}u^{\hat{\nu}'}$, in the proper reference frame of the traveler imposes the constraint

$$|\vec{a}| = \left|\left(1-\frac{b}{r}\right)^{1/2} e^{-\Phi}\left(\gamma e^{\Phi}\right)'\right| \leq g_{\oplus}\,. \tag{2.68}$$

For a finite constant redshift function, $\Phi' = 0$, this may reduces to

$$|\vec{a}| = \left|\left(1-\frac{b}{r}\right)^{1/2}\gamma' c^2\right| \leq g_{\oplus}\,. \tag{2.69}$$

Interestingly, for the observer having a constant velocity, $v = \text{const}$, $|\vec{a}| = 0$, naturally.

• Tidal acceleration felt by a traveler:

It is crucial to ensure that an observer moving through the wormhole does not experience destructive tidal forces. The tidal acceleration experienced by a traveler is expressed as $\Delta a^{\hat{\mu}'} = -R^{\hat{\mu}'}{}_{\hat{\nu}'\hat{\alpha}'\hat{\beta}'} u^{\hat{\nu}'} \eta^{\hat{\alpha}'} u^{\hat{\beta}'}$, where $u^{\hat{\mu}'} = \delta^{\hat{\mu}'}{}_{\hat{0}'}$ denotes four-velocity of the traveler and $\eta^{\hat{\alpha}'}$ represents the difference between two points of their body, say for instance $|\eta^{\hat{i}'}| \approx 2\,\text{m}$. Notice that, $\eta^{\hat{\alpha}'}$ is entirely spatial in the proper frame of the traveler, as $u^{\hat{\mu}'}\eta_{\hat{\mu}'} = 0$, resulting in $\eta^{\hat{0}'} = 0$. So, using the restriction $|\Delta a^{\hat{\mu}'}| \leq g_{\oplus}$, and imposing a Lorentz transformation of observer's frame to traveler's frame followed by some rigorous calculations (follow [321] for complete calculations), one may obtain the following tidal acceleration on a traveler during a radial motion through the wormhole:

$$\left|\left(1-\frac{b}{r}\right)\left[\Phi'' + (\Phi')^2 - \frac{b'r-b}{2r(r-b)}\Phi'\right]\right| \left|\eta^{\hat{1}'}\right| \;\leq\; g_{\oplus}\,, \tag{2.70}$$

$$\left|\frac{\gamma^2}{2r^2}\left[v^2\left(b'-\frac{b}{r}\right) + 2(r-b)\Phi'\right]\right| \left|\eta^{\hat{2}'}\right| \;\leq\; g_{\oplus}\,. \tag{2.71}$$

These two expressions put important restriction on the redshift function and observer's velocity at the throat r_0, as given by

$$|\Phi'(r_0)| \;\leq\; \frac{2g_{\oplus}\, r_0}{(1-b')\left|\eta^{\hat{1}'}\right|}\,, \tag{2.72}$$

$$\gamma^2 v^2 \;\leq\; \frac{2g_{\oplus}\, r_0^2}{(1-b')\left|\eta^{\hat{2}'}\right|}\,. \tag{2.73}$$

For a finite and constant redshift function wormhole, i.e., $\Phi' = 0$, Eq. (2.71) yields

$$\frac{\gamma^2 v^2}{2r^2}\left|\left(b'-\frac{b}{r}\right)\right| \left|\eta^{\hat{2}'}\right| \;\leq\; g_{\oplus}\,, \tag{2.74}$$

which means an observer at rest with $v = 0$, always measures null tidal force (zero-tidal force).

Note that velocity independent tidal forces render a wormhole non-traversable. For example, the velocity dependence can be avoided when $R_{\hat{\theta}\hat{t}\hat{\theta}\hat{t}} = -R_{\hat{\theta}\hat{r}\hat{\theta}\hat{r}}$, i.e.,

$$b' - \frac{b}{r} = -2r\left(1-\frac{b}{r}\right)\Phi'\,, \tag{2.75}$$

or

$$e^{2\Phi(r)} = e^{2\Phi(\infty)}\left(1-\frac{b}{r}\right)\,. \tag{2.76}$$

It provides the insight that $r = r_0$ contains a horizon, which makes the wormhole non-traversable.

2.2.4 Rotating 'Teo' wormhole

In 1998, Edward Teo investigated the stationary, axisymmetric (3+1) dimensional geometry of a traversable wormhole [368] given by the line element

$$ds^2 = -N^2 dt^2 + e^{\mu}\, dr^2 + r^2 K^2 [d\theta^2 + \sin^2\theta (d\phi - \omega\, dt)^2]\,, \tag{2.77}$$

where the unknowns N, K, ω and μ are functions of both r and θ. Here, $\omega(r,\theta)$ can be thought of as the angular velocity of a freely falling body. There are two killing vectors in the spacetime, one with the timelike, that produces time translation, and the other with the spacelike, produces invariant rotation with respect to ϕ. Of course the metric (2.77) reproduces the Morris-Thorne metric (2.32) in the rotation-less limit along with the symmetry

$$N(r,\theta) \to \mathrm{e}^{\Phi(r)}, \quad b(r,\theta) \to b(r)\,, \quad K(r,\theta) \to 1\,, \quad \omega(r,\theta) \to 0\,, \tag{2.78}$$

where

$$e^{-\mu(r,\theta)} = \left(1 - \frac{b(r,\theta)}{r}\right)\,. \tag{2.79}$$

In this configuration, the wormhole throat is located at $b(r_0) = r_0$, as in the Morris-Thorne geometry. Suppose $K(r,\theta)$ is a positive function, in the non-decreasing order, where one may comfortably denote the proper radial distance R, as $R \equiv rK$, with $R_r > 0$, in the $(2+1)$-dimension. An event horizon emerges for $N = 0$, thus to enforce non-singularity, the θ derivatives of N, b, and K are vanishing at the rotational symmetry axis. Note that the derivatives in r and θ are written in the subscripts.

The scalar curvature (i.e., R) of the metric is highly complicated, but it becomes simplified at the throat $r = r_0$.

$$\begin{aligned} R \;=\; & -\frac{1}{r^2K^2}\left(\mu_{\theta\theta} + \frac{1}{2}\mu_\theta^2\right) - \frac{\mu_\theta}{Nr^2K^2}\frac{(N\sin\theta)_\theta}{\sin\theta} \\ & -\frac{2}{Nr^2K^2}\frac{(N_\theta\sin\theta)_\theta}{\sin\theta} - \frac{2}{r^2K^3}\frac{(K_\theta\sin\theta)_\theta}{\sin\theta} \\ & +e^{-\mu}\,\mu_r\,\left[\ln(Nr^2K^2)\right]_r + \frac{\sin^2\theta\,\omega_\theta^2}{2N^2} + \frac{2}{r^2K^4}\,(K^2 + K_\theta^2)\,. \end{aligned} \tag{2.80}$$

The complicated ones in the expression are those involving μ_θ and $\mu_{\theta\theta}$, specifically:

$$\mu_\theta = \frac{b_\theta}{(r-b)}\,, \qquad \mu_{\theta\theta} + \frac{1}{2}\mu_\theta^2 = \frac{b_{\theta\theta}}{r-b} + \frac{3}{2}\frac{{b_\theta}^2}{(r-b)^2}\,. \tag{2.81}$$

Thus, to prevent curvature singularities, it is necessary to enforce $b_\theta = 0$ and $b_{\theta\theta} = 0$ at the throat. This requirement indicates that the throat is situated at a constant radius r.

Hence, it can be inferred that the spacetime characterizes a rotating wormhole configuration, featuring angular velocity ω, proper radial distance K, analogous redshift function N and the shape function b. The shape function b remains independent of θ at the throat ($b_\theta = 0$) and satisfies $b \leq r$, and the flaring-out condition $b_r < 1$.

In Reference [368], it was demonstrated by Teo that the NEC is breached in specific regions while upheld in others. Consequently, an observer falling into the wormhole could navigate around the throat, evading the need for exotic matter support. Nonetheless, it is essential to stress that complete avoidance of exotic matter remains unattainable.

2.2.5 Evolving wormholes

For a time-dependent wormhole solution in a cosmological background, one may start with the following line element

$$ds^2 = A^2(t)\left[-e^{2\Phi(r)}\,dt^2 + \frac{dr^2}{1-kr^2-\frac{b(r)}{r}} + r^2 d\Omega^2\right], \tag{2.82}$$

where $A^2(t)$ is a positive definite conformal factor. Another approach is to express the metric (2.82) in terms of "physical time" rather than "conformal time" by substituting t with $\tau = \int A(t)dt$, and consequently $A(t)$ with $R(\tau)$, where the latter is the function of the proper time [387, 388]. With the limit, $b(r) \to 0$ and $\Phi(r) \to 0$, the line element (2.82) reduces to FRW metric, whereas for $A(t) \to$ const. and $k \to 0$, it reduces to the static wormhole metric (2.32).

In the orthonormal reference frame, where the cosmological constant is absorbed in the energy-momentum tensor, so that $G_{\hat{\mu}\hat{\nu}} = R_{\hat{\mu}\hat{\nu}} - \frac{1}{2}g_{\hat{\mu}\hat{\nu}}R = 8\pi T_{\hat{\mu}\hat{\nu}}$,, the field equations are obtained to be

$$\rho(r,t) = \frac{1}{8\pi}\frac{1}{A^2}\left[3e^{-2\Phi}\left(\frac{\dot{A}}{A}\right)^2 + \left(3k + \frac{b'}{r^2}\right)\right], \tag{2.83}$$

$$\tau(r,t) = -\frac{1}{8\pi}\frac{1}{A^2}\left\{e^{-2\Phi(r)}\left[\left(\frac{\dot{A}}{A}\right)^2 - 2\frac{\ddot{A}}{A}\right] - \left[k + \frac{b}{r^3} - 2\frac{\Phi'}{r}\left(1 - kr^2 - \frac{b}{r}\right)\right]\right\}, \tag{2.84}$$

$$f(r,t) = -\frac{1}{8\pi}\left[2\frac{\dot{A}}{A^3}\,e^{-\Phi}\,\Phi'\left(1-kr^2-\frac{b}{r}\right)^{1/2}\right], \tag{2.85}$$

$$p(r,t) = \frac{1}{8\pi}\frac{1}{A^2}\left\{e^{-2\Phi(r)}\left[\left(\frac{\dot{A}}{A}\right)^2 - 2\frac{\ddot{A}}{A}\right] + \left(1-kr^2-\frac{b}{r}\right)\times \right.$$
$$\left.\times\left[\Phi'' + (\Phi')^2 - \frac{2kr^3+b'r-b}{2r(r-kr^3-b)}\Phi' - \frac{2kr^3+b'r-b}{2r^2(r-kr^3-b)} + \frac{\Phi'}{r}\right]\right\}, \tag{2.86}$$

where $f(r,t) = -T_{\hat{t}\hat{r}}$ represents the radially outward energy flux. The overdot and prime denotes differentiation with respect to t and r respectively. The presence of an off-diagonal component in the energy-momentum tensor arises from the temporal variation of $A(t)$ and/or the r dependence of the redshift function $\Phi(r)$.

The initial objective for studying evolving wormholes was to utilize inflation to expand an initially small, potentially submicroscopic wormhole, for instance, see studies by Thomas Roman [395]. Later, other researches have explored numerous interesting properties [387–389].

2.3 Time-travel paradoxes

A backward time-travel inevitably invites the specter of time-travel paradoxes. From science fiction to numerous movies, and recently the web-series have made us very much aware about the severe complexities and mind-boggling aspects of time-travel encounters. Say for example, encounter with one's past self, or with someone who will murder the traveler in the future, or with the time-machine that will be created in the future, or with Rabindranath Tagore, or a thief who stole his Nobel award and went back to the future, anything could happen when *Chronology* is violated. From these visualizations of our imagination, these paradoxes can be broadly categorized into two groups: *consistency paradoxes* and *causal loops*. Consistency paradoxes, exemplified by the classical grandfather paradox, emerge when the possibility of altering events in the past is contemplated. For instance, envision a time traveler journeying to the past and encountering their grandfather. If, driven by homicidal intentions, the time traveler eliminates their grandfather, preventing the birth of their father, their own existence becomes untenable. This scenario illustrates just one iteration of the grandfather paradox, which can manifest in myriad forms limited only by imagination. In contrast, causal loops involve self-contained information or objects trapped within spacetime. Consider a time traveler who ventures back to their past and furnishes their younger self with a manual detailing the construction of a time machine. The younger version then spends years constructing the time machine and eventually returns to the past to deliver the manual to their younger self. Here, the time machine exists in the future because it was built in the past by the younger version, and its construction was facilitated by the manual received from the future. While each component of this loop appears internally consistent, the paradox arises when considering the loop as a whole. This raises the question: what is the source of the manual, appearing seemingly out of thin air? Despite no violations of causality, the manual exists in spacetime without ever being created. Gott and Li [9] delved into various iterations of these causal loops, exploring the intriguing concept of whether the Universe could potentially create itself, leading to the emergence of closed timelike curves (CTCs) when tracing back through the original inflationary state, thereby posing a challenge to the notion of a first cause.

Recently, in a deterministic model of CTCs [507], a collection of areas devoid of CTCs is considered, yet these areas could potentially be traversed by such curves. Individuals within these locations receive classical states from past boundary, perform deterministic operations, and subsequently transmit the states through the future boundary. The states noticed by each individual in their past are fixed by the dynamics outside the locations, depending on the states created by other individuals. A straightforward characterization was established for all operations concerning up to three regions. Furthermore, it was revealed that, among three regions, processes devoid

of causal ordering exhibit fundamental similarity.

However, Tobar and Costa [508] formulated a description of deterministic operations amidst the existence of CTCs across numerous localized regions. Their demonstrations have shown that non-trivial time-travel between multiple regions can coexist with the absence of a logical paradox, provided that once the outcomes of all regions except two are determined, only unidirectional signaling remains feasible. The identification of unique and intricate quadripartite process functions that coexist with CTCs underscores the notion that when multiple localized areas interact while CTCs are present, a diverse array of communication scenarios emerges. These scenarios maintain the freedom of choice of observers in every location, without leading to logical contradictions such as the grandfather paradox. This is the well-established description of the potential emergence of *paradox-free time-travel*.

2.4 The Chronology Protection Conjecture

As discussed, the violation of causality may lead to severe disturbances in the chronology, in terms of time-travel (paradoxes). This deeply unsettling situation has prompted Hawking to propose his chronology protection conjecture [263]. He investigated the scenario wherein causality violations occur within a finite region of spacetime devoid of curvature singularities. Such regions typically feature a Cauchy horizon, compactly generated, often encompassing one or more incomplete closed null geodesics. Geometric parameters can be defined to quantify the Lorentz boost and area expansion along these closed null geodesics. If the causality violation originates from a non-compact initial surface, the averaged weak energy condition must be breached on the Cauchy horizon. This implies that closed timelike curves with finite lengths cannot be created by cosmic strings. Even if quantum theory permits violations of the weak energy condition, the energy-momentum tensor's expectation value would escalate substantially if timelike curves nearly close. It appears that the resultant back reaction would prevent the emergence of closed timelike curves. According to Hawking, these findings strongly endorse the *chronology protection conjecture*, for which "the laws of physics prohibit the appearance of closed timelike curves."

Note that there are still counter-arguments against the chronology protection conjecture. Therefore, one may finally conclude that there have been certain attempts to disprove the possibility of time travel, but none of them are complete. However, the justifications for time travel are not complete either. The scenario has been beautifully explained by Michio Kaku:

> "Originally, the burden of proof was on physicists to prove that time travel was possible. Now the burden of proof is on physicists to prove there must be a law forbidding time travel."

CHAPTER 3

THE ROLE OF CLOSED TIMELIKE CURVES IN PARTICLE MOTION WITHIN VAN STOCKUM SPACETIME: A GENERALIZATION

3.1 Prelude

The current chapter delves into the analysis of particle dynamics within the van Stockum spacetime framework, taking into account the presence of closed timelike curves (CTCs). Investigation encompasses both inertial test particles with zero and non-zero angular momentum within this particular geometric context. The examination reveals that solely test particles endowed with non-zero angular momentum are observable in proximity to CTCs. Furthermore, study extends to determining the minimum energy threshold for particles and the extent of backward temporal displacement along closed timelike geodesics (CTGs) bounded by a Cauchy horizon. Lastly, a comprehensive framework for the obtained results in general axially symmetric spacetimes is delineated, supported by pertinent illustrative instances.

The chapter is arranged as follows: the study is initiated with the geodesic motion in van Stockum interior metric in Section 3.2, where the radial null-like and timelike motions are extensively investigated in terms of spacetime diagrams. The spacetime diagram technique is mostly helpful for examining the geodesic structure within a geometry. Thus, the results obtained in Section 3.2 have been accommodated to describe the regions of different angular momentum particles in Section 3.3. Section 3.4 is particularly dedicated to the investigation of closed timelike curves and closed timelike geodesics in the interior van Stockum space. Finally, the extensive results of these sections are utilized in a general axisymmetric spacetime metric with prominent examples in Section 3.5.

3.2 van Stockum interior geodesics

The interior van Stockum metric is written as

$$ds^2 = -dt^2 + 2ar^2 d\phi dt + r^2\left(1 - a^2r^2\right)d\phi^2 + e^{-a^2r^2}\left(dr^2 + dz^2\right), \tag{3.1}$$

with 'a' being the angular velocity of the cylinder. The ranges of four cylindrical coordinates are: $t : \{-\infty, +\infty\}$, $r : \{0, +\infty\}$, $\phi : \{0, 2\pi\}$ and $z : \{-\infty, +\infty\}$. Now, by using the Euler-Lagrange equation of motion, the first order geodesic equations are readily obtained to be

$$\dot{t} = \left(1 - a^2r^2\right)E + aP_\phi\,, \tag{3.2}$$

$$\dot{\phi} = \frac{P_\phi}{r^2} - aE\,, \tag{3.3}$$

$$\dot{z} = P_z e^{a^2r^2}\,, \tag{3.4}$$

$$\dot{r}^2 = e^{a^2r^2}\left[-\epsilon + \left(1 - a^2r^2\right)E^2 + 2aEP_\phi - \frac{P_\phi^2}{r^2} - P_z e^{a^2r^2}\right], \tag{3.5}$$

where E, P_ϕ and P_z are the constants of motion corresponding to t, ϕ and z dynamics. They are termed as the total energy of the test particle, total angular momentum, and momentum along z direction respectively. $\epsilon = 0, 1$, and -1 defines null, timelike, and spacelike signatures. Therefore, with the required expressions in hand, one may now delve into the investigation of radial geodesic motions.

Note that, the angular velocity in angular momentum-less test particles (both null-like and timelike) happens to be non-zero, since Eq. (3.3) provides

$$\dot{\phi} = -aE\,. \tag{3.6}$$

Opher *et al.* described this to be the effect of spacetime dragging. The negative sign effectively denotes that this dragging is counter-rotating with the spacetime rotation.

3.2.1 Radial null geodesics

By applying $\epsilon = 0$, the r geodesic equation for photons (null-like) is given by

$$\dot{r}^2 = e^{a^2r^2}\left[\left(1 - a^2r^2\right)E^2 + 2aEP_\phi - \frac{P_\phi^2}{r^2} - P_z e^{a^2r^2}\right]. \tag{3.7}$$

One may now divide (3.2) by (3.7), to obtain the radial null geodesic equation as follows:

$$\frac{dt}{dr} = \frac{dt/d\lambda}{dr/d\lambda} = \frac{\dot{t}}{\dot{r}} = \pm\frac{e^{-\frac{a^2r^2}{2}}\left[\left(1 - a^2r^2\right)E + aP_\phi\right]}{\sqrt{\left(1 - a^2r^2\right)E^2 + 2aEP_\phi - \frac{P_\phi^2}{r^2} - P_z e^{a^2r^2}}}\,. \tag{3.8}$$

The solutions of Eq. (3.8) is introduced for zero and non-zero values of angular momentum (AM) of photons, i.e., P_ϕ. Consequently, it will be convenient to define the motion in a constant z slice by assuming $P_z = 0$, such that the coaxial movements of the particles are free.

3.2.1.1 $P_\phi = 0$ motion

For $P_\phi = P_z = 0$, the radial null geodesic equation (3.8) becomes

$$\frac{\dot{t}}{\dot{r}} = \pm e^{-\frac{a^2 r^2}{2}} \sqrt{1 - a^2 r^2}\,. \tag{3.9}$$

Notice that the equation is free of the energy of particles, while only depending on the angular velocity of the dust cylinder. However, it is not surprising, since the coaxial motion-less, zero-angular momentum interior photons (including dust) necessarily store their energy in the angular velocity, as verified from Eq. (3.3).

Further, with the standard numerical tool, one may integrate Eq. (3.9) for the spacetime diagram of radial motion of photons. Thus, the expression is approximated for figure 3.1 with different values of angular velocity, i.e., $a = 1$ and $a = \frac{1}{2}$. It is observed that the maximum radii of photon orbits are restricted at $ar = 1$ line. Physically, the inward directed acceleration vanishes at the symmetry axis (i.e., at $r = 0$) and increases with the outward motion. Again, as the particles reach the $ar = 1$ boundary, their velocity vanishes and they are attracted inside and subsequently repeat the motion. They perform this dynamics endlessly [260].

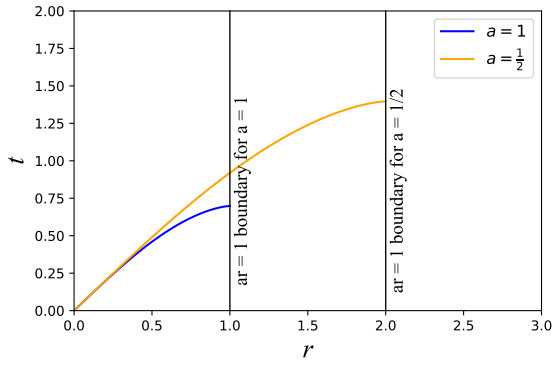

Figure 3.1: Spacetime diagram of radial null geodesics with $P_\phi = 0$. The $ar = 1$ boundary is exhibited with vertical grid line.

3.2.1.2 $P_\phi \neq 0$ motion

For $P_\phi \neq 0$, (3.8) is modified to

$$\frac{\dot{t}}{\dot{r}} = \pm \frac{e^{-\frac{a^2 r^2}{2}} \left[\left(1 - a^2 r^2\right) E + a P_\phi\right]}{\sqrt{\left(1 - a^2 r^2\right) E^2 + 2aEP_\phi - \frac{P_\phi^2}{r^2}}}\,. \tag{3.10}$$

Note that the motion is restricted at the certain limit of radial direction where the denominator of Eq. (3.10) vanishes for fixed a, E, P_ϕ. One may estimate this limit by considering

$$\left(1 - a^2 r^2\right) E^2 + 2aEP_\phi - \frac{P_\phi^2}{r^2} = 0\,. \tag{3.11}$$

It is however observed that this expression determines two non-zero limits in the radial direction within which the orbits are confined. These points are termed as r_{max}

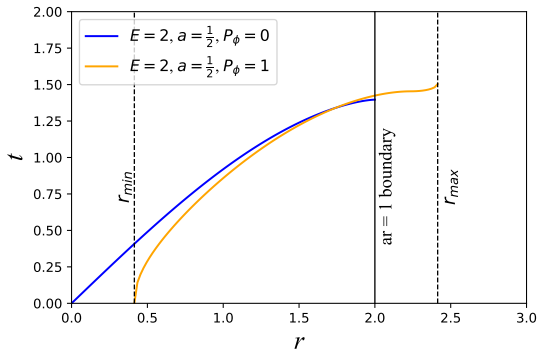

(a) $r_{min} = 0.414$, $r_{max} = 2.414$

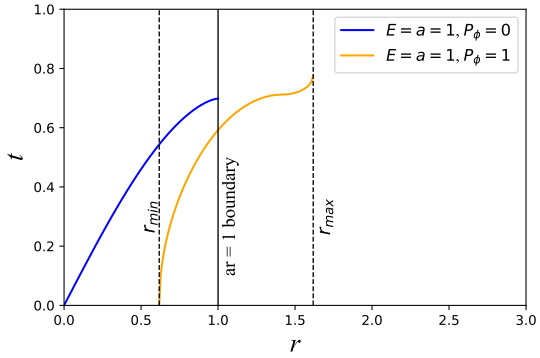

(b) $r_{min} = 0.618$, $r_{max} = 1.618$

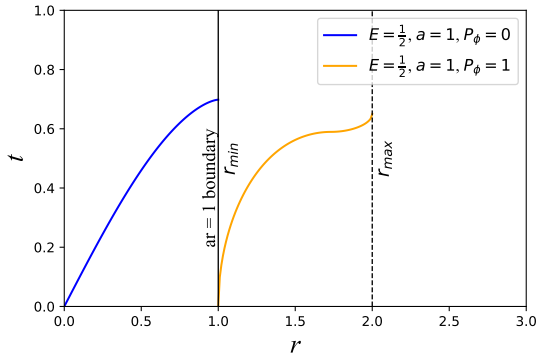

(c) $r_{min} = 1$, $r_{max} = 2$

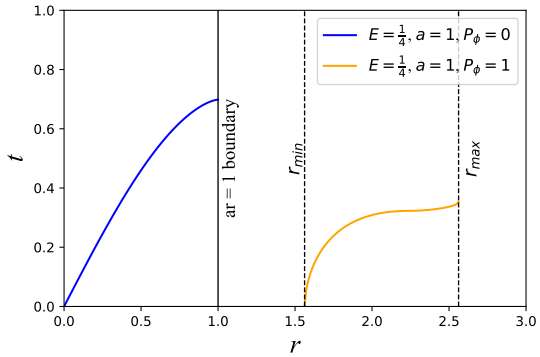

(d) $r_{min} = 1.562$, $r_{max} = 2.562$

Figure 3.2: Spacetime diagrams of radial null geodesics with $P_\phi = 1$. The vertical gridlines represent different confinement boundaries in each plot. The captions under each figure note the corresponding minimum and maximum confinement radii.

and r_{min}, respectively for the maximum and minimum radius of confinement. Their physically realizable expressions are given by

$$r_{max} = \frac{E + \sqrt{E^2 + 4aEP_\phi}}{2aE}, \tag{3.12}$$

$$r_{min} = \frac{-E + \sqrt{E^2 + 4aEP_\phi}}{2aE}. \tag{3.13}$$

Figure 3.2 exhibits the spacetime diagrams of non-zero AM photons corresponding to Eq. (3.10). These orbits are plotted along with zero AM motions (keeping other parameters i.e., a, E, fixed) for a comparable understanding.

As mentioned, the movement of non-zero AM photons is bounded inside the cylindrical shell of radius r_{min} and r_{max}. Notice that, with the variation of parameter choices, location of this shell fluctuates. For instance, as the total energy of the photons (E) decreases, the shell shifts radially outward for a fixed value of a and P_ϕ, as seen from figures 3.2b, 3.2c and 3.2d. Interesting insights arising from these orbits will be discussed in forthcoming sections.

Further, one may observe from equations (3.7) and (3.10) that the velocity of photons vanish at r_{min} and r_{max}. At r_{min}, although the acceleration vanishes, the total angular momentum leads to an outward pull to the photons, which again vanishes at r_{max} and they are drawn inward.

3.2.2 Radial timelike geodesics

By choosing $\epsilon = 1$ in Eq. (3.5), the r geodesic for timelike motion is obtained as

$$\dot{r}^2 = e^{a^2r^2}\left[-1 + (1-a^2r^2)E^2 + 2aEP_\phi - \frac{P_\phi^2}{r^2} - P_z e^{a^2r^2}\right], \tag{3.14}$$

which can be modified further to obtain the radial timelike geodesic equation:

$$\frac{\dot{t}}{\dot{r}} = \pm\frac{e^{-\frac{a^2r^2}{2}}\left[(1-a^2r^2)\,E + aP_\phi\right]}{\sqrt{-1 + (1-a^2r^2)\,E^2 + 2aEP_\phi - \frac{P_\phi^2}{r^2} - P_z e^{a^2r^2}}}. \tag{3.15}$$

Hence, with freeing the coaxial movement of the massive (timelike) particles i.e., $P_z = 0$, the zero and non-zero AM motions are discussed separately.

3.2.2.1 $P_\phi = 0$ motion

For zero AM particles, Eq. (3.15) yields

$$\frac{\dot{t}}{\dot{r}} = \pm\frac{Ee^{-\frac{a^2r^2}{2}}(1-a^2r^2)}{\sqrt{-1 + (1-a^2r^2)E^2}}. \tag{3.16}$$

Note that this equation is real-valued and physically realizable only when the following inequality holds:

$$E > \pm\frac{1}{\sqrt{1-a^2r^2}}. \tag{3.17}$$

The corresponding spacetime diagram of particles (with relevant choices of parameters) for Eq. (3.16) has been exhibited in Fig. 3.3.

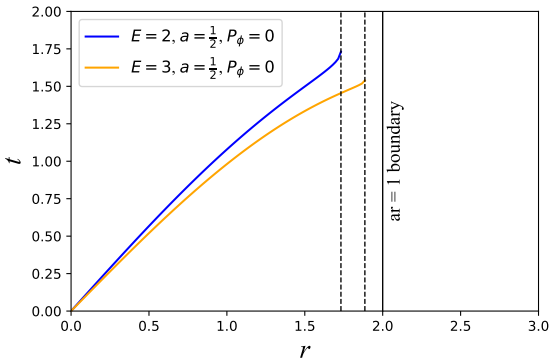

Figure 3.3: Spacetime diagram of radial timelike geodesics with $P_\phi = 0$. Apart from the $ar = 1$ boundary in solid grid line, the vertical dashed lines represent corresponding confinement radii ($r = 1.732$ and $r = 1.886$ respectively) for each plot.

It is evident from both the figure 3.3, and Eq. (3.17) that these particles are always confined within $ar < 1$. Nevertheless, Eq. (3.17) predicts the restriction of radial motion for $E = 2, a = 1/2$ and $E = 3, a = 1/2$ at $r = 1.732$ and $r = 1.886$ respectively. Interestingly, referring to Eq. (3.6), the spacetime dragging is linearly dependent on the energy of test particles. Therefore, from Eq. (3.17), it is noted that the dragging effect also forbids zero AM massive particles outside the $ar = 1$ boundary.

3.2.2.2 $P_\phi \neq 0$ motion

For non-zero AM massive particles, Eq. (3.15) modified to

$$\frac{\dot{t}}{\dot{r}} = \pm \frac{e^{-\frac{a^2 r^2}{2}} \left[\left(1 - a^2 r^2\right) E + a P_\phi \right]}{\sqrt{-1 + \left(1 - a^2 r^2\right) E^2 + 2aEP_\phi - \frac{P_\phi^2}{r^2}}} \,. \tag{3.18}$$

For this solution to be physically realizable, the following restriction appears:

$$\left(1 - a^2 r^2\right) E^2 + 2aEP_\phi - \left(1 + \frac{P_\phi^2}{r^2}\right) > 0 \,. \tag{3.19}$$

Notice that, similar to the non-zero AM photons, the motion of non-zero AM massive particles are also restricted between a minimum and maximum radius, i.e., $r_{min-time}$ and $r_{max-time}$. One may compute these two radii from the roots of the denominator in Eq. (3.18) as follows:

$$\left(arE - \frac{P_\phi}{r}\right) = \pm\sqrt{E^2 - 1} \,, \tag{3.20}$$

where the respective positive and negative right hand side provides $r_{max-time}$ and $r_{min-time}$ as given by

$$r_{max-time} = \frac{\sqrt{E^2 - 1} + \sqrt{E^2 - 1 + 4aEP_\phi}}{2aE} \,, \tag{3.21}$$

$$r_{min-time} = \frac{-\sqrt{E^2 - 1} + \sqrt{E^2 - 1 + 4aEP_\phi}}{2aE} \,. \tag{3.22}$$

Similar to the null-like motion, numerically integrated spacetime diagram of Eq. (3.18) has been plotted in Fig. 3.4 along with corresponding plot of zero AM particles for the same choices of parameters (i.e., a and E). The dashed vertical gridlines in the figure, that provides the $r_{max-time}$ and $r_{min-time}$ restriction, have been predicted by equations (3.21) and (3.22). Likewise the null geodesics, timelike motion is also confined within the cylindrical shell of radii r_{min} to r_{max}. One may now compare Fig. 3.2a with 3.4a (since they share the same parameter choices), where it is comfortably observed that the motion of timelike particles are always bounded within the confinement of null-like motion. For instance, the maximum radial reach of zero AM massive particles are $ar = 1$, where the cylindrical shell of non-zero AM particle motion is always situated within the cylindrical shell of non-zero AM null-like motion. Thus, $r_{min-time}$ and $r_{max-time}$ does not necessarily coincide r_{min} and r_{max}.

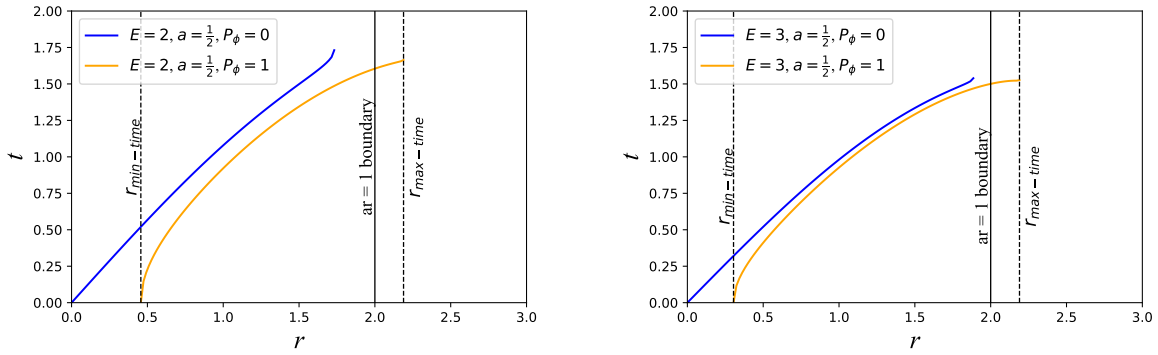

(a) $r_{min-time} = 0.457$, $r_{max-time} = 2.189$ (b) $r_{min-time} = 0.304$, $r_{max-time} = 2.19$

Figure 3.4: Spacetime diagrams of radial timelike geodesics with $P_\phi = 1$. The vertical gridlines represent different confinement boundaries in each plot.

3.3 The characteristic regions

It is interesting to note that the presence of the $ar = 1$ boundary, r_{min} and r_{max}, delineates distinct regions of particle motion, where the characteristics can be zero or non-zero AM. These boundaries are entirely contingent upon and fluctuate with the angular momentum (P_ϕ) and energy (E) of the particles. For example, readers are referred to observe figures 3.2a and 3.2b. Hence, one may consider to distinguish the regions as follows:

(i) **Region I:** From the symmetry axis to r_{min}, where only AM-less particles can exist.

(ii) **Region II:** Region between r_{min} and $ar = 1$ boundary can be termed as the mixed region, where both zero and non-zero AM particles can be found.

(iii) **Region III:** $ar = 1$ boundary to r_{max}, which is purely a non-zero AM particle region.

Note that this observation is also valid for massive particles, as concluded from Fig. 3.4. As already well-established, null-like photon movement corresponds to the limitation of timelike massive particle motion. For instance, the r_{min} to r_{max} shell determines the restriction of $r_{min-time}$ to $r_{max-time}$ shell, just like the light cone in worldline dynamics.

For another definition of the van Stockum interior and exterior regions, it is noted that the primary assumption of the interior metric is $r < R$, where R is the radius of the dust cylinder; and beyond this radius, there lies the exterior region. Therefore, when r_{max} is larger than R, the interior solution is merged with the exterior solution, leading to a completely different aspect of the current study, which is not considered here momentarily. Hence, restricting the present attention to a pure interior particle motion, it is concluded that the region outside r_{max}, i.e., $r_{max} < r < R$ is a pure empty space, where even the photons are forbidden to exist. So, observers residing outside the $r > r_{max}$ surface (the best place being the exterior region), can't see the movement

of particles inside the cylinder. The region will appear as a perfect dark cylinder to their eyes.

The fluctuation in the locations of $ar = 1$, r_{min} and r_{max} surfaces with E, P_ϕ and a is another point of interest. Referring to figures 3.2a and 3.2b, although the $ar = 1$ boundary lie within r_{min} to r_{max} cylindrical shell, figures 3.2c and 3.2d indicate that the shell gradually shifts away from the symmetry axis with the loss of particle energy, E (for fixed value of P_ϕ and a). Regions I, II, and III, all are present in figures 3.2a and 3.2b. But, for $P_\phi = a = 1$, $E = 1/2$ is the critical point when the shell from r_{min} to r_{max} has shifted so much that r_{min} has coincided with the $ar = 1$ boundary, and therefore the mixed region (Region II) has vanished. Consequently, if the particle energy (E) decreases further, Regions I and III have completely separated as shown in Fig. 3.2d. This is the case where Region II is forbidden, and the region between Regions I and III is pure empty space where the existence of particles is completely restricted.

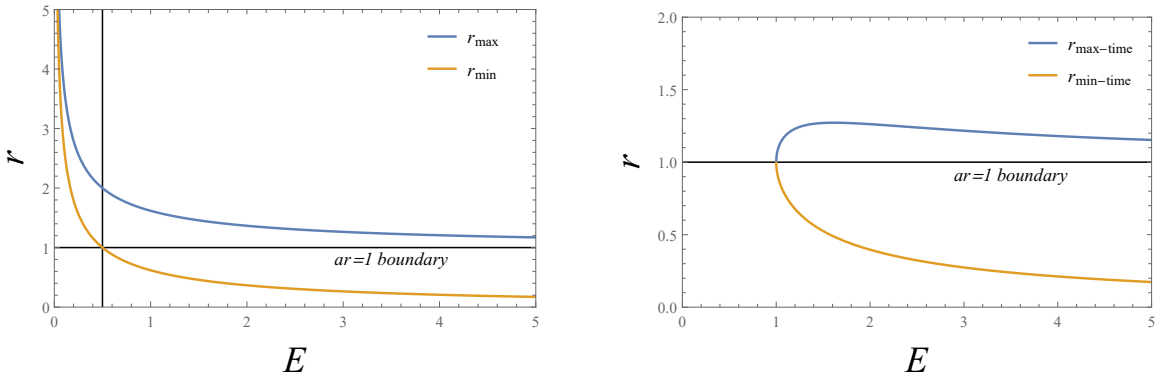

(a) Null geodesics

(b) Timelike geodesics

Figure 3.5: Variation of different confinement radii (for null and timelike geodesics) with energy (E) of the photon (for (a)) and massive particle (for (b)), for $P_\phi = 1, a = 1$. The vertical grid line in (a) shows the coincidence of r_{min} with $ar = 1$ for $E = 1/2, P_\phi = 1, a = 1$.

Hence, it is a matter of interest whether any relationship between E and P_ϕ supports the possibility of r_{min} and $ar = 1$ coincidence. Consider Eq. (3.13) with $a = \frac{1}{r}$ such that $ar = 1$ is consistently maintained. Therefore, it reduces to

$$r_{min} = r = \frac{-E + \sqrt{E^2 + \frac{4EP_\phi}{r}}}{\frac{2E}{r}}, \tag{3.23}$$

which further provides the following condition

$$E = \frac{P_\phi}{2r}. \tag{3.24}$$

The choice of parameters in Fig. 3.2c obeys the condition (3.24), and thus r_{min} and $ar = 1$ boundary coincide. On the other hand, when $E < \frac{P_\phi}{2r}$, Region I and Region

III completely separate from each other, as given by Fig 3.2d. Fig. 3.5a offers the variation of r_{min} and r_{max} with photon energy (E), for $P_\phi = 2$ and $a = 1$.

Another realization emerges from Eq. (3.20) where one may observe that, for $E \leq 1$, massive particle movement is completely forbidden. Note that, with the same parameter choices, however, photons have no such limitation. In this particular region, photons exist while the presence of massive particles is prohibited. This unique region can be aptly termed as a *"pure null region"*. Interestingly, the occurrence of r_{min} and $ar = 1$ coincidence, and the separation of Region I and Region III occurs under this specific condition for photons.

Fig. 3.5b offers the variation of $r_{min-time}$ and $r_{max-time}$ with massive test particle energy E, for $P_\phi = 2$ and $a = 1$. It clearly exhibits the restriction of massive particle movement at $E \leq 1$.

3.4 CTCs in van Stockum interior space-time

According to the definition, the van Stockum interior solution contains closed timelike curves corresponding to the ϕ coordinate with t, r, z being constants. From the timelike $g_{\phi\phi}$ component, it is found that the causality violating region appears at $ar > 1$ region. Therefore, for the CTCs, the line element (3.1) takes the form

$$ds^2 = r^2(1 - a^2r^2)d\phi^2 \,. \tag{3.25}$$

Now, using the Euler-Lagrange dynamics on this equation, the angular velocity of the CTC is given by

$$\dot{\phi} = \frac{P_\phi}{r^2(1 - a^2r^2)} \,, \tag{3.26}$$

where P_ϕ is the angular velocity of the particles orbiting the CTCs. This expression does not involve any separate space-time dragging term. The only characteristic term present here is angular momentum. Therefore, particles only traverse these curves with non-zero AM. Notice that Eq. (3.26) disallows the motion of angular momentum-less particles in the vicinity of CTC.

Now, if the assumption of CTC, i.e., t, r, z to be constant, which leads to $\dot{t} = \dot{r} = \dot{z} = 0$, is imposed on the geodesic equations (3.2), (3.4) and (3.5), one gets

$$\dot{t} = 0 = (1 - a^2r^2)E + aP_\phi \,, \tag{3.27}$$

$$\dot{z} = 0 = P_z e^{a^2r^2} \,, \tag{3.28}$$

$$\dot{r}^2 = 0 = e^{a^2r^2}\left[-1 + \left(1 - a^2r^2\right)E^2 + 2aEP_\phi - \frac{P_\phi^2}{r^2} - P_z e^{a^2r^2}\right] . \tag{3.29}$$

Since, $e^{a^2r^2} \neq 0$ and $P_z = 0$ (from (3.28)), the following modifications are obtained

$$(1 - a^2r^2)E = -aP_\phi \,, \tag{3.30}$$

$$-1 + (1 - a^2r^2)E^2 = \frac{P_\phi^2}{r^2} - 2aEP_\phi \,. \tag{3.31}$$

Hence, Equations (3.30) and (3.31) approximate the energy required by the particles to traverse the CTC as

$$E = \pm \frac{ar}{\sqrt{a^2r^2 - 1}}\,, \tag{3.32}$$

which also re-establishes the position of CTCs to be $ar > 1$.

Using the same treatment, one may now show that the energy required by a particle to traverse closed spacelike geodesics (CSG) is

$$E = \pm \frac{ar}{\sqrt{1 - a^2r^2}}\,, \tag{3.33}$$

suggesting that CSG appears in the spacetime at $ar < 1$ region of the cylinder. So, $ar = 1$ boundary separates the CTGs and CSGs. Alongside, it is the position where closed null geodesics (CNGs) are possible to appear. Thus, the $ar = 1$ boundary is nothing but the Cauchy horizon.

3.4.1 Backward time jump in CTG

If equations (3.30) and (3.32) are substituted in Eq. (3.3), one gets

$$\dot{\phi} = -\frac{E}{ar^2} = \mp \frac{1}{r\sqrt{a^2r^2 - 1}}\,. \tag{3.34}$$

Consider τ_1 and τ_2 to be the proper time of a particle at $\phi = 0$ and $\phi = 2\pi$ respectively, then the backward time jump $\Delta\tau = \tau_2 - \tau_1$ for the particle in CTG occurs when it just crosses $\phi = 2\pi$ position, i.e.,

$$2\pi = \mp \frac{1}{r\sqrt{a^2r^2 - 1}}(\tau_2 - \tau_1) = \mp \frac{1}{r\sqrt{a^2r^2 - 1}}(\Delta\tau)\,. \tag{3.35}$$

For a non-negative energy of the particle, this expression provides

$$\Delta\tau = -2\pi r\sqrt{a^2r^2 - 1}\,, \tag{3.36}$$

where the negative sign denotes a backward time jump.

The expression in Eq. (3.36) represents the constant nature of backward time jump for a CTG at fixed radius r, which offers the remarkable feature that after each rotation, the particle always reappears at the same proper time it started. This also means that the particle cannot escape the CTG loop (at constant radius r) for an infinite time, according to the observer's frame of reference. In terms of the particle's frame of reference, it travels the loop for a certain time and eventually gets back to the same initial position for infinite rotations.

3.4.2 Dependence on angular momentum (P_ϕ)

Until now, it is clearly observed that zero-angular momentum particles are restricted within the $ar < 1$ region. But, non-zero AM particles, i.e., with $P_\phi \neq 0$, can fluently traverse $ar > 1$ region where CTGs are allowed to exist. Therefore, only non-zero AM

particles can traverse the closed timelike geodesics in van Stockum interior solution. From equation (3.30),

$$E = -\frac{aP_\phi}{1-a^2r^2}\,, \tag{3.37}$$

which suggests that the particles must have a non-zero AM otherwise, they have no energy to survive the journey.

A 3d parametric plot has been exhibited in Fig. 3.6 to represent the closed timelike geodesic at the cylindrical shell of radius $ar = 1$ boundary to $r_{max-time}$, i.e., Region III.

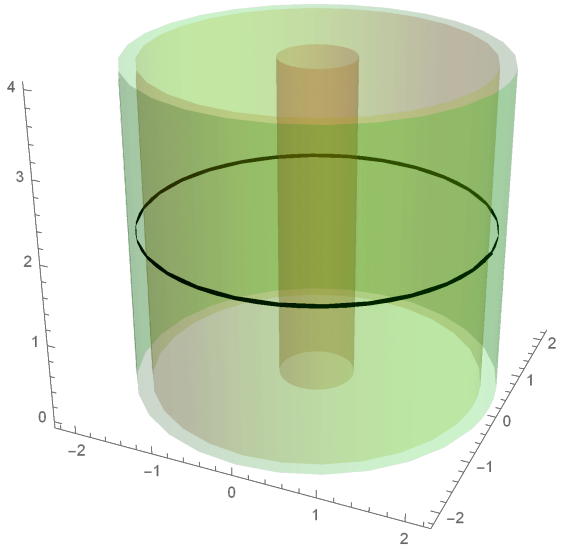

Figure 3.6: Three-dimensional parametric plot capturing a CTG orbit between $ar = 1$ and $r_{max-time}$, for $E = 2, P_\phi = 1, a = 1/2$. The $r_{min-time}, ar = 1, r_{max-time}$, and the CTG are respectively located at $r = 0.457, r = 2, r = 2.189$, and $r = 2.1$.

3.5 A generalized formulation

Previous sections have briefly investigated that the AM-less particles are forbidden in the vicinity of CTCs. This leads to the examination of a general axisymmetric spacetime line element to know whether they all exhibit the same feature irrespective of their choices of metric coefficients.

3.5.1 Closed timelike curves

To start the generalized description of CTCs, consider the general stationary, axisymmetric, rotating line element as given by [224]

$$ds^2 = -Fdt^2 + 2Md\phi dt + Ld\phi^2 + H_1dr^2 + H_2dz^2\,, \tag{3.38}$$

where F,M, L, H_1 and H_2 are the metric components g_{ij}, which can be arbitrary functions of r, t, z together or individually. The azimuthal curve in Eq. (3.38) with $\{t, r, z\} =$ const., and $L < 0$ denotes the closed timelike curve, whereas corresponding curve with $L = 0$ describes a closed null curve.

The Lagrangian of the metric is readily given by

$$2\mathcal{L} = -F\dot{t}^2 + 2M\dot{\phi}\dot{t} + L\dot{\phi}^2 + H_1\dot{r}^2 + H_2\dot{z}^2\,, \tag{3.39}$$

for which the calculation of first order geodesic equations in terms of canonical momentum $P_q = \frac{\partial\mathcal{L}}{\partial\dot{q}}$ is straightforward using the Euler-Lagrange equation, as given by

$$\begin{aligned} P_t &= -E = -F\dot{t} + M\dot{\phi}\,, \\ P_\phi &= M\dot{t} + L\dot{\phi}\,, \\ P_z &= H_2\dot{z}\,. \end{aligned} \tag{3.40}$$

Here, E, P_ϕ, P_z are the integration constants denoted by total energy, angular momentum, and momentum along z direction respectively for a test particle. The set of simplified geodesic equations are now given by

$$\dot{t} = \frac{P_\phi M + EL}{M^2 + LF}\,, \tag{3.41}$$

$$\dot{\phi} = \frac{P_\phi F - EM}{M^2 + LF}\,, \tag{3.42}$$

$$\dot{z} = \frac{P_z}{H_2}\,. \tag{3.43}$$

Note that, $\dot{\phi}$ is the angular velocity of the particle, which is non-zero even for zero AM. This is interpreted as the spacetime dragging term, as given by

$$\dot{\phi} = -\frac{EM}{M^2 + LF}\,, \tag{3.44}$$

where the negative sign denotes the counter-rotation with the orientation of spacetime rotation. Thus, for the dynamics of CTC, AM-less particles cannot be avoided alone just because of the absence of their rotation.

Now, by using geodesic equations (3.41), (3.42) and (3.43), the radial null geodesic for the metric (3.38) is given by

$$\dot{r}^2 = \frac{E^2L - P_\phi^2 F + 2MEP_\phi}{(M^2 + LF)H_1} - \frac{P_z^2}{H_1H_2}\,. \tag{3.45}$$

Considering the coaxial movement to be free, one obtains

$$\frac{\dot{t}}{\dot{r}} = \frac{dt}{dr} = \frac{(P_\phi M + EL)\sqrt{H_1}}{\sqrt{(M^2 + LF)(E^2L - P_\phi^2 F + 2MEP_\phi)}}\,. \tag{3.46}$$

Notice, the expression inside the square root in the denominator must be greater than zero to maintain the equation real. Since the Lorentzian signature of the metric ($(M^2 + LF) > 0$) is true, it determines the following relation

$$(E^2L - P_\phi^2 F + 2MEP_\phi) > 0\,, \tag{3.47}$$

which provides the radial geodesic confinement condition for photons. Therefore, for zero AM photons, one may obtain $E^2L > 0$; and since the energy of photons is always non-zero, it simplifies to

$$L > 0\,. \tag{3.48}$$

This condition represents the necessary requirement for achieving confinement of photon trajectories devoid of angular momentum. The emergence of CTCs, indicative of causality violation, occurs within the region where $L < 0$. Given that the boundary delineating photon confinement signifies the utmost limitation for timelike particles, this condition consistently prevents angular momentum-less massive particles from venturing into the CTC region.

Further, for CTCs, the metric given by (3.38) takes the form

$$ds^2 = Ld\phi^2\,, \tag{3.49}$$

where the angular momentum corresponding to ϕ geodesic is given by

$$\dot{\phi} = \frac{P_\phi}{L}\,. \tag{3.50}$$

To maintain this expression in CTCs, one may note that the geodesic equation (3.42) necessarily demands M to be zero, for which the spacetime dragging term (3.44) vanishes. Therefore, it can be concluded that the CTCs may not be the result of the spacetime dragging effect. Moreover, Eq. (3.50) also claims that AM-less particles cannot be present in the vicinity of CTCs.

These explanations perfectly fit with the corresponding discussions in van Stockum interior solution.

3.5.2 Closed timelike geodesics

Considering the metric given by Eq. (3.38) allows for the CTGs, the radial timelike geodesic is given by

$$\dot{r}^2 = \frac{-M^2 - LF + E^2L - P_\phi^2F + 2MEP_\phi}{(M^2 + LF)H_1} - \frac{P_z^2}{H_1H_2}\,. \tag{3.51}$$

Now, according to the condition of CTG, i.e., $\dot{t} = \dot{r} = \dot{z} = 0$, equations (3.41), (3.43) and (3.51) become

$$P_\phi M + EL = 0\,, \tag{3.52}$$

$$P_z = 0\,, \tag{3.53}$$

$$-M^2 - LF + E^2L - P_\phi^2F + 2MEP_\phi = 0\,, \tag{3.54}$$

where Eq. (3.52) further gives,

$$P_\phi = -\frac{EL}{M}\,. \tag{3.55}$$

From this relation, it is evident that for $P_\phi = 0$, E must also be zero, since $L \neq 0$ for any closed timelike orbits. This implies that for $P_\phi = E = 0$, $M^2 + LF = 0$ in Eq.

(3.54) which directly contradicts the Lorentzian signature of the metric. Therefore, it is evident that P_ϕ cannot be zero, suggesting that AM-less particles are forbidden in CTGs.

Now, plugging the value of P_ϕ from Eq. (3.55) in (3.54) by maintaining the Lorentzian signature, one gets

$$E = \pm\frac{M}{\sqrt{-L}}\,. \tag{3.56}$$

This is the expression of the total amount of energy required by a particle to traverse a CTG.

On the other hand, imposing equations (3.55) and (3.56) in (3.42), it gives

$$\dot{\phi} = -\frac{E}{M} = \mp\frac{1}{\sqrt{-L}}\,, \tag{3.57}$$

which can be integrated to obtain the total backward time jump for a particle in a full rotation around CTG, as

$$\Delta\tau = \mp 2\pi\sqrt{-L}\,, \tag{3.58}$$

where $\Delta\tau = (\tau_2 - \tau_1)$ is the backward time jump. Note that, τ_1 and τ_2 are the proper time of the massive particle at $\phi = 0$ and $\phi = 2\pi$ respectively.

The relations given by equations (3.56) and (3.58) have to be fulfilled by every CTGs present in stationary, axisymmetric, rotating metric as in Eq. (3.38). These are however not the sufficient conditions for the CTCs which are non-geodesics.

3.5.3 Examples on the generalized formulation

In this section, the above generalization is imposed and tested for a couple of well-established axially symmetric solutions allowing CTCs.

3.5.3.1 Gödel's universe

The metric that describes Gödel's cosmological universe is given by [235]

$$ds^2 = 4a^2\left[dt^2 - dr^2 + \left(sinh^4 r - sinh^2 r\right)d\phi^2 + 2\sqrt{2}sinh^2 r\,d\phi dt - dz^2\right]. \tag{3.59}$$

Considering a different set of coordinates (t', r, ϕ), and suppressing the z coordinate, one gets

$$ds^2 = 2\omega^{-2}\left[-dt'^2 + dr^2 - \left(sinh^4 r - sinh^2 r\right)d\phi^2 + 2\sqrt{2}sinh^2 r\,d\phi dt\right], \tag{3.60}$$

where a and ω are arbitrary positive numbers. Now, in terms of the general metric (3.38), the metric components are: $F(r) = 2\omega^{-2}$, $M(r) = 2\omega^{-2}\sqrt{2}sinh^2 r$, $L(r) = -2\omega^{-2}(sinh^4 r - sinh^2 r)$, $H_1(r) = 2\omega^{-2}$.

In this cosmological solution, Gödel investigated that a causality violating closed timelike loop appears at $r > ln(1+\sqrt{2})$. Alongside, the CTC present here is non-geodesic in nature [2, 243]. Note that, a simple technique to check whether a spacetime

allows for the CTGs is investigated by Grøn and Johannesen in [262], where the geodesic confinement in Gödel's solution is extensively examined by Novello *et al.* [249].

To eliminate the potential for zero-AM particles to travel within these CTCs, the confinement of AM-less photon trajectories are investigated. This analysis delineates the limitation on the movement of massive particles without angular momentum beyond the confinement boundary.

Now to check the confinement of zero AM photons, Eq. (3.48) is used as

$$-2\omega^{-2}(sinh^4 r - sinh^2 r) > 0\,, \tag{3.61}$$

which simplifies to $r < ln(1+\sqrt{2})$. This finding implies that the farthest radial extent achievable by AM-less photons is $ln(1+\sqrt{2})$. Consequently, it decisively eliminates the potential for movement of timelike particles devoid of angular momentum into the region containing closed timelike curves (CTCs).

3.5.3.2 Bonnor's rotating dust

Bonnor's line element of rotating dust cloud [239] is given by

$$ds^2 = -dt^2 + 2nd\phi dt + (r^2 - n^2)d\phi^2 + e^{\mu}(dr^2 + dz^2)\,, \tag{3.62}$$

where

$$n = \frac{2hr^2}{R^3}\,, \qquad \mu = \frac{h^2r^2(r^2-8z^2)}{2R^8}\,, \qquad R^2 = (r^2+z^2)\,. \tag{3.63}$$

Bonnor described 'h' to be the rotation parameter. Therefore, in terms of the general metric (3.38), the metric components are: $F(r,z) = 1$, $M(r,z) = n$, $L(r,z) = (r^2 - n^2)$, and $H_1(r,z) = H_2(r,z) = e^{\mu}$. Note that this spacetime allows for non-geodesic closed timelike curves [262].

The region where causality violation occurs, resulting in the appearance of CTCs, can be determined by the condition $L < 0$. At the position $z = 0$, this condition transforms into

$$r^4 < 4h^2\,. \tag{3.64}$$

Conversely, the confinement of AM-less photons at $z = 0$ is characterized by $L > 0$, which can be expressed as

$$r^4 > 4h^2\,. \tag{3.65}$$

Thus, it demonstrates the absence of movement of angular momentum-less timelike massive particles in the vicinity of closed timelike curves.

3.6 Discussions

There are a number of different observations made in this chapter which are as follows:

1. Opher *et al.* noted that within the van Stockum solution, *"The gravitational collapse of a cylinder with rotation can never develop singularities at the axis"* [260].

The present study reveals that any particle confined within the dust cylinder cannot escape, assuming the radius of the dust cylinder R always exceeds r_{max}. While the dust cylinder may not exhibit the characteristics of a typical black hole, to external observers, it perpetually presents itself as a perfectly black cylindrical region.

2. In the van Stockum solution, there may exist unphysical imaginary timelike geodesic solutions. However, by imposing the same parameter choices, physically realizable null trajectories can be identified. Interestingly, in these regions, only photons are permitted to exist, leading to the emergence of what is termed as a "pure null region."

3. For photons with energies exceeding $\frac{P_\phi}{2r}$ (where r represents the radial position of the $ar = 1$ boundary) in van Stockum space, the $ar = 1$ boundary consistently lies between r_{min} and r_{max}. When the energy equals $\frac{P_\phi}{2r}$, r_{min} aligns with the $ar = 1$ boundary. However, for energies below $\frac{P_\phi}{2r}$, the $ar = 1$ boundary is no longer restricted within r_{min} to r_{max}. Instead, the cylindrical shell ranging from r_{min} to r_{max} shifts outward to the $ar = 1$ boundary. These latter two scenarios are only applicable in a pure null region.

4. In the van Stockum interior, the region of spacetime where causality is violated (i.e., $ar > 1$) spans from $ar = 1$ to r_{max}, which corresponds to Region III as described. This region exclusively accommodates particles with non-zero AM, implying that particles without AM are entirely prohibited from traversing CTCs. Thus, angular momentum emerges as a crucial factor for determining the eligibility of particles to move along closed timelike trajectories.

5. The absence of particles without angular momentum in closed timelike geodesics can be demonstrated more straightforwardly. In van Stockum, this is expressed by equation (3.37), with the general confirmation provided in equation (3.55).

6. The preceding section's comprehensive overview affirms that axially symmetric rotating spacetimes accommodating CTCs also exhibit spacetime dragging. This phenomenon is contingent upon the qualitative behaviour of the metric coefficients [509]. Our investigation delves into the impact of spacetime dragging on particle motion along closed timelike orbits. Spacetime dragging is the mechanism responsible for inducing rotational motion in particles devoid of angular momentum. However, this dragging effect is prohibited within closed timelike curves. Instead, particles traverse CTCs solely due to their angular momentum.

7. Referring to equations (3.26) and (3.50), it is evident that the angular velocity of particles within closed timelike curves (CTCs) does not incorporate distinct spacetime dragging terms. This suggests that the formation of CTCs may not be contingent upon spacetime dragging. A comparable rationale can be identified in the examination of counter-rotation within CTCs [291, 510].

8. A concise investigation into closed timelike geodesics is conducted, wherein the backward time jump and the energy required for traversal within a CTG are determined. The time jump remains constant, causing the particle to return to its original state with each rotation, akin to an endless cycle that never fascinates a time traveler. The magnitude of the jump increases as the loop is extended further away from the axis in the interior solution of van Stockum.

9. The outcomes of the general description are applied to several familiar spacetimes like Gödel and Bonnor metrics. It is demonstrated that all spacetimes conforming to the format described in equation (3.38) prohibit angular momentum-less particles from traversing closed timelike orbits.

CHAPTER 4

ON THE ROLE OF CLOSED TIMELIKE CURVES AND CONFINEMENT STRUCTURE AROUND KERR-NEWMAN SINGULARITY

4.1 Prelude

In the realm of Einstein's General Relativity (GR), the study of geodesic motion around black holes is a captivating field, intricately linked to various astronomical phenomena such as black hole shadows, light deflection, and planetary perihelion shifts. With upcoming advancements in experimental capabilities, including the LIGO [511], the Event Horizon Telescope [512], and others like ATHENA [513], SKA [514], and eLISA [515] are poised to delve into the mysteries surrounding black hole horizon phenomena with unprecedented precision.

The Kerr-Newman solution of the Einstein-Maxwell field equations characterizes the gravitational field of a charged rotating black hole [274]. Notably, it can also describe a naked singularity under specific metric parameter limits. This solution can reduced to the Kerr [237], Schwarzschild, and Reissner-Nordström [516, 517] metrics with tailored choices of the black hole's angular momentum (a) and electric charge (Q). While many astrophysical black hole candidates are anticipated to exhibit rotation, they are mostly expected to possess negligible or no net charge. However, certain accretion scenarios suggest the plausibility of black holes with both net charge and spin [518–520], thus igniting recent interest in Kerr-Newman black holes. This solution is significant both phenomenologically and conceptually as it offers an idealized framework to explore the interplay between gravitoelectric, gravitomagnetic, and electromagnetic aspects of gravity. For an in-depth review of the Kerr-Newman metric, readers can refer to [521].

Investigating the gravitational field and associated phenomena within a specific

metric entails examining the geodesic motion of test particles in the spacetime. Various facets of geodesic motion in Kerr-Newman geometry have been explored over time, for instance, refer to [522–539]. Pugliese *et al.* specifically studied equatorial orbits of neutral test particles, distinguishing between black hole and naked singularity scenarios using an effective potential approach [540]. In this study, of particular note is the existence of an empty region surrounding the central singularity, preventing test particles from interacting with the singular point, which holds relevance to the present chapter.

In this chapter, the motion of particles surrounding the naked singularity and black hole within Kerr-Newman spacetime is delved into, with particular focus on closed timelike orbits. It is obtained that both the naked singularity (NS) and black hole (BH) are shrouded by regions where causality is violated, effectively concealing the singularity. Moreover, the Cauchy surface consistently resides within the inner horizon in non-extremal black holes. For neutral particles and those possessing charge with same polarity as the source, only particles with positive angular momentum are permitted to traverse the closed timelike curves. Conversely, for particles with opposite polarity charge to the source, the significant Coulomb attraction draws all particles within the Cauchy surface, enabling their presence in closed timelike curves regardless of their angular momentum. Nonetheless, in both the NS and BH scenarios (both extremal and non-extremal), test particles are confined at a substantial distance from the singular point, thus ensuring the existence of an empty region surrounding the singularity that prevents particle interaction with it. The radius of this empty region, contingent upon source parameters and characteristics of particles, is scrutinized through a precise expression.

The chapter commences with a concise overview of the Kerr-Newman geometry in Section 4.2, emphasizing horizon features and the presence of closed timelike curves (CTCs). Following this, Section 4.3 delves into the derivation of geodesic equations for neutral particles. Sections 4.4 and 4.5 are dedicated to a detailed examination of geodesic motion and the behaviour of neutral test particles within CTCs for both naked singularities and black holes, including non-extremal and extremal cases. The study of the expression for confinement radius is conducted in section 4.6. Moving on to Section 4.7, a transition is made to the discussion of the motion of charged particles, synthesizing the concepts introduced earlier. Finally, the chapter concludes with a summary of findings in Section 4.8.

4.2 Kerr-Newman Geometry

The Kerr-Newman spacetime, which is asymptotically flat, axisymmetric, and stationary, can be determined from the solution of the Einstein-Maxwell field equation:

$$G_{\mu\nu} = -2\left(g^{\alpha\beta}F_{\mu\alpha}F_{\nu\beta} - \frac{1}{4}g_{\mu\nu}F_{\alpha\beta}F^{\alpha\beta}\right), \tag{4.1}$$

where $G_{\mu\nu}$ and $F^{\mu\nu}$ represent the Einstein tensor and electromagnetic tensor respectively. The metric is expressed in the Boyer-Lindquist form as

$$ds^2 = \frac{\rho^2}{\Delta}dr^2 + \frac{sin^2\theta}{\rho^2}\left[(r^2+a^2)d\phi - adt^2\right]^2 - \frac{\Delta}{\rho^2}\left[asin^2\theta d\phi - dt\right]^2 + \rho^2 d\theta^2\,, \tag{4.2}$$

with

$$\Delta = r^2 - 2Mr + a^2 + Q^2\,, \tag{4.3}$$

$$\rho^2 = r^2 + a^2 cos^2\theta\,. \tag{4.4}$$

Here, M denotes the mass (always assumed to be greater than zero), a represents the angular momentum of the spacetime, and Q stands for the electric charge of the gravitational source. The metric description simplifies to the Schwarzschild metric when $Q = a = 0$, while the Kerr and Reissner-Nordström metrics are obtained by setting $Q = 0$ and $a = 0$, respectively.

Horizons are formed in the spacetime when the condition $\Delta = 0$ is satisfied, resulting in $r_\pm = M \pm \sqrt{M^2 - a^2 - Q^2}$. Here, r_+ and r_- denote the outer horizon (the event horizon for Kerr-Newman black hole) and inner horizon, respectively. However, the null coordinate expression of the metric shows no singularity at $\Delta = 0$. Although understanding the physical significance of the coordinate singularity is crucial in the geometry context, the only genuine singularity of the spacetime occurs at $r = 0$.

At this juncture, three observations can be inferred from the expression of $r_\pm$ [521]:

1. When $M^2 > (a^2 + Q^2)$, both the inner and outer horizons coexist, with the singularity concealed behind the event horizon. The region within the black hole, delineated by $r < r_+$, remains hidden from an observer situated at infinity.

2. In the scenario where $M^2 = (a^2 + Q^2)$, the inner and outer horizons coincide at $r = M$, defining the Kerr-Newman extremal black hole.

3. When $M^2 < (a^2 + Q^2)$, the event horizon is absent, and the geometry features a naked singularity. A crucial implication of this condition is the breach of causality, where closed timelike orbits are not ensconced within an event horizon.

In a stationary, axisymmetric spacetime, describing a closed timelike curve involves considering $g_{\phi\phi}$ to be negative, along with constant t, r, θ [224]. In the Kerr-Newman metric, this condition translates to the expression:

$$r^4 + a^2(r^2 + 2Mr - Q^2) < 0\,, \tag{4.5}$$

when considering a curve in the equatorial slice of the geometry. The boundaries of these regions are determined explicitly by solving $r^4 + a^2(r^2 + 2Mr - Q^2) = 0$, yielding radii given by the roots:

$$r_\pm^+ \equiv \frac{1}{2}\sqrt{\zeta} \pm \frac{1}{2}\sqrt{-2a^2 - \zeta - \frac{4a^2M}{\sqrt{\zeta}}}\,, \tag{4.6}$$

$$r_\pm^- \equiv -\frac{1}{2}\sqrt{\zeta} \pm \frac{1}{2}\sqrt{-2a^2 - \zeta + \frac{4a^2M}{\sqrt{\zeta}}}\,, \tag{4.7}$$

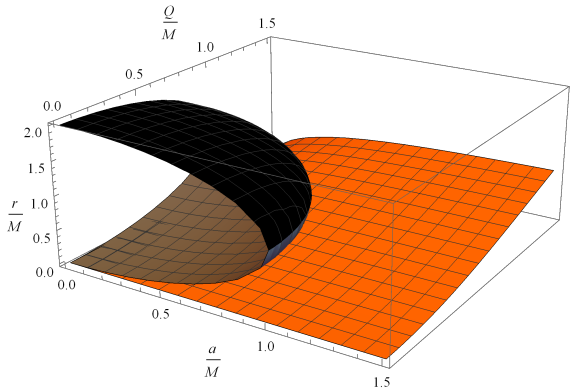

Figure 4.1: The boundary of the CTC r_+^- (orange surface), along with the inner (gray surface) and outer (black surface) horizons, is exhibited as a function of $a/M \in (0, 1.5)$ and $Q/M \in (0, 1.5)$. In the Kerr-Newman black hole, r_+^- always resides within the event horizon, while in naked singularity, the CTC is open, covering the central singularity at $r = 0$.

where

$$\zeta \equiv -\frac{2a^2}{3} + \frac{2^{1/3}(a^4 - 12a^2Q^2)}{3\left(2a^6 + 108a^4M^2 + 72a^4Q^2 + \sqrt{-4(a^4 - 12a^2Q^2)^3 + (2a^6 + 108a^4M^2 + 72a^4Q^2)^2}\right)^{1/3}}$$
$$+ \frac{\left(2a^6 + 108a^4M^2 + 72a^4Q^2 + \sqrt{-4(a^4 - 12a^2Q^2)^3 + (2a^6 + 108a^4M^2 + 72a^4Q^2)^2}\right)^{1/3}}{3 \times 2^{1/3}} . \tag{4.8}$$

Therefore, when considering a CTC within the Kerr geometry, only Eq. (4.8) undergoes a change in value when $Q = 0$, while Eqs. (4.6) and (4.7) remain unchanged. It is observed that for fixed source parameters (a, Q, M), both ζ and M are always positive, resulting in complex radii for $r_\pm^+$. Conversely, r_+^- yields real positive values, and r_-^- provides real negative values. The behaviour of r_+^- in relation to the inner and outer horizons is depicted in Fig. 4.1. It is noteworthy that until the inner and outer horizons coincide, the boundary of the CTC, represented by r_+^-, always remains within the horizons. Beyond this point, the values of source parameters a/M and Q/M determine the presence of a naked singularity, where the horizons vanish. Additionally, as Q/M decreases, the CTC region moves closer to the central singularity, and as $Q/M \to 0$, it approaches the singularity at $r = 0$. This trend is similarly observed for $a/M \to 0$. Consequently, for both Kerr and Reissner-Nordström cases, the causality-violating region is situated near the singularity. However, the Cauchy surface, indicated by the orange surface, always remains within the inner horizon (gray surface), representing the type of particle motion possible within the inner horizons of a rotating black hole.

For CTC formation, the azimuthal coordinate ϕ must exhibit timelike characteristics while keeping other coordinates (t, r, θ) constant. Therefore, according to Eq. (4.2), the spacetime metric becomes:

$$ds^2 = \frac{r^4 + a^2(r^2 + 2Mr) - a^2Q^2}{r^2} d\phi^2 . \tag{4.9}$$

For ϕ to be timelike, the source charge Q must significantly influence, satisfying relation (4.5). The CTC region, i.e., causality violating region is defined by $r < r_+^-$. Utilizing the Lagrangian formulation $\mathcal{L} = \frac{1}{2} g_{\alpha\beta}\dot{x}^\alpha \dot{x}^\beta$, within the CTC region, one may have $2\mathcal{L} = \bar{A}\dot{\phi}^2$, where $\bar{A} = \frac{r^4+a^2(r^2+2Mr)-a^2Q^2}{r^2}$. Consequently, the angular momentum (L_c) of a timelike particle is conserved and given by:

$$L_c = \bar{A}\dot{\phi}\,, \tag{4.10}$$

where $\bar{A}$ is negative in the CTC region, ensuring the timelike nature of the angular coordinate ϕ. Hence, the angular velocity $\dot{\phi}$ of any test particle relies on its angular momentum as:

• Test particles with positive angular momentum ($L_c > 0$) exhibit counter-rotating angular velocity, facilitating CTC formation, as the CTC counter-rotates with the source spin, opposing the rotation direction of the singularity. Detailed discussions can be found in [291].

• Conversely, test particles with negative angular momentum ($L_c < 0$) demonstrate co-rotating angular velocity, hindering CTC formation.

Additionally, it is important to clarify that the presence of timelike geodesics or curves within the region $r < r_+^-$ does not necessarily imply causality violation to form closed timelike geodesics (CTGs) (for further details, see references [541–543]).

4.3 The Equatorial Geodesics

To derive the geodesic equations for the metric (4.2), one can employ the Lagrangian approach. In this study, sole focus is placed on equatorial geodesic motion, with θ being set to $\pi/2$. Consequently, the geodesic equation associated with θ is omitted throughout our analysis. The first-order geodesic equations are obtained from the canonical momentum corresponding to the Euler-Lagrange dynamics as

$$\dot{t} = \frac{E(r^4 + a^2(r^2 + 2Mr - Q^2)) - aL(2Mr - Q^2)}{r^2(r^2 + a^2 - 2Mr + Q^2)}\,, \tag{4.11}$$

$$\dot{\phi} = \frac{aE(2Mr - Q^2) + L(r^2 - 2Mr + Q^2)}{r^2(r^2 + a^2 - 2Mr + Q^2)}\,, \tag{4.12}$$

$$\dot{r}^2 = \frac{\begin{array}{r}(E^2-\mu)\,r^4 + 2Mr^3\mu - (-a^2E^2 + L^2 + a^2\mu + Q^2\mu)\,r^2 \\ + (-aE + L)^2\,(2Mr - Q^2)\end{array}}{r^4}\,. \tag{4.13}$$

In this context, the constants of motion, denoted as $E = -\frac{\partial \mathcal{L}}{\partial \dot{t}} = -g_{\alpha\beta}\xi_t^\alpha u^\beta$ and $L = \frac{\partial \mathcal{L}}{\partial \dot{\phi}} = g_{\alpha\beta}\xi_\phi^\alpha u^\beta$, are associated with the total energy and angular momentum of the test particle with mass μ. These constants are determined by the canonical momentum of the Lagrangian with respect to the time and azimuthal coordinates, where $\xi_t = \partial t$ and $\xi_\phi = \partial\phi$ represent the timelike and spacelike killing vectors, respectively, indicating the space's stationarity and the source's axial symmetry.

Several observations can be made regarding the co-rotation effect and circular motion of test particles in spacetime. For instance, in the ϕ geodesic equation (4.12), setting $L = 0$ yields a non-zero angular velocity $\dot{\phi}$, expressed as:

$$\dot{\phi} = \frac{aE(2Mr - Q^2)}{r^2(r^2 + a^2 - 2Mr + Q^2)} \,. \tag{4.14}$$

This phenomenon can be interpreted as spacetime dragging. Consequently, even when considering $L = 0$, particles lacking angular momentum still exhibit co-rotation with spacetime. Moreover, if the spacetime's angular momentum vanishes ($a = 0$), the dragging effect disappears.

The feasibility of circular motion for test particles can be described through the classical effective potential approach. Test particle dynamics can be likened to one-dimensional classical particle motion within the effective potential $V(r)$. The effective potential for equatorial timelike geodesics is expressed as [14]:

$$V = \frac{-B \pm \sqrt{B^2 - 4AC}}{2A} \,, \tag{4.15}$$

where A, B, and C are derived directly from the radial timelike geodesic equation (i.e., Eq. (4.13)), and are defined as:

$$A = r^4 + a^2(r^2 + 2Mr - Q^2) \,, \tag{4.16}$$
$$B = -2aL(2Mr - Q^2) \,, \tag{4.17}$$
$$C = -\mu r^4 + 2Mr^3\mu - (L^2 + a^2\mu + Q^2\mu)r^2 + L^2(2Mr - Q^2) \,. \tag{4.18}$$

The circular orbits of test particles can be determined by solving the following equations simultaneously:

$$V'(r, L, a, Q) = 0 \,, \qquad \text{and} \qquad V = \frac{E}{\mu} \,. \tag{4.19}$$

Here, the prime symbol denotes differentiation with respect to r.

The primary objective of this chapter is to delineate the motion of test particles associated with both black holes and naked singularities as a function of angular momentum (L). To investigate circular motion dynamics, the condition $V' = 0$ is examined and resolved in terms of angular momentum (AM). The solution is generally expressed as

$$\frac{L_\pm}{\mu} \equiv \frac{1}{r^2}\left[\frac{\mathcal{X} \pm 2M^2\sqrt{\mathcal{Y}}}{\mathcal{Z}}\right]^{1/2} \,, \tag{4.20}$$

where $L = \pm L_\pm$, with

$$\mathcal{X} \equiv r^2\left\{-\left(Q^2 - Mr\right)r^4\left[2Q^2 + (r - 3M)r\right] + a^4\left(Q^2 - Mr\right)\left[2Q^2 - (5M + r)r\right] + a^2\left[2Q^6 + Q^4(r - 11M)r - 2Q^2(r - 2M)r^2(5M + r) + 2Mr^3[r(3M + r) - 6M^2]\right]\right\} \,, \tag{4.21}$$
$$\mathcal{Y} \equiv -a^2\left(Q^2 - rM\right)r^4\left[a^2 + Q^2 + (r - 2M)r\right]^2\left[a^2\left(Q^2 - Mr\right) + \left(2Q^2 - 3Mr\right)r^2\right]^2 \,, \tag{4.22}$$
$$\mathcal{Z} \equiv 4a^2\left(Q^2 - rM\right) + \left[2Q^2 + (r - 3M)r\right]^2 \,. \tag{4.23}$$

The associated energy is derived from Equation (4.19), given by

$$E(\pm L_{\mp}) = \frac{-(\pm L_{\mp})\,(Q^2 - 2Mr) + \sqrt{\begin{array}{l} r^2\left[a^2 + Q^2 + (r-2M)r\right] \times \\ \quad \left(r^2\left(L_{\mp}^2 + r^2\right) + a^2\left[r(2M+r) - Q^2\right]\right) \end{array}}}{r^4 + a^2\left[r(2M+r) - Q^2\right]}. \quad (4.24)$$

In this context, L_+ and L_- respectively represent the positive and negative segments of angular momentum. Pugliese *et al.* briefly examined the well-defined region of energy and angular momentum in orbital coordinates and source parameters, also analyzing regions where circular motion occurs [540]. However, delving into the region of space occupied by circular orbits is not pertinent to the current investigation. Instead, the focus lies on understanding the relationship between the effective potential and angular momentum.

This chapter delves into exploring the space region where geodesic trajectories and closed timelike curves within a Cauchy horizon are feasible. To study motion around CTCs in Kerr-Newman geometry, various techniques are employed, including geodesics in spacetime diagrams, velocity analysis, and effective potentials in radial timelike geodesics. It is well-known from textbook discussions that CTCs manifest in certain rotating spacetimes within specific spatial regions. Despite the complete geodesic structure of a metric, there are constraints for particles with diverse characteristics. In the $r-t$ spacetime diagram, the expression for dt/dr is derived from the geodesic equations (4.11) and (4.13). Trajectories are examined concerning the zero, positive, and negative values of angular momentum (AM) of test particles. Particles with positive AM co-rotate with spacetime, negative AM particles counter-rotate, while those with zero AM only rotate due to spacetime dragging. Without loss of generality, the initial focus is on neutral particle scenarios with positive charge and positive angular momentum of spacetime ($Q > 0$ and $a > 0$), whereas the latter section deals with the motion of charged particles. The discussion commences with horizon-less naked singularities followed by non-extremal and extremal black holes.

4.4 Naked Singularity

In this section, the motion of neutral test particles around the Kerr-Newman naked singularity will be discussed in detail. Focusing on the effective potential and zero AM particles, the solution of the equations

$$V'(r, L, a, Q) = 0\,, \quad \text{and} \quad L = 0\,, \quad (4.25)$$

identifies specific circular motion in the geometry, with the real solution existing solely in the naked singularity. Typically, the gravitational component of the effective potential dictates the motion described by Eq. (4.25), and motion with $L = 0$ occurs only when forces are balanced in the configuration. This phenomenon can be interpreted as a repulsive gravity effect, as discussed in [544].

Furthermore, characterizing particle motion with non-zero angular momentum becomes more intricate in Kerr-Newman (KN) naked singularities. Thus, to prepare for

the study, the radial null geodesic equations for naked singularities are expressed in terms of dt/dr, as

- **Geodesics with zero angular momentum:**

$$\frac{dt}{dr} = \pm \frac{\sqrt{r^4 + a^2(r^2 + 2Mr - Q^2)}}{(r^2 + a^2 - 2Mr + Q^2)}, \tag{4.26}$$

- **Geodesics with non-zero angular momentum:**

$$\frac{dt}{dr} = \pm \frac{E(r^4 + a^2(r^2 + 2Mr - Q^2)) - aL(2Mr - Q^2)}{(r^2 + a^2 - 2Mr + Q^2)\sqrt{\begin{array}{l} E^2r^4 - (-a^2E^2 + L^2)r^2 \\ \quad + (-aE + L)^2(2Mr - Q^2) \end{array}}}. \tag{4.27}$$

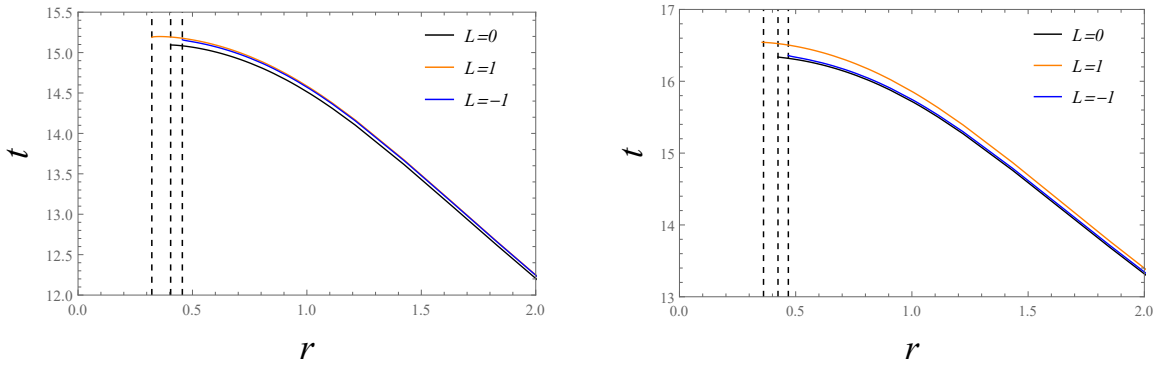

(a) (b)

Figure 4.2: (a) Spacetime diagram illustrating radial null geodesics around naked singularity. Trajectories for photons with both zero and non-zero AM are depicted, where $E = 2$ and $a = Q = M = 1$. The confinement of trajectories with $L = 0$, $L = 1$, and $L = -1$ occurs respectively at $r = 0.405$, $r = 0.322$, and $r = 0.456$, indicated by vertical dashed lines. (b) Spacetime diagram illustrating radial timelike geodesics around naked singularity. Trajectories for massive particles with both zero and non-zero AM are depicted, where $E = 2$, $\mu = 1$, and $a = Q = M = 1$. The confinement of trajectories with $L = 0$, $L = 1$, and $L = -1$ occurs respectively at $r = 0.424$, $r = 0.362$, and $r = 0.468$, indicated by vertical dashed lines.

The spacetime diagram illustrating the numerical integration of Eq. (4.26) and (4.27), is depicted in Fig. 4.2a. For both positive and negative angular momentum values, $L = 1$ and $L = -1$ are selected, along with a photon energy of $E = 2$, and parameters for the naked singularity source, $a = Q = M = 1$. Closed timelike curves emerge for orbital radii $r < 0.405$, directly obtained from r_+^- in Eq. (4.7).

It is worth noting from Eq. (4.26) that trajectories of angular momentum-less photons remain independent of associated particle energy. This behaviour resembles that of angular momentum-less photons in the axisymmetric van Stockum spacetime of the previous chapter. As observed in the figure, these particles are prevented from

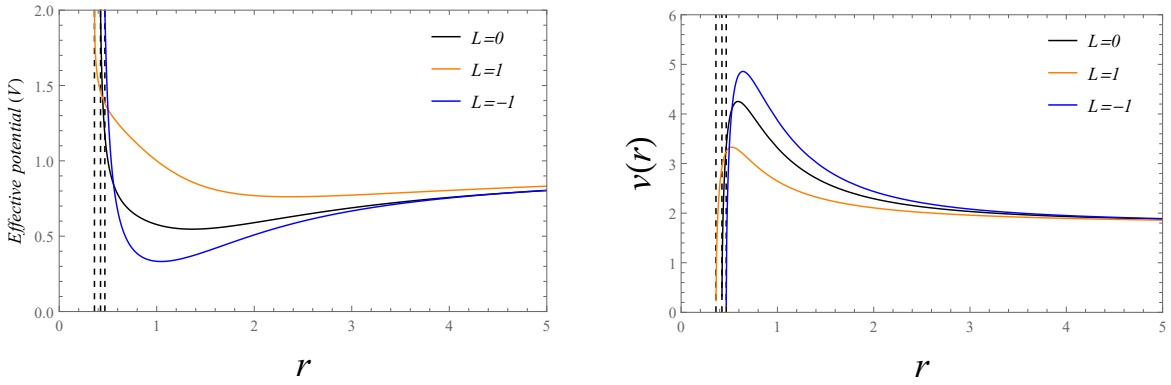

(a) (b)

Figure 4.3: (a) The effective potential and (b) the velocity in terms of proper time for both zero and non-zero AM test particles, with parameters $E = 2$, $\mu = 1$, and $a = Q = M = 1$. The black vertical dashed lines indicate points where the plots reach positive infinity or zero, aligning precisely with the confinement points depicted in Fig. 4.2b.

interacting with the central singularity at $r = 0$, consistently maintaining trajectories at a significant distance from the singular point.

Moreover, upon examination of Fig. 4.2a, it is apparent that zero and negative ($L = -1$) angular momentum photons are respectively confined to $r = 0.405$ and $r = 0.456$, precluding their approach to $r < 0.405$ where CTCs emerge. Thus, it is evident that zero and negative angular momentum photons cannot traverse CTCs. However, positive angular momentum ($L = 1$) photons can traverse up to $r = 0.322$, indicating their presence within CTCs.

4.4.1 Timelike motion

For massive particles, i.e., $\mu \neq 0$, corresponding geodesic equations are written as

- **Geodesics with Zero angular momentum:**

$$\frac{dt}{dr} = \pm \frac{E(r^4 + a^2(r^2 + 2Mr - Q^2))}{(r^2 + a^2 - 2Mr + Q^2)\sqrt{\begin{array}{r}(E^2 - \mu)r^4 + 2Mr^3\mu - r^2\mu(a^2 + Q^2) \\ + a^2E^2(r^2 + 2Mr - Q^2)\end{array}}}, \tag{4.28}$$

- **Geodesics with Non-zero angular momentum:**

$$\frac{dt}{dr} = \pm \frac{E(r^4 + a^2(r^2 + 2Mr - Q^2)) - aL(2Mr - Q^2)}{(r^2 + a^2 - 2Mr + Q^2)\sqrt{\begin{array}{r}(E^2 - \mu)r^4 + 2Mr^3\mu - (-a^2E^2 + L^2 \\ + a^2\mu + Q^2\mu)r^2 + (-aE + L)^2(2Mr - Q^2)\end{array}}}. \tag{4.29}$$

The spacetime diagram depicted by equations (4.28) and (4.29) for massive particles, considering both zero and non-zero AM, is illustrated in Fig. 4.2b. Here, parameters are set to $a = Q = M = 1$, $\mu = 1$ and $E = 2$. For nonzero AM, values of

L are chosen as $L = 1$ and $L = -1$. These trajectories exhibit confinement points, marked by vertical black dashed lines, following the same methodology as in the prior scenario. However, due to their inbound masses, these particles traverse spacetime less extensively compared to photons. Moreover, the plot reveals particle motion within a closed timelike loop. Only test particles with positive AM are capable of crossing the boundary at $r = 0.405$, allowing access to the CTC.

To depict the confinement phenomenon in a physical context, the effective potential approach can be employed. Fig. 4.3a illustrates a plot of the effective potential derived from Eq. (4.15), using the same parameter values as in Fig. 4.2b. The figure reveals that the singularity is enveloped by the classical effective potential, which tends towards positive infinity at the confinement point, thereby preventing timelike geodesics from reaching the singularity.

In the gravitational field context, it is anticipated that a particle falling into the naked singularity from spatial infinity would encounter regions of increasingly stronger gravitational field as it approaches the singularity along the symmetry axis. At the minimum of the effective potential depicted in Fig. 4.3a, the particle experiences maximum gravitational attraction, followed by an increasingly higher order of inner repulsion near the confinement point. Finally, as the particle hits the confinement or inner turning point, the gravitational attraction and the repulsion balances. This phenomenon mirrors the nature of light cones in axial geometry. Qualitatively, the inner region up to the minima behaves as the source of gravity, with spacetime curvature dropping to zero as $r \to \infty$.

Further, Fig. 4.3b presents the velocity attained by the infalling particle in terms of proper time, utilizing the radial four-velocity expression provided by Eq. (4.13). It is evident that particles reach maximum velocity at the minima of effective potential, experiencing the strongest gravitational field. As they approach the singularity, the geometry's peculiar nature causes them to decelerate until they reach zero velocity. Additionally, it is noticeable that the lower minima of the potential attract and repel positive AM particles less strongly than the other two, allowing them to penetrate deeper into spacetime towards the CTC region, unlike zero and negative AM particles.

4.5 Black Hole

In this section, the existence of CTCs and the behaviour of particles traversing them in Kerr-Newman black holes will be explored in detail. CTCs in Kerr-Newman non-extremal black holes are situated inside the inner horizon, rendering them undetectable to observers at infinity. However, accessing the CTC for a particle entails crossing two horizons, where significant spaghettification effects may occur, making the journey challenging. Nonetheless, studying geodesic behaviour and CTCs in rotating black holes is crucial for advancing our understanding of their inner structure.

It is worth noting that while the fundamental geodesic equations for analyzing radial geodesics in Kerr-Newman black holes are akin to those for naked singularities, a condition of $M^2 > (a^2 + Q^2)$ must be met for the chosen source parameters.

Despite the presence of both inner and outer horizons in Kerr-Newman non-extremal

black holes, the spacetime diagram illustrating radial null geodesics concerning an observer at infinity is depicted in the top panel of Fig. 4.4 (computed by numerically integrating Eq. (4.26) and (4.27)). Here, the motions of $L = 0$, $L = 1$, and $L = -1$ are displayed separately for $E = 2$, $a = Q = 1$, and $M = 2$. For these chosen source parameter values, the CTC, inner, and outer horizons manifest at orbital radii of $r_{ctc} = 0.235$, $r_{in} = 0.586$, and $r_{out} = 3.414$, respectively.

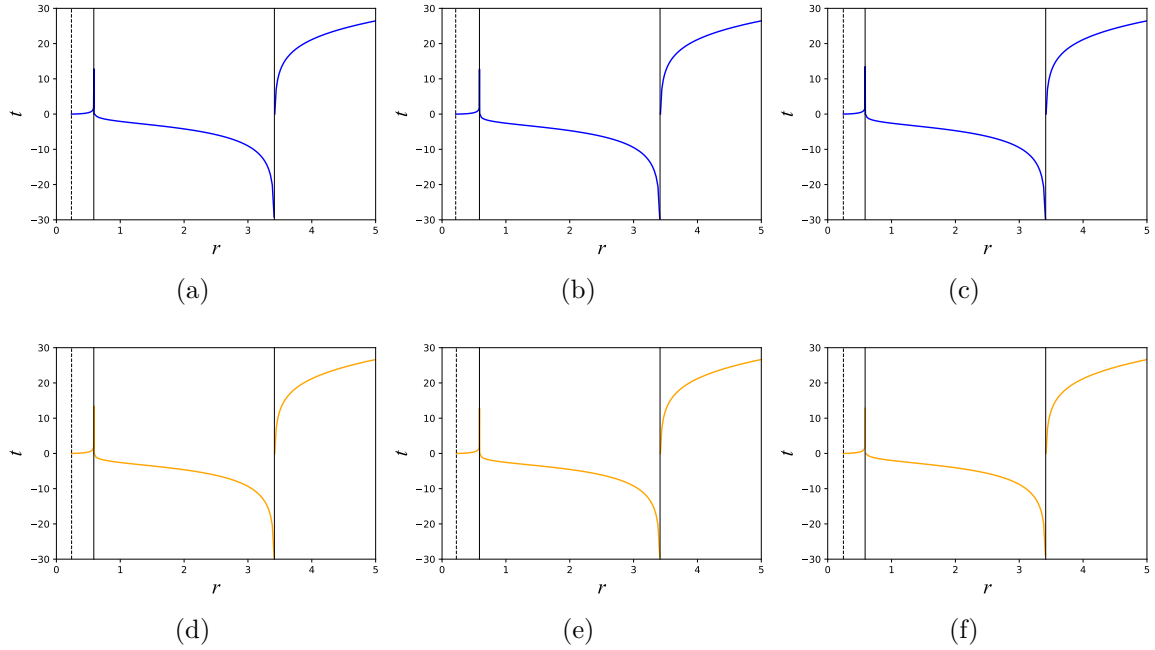

Figure 4.4: TOP PANEL: Spacetime diagrams illustrating radial null geodesics in KN black hole with $r_{ctc} = 0.235$, $r_{in} = 0.586$, and $r_{out} = 3.414$. Plots are presented for $E = 2$, $a = Q = 1$, and $M = 2$, categorized by the angular momentum of photons as (a) $L = 0$, (b) $L = 1$, and (c) $L = -1$. The confinement points are depicted by vertical dashed lines, located at $r = 0.235$, $r = 0.214$, and $r = 0.245$ respectively.
BOTTOM PANEL: Spacetime diagrams illustrating radial timelike geodesics in KN black hole with $r_{ctc} = 0.235$, $r_{in} = 0.586$, and $r_{out} = 3.414$. Plots are presented for $E = 2$, $\mu = 1$, $a = Q = 1$, $M = 2$, categorized by the angular momentum of particles as (d) $L = 0$, (e) $L = 1$, and (f) $L = -1$. The confinement points are depicted by vertical dashed lines, located at $r = 0.238$, $r = 0.224$, and $r = 0.246$ respectively. The left and right solid vertical lines represent inner and outer horizons respectively.

The motion of particles within the KN black hole exhibits complexities unlike those in naked singularities. Trajectories seem to linger infinitely near the horizons, as evident from the figures. It is a well-established concept in textbook literature that in Schwarzschild black holes, infalling geodesics take infinite time to reach the event horizon, yet, in terms of proper time, they reach the singularity within finite time [2,13,14]. A similar phenomenon occurs at the inner and outer horizons of Kerr-Newman black holes, except trajectories avoid approaching the central singularity at the confinement points. Nevertheless, it is apparent that, akin to naked singularities, all three motions

are confined at specific points within the inner horizon, albeit significantly distant from the singularity at $r = 0$. Moreover, particle characteristics within CTCs resemble those of naked singularities. Motion with $L = 0$ is restricted to the CTC's limiting radius, where negative angular momentum photons avoid the radial boundary where CTCs exist. Therefore, zero and negative angular momentum particles are prohibited in closed timelike orbits.

4.5.1 Timelike motion

For the spacetime diagram illustrating radial timelike geodesics, one can adopt Eq. (4.28) and (4.29) for the non-extremal black hole source parameters. Setting $E = 2,\ \mu = 1,\ M = 2$, and $a = Q = 1$, the plots are presented in the bottom panel of Fig. 4.4, featuring distinct frames for motions with $L = 0,\ L = 1$, and $L = -1$.

Similar to the photon trajectories, the trajectories of massive particles exhibit an asymptotic nature, resulting in infinite time consumption at the horizons. While the confinement of particle trajectories confirms the presence of positive AM test particles exclusively in the CTC, the inbound motions depicted in Fig. 4.4 (lower panel) requires refinement in terms of proper time (τ). In this scenario, Eq. (4.13) is directly utilized for timelike motion by rearranging the numerator and denominator as shown below:

$$\frac{d\tau}{dr} = \frac{r^2}{\sqrt{\begin{aligned}(E^2-\mu)r^4 + 2Mr^3\mu - (-a^2E^2 + L^2 + a^2\mu + Q^2\mu)r^2 \\ + (-aE + L)^2(2Mr - Q^2)\end{aligned}}}\,. \tag{4.30}$$

Utilizing numerical integration of this equation, one can accurately compute the radial geodesics without the inconsistency inherent in coordinate time. Fig. 4.5a displays plots for zero and non-zero AM particles using the same source parameters as in Fig. 4.4. Notably, the geodesics exhibit smooth behaviour at the inner and outer horizons, now reaching the confinement points within finite times. This outcome reaffirms that the confinement points coincide with those depicted in Fig. 4.4 (bottom panel), underscoring the inadequacy of coordinate time in describing geodesic motion in black holes.

To delve further into the characteristics of motion within the non-extremal black hole, the intention is to examine the velocity of radially infalling particles, focusing on specific points of interest for particles with varying AM. Fig. 4.5b visualizes the velocities of test particles with different AM, highlighting the turning points where velocity drops to zero and confinement occurs.

In terms of gravitational field dynamics, particles falling from spatial infinity approach the event horizon, where gravitational attraction progressively intensifies. As they near the event horizon, the increasingly strong gravitational field causes spacetime curvature to bend profoundly, preventing geodesics from escaping. The presence of coordinate singularities at the horizons affects coordinate time, as depicted in Fig. 4.4. Considering the outer horizons, an infalling particle experiences negative time infinity, but as one moves leftward, it emerges from negative infinity and approaches positive time infinity at the inner horizon. However, the inconsistency diminishes in terms of

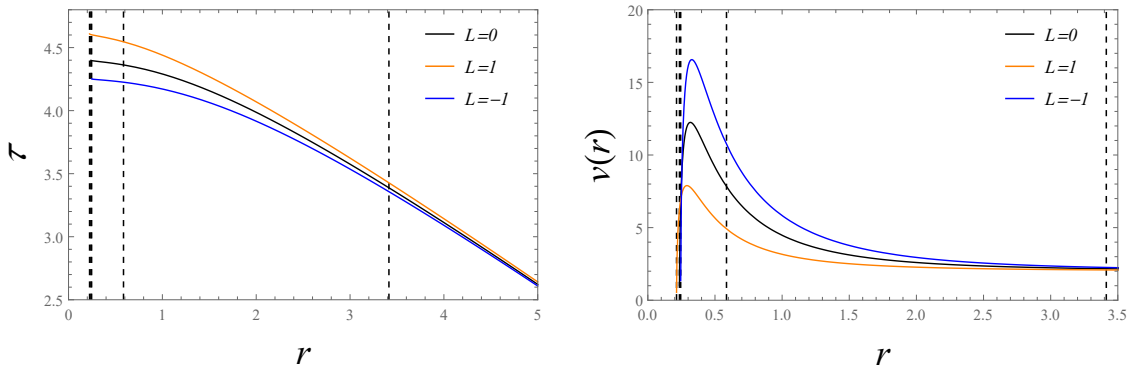

(a) (b)

Figure 4.5: (a) Spacetime diagram illustrating radially infalling particles against proper time (τ) in KN non-extremal black hole. For $E = 2,\ \mu = 1,\ a = Q = 1$ and $M = 2$, trajectories with different AM are depicted with the confinement points. (b) Velocity of the particles in KN non-extremal black hole for the same parameter choices. Velocities with respect to proper time (τ) hit zero at the confinement points. In both of the plots, vertical dashed lines at $r_{in} = 0.586$, and $r_{out} = 3.414$ denote inner and outer horizons, respectively.

proper time, with particle velocity increasing between the outer and inner horizons. Upon crossing the inner horizon, the particle encounters a significantly higher gravitational field, reaching its peak near the Cauchy surface where velocity peaks. Subsequently, the dominance of gravity's repulsive field causes velocity to plummet rapidly, eventually reaching zero at the confinement radius where the gravitational attraction and the inner repulsion balances. Notably, particles are barred from interacting with the central singularity in both non-extremal black holes and naked singularities of KN spacetime. A potent repulsive gravitational effect is presumed to be present, varying in intensity based on particle characteristics, such as angular momentum.

4.5.2 Extremal Black hole

Up to this juncture, our focus has been on non-extremal black holes. However, it is pertinent to explore the scenario with extremal black holes. Examining the Kerr-Newman extremal black hole, where the event horizon is defined by $r_H = M = \sqrt{a^2 + Q^2}$, sheds light on the behaviour of particles near the CTC. Fig. 4.6 illustrates the confinement radius for various AM timelike particles in this context. The figure showcases the numerical solution of Eq. (4.28) and (4.29), considering parameters such as $M = \sqrt{2},\ a = Q = 1,\ \mu = 1$, and $E = 2$. The Cauchy surface emerges at $r = 0.315$, situated within the event horizon, $r_{horizon} = 1.414$. As depicted in the figure, akin to non-extremal black holes, infalling particles experience repulsion before reaching the singularity and are confined to positions significantly distant from $r = 0$. Consequently, only particles with positive angular momentum manage to breach the Cauchy horizon and are capable of traversing the CTC.

4.6 The Confinement radius

A noteworthy implication arising from this discourse concerns the restriction of geodesic paths. The calculation of the confinement radius, typically derived from the real roots of the expression within the square-root term of Eq. (4.13), is of particular interest. Although obtaining an analytical solution poses a challenge, the roots are expressed as follows:

$$r^1_{\pm} \equiv -\frac{B}{4A} - \frac{\sqrt{\delta+\chi}}{2} \pm \frac{1}{2}\sqrt{2\delta - \chi - \frac{\epsilon}{4\sqrt{\delta+\chi}}}\,, \tag{4.31}$$

$$r^2_{\pm} \equiv -\frac{B}{4A} + \frac{\sqrt{\delta+\chi}}{2} \pm \frac{1}{2}\sqrt{2\delta - \chi + \frac{\epsilon}{4\sqrt{\delta+\chi}}}\,; \tag{4.32}$$

where [1]

$$\chi = \frac{2^{1/3}\alpha}{3A\left(\beta + \sqrt{-4\alpha^3+\beta^2}\right)^{1/3}} + \frac{\left(\beta + \sqrt{-4\alpha^3+\beta^2}\right)^{1/3}}{3\times 2^{1/3}A}\,,$$
$$\delta = \frac{B^2}{4A^2} + \frac{2F}{3A}\,,$$
$$\epsilon = -\frac{B^3}{A^3} - \frac{4BF}{A^2} - \frac{8G}{A},$$
$$\alpha = F^2 - 3BG - 12AH\,,$$
$$\beta = -2F^3 + 9BFG + 27AG^2 - 27B^2H - 72AFH\,,$$
$$A = E^2 - \mu\,,$$
$$B = 2M\mu\,,$$
$$F = -a^2E^2 + L^2 + (a^2+Q^2)\mu\,,$$
$$G = 2M(-aE+L)^2\,,$$
$$H = Q^2(-aE+L)^2\,.$$

Depending on parameter selections, equations (4.31) and (4.32) consistently yield two complex roots, one positively definite and one negatively definite real root. Of these, only the positive real root is physically meaningful and is utilized exclusively throughout the analysis to precisely determine the confinement radius of geodesics within both black hole and naked singularity contexts. Generally, r^1_+ serves as the positive definite confinement radius.

Let us delve deeper into the minimum confinement radius, which signifies the maximum radial extent of particles towards the singularity. It is crucial to mention the critical point $aE = L$ at which r^1_+ terminates for photons. However, one may visualize the dependence of the confinement radius on the angular momentum of test particles while keeping other parameters constant. The results for naked singularities

[1] It is important to note that the A and B mentioned here are distinct from those in the effective potential, as outlined by Eq. (4.15).

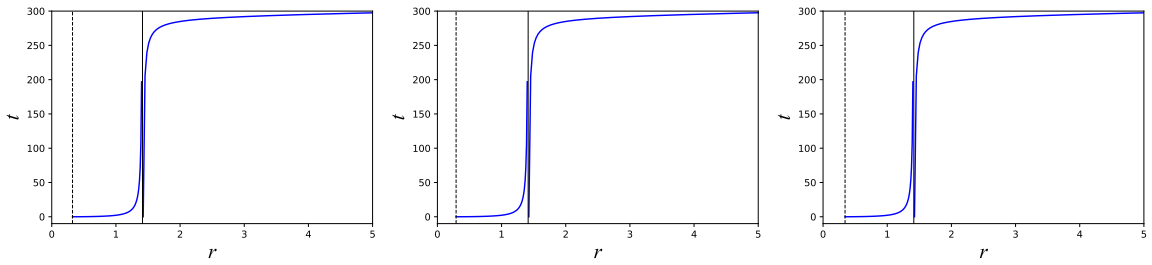

(a) (b) (c)

Figure 4.6: Spacetime diagrams illustrating radial timelike geodesics in KN extremal black hole with $r_{ctc} = 0.315$ and $r_{horizon} = M = 1.414$. Plots are presented for $E = 2,\ \mu = 1,\ a = Q = 1,\ M = \sqrt{2}$, categorized by the angular momentum of particles as (a) $L = 0$, (b) $L = 1$, and (c) $L = -1$. The confinement points are depicted by vertical dashed lines, positioned at $r = 0.324$, $r = 0.291$, and $r = 0.343$ respectively. The solid vertical line represents the event horizon.

are depicted in Fig. 4.7a. It reveals an empty region around the singularity where the minimum confinement radius occurs at $L = 1.4437$. The value of r_+^1 is complex for angular momenta around $L = aE = 1.6$, ranging from $L = 1.52$ to $L = 1.755$. Interestingly, this range coincides with the transition of r_+^2 from complex to real values. This missing information is incorporated in Fig. 4.7a using r_+^2. Additionally, as $L > aE$, the confinement radius gradually increases, surpassing the CTC radius after a certain threshold, indicating the absence of particles in the CTC region for those angular momentum values.

Fig. 4.7b displays the corresponding plot for black holes. Here, r_+^1 becomes complex within the range $L = 1.522$ to $L = 1.73$, with the minimum confinement radius, i.e., 0.17735 occurring at $L = 1.4437$. Similarly, r_+^2 is plotted within the complex range. The angular momentum value $L = 1.4437$ is considered critical for $a = 0.5$ and $E = 3.2$ for both naked singularities and black holes. However, a crucial observation from this investigation is that positive angular momentum alone is not always sufficient for a particle to traverse the CTC. For significantly small positive angular momentum values (i.e., $L << aE$) in timelike particles, they cannot pass through the Cauchy surface. Similarly, the same holds true for any timelike particle with $L > aE$ in the interior of a black hole, albeit for only certain values in naked singularities.

4.7 Motion of charged particles

Since the dynamics of neutral test particles have been extensively studied, attention is now directed towards examining the behaviour of charged particles in the Kerr-Newman geometry. The Lagrangian density for a test particle with mass μ and charge q moving within the background described by the line element in Eq. (4.2) is expressed as

$$\mathcal{L} = \frac{1}{2} g_{\alpha\beta} \dot{x}^\alpha \dot{x}^\beta + \epsilon A_\alpha x^\alpha \,, \tag{4.33}$$

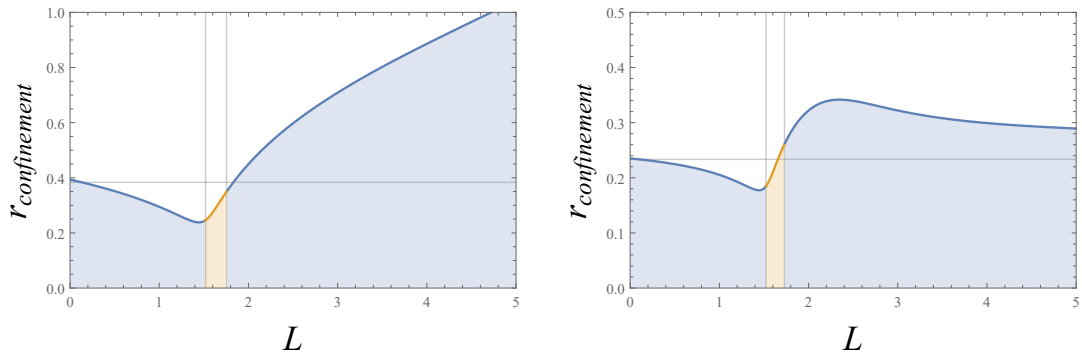

(a) (b)

Figure 4.7: (a) Variation of the confinement radius with the angular momentum of test particles in naked singularity for $\mu = 1$, $M = Q = 1$, $a = 0.5$, and $E = 3.2$. At $L = 1.4437$, the confinement radius $r_{\text{confinement}}$ reaches its minimum value of 0.23809, resulting in a void encircling the singularity. (b) A similar plot for the interior geometry of a non-extremal black hole with $\mu = 1$, $M = 2$, $Q = 1$, $a = 0.5$, and $E = 3.2$. The minimum confinement radius $r_{\text{confinement}}$ is 0.17735, occurring at $L = 1.4437$. In both plots, the blue and orange lines represent r_+^1 and r_+^2 respectively, while the horizontal gridline indicates the CTC radius.

where A_α represents the components of the electromagnetic 4-potential with $A = \frac{Q}{r}dt$, and $F = dA = -\frac{Q}{r^2}dt \wedge dr$. Here, the overdot notation signifies differentiation with respect to proper time, and the specific charge is denoted as $\epsilon = q/\mu$. The equations of motion can be derived using the Euler-Lagrange equation, yielding

$$\dot{x}^\alpha \nabla_\alpha \dot{x}^\beta = \epsilon F^\beta_\gamma \dot{x}^\gamma \,. \tag{4.34}$$

After a series of calculations, the geodesic equations are obtained in terms of conserved quantities (L and E), expressed as follows:

$$\dot{t} = -\frac{aL(2Mr - Q^2)}{r^2(r^2 - 2Mr + a^2 + Q^2)} + \frac{r^4 + a^2(r^2 + 2Mr - Q^2)}{r^2(r^2 - 2Mr + a^2 + Q^2)}\left(E + \frac{\epsilon Q}{r}\right) , \tag{4.35}$$

$$\dot{\phi} = \frac{L(r^2 - 2Mr + Q^2)}{r^2(r^2 - 2Mr + a^2 + Q^2)} + \frac{a(2Mr - Q^2)}{r^2(r^2 - 2Mr + a^2 + Q^2)}\left(E + \frac{\epsilon Q}{r}\right) , \tag{4.36}$$

$$\dot{r}^2 = \frac{\begin{array}{c}(Er\mu + qQ)^2(r^4 + a^2(r^2 + 2Mr - Q^2)) + 2aL\mu r(Er\mu + qQ)(Q^2 - 2Mr) \\ + r^3\mu(r\epsilon\mu - 2qQ)(r^2 - 2Mr + a^2 + Q^2) - L^2r^2\mu^2(r^2 - 2Mr + Q^2)\end{array}}{r^6\mu^2} . \tag{4.37}$$

Here, the derivations of the effective potential are skipped, which can be acquired through a straightforward method or by following the steps outlined in section 4.3. Instead, the focus is shifted directly to the expressions necessary for constructing the

spacetime diagram. After dividing Eq. (4.35) by (4.37), the resulting expression is formulated as:

$$\frac{dt}{dr} = \pm \frac{\left[(r^4 + a^2(r^2 + 2Mr - Q^2))(Er + \epsilon Q) - aLr(2Mr - Q^2)\right]\mu}{(r^2 - 2Mr + a^2 + Q^2)} \cdot \tag{4.38}$$
$$\times \sqrt{\begin{array}{l}(Er\mu + qQ)^2(r^4 + a^2(r^2 + 2Mr - Q^2)) \\ \quad + 2aL\mu r(Er\mu + qQ)(Q^2 - 2Mr) + r^3\mu(r\epsilon\mu - 2qQ) \\ \quad\quad \times (r^2 - 2Mr + a^2 + Q^2) - L^2r^2\mu^2(r^2 - 2Mr + Q^2)\end{array}}$$

The numerical integration of this equation yields spacetime diagrams visualized in Fig. 4.8. Utilizing the same source parameters as detailed in sections 4.4 and 4.5, the effects of charged particles are examined. Notably, when test particles carry positive charges, such as $q = +1$ (with a source charge $Q = +1$), their behaviour mirrors that of neutral test particles. In both the naked singularity and black hole scenarios, the gravitational force, originating from the inner region of the geometry, increases as the particle approaches the singularity from spatial infinity. The presence of positive AM enables particles to co-rotate with the spacetime, offering an additional impetus that allows them to withstand gravitational repulsion better in the inner region, consequently moving further towards the singularity. This interaction between gravitational and electromagnetic forces is particularly pronounced when particles carry positive charges. The Coulomb interaction introduces additional repulsion, causing the confinement radii to expand, except for counter-rotating (negative AM) particles. Surprisingly, for negative AM particle motion, gravitational repulsion and electromagnetic repulsion act oppositely, leading to inward movement of the confinement radii. Despite identical charges causing repulsion, counter-rotation generates an inward pull that counters gravitational repulsion, resulting in inward movement of the confinements.

However, particles with positive AM still manage to cross the Cauchy radius and traverse the CTC. In the case of the naked singularity, particles with $L = +1$ reach a radial position of $r = 0.4039$, just inside the CTC region at $r < 0.4047$. Similarly, in the black hole scenario, these particles reach up to $r = 0.2351$, within the CTC region at $r < 0.2354$.

For negatively charged particles ($q = -1$) interacting with a positively charged source ($Q = +1$), their behaviour contrasts significantly with neutral particles. In this scenario, particles are strongly attracted towards the inner region, with negative AM particles experiencing the strongest attraction. This phenomenon can be understood through Coulomb's law, where particles of the same charge repel each other, but attract when the charges are opposite. Consequently, both the confinement radii for naked singularities and black holes are notably pulled inward. Unlike the neutral case, negative AM particles are confined closest to the center, followed by particles with no AM, and then positive AM particles at the outermost position. This observation suggests that Coulombic interaction dominates over gravitational interaction, which was predominant in the dynamics of neutral particles. Importantly, all particles now have the capability to traverse CTCs in both naked singularities and black holes. By comparing the position of the CTCs (appearing inside radii of $r = 0.4047$ for naked singularities and $r = 0.2354$ for black holes) with the confinement radii provided in Fig. 4.8 for negatively charged particles, the presented results can be verified.

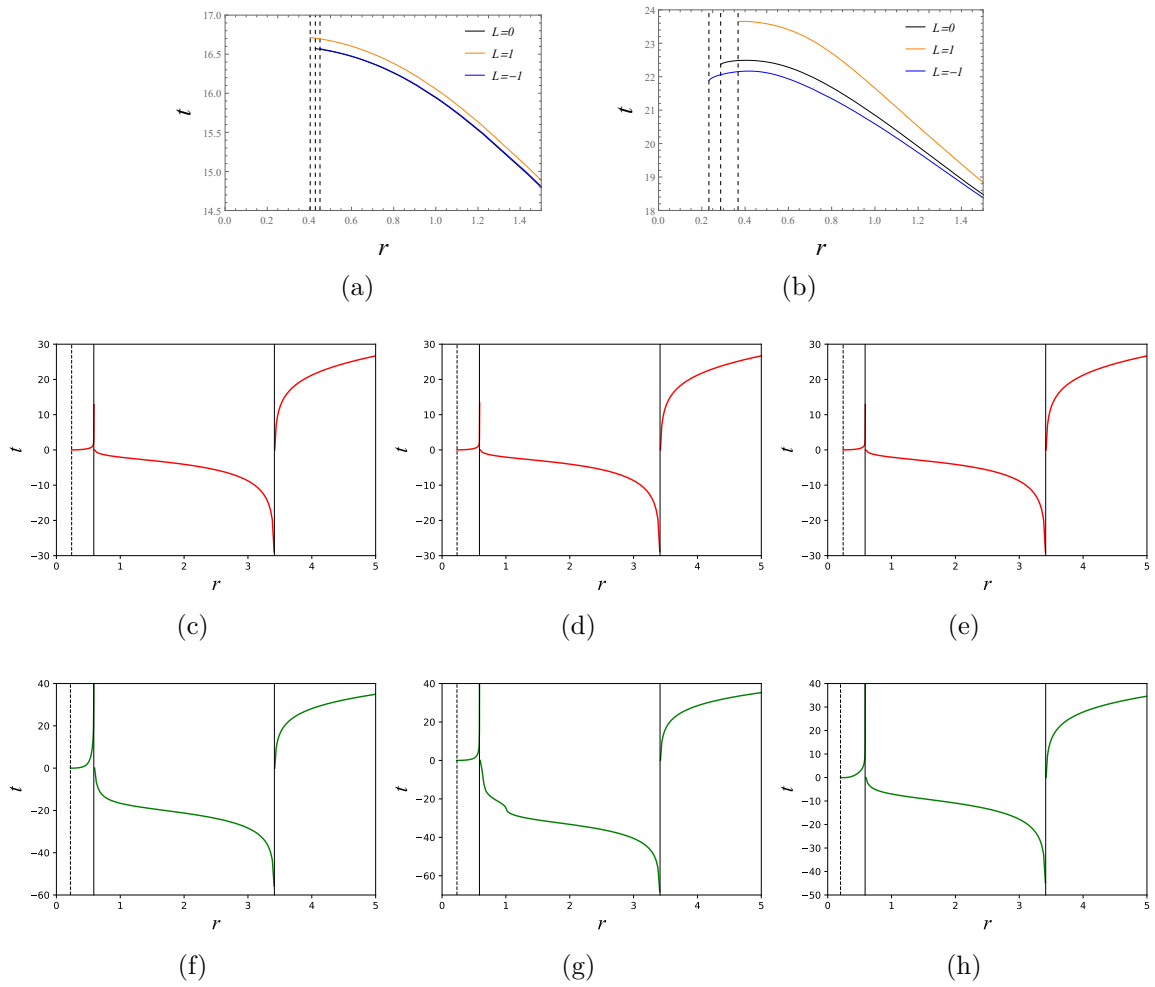

Figure 4.8: TOP PANEL: Spacetime diagrams illustrating radial timelike geodesics of charged particles in KN naked singularity. (a) Trajectory of positive charged particles ($q = +1$) with different AM for $M = a = Q = 1$, $\mu = \epsilon = 1$ and $E = 2$. The confinement points of $L = 0$, $L = 1$ and $L = -1$ motions are located at $r = 0.428$, $r = 0.4039$ and $r = 0.450$ respectively. (b) Corresponding plot for negative charged particles ($q = -1$) with confinement points at $r = 0.287$, $r = 0.367$ and $r = 233$ respectively.
MIDDLE PANEL: Spacetime diagrams of positive charged particles ($q = +1$) in non-extremal black hole for $M = 2$, $a = Q = 1$, $\mu = \epsilon = 1$ and $E = 2$. The (c) $L = 0$, (d) $L = 1$, (e) $L = -1$ trajectories are confined at $r = 0.239$, $r = 0.2351$, $r = 0.242$ respectively, and are denoted by vertical dashed lines.
BOTTOM PANEL: Spacetime diagrams of negative charged particles ($q = -1$) in non-extremal black hole for $M = 2$, $a = Q = 1$, $\mu = \epsilon = 1$ and $E = 2$. The (f) $L = 0$, (g) $L = 1$, (h) $L = -1$ trajectories are confined at $r = 0.22$, $r = 0.233$, $r = 0.201$ respectively, and are denoted by vertical dashed lines. The CTC and the event horizons (left and right solid vertical lines) are positioned at $r_{ctc} = 0.235$, $r_{in} = 0.586$ and $r_{out} = 3.414$.

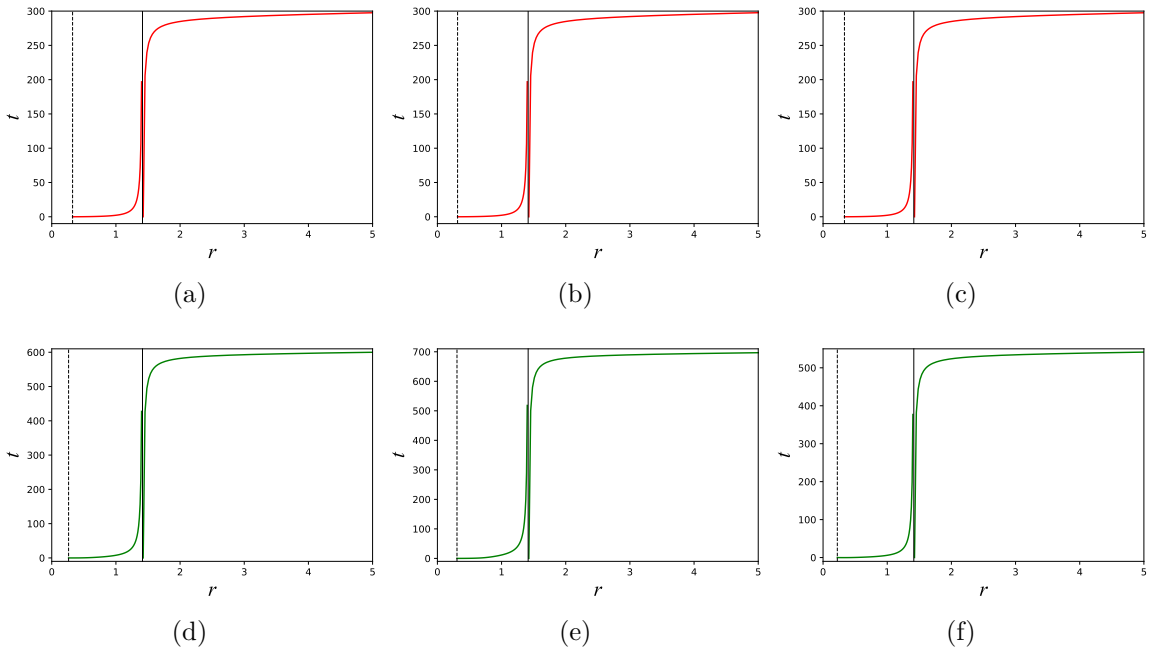

Figure 4.9: TOP PANEL: Spacetime diagrams of positive charged particles ($q = +1$) in KN extremal black hole for $M = \sqrt{2},\ a = Q = 1,\ \mu = \epsilon = 1$ and $E = 2$. The (a) $L = 0$, (b) $L = 1$, (c) $L = -1$ trajectories are confined at $r = 0.325,\ r = 0.3144,\ r = 0.333$ respectively, and are denoted by vertical dashed lines.
BOTTOM PANEL: Spacetime diagrams of negative charged particles ($q = -1$) in KN extremal black hole for $M = \sqrt{2},\ a = Q = 1,\ \mu = \epsilon = 1$ and $E = 2$. The (d) $L = 0$, (e) $L = 1$, (f) $L = -1$ trajectories are confined at $r = 0.262,\ r = 0.305,\ r = 0.222$ respectively, and are denoted by vertical dashed lines. The CTC and the event horizon (solid vertical line) are positioned at $r_{ctc} = 0.315$ and $r_{horizon} = 1.414$ respectively.

The confinement of geodesics within the Kerr-Newman extremal black hole has been examined with both positive ($q = +1$) and negative ($q = -1$) charges assigned to massive particles. Using identical source parameter values as the neutral particle scenario (i.e., $M = \sqrt{2}$ and $a = Q = 1$), the confinement radii of charged particles were determined, as depicted in Fig. 4.9. Notably, it is evident that the discussions regarding the origins of confinement in non-extremal black holes remain applicable in extremal Kerr-Newman black holes. The confinement radii for identically charged particles, except for negative AM particle geodesics, are shifted outward due to Coulomb repulsion, permitting only positive AM particles within the CTC region. Conversely, for oppositely charged particles, all confinement boundaries are significantly drawn inward by Coulomb attraction, allowing each particle to reside in the vicinity of CTCs.

Additionally, it is notable that charge conservation holds true in the context of charged particle motion. Reversing the charge sign in the source ($Q = -1$) leads to a reversal in all characteristics. Specifically, the plots' nature and the confinement points for $Q = -1,\ q = +1$ correspond to those of $Q = +1,\ q = -1$; similarly, for $Q = -1,\ q = -1$, they mirror those of $Q = +1,\ q = +1$.

4.8 Discussions

This study conducts a comprehensive examination of closed timelike curves and the behaviour of test particles along their trajectories within the equatorial slice of KN spacetime. Initially, the investigation focuses on determining the position of CTCs within the orbital region of the geometry, identifying two real roots, of which only one is physically feasible. Graphical representations of the inner and outer horizons, along with the CTC region, reveal that the Cauchy surface consistently lies within the inner horizon, while the central singularity at $r = 0$ is encompassed by CTCs, irrespective of whether the spacetime represents a black hole or a naked singularity.

Analysis of the geodesic equations reveals the presence of spacetime dragging effects on zero AM test particles. However, positive and negative AM particles, which respectively co-rotate and counter-rotate with the spacetime spin, eventually converge at the confinement point, prohibiting them from reaching the central singularity at $r = 0$. This results in an empty region surrounding the singularity where particle motion is entirely restricted. Previous work by Pugliese *et al.* [540] examined the radius of this forbidden area in terms of circular motion, denoted as $r_* = Q^2/M$, covering the singularity and located inside the outer horizon. They argued that while this boundary is independent of source parameters, it is a characteristic of the gravitational field generated by the electric charge. In the Reissner-Nordström metric, this radius represents the limiting radius of AM-less particles [545]. In this study, the explicit expressions for this radius are provided by Eq. (4.31) and (4.32), which in contrast represent the limiting radius for positive AM particles in neutral and identically charged (with the source) particle motions, while for oppositely charged particles, it represents the limiting radius for negative AM particles. Despite variations in the confinement of different AM test particles, the empty region lies significantly within the inner horizon for black holes. Furthermore, this boundary depends not only on the source parameters but also results from particle characteristics, such as energy and angular momentum.

As discussed, for both neutral and identically charged particle motions, an observer residing on the singularity initially perceives the region where positive AM particles are located. These particles can orbit within the CTCs until the zero AM confinement radius, where only zero and positive AM particles are present. Subsequently, beyond the negative AM confinement radius, all three particle types are permitted. Conversely, for motions involving oppositely charged particles, the observer observes the confinement of negative AM, zero AM, and positive AM particles, respectively. However, due to Coulomb attraction, all particles are capable of traversing the CTCs collectively.

Besides the spacetime diagram, the motion of particles within both the black hole and the naked singularity is examined in terms of velocity and/or the effective potential of timelike geodesics. Infalling geodesics experience increasingly stronger gravitational fields as they approach the singularity gradually. Consequently, velocity steadily increases until reaching a radius close to the singularity, where the dominant effect of repulsive gravity causes velocity to drop to zero, preventing further approach to the singularity. The growing repulsive gravity near the central singularity obscures it from external view, impeding the study of the singular point through particle motions.

The motion of test particles within a black hole always holds a particular point of interest. Despite certain limitations in defining infalling geodesics at the coordinate singularity, coordinate time helps identify the presence and maximum radial extent of test particles within the outer and inner horizons. Additionally, infalling trajectories are examined in terms of proper time within the geometry, elucidating the results alongside particle characteristics within CTCs inside the inner horizon.

For neutral particles, the confinement radius for zero AM photons coincides with the boundary of CTCs. As illustrated in Fig. 4.2, zero AM particle geodesics are feasible only at $r > 0.405$, while CTCs exist within a radius of $r < 0.405$. Consequently, only positive AM particles can access regions near CTCs in the naked singularity scenario. This finding holds true for KN black holes as well, as discussed in section 4.5, with relevant figures such as Fig. 4.4 and 4.5 providing examples. Hence, CTCs exclusively accommodate particles with positive AM, excluding those with zero and negative AM.

In the KN geometry, the trajectory of an infalling charged particle does not exhibit significant differences compared to neutral particles. For particles with identical charges, CTCs still only permit positive AM particles nearby, albeit with the confinement radius primarily shifting outward. Conversely, for particles with opposite charges, strong Coulomb attraction dominates over gravitational interaction, drawing all particle types within the Cauchy surface radius, enabling them to traverse the CTC.

This study not only examines particle characteristics within CTCs but also sheds light on particle motion in the equatorial orbit of KN black holes and naked singularities. Thus, it may offer new insights into discussions on naked singularities and black hole interior structure, particularly regarding the formation, structure, and accretion disk scenarios.

CHAPTER 5

GEODESIC MOTION IN TRAVERSABLE WORMHOLES: POSSIBILITY OF CLOSED TIMELIKE GEODESICS

5.1 Prelude

In generic traversable wormholes, particle motion is expected to potentially violate causality, leading to closed timelike orbits within the geometry. The investigation focuses on whether geodesic motion itself violates causality through closed timelike geodesics within their orbits. Motivated by this inquiry, the current chapter delves into the examination of a general wormhole solution within the framework of Einstein's gravity, characterized by an exponential shape function, encompassing both ultrastatic and finite redshift geometries. The investigation focuses on the geodesic motion surrounding these wormholes, revealing a noteworthy phenomenon: the deflection angle of orbiting photons shifts to a negative value beyond a certain threshold, indicating the emergence of a repulsive gravitational effect present in both ultrastatic and finite redshift wormholes. The analysis showcases a variety of timelike trajectories, both unbounded and bounded, depicted on wormhole embedding diagrams. Notably, certain bounded orbits exhibit intersection points, potentially leading to the violation of causality in geodesic paths. Furthermore, a distinct category of closed timelike geodesics is identified within the unstable circular trajectory at the wormhole throat. Ultimately, the trajectories are categorized concerning the family of closed timelike geodesic (CTG) orbits.

In the present chapter, the focus lies on investigating the geodesic motion of test particles around a traversable wormhole, with particular attention given to the potential existence of closed timelike geodesics within their paths. In Section 5.2, the wormhole model has been revisited within Einstein's gravity framework, with additional computations included concerning the field equations employing an exponential shape function within a specific redshift geometry. Concurrently, the respective null and

weak energy conditions for the geometry have been examined in Section 5.3. Section 5.4 is dedicated to discussing the characteristics of wormhole geometry and geodesic equations, encompassing topics such as the deflection angle of photons and the existence of circular timelike geodesics. Following this, in Section 5.5, diverse geodesic trajectories on the wormhole embedding diagram are showcased, preceding the classification of these trajectories. Finally, the analysis concludes with summarizing remarks presented in Section 5.6.

5.2 The Morris-Thorne model

In this section, a concise overview of the Morris-Thorne wormhole solution is provided before delving into the examination of particle dynamics within this geometry. Specific selections of the shape function and redshift function are opted for among the array of possibilities, with a focus on their impact on geodesic motion.

The static spherically symmetric Morris-Thorne wormhole is described by the metric

$$ds^2 = -e^{2\Phi(r)}dt^2 + \left(1 - \frac{b(r)}{r}\right)^{-1} dr^2 + r^2 d\Omega^2 \,. \tag{5.1}$$

Here, $d\Omega^2 = d\theta^2 + sin^2\theta d\phi^2$ represents the metric on the two-sphere $\mathbb{S}^2$, while $b(r)$ and $\Phi(r)$ denote the shape function and redshift function of the wormhole, respectively. The range of angular coordinates θ and ϕ is given by: $\theta : \{0, \pi\}$, $\phi : \{0, 2\pi\}$. It is crucial that the redshift function remains finite everywhere to ensure the absence of singularities and horizons. Additionally, both the shape function and redshift function must satisfy the following conditions:

(i) At the wormhole throat (b_0), the shape function satisfies $b(b_0) = b_0$, indicating the minimum radius at the throat. Thus, the radial coordinate ranges from b_0 to ∞.

(ii) For $r > b_0$, the condition $\frac{b(r)}{r} \leq 1$ is upheld to ensure that the radial component of the metric $g_{rr} < 0$ (with equality only at the throat).

(iii) As $r \to \infty$, both $\frac{b(r)}{r} \to 0$ and $\Phi(r) \to 0$ to maintain an asymptotically flat geometry.

(iv) The *flaring-out condition*, given by $(-rb'(r) + b(r)) > 0$ for $r > b_0$, must be satisfied.

(v) At $r = b_0$, $b'(r) \leq 1$.

Furthermore, disregarding any matter coupling, the energy-momentum tensor of an anisotropic fluid is expressed as $T^{\nu}_{\mu} = \text{diag}(-\rho,\ p_r,\ p_t,\ p_t)$, where ρ, p_r, and p_t represent the total energy density, radial pressure, and tangential pressure of the fluid,

respectively. Upon straightforward calculations of the Einstein field equation for the geometry given by (5.1), the following results are obtained:

$$\rho = -\frac{b'}{8\pi r^2}\,, \tag{5.2}$$

$$p_r = -\frac{b}{8\pi r^3} + \left(1-\frac{b}{r}\right)\frac{\Phi'}{4\pi r}\,, \tag{5.3}$$

$$p_t = \frac{1}{8\pi}\left(1-\frac{b}{r}\right)\left(\Phi'' + (\Phi')^2 - \frac{rb'-b}{2r(r-b)}\Phi' + \frac{\Phi'}{r} - \frac{rb'-b}{2r^2(r-b)}\right)\,, \tag{5.4}$$

where the prime indicates differentiation with respect to r. Natural units, where $G = c = 1$, were utilized in the calculations.

Next, the analysis shifts towards examining the characteristics and potential matter content of the wormhole model. In this regard, attention is directed to a particular shape function for the wormhole, known as the exponential shape function, which is defined as:

$$b(r) = re^{-(r-b_0)}\,. \tag{5.5}$$

The properties and significance of this shape function have been extensively explored in various studies [120,546], confirming its compatibility with desired attributes. In [546], the importance of the shape function and the tidal forces experienced by travelers through the wormhole in this particular case are thoroughly discussed. While the choice of the exponential shape function in this chapter is arbitrary, the results, particularly regarding the geodesic motions of test particles, are consistent with those obtained from other typical shape functions and wormhole models, such as the Ellis wormhole and wormholes supported by conformally coupled massless scalar fields. These will be briefly addressed in subsequent sections.

Additionally, when discussing wormhole properties concerning the shape function, a zero-tidal force wormhole is initially considered. This type, also termed the ultrastatic wormhole, holds a specific point of interest where $\Phi(r) = 0$. In this scenario, within a frame devoid of gravitational acceleration, a particle dropped from rest remains at rest [463]. Subsequently, a tidal force is introduced to the geometry, incorporated through the redshift function expressed as:

$$\Phi(r) = \frac{\gamma}{2r}\,, \tag{5.6}$$

where γ represents an arbitrary constant. The value of γ, except for zero, ensures finite redshift. Upon substituting the shape and redshift functions into the field equations (5.2), (5.3), and (5.4), the expressions for ρ, p_r, and p_t are obtained as:

$$\rho = -\left(\frac{1-r}{8\pi r^2}\right)e^{(b_0-r)}\,, \tag{5.7}$$

$$p_r = \frac{1}{8\pi r^3}\left(-\gamma + (\gamma - r)e^{(b_0-r)}\right)\,, \tag{5.8}$$

$$p_t = \frac{\gamma}{16\pi r^3}\left(1+\frac{\gamma}{2r}\right)\left(1-e^{(b_0-r)}\right) + \frac{e^{(b_0-r)}}{16\pi r}\left(1-\frac{\gamma}{2r}\right)\,. \tag{5.9}$$

It is worth noting that when $\gamma = 0$, the zero-tidal force wormhole configuration is obtained. Therefore, in this literature, the investigation of zero-tidal force wormholes is conducted under the condition $\gamma = 0$. Subsequently, the choice of $\gamma = 1$ is adopted for analyzing non-zero tidal forces in the study, which proves to be a convenient option for further analysis.

5.3 Energy Conditions

Constructing a traversable wormhole necessitates threading its throat with matter that violates the weak energy condition (consequently, the null energy condition), known as exotic matter.

In the framework of GR, adherence to the inequality $T_{\mu\nu}X^{\mu}X^{\nu} \geq 0$, where X^{μ} is any null vector, is crucial. This corresponds to the NEC, expressed as $\rho + p_i \geq 0$ in terms of the pressure p_i. The WEC extends NEC by requiring positive local energy density $T_{\mu\nu}V^{\mu}V^{\nu} \geq 0$, for any timelike observer, where V^{μ} is a timelike vector. In principal pressure form, WEC corresponds to $\rho \geq 0$ and $\rho + p_i \geq 0, \forall\ i$.

In the current analysis, evaluating ρ, $(\rho + p_r)$, and $(\rho + p_t)$ from equations (5.7), (5.8) and (5.9) is straightforward. Plots of these energy condition components for zero-tidal force ($\gamma = 0$) and non-zero tidal force ($\gamma = 1$) wormholes are displayed in Fig. 5.1, whereas the transition points from positive to negative values are summarized in Table 5.1. It is noted that values below the throat radius are excluded from consideration.

Regardless of tidal force, $\rho \geq 0$ holds in $r \in [\ b_0, \infty)$, with equality at the throat. Additionally, $(\rho + p_t)$ satisfies the conditions for both cases. However, NEC and WEC are violated due to $(\rho + p_r)$, indicating presence of exotic matter. For $\gamma = 0$, violation occurs in $r \in [b_0, 2]$, while NEC and WEC are upheld for $r \in [\ 2, \infty)$. In the case of non-zero tidal force ($\gamma = 1$), $(\rho + p_r)$ is violated entirely, suggesting exotic matter presence throughout the geometry. Thus, the results affirm the theoretical basis for constructing a traversable wormhole.

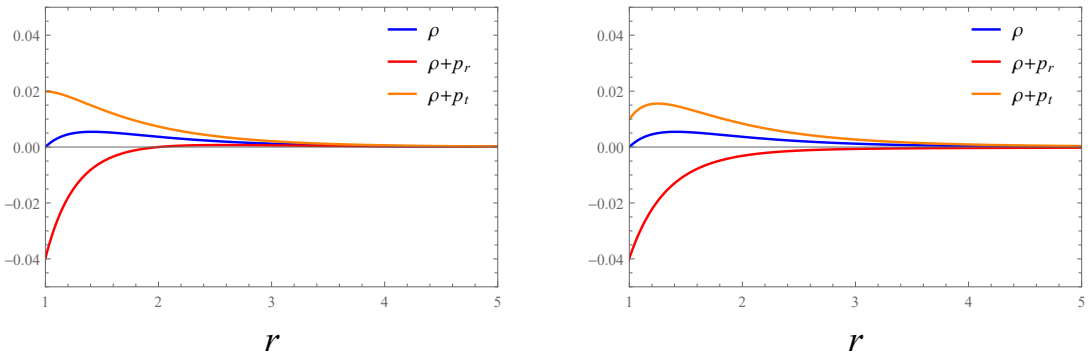

Figure 5.1: The variation of null and weak energy condition components ρ, $(\rho+p_r)$, $(\rho+p_t)$ against radial parameter r, for (a) zero-tidal force wormhole (i.e. $\gamma = 0$), (b) non-zero tidal force wormhole with $\gamma = 1$. Here, the throat radius is $b_0 = 1$.

γ	Terms	Result
$\gamma = 0$	ρ	≥ 0 for $r \in [\ 1, \infty)$
	$\rho + p_r$	≥ 0 for $r \in [\ 2, \infty)$
	$\rho + p_t$	≥ 0 for $r \in [\ 0.67, \infty)$
$\gamma = 1$	ρ	≥ 0 for $r \in [\ 1, \infty)$
	$\rho + p_r$	Always < 0
	$\rho + p_t$	≥ 0 for $r \in [\ 0.89, \infty)$

Table 5.1: Numerical results for the possible regions where respective energy condition components are satisfied.

5.4 The Geometry and Geodesics

Before delving into discussions regarding geodesics and particle dynamics within traversable wormholes, several pertinent concepts need to be highlighted.

The wormhole's shape can always be envisioned by considering constant time slices in the equatorial plane. The geometry can be embedded into a higher-dimensional ordinary 3D Euclidean space described by the metric

$$ds^2 = dz^2 + dr^2 + r^2 d\phi^2 \,. \tag{5.10}$$

The embedding function can then be expressed as

$$\frac{dz}{dr} = \pm \left(\frac{r}{b(r)} - 1 \right)^{-1/2} \,. \tag{5.11}$$

Here, the radial coordinate ranges from spatial infinity $r = \infty$ to the throat radius $r_{min} = b_0$. Notably, the embedding function $z(r)$ flares out in the throat region, where the flaring-out condition is obtained by

$$\frac{d^2 r}{dz^2} = \frac{b(r) - r b'(r)}{2b(r)^2} > 0 \qquad \text{for } r \geq b_0 \,. \tag{5.12}$$

Referring to Eq. (5.1), it is evident that the radial coordinate r is not sufficient to describe the entire spacetime due to its coordinate singularity at the throat. Thus, it only covers one side of the throat. To address this limitation, the proper radial distance $l(r)$ is introduced to characterize the entire spacetime. This reformulates Eq. (5.1) as:

$$ds^2 = -e^{2\Phi(r(l))} dt^2 + dl^2 + r(l)^2 d\Omega^2 \,, \tag{5.13}$$

where $l(r)$ is defined as:

$$l(r) = \pm \int_{b_0}^{r} \left(1 - \frac{b(r)}{r} \right)^{-1/2} dr \,. \tag{5.14}$$

Here, the throat is situated at $l = 0$, with spatial infinities at $l \to \pm\infty$ defining the two asymptotic sides of the wormhole throat. The sign of the proper radius denotes

the upper and lower universes, where the upper universe can be identified with our own if the wormhole connects two distinct universes. Otherwise, if it connects distant regions within our universe, the upper and lower universes represent our locality and the distant sublocality within the same universe.

To derive the geodesic equations on the equatorial plane ($\theta = \frac{\pi}{2}$) for the wormhole metric defined in equation (5.1), the Lagrangian equation of motion given by $\mathcal{L} = \frac{1}{2} g_{\alpha\beta} \frac{dx^\alpha}{d\tau} \frac{dx^\beta}{d\tau}$ is considered. The first-order geodesics are then obtained from the canonical conserved momentum, yielding:

$$\dot{t} = E e^{-2\Phi(r)} \,, \tag{5.15}$$

$$\dot{\phi} = \frac{L}{r^2} \,, \tag{5.16}$$

$$\dot{r}^2 = \left(1 - \frac{b(r)}{r}\right) \left(E^2 e^{-2\Phi(r)} - \frac{L^2}{r^2} + \varepsilon\right) \,, \tag{5.17}$$

where $\varepsilon = 1, 0, -1$ represents spacelike, null, and timelike geodesics, respectively. The parameters E and L denote the total energy and angular momentum of the test particle, respectively. The overdot indicates differentiation with respect to the affine parameter for null geodesics and proper time for timelike geodesics.

For radial null geodesics, Eq. (5.17) is modified to

$$\dot{r}^2 = \left(1 - \frac{b(r)}{r}\right) \left(E^2 e^{-2\Phi(r)} - \frac{L^2}{r^2}\right) \,. \tag{5.18}$$

Therefore, to investigate the photon trajectories, the following equation is introduced:

$$\left(\frac{dr}{d\phi}\right)^2 = \left(1 - \frac{b(r)}{r}\right) \left(\frac{E^2}{L^2} r^4 e^{-2\Phi(r)} - r^2\right) \,. \tag{5.19}$$

If a photon source with a radius of r_s influences the geometry, photons originating from spatial infinity will not reach the surface if the solution satisfies the condition $r_0 > r_s$, where r_0 represents the distance of closest approach or the turning point, such that one gets

$$\frac{L^2}{E^2} = r_0^2 e^{-2\Phi(r_0)} \qquad \left(\text{if } \frac{b(r)}{r} \neq 1, \text{ for any } r > r_s\right) \,. \tag{5.20}$$

This condition is characterized by $\dot{r}^2 = 0$, indicating that photons neither approach nor recede from the surface, thus, the impact parameter is given by

$$\mu = \frac{L}{E} = \pm\, r_0 e^{-\Phi(r_0)} \,. \tag{5.21}$$

When a photon originates from spatial infinity, denoted as $\lim_{r\to\infty} \left(r, -\frac{\pi}{2} - \frac{\alpha}{2}\right)$, and passes through the turning point located at $(r_0, 0)$, eventually reaching $\lim_{r\to\infty} \left(r, \frac{\pi}{2} + \frac{\alpha}{2}\right)$, the resulting deflection angle $\alpha(r_0)$ is determined according to [547], as

$$\alpha(r_0) = -\pi + 2 \int_{r_0}^{\infty} \frac{dr}{r \left[\left(1 - \frac{b(r)}{r}\right) \left(\left(\frac{r e^{\Phi(r_0)}}{r_0 e^{\Phi(r)}}\right)^2 - 1\right)\right]^{1/2}} \,. \tag{5.22}$$

The existence of a photon sphere confines photons within a fixed radius r, preventing them from reaching the asymptotic limit $\lim_{r\to\infty}\left(r, \frac{\pi}{2}+\frac{\alpha}{2}\right)$, resulting in a divergent integral. By incorporating the shape and redshift function from Eq. (5.5) and (5.6), the deflection angle given by Eq. (5.22) has been numerically integrated. Figure 5.2 illustrates the variation of the deflection angle with r_0 for a throat radius $b_0 = 1$. Notably, the deflection angle becomes negative beyond a certain distance for both zero and non-zero tidal force wormholes, indicating a repulsive gravitational effect on the geometry.

This repulsive gravity phenomenon is familiar in modified gravity theories involving exotic matter and phantom energies [548–553]. Notably, the dRGT massive gravity [157, 158] is recognized as a common source, where massive gravitons may play a significant role (it will be briefly addressed in the next chapter). Panpanich *et al.* investigated the repulsive gravity effect through negative deflection angles in a black hole geometry [554]. However, this effect is not attributed to the introduction of exponential shape function. Instead, the choice of the redshift function (5.6) can readily yield negative deflection angles with well-known shape functions like the Ellis wormhole shape. Comparing transition points for $\gamma = 0$ and $\gamma = 1$, it is evident that the repulsive effect is more pronounced in wormhole geometries with finite tidal forces.

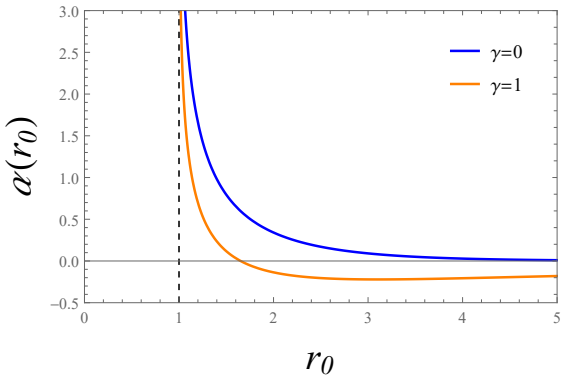

Figure 5.2: Plot demonstrating deflection angle for different redshift wormhole configuration (with $\gamma = 0$, and $\gamma = 1$). The deflection angles become negative at $r_0 = 4.05$, and $r_0 = 1.65$ respectively, for $\gamma = 0$, and $\gamma = 1$. The vertical dashed line denotes throat radius $b_0 = r_0 = 1$.

5.4.1 Timelike geodesics

In this subsection, several important motions of massive particles within wormhole geometries will be examined. Cataldo *et al.* briefly addressed the initial velocity, position, and accelerations of radial timelike geodesics around ultrastatic wormholes [463]. Now, the comprehensive analysis of non-radial timelike geodesic accelerations can be obtained through differentiation of the first-order radial timelike geodesic equation presented in Eq. (5.17), as

$$\ddot{r} = \left(1 - e^{-(r-b_0)}\right)\frac{L^2}{r^3} + \frac{1}{2}\left(E^2 - \frac{L^2}{r^2} - 1\right)e^{-(r-b_0)}\,. \tag{5.23}$$

At this juncture, examination of circular timelike geodesics, which hold particular significance, is imminent. Conventionally, it is established that circular timelike geodesics

are confined to the throat, where the radial velocity vanishes, i.e., $\dot{r} = 0$. At this point, the acceleration for $\dot{r} = 0$ is given by

$$\ddot{r} = \left(1 - e^{-(r-b_0)}\right) \frac{L^2}{r^3} \,. \tag{5.24}$$

As the acceleration becomes zero at $r = b_0$, it is evident that circular timelike geodesics exclusively exist at the throat.

For ultrastatic wormholes, the radial geodesic equation expressed in terms of proper distance can be formulated as

$$\left(\frac{dl}{ds}\right)^2 = E^2 - V(L, l) \,, \tag{5.25}$$

where the potential associated with conserved momentum and proper distance is represented by

$$V(L, l) = \frac{L^2}{r(l)^2} + \varepsilon \,, \tag{5.26}$$

which remains positive for $L \neq 0$ and tends to zero as $l \to \pm\infty$. The important relations on this account is given by

$$\left.\frac{dV}{dl}\right|_{l=0} = 0 \,, \tag{5.27}$$

$$\left.\frac{d^2V}{dl^2}\right|_{l=0} = -\frac{L^2}{r^4}\left(\frac{b(r)}{r} - b'(r)\right)\Bigg|_{l=0} < 0 \,. \tag{5.28}$$

Equation (5.27) indicates that the potential reaches a global maximum at the throat, with the inequality in Eq. (5.28) arising from the flaring out condition. When $r(l)$ is concave up, the sole turning point occurs at $l = 0$, distinguishing bound orbits from transmitting unbounded orbits. Stable circular geodesic orbits can exist even if $r(l)$ is not strictly concave up, with the potential well exhibiting oscillatory motion around turning points [462, 474].

Timelike geodesic trajectories can be categorized into bounded and unbounded orbits. Bound orbits involve geodesics originating from spatial infinity, reaching the throat, and returning to the same spatial infinity, while unbounded trajectories entail geodesics passing through the throat to access other universes or distant points within the same universe. In traversable wormholes, it is critical that timelike massive particle trajectories originating from one universe traverse the throat to reach the other universe or a distant point within the same universe. This unbounded trajectory is also referred to as the escape orbit.

To distinguish these particle orbits with analytic expressions, it is necessary to recall Eq. (5.17) in terms of proper distance, as

$$\dot{l}^2 = \left(E^2 e^{-2\Phi(r)} - \frac{L^2}{r^2} - 1\right) \,. \tag{5.29}$$

When a particle approaching from infinity gets deflected after reaching the throat at a closest distance b_0, the condition for a bound orbit can be expressed as follows:

$$\left(E^2 e^{-2\Phi(b_0)} - \frac{L^2}{b_0^2} - 1\right) \leq 0\,, \tag{5.30}$$

which can be further simplified to:

$$\frac{L}{\sqrt{E^2 e^{-2\Phi(b_0)} - 1}} \geq b_0\,. \tag{5.31}$$

Otherwise, the trajectory constitutes an escape orbit.

With the specified parameters chosen in this chapter, the bound orbit condition given by Eq. (5.31) is adapted as follows:

$$\frac{L}{\sqrt{E^2 e^{-\gamma/b_0} - 1}} \geq b_0\,. \tag{5.32}$$

For a zero-tidal force wormhole, it is expressed as:

$$\frac{L}{\sqrt{E^2 - 1}} \geq b_0\,. \tag{5.33}$$

Now, in the following section, different bound and escape trajectories of a timelike test particle will be examined thoroughly for both zero and non-zero tidal force wormhole configuration.

5.5 The Geodesic Trajectories and CTG

To derive the trajectories of massive particles, the geodesic equation can be expressed as

$$\left(\frac{dr}{d\phi}\right)^2 = \left(1 - e^{-(r-b_0)}\right)\left[\left(\frac{E^2 e^{-\gamma/r} - 1}{L^2}\right) r^4 - r^2\right]\,, \tag{5.34}$$

where the expressions for the wormhole shape function and redshift function from Eq. (5.5) and (5.6) have been incorporated into Eq. (5.17). This equation is further modified in terms of proper length as follows:

$$\left(\frac{dl}{d\phi}\right)^2 = \left[\left(\frac{E^2 e^{-\gamma/r(l)} - 1}{L^2}\right) r(l)^4 - r(l)^2\right]\,. \tag{5.35}$$

To visualize the solution of Eq. (5.35) in the context of wormhole embedding, the equation for the embedding function is revisited, as given by Eq. (5.11), and the proper distance described in Eq. (5.14). Utilizing the selected shape function (i.e., Eq. (5.5)), analytical solutions for these equations are obtained as

$$z(r) = \pm 2 \arctan\sqrt{e^{(r-b_0)} - 1}\,, \tag{5.36}$$

$$l(r) = \pm 2 \log\left[e^{r/2}(1 + \sqrt{1 - e^{(b_0 - r)}})\right]\,. \tag{5.37}$$

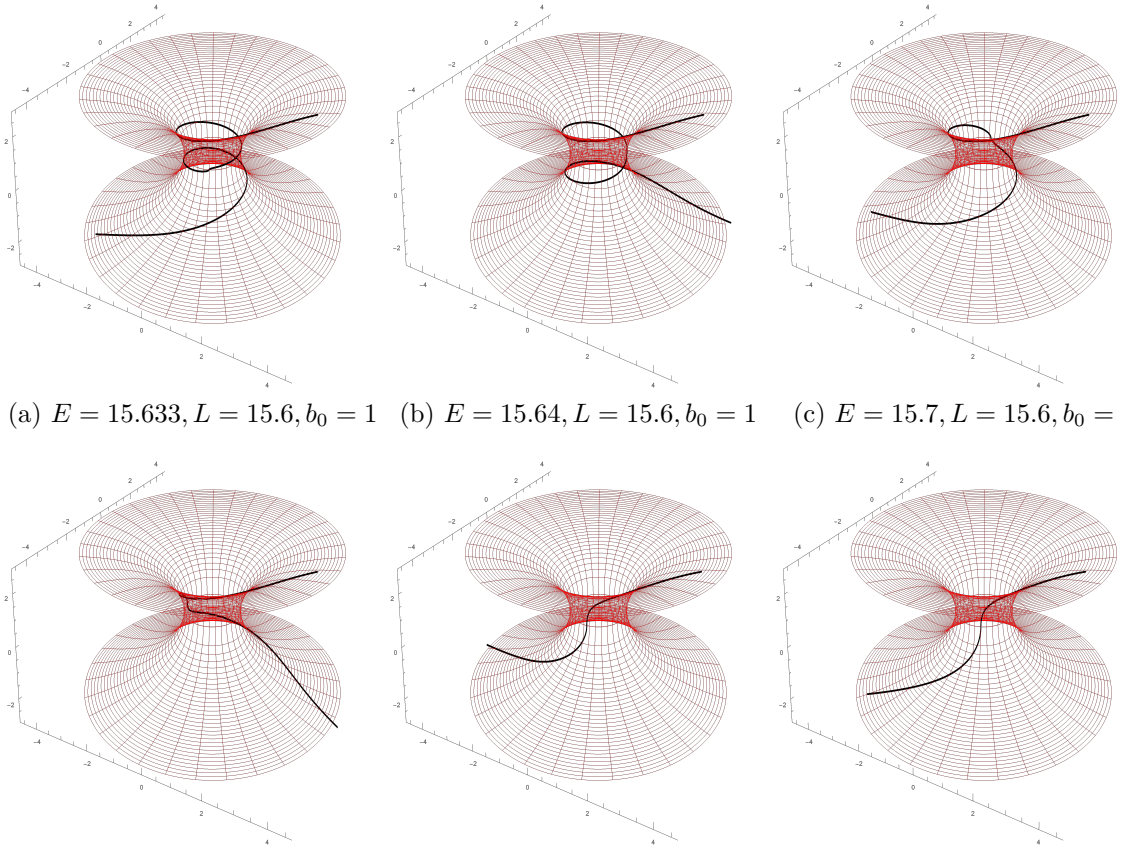

(a) $E = 15.633, L = 15.6, b_0 = 1$ (b) $E = 15.64, L = 15.6, b_0 = 1$ (c) $E = 15.7, L = 15.6, b_0 = 1$

(d) $E = 16.1, L = 15.6, b_0 = 1$ (e) $E = 20.5, L = 15.6, b_0 = 1$ (f) $E = 23.5, L = 15.6, b_0 = 1$

Figure 5.3: Escape orbits of $dl/d\phi$ motion for zero-tidal force wormhole with $\gamma = 0$. The isometric wormhole embedding is employed for a throat radius $b_0 = 1$. Different geodesic trajectories are visualized for gradually increasing particle energy (E), at a fixed angular momentum $L = 15.6$. Orbits originating from the upper universe traverse the throat and transition into the lower universe.

To generate trajectory plots, Eq. (5.37) is inverted for use in Eq. (5.35). Since the final expression of Eq. (5.35) poses challenges for analytical solution, numerical methods are employed for solving the equation, facilitating 3D parametric plotting on wormhole embeddings to depict orbits. The isometric embedding of the traversable wormhole is visualized by plotting Eq. (5.36). Subsequently, orbits are computed for varying values of energy (E) with a fixed angular momentum ($L = 15.6$) of the test particles.

The primary objective of this chapter is to examine both bounded and unbounded orbits on the wormhole embedding for zero and non-zero tidal force scenarios ($\gamma = 0$ and $\gamma = 1$), thereby exploring the possibility of closed timelike geodesics within their trajectories. Additionally, the effect of tidal force on geodesics is investigated. Various particle motions are illustrated within the wormhole geometry in Figures 5.3, 5.4, 5.5, and 5.6. Escape and bound orbits of a zero-tidal force wormhole are depicted in Fig. 5.3 and 5.4 for different values of energy (E), angular momentum (L) of the particle.

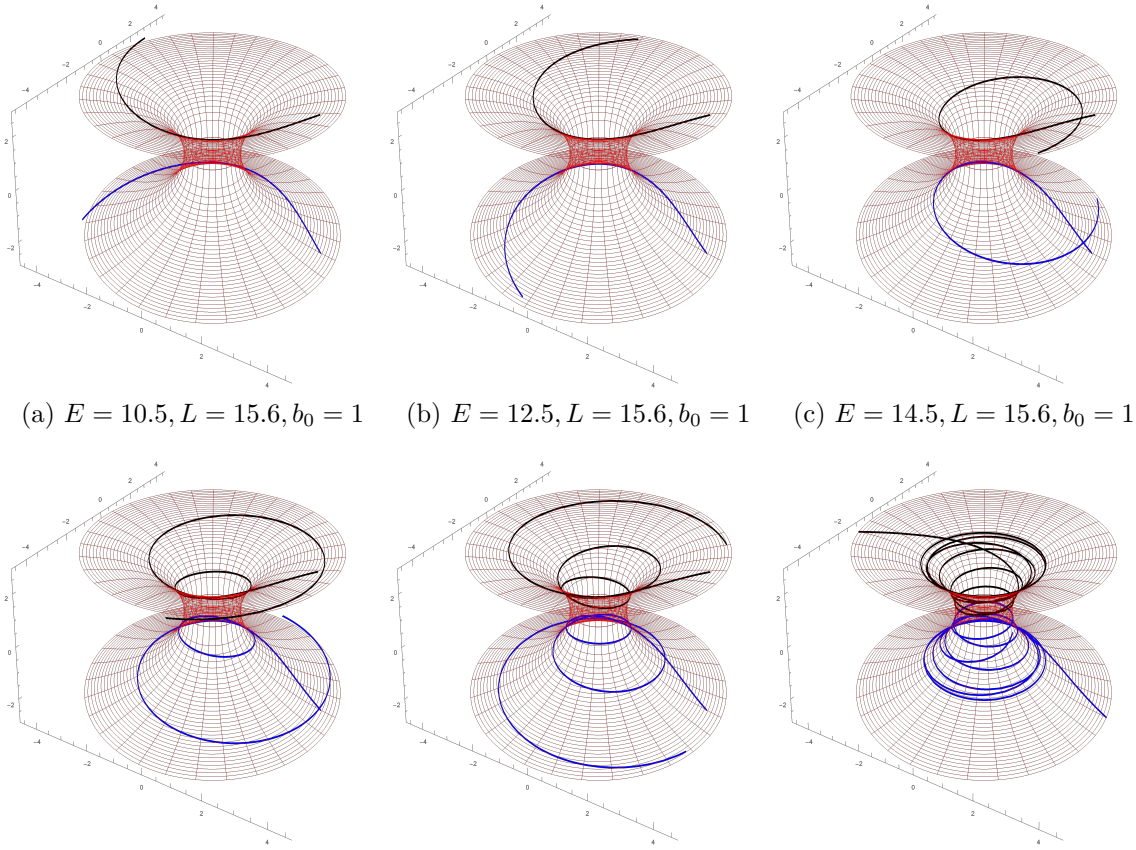

(a) $E = 10.5, L = 15.6, b_0 = 1$ (b) $E = 12.5, L = 15.6, b_0 = 1$ (c) $E = 14.5, L = 15.6, b_0 = 1$

(d) $E = 15.5, L = 15.6, b_0 = 1$ (e) $E = 15.6, L = 15.6, b_0 = 1$ (f) $E = 15.63, L = 15.6, b_0 = 1$

Figure 5.4: Bound orbits of $dl/d\phi$ motion for zero-tidal force wormhole with $\gamma = 0$. The isometric wormhole embedding is employed for a throat radius $b_0 = 1$. Different geodesic trajectories are visualized for gradually increasing particle energy (E), at a fixed angular momentum $L = 15.6$. Orbits originated from the upper (lower) universe are deflected around the throat region and re-enter the same universe. The trajectories depicted in black and blue in the upper and lower universes, respectively, represent the outcomes of positive and negative segments of $dl/d\phi$. Trajectories in (c)-(f) exhibit intersecting closed timelike geodesic orbits.

The trajectories' evolution for non-zero tidal force ($\gamma = 1$) is examined in Fig. 5.5 and 5.6. In all these scenario, throat radius is fixed at $b_0 = 1$, and the angular momentum of the test particle is maintained at $L = 15.6$ to demonstrate variations with increasing energy (E). In wormholes with tidal force, trajectories are expected to exhibit smaller deviations due to reduced deflection angles. This expectation is confirmed in Fig. 5.5 and 5.6, where higher energy is required to replicate trajectories as in Fig. 5.3 and 5.4 for the same values of L and b_0. In bound orbits, particles remain within the same universe. Consequently, positive and negative solutions of Eq. (5.35) depict identical trajectories in the upper and lower universes of the wormhole respectively. These trajectories in the lower universe are represented by blue lines, as seen in the figures.

It is notable that certain bound orbits, displayed in Fig. 5.4 and 5.6 exhibit in-

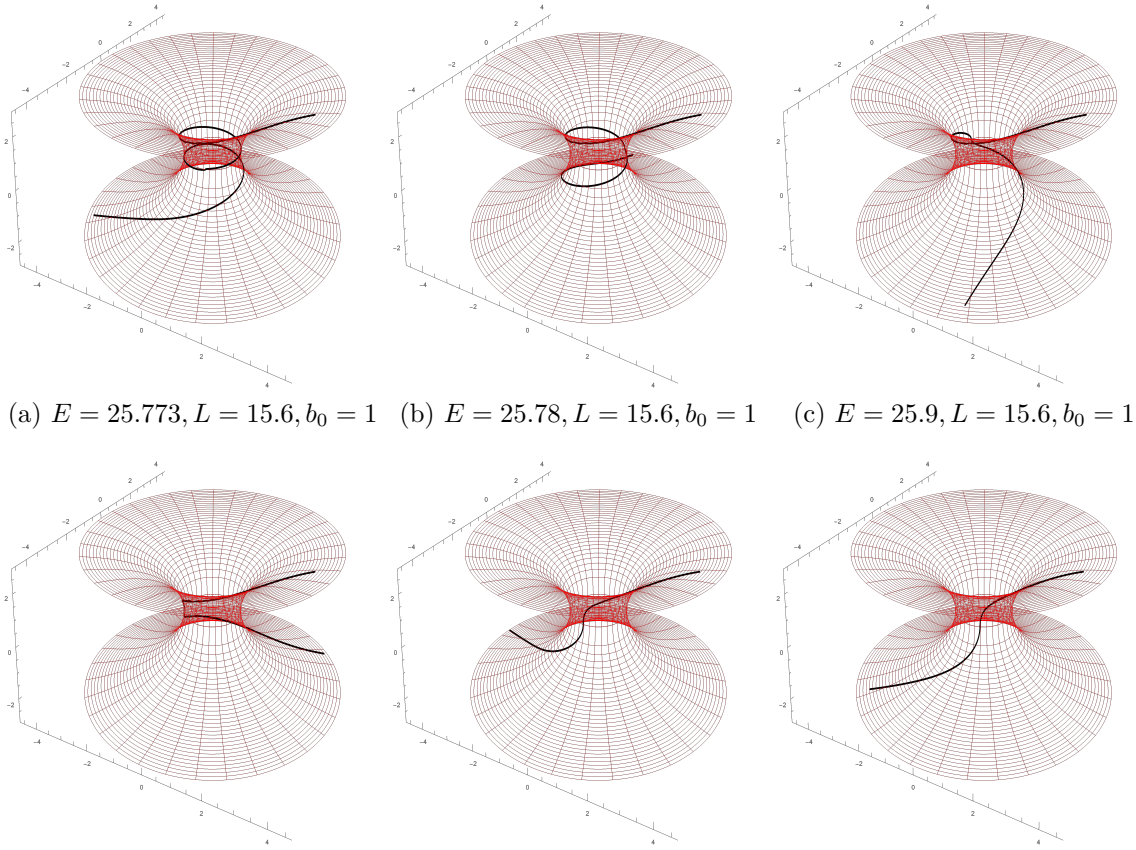

(a) $E = 25.773, L = 15.6, b_0 = 1$ (b) $E = 25.78, L = 15.6, b_0 = 1$ (c) $E = 25.9, L = 15.6, b_0 = 1$

(d) $E = 26.5, L = 15.6, b_0 = 1$ (e) $E = 30.5, L = 15.6, b_0 = 1$ (f) $E = 35.5, L = 15.6, b_0 = 1$

Figure 5.5: Escape orbits of $dl/d\phi$ motion for non-zero tidal force wormhole with $\gamma = 1$. The isometric wormhole embedding is employed for a throat radius $b_0 = 1$. Different geodesic trajectories are visualized for gradually increasing particle energy (E), at a fixed angular momentum $L = 15.6$. Orbits originating from the upper universe traverse the throat and transition into the lower universe.

tersection points, a phenomenon consistent with findings in prior research [462–464]. These intersections, discussed extensively in [555], occur when a light flash emitted by an observer coincides with its trajectory at previous points while traversing the wormhole embedding. This raises intriguing questions about the nature of these intersection points, suggesting they might replicate past events.

These causal points present a particle with two choices: to remain on its current orbit to move towards future, or to follow its past trajectory, eventually returning to the same point after a certain duration. For massive particles and photons, these intersecting orbits may resemble closed timelike or null orbits, respectively.

In most wormhole classifications, intersecting closed timelike geodesics (CTGs) are observed only in bound orbits. Consequently, a particle must exist in the same universe (or sublocality) to engage in CTG motion. However, it is not entirely implausible to encounter CTGs in escape orbits, as seen in [464].

Recalling the explanation from section 5.4.1 concerning circular timelike geodesics

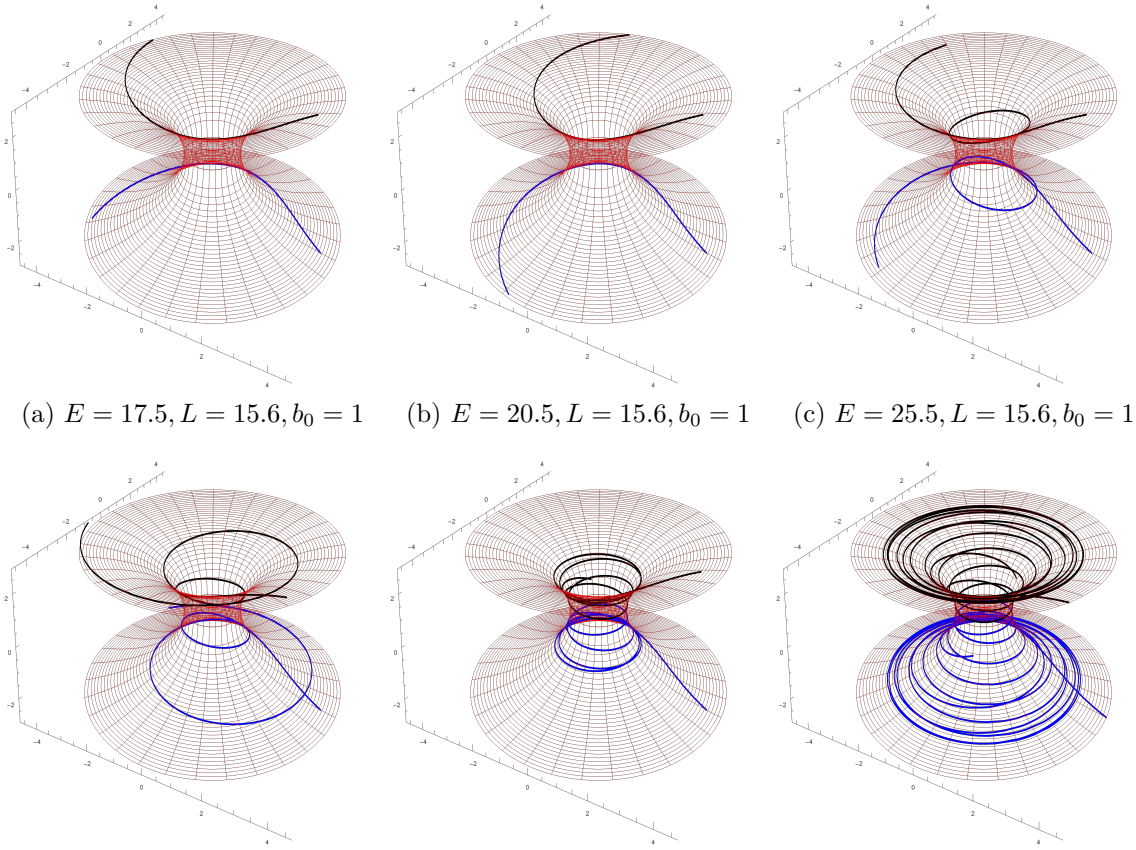

(a) $E = 17.5, L = 15.6, b_0 = 1$ (b) $E = 20.5, L = 15.6, b_0 = 1$ (c) $E = 25.5, L = 15.6, b_0 = 1$

(d) $E = 25.7, L = 15.6, b_0 = 1$ (e) $E = 25.77, L = 15.6, b_0 = 1$ (f) $E = 25.772, L = 15.6, b_0 = 1$

Figure 5.6: Bound orbits of $dl/d\phi$ motion for non-zero tidal force wormhole with $\gamma = 1$. The isometric wormhole embedding is employed for a throat radius $b_0 = 1$. Different geodesic trajectories are visualized for gradually increasing particle energy (E), at a fixed angular momentum $L = 15.6$. Orbits originated from the upper (lower) universe are deflected around the throat region and re-enter the same universe. The trajectories depicted in black and blue in the upper and lower universes, respectively, represent the outcomes of positive and negative segments of $dl/d\phi$. Trajectories in (c)-(f) exhibit intersecting closed timelike geodesic orbits.

at the throat, a distinct class of orbits is presented in Fig. 5.7. However, similar orbits have been documented previously in studies by [462, 464]. These orbits exemplify closed timelike geodesic trajectories at the wormhole throat, resembling closed timelike orbits observed in cylindrical wormholes [556–558] and other cylindrically symmetric rotating spacetimes [224]. A particle entering from the lower universe forms a closed timelike orbit at the throat, perpetually rotating without escaping. This specific orbit entails the particle traversing for a duration before returning to its initial entry point. Analogous scenarios are observed in closed timelike geodesics of cylindrically symmetric spacetimes, as detailed in chapter 3. However, these circular timelike geodesics at the throat exhibit high instability upon introducing minor parameter deviations.

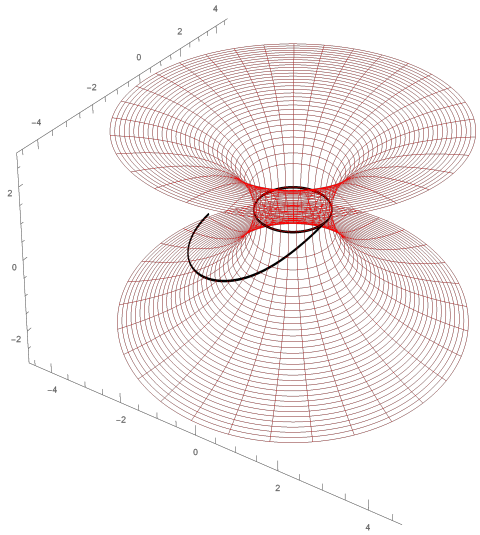

Figure 5.7: Unstable bound orbit at the throat, for $E = 1545, L = 1566, b_0 = 1$, exhibiting closed timelike geodesic. Particle originating from the lower universe is trapped at the throat creating infinite closed loop.

Classification of $dl/d\phi$ orbits:
In this classification, various trajectories are distinguished in terms of CTGs, as observed during the investigation of motion on the isometric embedding concerning $dl/d\phi$. These timelike orbits are categorized as follows:
• **Unbounded escape orbit:** This trajectory involves a geodesic path originating from one asymptotic region, crossing the wormhole throat, and reaching the other asymptotic region.
• **Bound orbit:** In this scenario, a geodesic remains predominantly within the same asymptotic region. Typically, it deviates from the vicinity of the throat and returns to the originating universe.
• **Intersecting CTG orbit:** This trajectory involves a geodesic intersecting its own path once or multiple times. Such intersections may enable closed timelike geodesic orbits, allowing for theoretical time reversal. Fig. 5.4c-5.4f and 5.6c-5.6f depict examples of this orbit. Furthermore, Fig. 5.4f, 5.6e, 5.6f exhibit families of interacting CTGs in this category.
• **Throat-CTG orbit:** Circular timelike geodesics are exclusively found at the throat, potentially leading to CTGs, although these trajectories are highly unstable. Figure 5.7 illustrates an example of this orbit.

5.6 Discussions

In this chapter, a Morris-Thorne type wormhole solution is investigated within Einstein's gravity, assuming an exponential shape function and a constrained redshift function specified by Eq. (5.5) and (5.6) respectively. The ultrastatic wormhole geometry (zero-tidal force) is retrieved when $\gamma = 0$, whereas for a non-zero tidal force wormhole, $\gamma = 1$ is considered. Visualizations of the behaviour of null and weak energy condition components are provided. While the energy density is positive in both cases, negativity is exhibited by $(\rho + p_r)$ at the throat region, indicating the presence of exotic fluid necessary for traversability.

In the subsequent section, the deflection angle of orbiting photons is analyzed, which becomes negative beyond a certain distance, signifying a repulsive gravitational effect on the geometry. It is observed that this effect is less pronounced in a non-zero tidal force wormhole compared to a zero-tidal force one. Nonetheless, the nature of the effect remains consistent regardless of the choice of shape and redshift function. The investigation reveals that common shape functions (e.g., Ellis wormhole) also yield this deflection angle property in the presence of a non-zero tidal force. Further exploration is warranted regarding the role of the repulsive gravity effect, possibly due to exotic matter at the throat, establishing an open field of discussion concerning this effect in wormhole geometries and its relation with the type of matter fluid.

In section 5.4.1, examination is made of circular timelike geodesics, which are only viable at the wormhole throat. Both bound and unbounded orbits are discussed in terms of the potential function with proper radial distance. Additionally, investigation is conducted on timelike bound orbit conditions in a finite redshift and in an ultrastatic wormhole. Various timelike geodesic escape and bound orbits, parameterized by particle energy and angular momentum, as well as the size and shape of the wormhole throat, are presented in a series of figures for both ultrastatic and non-zero tidal force wormholes. By numerically solving the $dr/d\phi$ equation for different parameter values, geodesic orbits are constructed on the isometric wormhole embedding. The gradual increase in particle energy (E) for a fixed angular momentum ($L = 15.6$) illustrates corresponding trajectory changes for a throat radius of $b_0 = 1$. Furthermore, the bound orbits, corresponding to positive and negative segments of Eq. (5.35) mirror each other in the upper and lower universes respectively.

Subsequently, the existence and characteristics of closed timelike geodesic trajectories were explored, particularly prevalent within bound orbits. These trajectories exhibit overlap with their past worldlines while traversing the wormhole embedding. At these intersection points, particles face a choice: to continue along present orbits or to follow past worldlines, leading them back to the same intersection points after a certain duration. Some orbits encounter these causal points once or twice, while others engage in a series of interacting CTGs. The question arises whether these CTGs arise due to the choice of the shape function considered in this study (specifically, the exponential shape function (5.5)). To address this concern, one may refer to previous studies [462–464], where although causal points were not explicitly mentioned, intersecting orbits were observed, facilitating CTGs. Additionally, it is noteworthy that these CTGs are necessarily geodesics.

Moreover, the unstable circular timelike orbit at the throat serves as another source of CTGs, as depicted in Fig. 5.7. It was observed that test particles entering this loop become indefinitely trapped, endlessly retracing their past selves after each rotation.

In conclusion, the bounded and unbounded orbits were categorized based on the presence of CTGs within their trajectories.

CHAPTER 6

STATIC WORMHOLE FORMATION IN dRGT MASSIVE GRAVITY: AN ANALYTIC DESCRIPTION

6.1 Prelude

Since the introduction of the traversable wormhole model, there has been considerable interest in exploring whether wormholes can be constructed using ordinary matter. Recent studies have discussed wormhole solutions in both Einstein gravity and modified gravity theories, suggesting the possibility of constructing wormholes with ordinary matter in modified gravity that satisfy all energy conditions [559]. Although the matter itself may be ordinary, the effective geometric matter, which serves as the matter source in modified gravity, violates the usual null energy condition. Several studies have explored non-exotic matter wormholes in various gravity scenarios as given in [430, 432, 560–568].

The current chapter examines the wormhole solution within both dRGT-$f(R,T)$ massive gravity and Einstein massive gravity frameworks. In both scenarios, the anisotropic pressure solution within an ultrastatic wormhole geometry yields a shape function dependent on parameters γ and Λ associated with massive gravity. However, the influence of these parameters leads to a departure from asymptotic flatness in spacetime. Analogous to the case of black hole solutions in massive gravity, this discrepancy emerges due to the repulsive nature of gravity, manifested in phenomena such as negative photon deflection angles beyond certain radial distances. It is observed that the repulsive effect induced by massive gravitons exerts significant influence on the spacetime geometry, compromising its asymptotic flatness. Nevertheless, within this framework, it is feasible to construct a wormhole supported by ordinary matter at its throat, satisfying all energy conditions, while the negative energy density is attributed to massive gravitons. Additionally, employing the TOV equation reveals the stability of the model under hydrostatic equilibrium conditions.

Thus, in this chapter, the derivation of the field equations governing the wormhole solution within the framework of $f(R,T)$ massive gravity is delved into, with thorough discussion provided in Section 6.2. Section 6.3 presents the solution for anisotropic pressure within the ultrastatic wormhole geometry, highlighting the emergence of a repulsive gravitational effect. To broaden the understanding of the interplay between asymptotic structure and repulsive gravity, the analysis is extended to investigate the wormhole solution within the dRGT extension of Einstein gravity, as detailed in Section 6.4. Meanwhile, Section 6.6 is dedicated to analyzing the stability of the model, whereas Section 6.5 delves into discussions regarding energy conditions and the underlying matter content. Finally, concluding discussions are provided in Section 6.7. Note that the study maintains a natural unit system throughout, for which $G = c = 1$.

6.2 The dRGT field equations

To explore the $f(R,T)$ gravity model within the framework of de Rham-Gabadadze-Tolley (dRGT) massive gravity, the corresponding action is formulated as follows:

$$S = \int d^4x\sqrt{-g}\left(\frac{1}{16\pi}\Big[f(R,T) + m_g^2\mathcal{U}(g,\phi^a)\Big] + \mathcal{L}_m\right), \tag{6.1}$$

where $f(R,T)$ represents a function dependent on R and T. $\mathcal{U}$ denotes the self-interacting potential of the graviton, characterized by the graviton mass m_g, $\mathcal{L}_m$ stands for the matter Lagrangian, and g signifies the determinant of the metric tensor $g_{\mu\nu}$. The potential $\mathcal{U}$ is defined in 4-dimension as follows:

$$\mathcal{U} = \mathcal{U}_2 + \alpha_3\mathcal{U}_3 + \alpha_4\mathcal{U}_4\,, \tag{6.2}$$

where α_3 and α_4 are two dimensionless free parameters. The parameters $\mathcal{U}_2$, $\mathcal{U}_3$ and $\mathcal{U}_4$ are written as

$$\begin{aligned}
\mathcal{U}_2 &= [\mathcal{K}]^2 - [\mathcal{K}^2]\,,\\
\mathcal{U}_3 &= [\mathcal{K}]^3 - 3[\mathcal{K}][\mathcal{K}^2] + 2[\mathcal{K}^3]\,,\\
\mathcal{U}_4 &= [\mathcal{K}]^4 - 6[\mathcal{K}]^2[\mathcal{K}^2] + 8[\mathcal{K}][\mathcal{K}^3] + 3[\mathcal{K}^2]^2 - 6[\mathcal{K}^4]\,,
\end{aligned} \tag{6.3}$$

where

$$\mathcal{K}^\mu{}_\nu = \delta^\mu_\nu - \sqrt{g^{\mu\lambda}\partial_\lambda\phi^a\partial_\nu\phi^b\mathcal{F}_{ab}}\,. \tag{6.4}$$

Here, the trace of $\mathcal{K}^\mu_\nu$ is denoted by $[\mathcal{K}]$, where $(\mathcal{K}^i)^\mu_\nu = \mathcal{K}^\mu_{\rho_1}\mathcal{K}^{\rho_1}_{\rho_2}...\mathcal{K}^{\rho_i}_\nu$. The Stückelberg field is represented by ϕ^a, and the explicit form of the reference fiducial metric $\mathcal{F}_{ab}$ is given by

$$\mathcal{F}_{ab} = \begin{pmatrix} 0 & 0 & 0 & 0\\ 0 & 0 & 0 & 0\\ 0 & 0 & c^2 & 0\\ 0 & 0 & 0 & c^2\sin^2\theta \end{pmatrix}. \tag{6.5}$$

In the unitary gauge fixed as $\phi^a = x^\mu\delta^a_\mu$, the expression becomes

$$\sqrt{g^{\mu\lambda}\partial_\lambda\phi^a\partial_\nu\phi^b\mathcal{F}_{ab}} = \sqrt{g^{\mu\lambda}\mathcal{F}_{\lambda\nu}}\,. \tag{6.6}$$

Upon varying the action with respect to the metric $g_{\mu\nu}$, one may obtain the field equation for the modified dRGT-$f(R,T)$ massive gravity theory as follows:

$$f_R(R,T)R_{\mu\nu} - \frac{1}{2}f(R,T)g_{\mu\nu} + (g_{\mu\nu}\Box - \nabla_\mu\nabla_\nu)f_R(R,T) \\ = -m_g^2 X_{\mu\nu} + 8\pi T_{\mu\nu} - f_T(R,T)(T_{\mu\nu} + \Theta_{\mu\nu})\,. \tag{6.7}$$

In the equations above, $f_R(R,T)$ and $f_T(R,T)$ represent the derivatives of $f(R,T)$ with respect to R and T respectively, while $\Box f_R = g^{\mu\nu}\nabla_\mu\nabla_\nu f_R$. Additionally, the variation of the trace of the energy-momentum tensor of the matter field, $T = g^{\mu\nu}T_{\mu\nu}$, is expressed as

$$\frac{\delta(g^{\alpha\beta}T_{\alpha\beta})}{\delta g^{\mu\nu}} = T_{\mu\nu} + \Theta_{\mu\nu}\,, \tag{6.8}$$

where $\Theta_{\mu\nu}$ and $T_{\mu\nu}$ are defined as

$$\Theta_{\mu\nu} \equiv g^{\alpha\beta}\frac{\delta T_{\alpha\beta}}{\delta g^{\mu\nu}}\,, \tag{6.9}$$

$$T_{\mu\nu} \equiv g_{\mu\nu}\mathcal{L}_m - \frac{2\partial(\mathcal{L}_m)}{\partial g^{\mu\nu}}\,. \tag{6.10}$$

Here, $T_{\mu\nu}$ can alternatively be expressed using the principal pressure terms as follows:

$$T_{\mu\nu} = (\rho + p_t)u_\mu u_\nu + p_t g_{\mu\nu} + (p_r - p_t)\chi_\mu\chi_\nu\,, \tag{6.11}$$

where u_μ represents the timelike unit vector, and χ_μ denotes a spacelike unit vector, satisfying $u_\mu u^\mu = -1$ and $\chi_\mu\chi^\mu = 1$. Assuming the Lagrangian matter density $\mathcal{L}_m = \rho$ universally, one may obtain $\Theta_{\mu\nu} = -2T_{\mu\nu} + \rho g_{\mu\nu}$.

Furthermore, $X_{\mu\nu}$ stands for the massive graviton tensor, expressed as

$$X^\mu_\nu = \mathcal{K}^\mu_\nu - [\mathcal{K}]\delta^\mu_\nu - \alpha\left[(\mathcal{K}^2)^\mu_\nu - [\mathcal{K}]\mathcal{K}^\mu_\nu + \frac{1}{2}\delta^\mu_\nu\left([\mathcal{K}]^2 - [\mathcal{K}^2]\right)\right] \\ + 3\beta\left[(\mathcal{K}^3)^\mu_\nu - [\mathcal{K}](\mathcal{K}^2)^\mu_\nu + \frac{1}{2}\mathcal{K}^\mu_\nu\left([\mathcal{K}]^2 - [\mathcal{K}^2]\right)\right] \\ - 3\beta\left[\frac{1}{6}\delta^\mu_\nu\left([\mathcal{K}]^3 - 3[\mathcal{K}][\mathcal{K}^2] + 2[\mathcal{K}^3]\right)\right]\,, \tag{6.12}$$

where α and β are two massive gravity parameters, represented by

$$\alpha = 1 + 3\alpha_3\,, \qquad \beta = \alpha_3 + 4\alpha_4\,, \tag{6.13}$$

whereas by definition,

$$\frac{m_g^2}{8\pi}X_{\mu\nu} = -(\rho^{(g)} + p_t^{(g)})u_\mu u_\nu - p_t^{(g)}g_{\mu\nu} - (p_r^{(g)} - p_t^{(g)})\chi_\mu\chi_\nu\,, \tag{6.14}$$

which represents the energy-momentum tensor of the massive gravity sector. Utilizing Eq. (6.12), the density and pressure components $\rho^{(g)}(r)$ and $p^{(g)}_{r,\perp}(r)$ of the massive

gravitons for static Morris-Thorne wormholes can be readily computed as [206]

$$\rho^{(g)}(r) \equiv \frac{m_g^2}{8\pi} X^t{}_t = -\frac{1}{8\pi}\left(\frac{2\gamma - \Lambda r}{r}\right), \tag{6.15}$$

$$p_r^{(g)}(r) \equiv -\frac{m_g^2}{8\pi} X^r{}_r = \frac{1}{8\pi}\left(\frac{2\gamma - \Lambda r}{r}\right), \tag{6.16}$$

$$p_{\theta,\phi}^{(g)}(r) \equiv -\frac{m_g^2}{8\pi} X_{\theta,\phi}^{\theta,\phi} = \frac{1}{8\pi}\left(\frac{\gamma - \Lambda r}{r}\right). \tag{6.17}$$

In the above equations, the effective cosmological constant Λ and a novel parameter γ are introduced and expressed as linear combinations of the parameters α and β. This formulation is given by

$$\Lambda \equiv -3m_g^2(1+\alpha+\beta), \qquad \gamma \equiv -m_g^2 c(1+2\alpha+3\beta). \tag{6.18}$$

Subsequently, through basic mathematical manipulations applied to Eq. (6.7), the final field equation is obtained to be

$$G_{\mu\nu} = 8\pi G_{eff} T_{\mu\nu} + T_{\mu\nu}^{eff} - \frac{1}{f_R(R,T)} m_g^2 X_{\mu\nu}, \tag{6.19}$$

where

$$G_{eff} = \frac{1}{f_R(R,T)}\left(1 + \frac{f_T(R,T)}{8\pi}\right), \tag{6.20}$$

$$T_{\mu\nu}^{eff} = \frac{1}{f_R(R,T)}\left[\frac{1}{2}\big(f(R,T) - R f_R(R,T) + 2\rho f_T(R,T)\big) g_{\mu\nu} - \big(g_{\mu\nu}\Box - \nabla_\mu\nabla_\nu\big) f_R(R,T)\right]. \tag{6.21}$$

It is worth noting that when $f(R,T) \equiv f(R)$, where $f_T(R,T) = 0$, the conventional $f(R)$ massive gravity solution is recovered. In the field equation, the energy-momentum tensor component ($T_{\mu\nu}$) of $f(R,T)$ gravity depicts the interaction between matter and curvature. This interaction can be understood as the coupling between curvature and matter arising from the exchange of energy and momentum between them. Conversely, when considering the total energy-momentum tensor, which combines the contributions from $f(R,T)$ and massive gravity sectors, it incorporates the interaction of massive gravitons with the curvature-matter coupling. This can be mathematically expressed as:

$$T_{\mu\nu}^{tot} = \text{diag}\left(-\rho - \rho^{(g)}, p_r + p_r^{(g)}, p_t + p_t^{(g)}, p_t + p_t^{(g)}\right). \tag{6.22}$$

However, the energy-momentum sector of $f(R,T)$ gravity, as proposed by Harko *et al.* [122], presents a critical issue by violating the energy conservation law and resulting in non-geodesic motion of test particles. Conversely, an alternative approach to $f(R,T)$ gravity, suggested by Chakraborty [569], demonstrates that maintaining conservation of the EM tensor results in a similar form of the field equation. Consequently, test

particles follow geodesic orbits, and the choice of Lagrangian is not entirely arbitrary. For the homogeneous and isotropic universe model, this approach yields field equations equivalent to Einstein gravity with a non-interacting 2-fluid system, where one component behaves as the usual perfect fluid and the other exhibits exotic properties.

Recently, in [570, 571], it was demonstrated that $f(R,T)$ gravity can accommodate a wormhole with non-exotic matter, where the ordinary EM tensor satisfies the null energy condition (NEC), while the additional curvature from modified gravity leads to NEC violation for the total EM tensor. The existence of ordinary matter wormholes in the context of modified gravity is briefly discussed in [559].

Mathematically, the EM tensor in massive gravity exhibits properties akin to anisotropic dark energy, with $p_r^{(g)} = -\rho^{(g)}$. This behaviour can effectively model various compact objects and astrophysical phenomena [166–173, 199]. Consequently, in $f(R,T)$-massive gravity, the interplay between massive gravitons and effective geometric matter (arising from curvature) can lead to exotic behaviour. Thus, if the EM sector of usual matter satisfies energy conditions and is dominated by the sum of gravitons and geometric matter, an ordinary matter wormhole may emerge.

To establish a traversable wormhole solution, the Morris-Thorne line element is considered [321]:

$$ds^2 = -e^{2\Phi(r)}dt^2 + \left(1 - \frac{b(r)}{r}\right)^{-1} dr^2 + r^2 d\Omega^2\,, \tag{6.23}$$

where $d\Omega^2 = d\theta^2 + \sin^2\theta d\phi^2$, and $\Phi(r)$ and $b(r)$ represent the redshift function and shape function respectively. Traversability of this particular wormhole geometry necessitates the following conditions:

1. The construction of the wormhole involves gluing two asymptotic regions at the wormhole throat, denoted by the minimum $r = r_0$. Thus, the radial coordinate spans the interval $r \in [\, r_0, \infty)$.

2. To prevent the presence of horizons and singularities, the redshift function $\Phi(r)$ must be finite everywhere, ensuring $e^{\Phi(r)} > 0$ for $r > r_0$.

   The ultrastatic wormhole, a specific case of interest, represents the zero-tidal force wormhole where $\Phi(r) = 0$, resulting in $e^{\Phi(r)} = 1$. In this scenario, a particle initially at rest remains stationary in a frame devoid of gravitational acceleration [321].

3. The flaring-out condition, $-rb'(r) + b(r) > 0$, needs to be satisfied at or near the throat $r = r_0$.

4. These conditions imply $b(r_0) = r_0$ and $b'(r_0) \leq 1$, $\forall r \geq r_0$, with equality of $b'(r_0)$ occurring solely at the throat. Moreover, for $r > r_0 \Rightarrow b(r) < r$.

5. Asymptotic flatness dictates $\Phi(r) \to 0$ and $b(r)/r \to 0$ as $r \to \infty$.

The redshift and shape functions must adhere to these conditions (for further details, refer to [321]).

The Einstein tensor components of the metric (6.23) are given as follows:

$$G_{tt} = \frac{b'}{r^2}\,, \tag{6.24}$$

$$G_{rr} = -\frac{b}{r^3} + 2\left(1-\frac{b}{r}\right)\frac{\Phi'}{r}\,, \tag{6.25}$$

$$G_{\theta\theta} = G_{\phi\phi} = \left(1-\frac{b}{r}\right)\left[\Phi'' + \Phi'^2 + \left(\frac{-rb'+2r-b}{2r(r-b)}\right)\Phi' - \frac{rb'-b}{2r^2(r-b)}\right]. \tag{6.26}$$

Utilizing these components, the computation of the field equation for $f(R,T)$ massive gravity from Eq. (6.19) can be readily performed. The components are obtained as

$$\begin{aligned}\rho =& \frac{f}{16\pi} + \frac{f_R}{8\pi}\left[\left(1-\frac{b}{r}\right)\left(\Phi''+\Phi'^2\right) - \frac{rb'+3b-4r}{2r^2}\Phi'\right] \\ &- \left(1-\frac{b}{r}\right)\frac{f_R''}{8\pi} + \left(\frac{rb'+3b-4r}{2r^2}\right)\frac{f_R'}{8\pi} + \left(\frac{2\gamma-\Lambda r}{8\pi r}\right),\end{aligned} \tag{6.27}$$

$$\begin{aligned}p_r =& -\frac{f}{16\pi} + \left(1-\frac{b}{r}\right)\frac{f_R'' f_T}{8\pi(8\pi+f_T)} - \frac{f_R'}{(8\pi+f_T)}\left[\left(\frac{rb'+3b-4r}{2r^2}\right)\frac{f_T}{8\pi}\right. \\ &\left. - \left(1-\frac{b}{r}\right)\left(\Phi'+\frac{2}{r}\right)\right] - \frac{f_R}{(8\pi+f_T)}\left[\left(\frac{-rb'-3b+4r}{2r^2}\right)\Phi'\frac{f_T}{8\pi}\right. \\ &\left. + \left(\frac{-rb'+b}{2r^2}\right)\left(\Phi'+\frac{2}{r}\right)\right] - \left(1-\frac{b}{r}\right)\left(\Phi''+\Phi'^2\right)\frac{f_R}{8\pi} - \left(\frac{2\gamma-\Lambda r}{8\pi r}\right),\end{aligned} \tag{6.28}$$

$$\begin{aligned}p_t =& -\frac{f}{16\pi} + \left(1-\frac{b}{r}\right)\frac{f_R''}{8\pi} - \frac{f_R'}{(8\pi+f_T)}\left[\left(\frac{rb'+3b-4r}{2r^2}\right)\frac{f_T}{8\pi} + \left(\frac{rb'+b-2r}{2r^2}\right)\right. \\ &\left. - \left(1-\frac{b}{r}\right)\Phi'\right] - \frac{f_R}{(8\pi+f_T)}\left[\left(\frac{r-b}{r^2} - \left(\frac{rb'+3b-4r}{2r^2}\right)\frac{f_T}{8\pi}\right)\Phi'\right. \\ &\left. - \frac{rb'+b}{2r^3}\right] - \frac{f_R f_T}{8\pi(8\pi+f_T)}\left(1-\frac{b}{r}\right)\left(\Phi''+\Phi'^2\right) - \left(\frac{2\gamma-\Lambda r}{8\pi r}\right).\end{aligned} \tag{6.29}$$

Now, to construct a wormhole solution, various approaches can be adopted, such as specifying choices for $\Phi(r)$, $b(r)$, and $f(R,T)$, among others. Another approach involves prescribing specific pressures (isotropic/anisotropic) or equations of state for p_r, p_t. However, pre-determining the shape function before obtaining the solution may neglect the influence of massive gravity on the shape. For instance, a wormhole solution in $f(R)$ massive gravity as proposed by Tangphati *et al.* [206]. Thus, in this current investigation, the anisotropic pressure solution in $f(R,T)$ massive gravity is explored, which demonstrates the impact of massive gravitons on the wormhole shape function.

6.3 Anisotropic solution

In the context of the anisotropic pressure fluid wormhole solution in dRGT-$f(R,T)$ massive gravity, a straightforward selection of $f(R,T)$ is opted for, such as $f(R,T) \equiv (\alpha R + \beta T)$ [1]. Here, the parameters $\alpha = 1$ and $\beta = 2\lambda$ yield the familiar linear $f(R,T)$ cosmology, specifically $f(R,T) \equiv (R + 2\lambda T)$ [122]. Notably, $f_R = \alpha$, $f_T = \beta$, and $f'_R = f''_R = 0$ for this particular choice. Additionally, an ultrastatic wormhole is selected for the specific solution, resulting in $\Phi'(r) = \Phi''(r) = 0$. Consequently, the reduced energy-momentum components can be directly computed as follows:

$$\rho = \frac{\alpha b'}{r^2(8\pi+\beta)} + \frac{2\gamma - \Lambda r}{2r(4\pi+\beta)}\,, \tag{6.30}$$

$$p_r = -\frac{\alpha b}{r^3(8\pi+\beta)} - \frac{2\gamma - \Lambda r}{2r(4\pi+\beta)}\,, \tag{6.31}$$

$$p_t = \frac{\alpha(-rb'+b)}{2r^3(8\pi+\beta)} - \frac{2\gamma - \Lambda r}{2r(4\pi+\beta)}\,. \tag{6.32}$$

The equation for the anisotropic pressure fluid is expressed as $p_t = \sigma p_r$, where $\sigma = 1$ indicates isotropic pressure condition ($p_t = p_r = p$). Conversely, for anisotropic pressure fluid, to maintain asymptotic flatness of the spacetime, σ must be negative. Therefore, for our specific selections, equations (6.31) and (6.32) can be directly employed to derive the shape function.

$$b(r) = \frac{r^2(8\pi+\beta)}{2\alpha(4\pi+\beta)}\left[\frac{-4\gamma(1-\sigma) + \Lambda r(1-2\sigma)}{(1-2\sigma)}\right] + Cr^{1+2\sigma}\,, \tag{6.33}$$

where C represents the constant of integration. It is to be noted that the shape function depends exclusively on the γ and Λ parameters of massive gravity, and consequently, on the mass of the graviton.
A notable observation is that when $\sigma = -1$ and $\gamma = \Lambda = 0$, the equation simplifies to the shape function of the so-called Ellis wormhole [349].
However, the position of the wormhole throat can be determined by finding the root of $\left(1 - \frac{b(r)}{r}\right) = 0$, which (within our region of interest) ultimately yields

$$1 + A\gamma r - B\Lambda r^2 + Cr^{2\sigma} = 0\,, \tag{6.34}$$

where

$$A = \frac{2(8\pi+\beta)}{\alpha(4\pi+\beta)}\left(\frac{1-\sigma}{1-2\sigma}\right)\,, \qquad B = \frac{(8\pi+\beta)}{2\alpha(4\pi+\beta)}\,. \tag{6.35}$$

For the Ellis wormhole, Eq. (6.34) transforms to

$$1 + \bar{A}\gamma r - B\Lambda r^2 + \frac{C}{r^2} = 0\,. \tag{6.36}$$

[1] Please note that the α and β parameters mentioned here are distinct from those used in the field equation of massive gravity. Henceforth, the coefficients of $f(R,T)$ will exclusively be denoted by α and β, except when discussing the deflection angle.

Equation (6.36) possesses four roots, with one real root determining the throat radius. Imposing condition 4 of the minimum requirements for wormhole geometry in section 6.2, i.e., $b(r = r_0) = r_0$, allows determination of C from (6.34) such that the throat radius r_0 is specified. Hence, the final shape function is expressed as

$$b(r) = r\left(\frac{r}{r_0}\right)^{2\sigma} - \frac{r(8\pi+\beta)}{2\alpha(4\pi+\beta)(1-2\sigma)} \times \left[4\gamma\,(1-\sigma)\left(r - r_0\left(\frac{r}{r_0}\right)^{2\sigma}\right) - \Lambda\,(1-2\sigma)\left(r^2 - r_0^2\left(\frac{r}{r_0}\right)^{2\sigma}\right)\right]. \tag{6.37}$$

As anticipated, the outcome reveals that in the absence of massive gravity effects (i.e., $\gamma = \Lambda = 0$), the expression aligns with the conventional solution of anisotropic pressure fluid in $f(R,T)$ gravity. However, the inclusion of r and r^2 terms respectively with γ and Λ in the second term of the shape function alters the asymptotic flatness of the spacetime. This effect closely resembles the behaviour observed in black hole solutions within dRGT massive gravity, as found in [554].

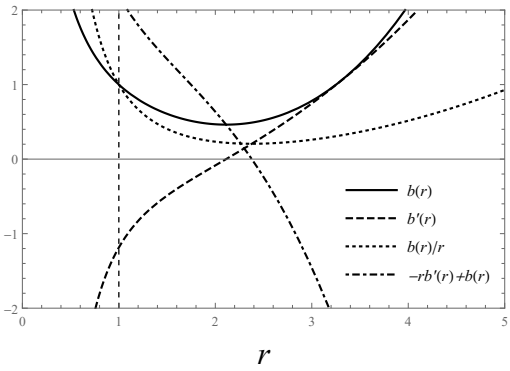

Figure 6.1: Nature of $f(R,T)$-massive gravity shape function according to the Morris-Thorne wormhole properties for $\alpha = 1, \beta = 2, \sigma = -1, \gamma = 0.06$, and $\Lambda = 0.07$. The vertical dashed line represent the throat radius $r_0 = 1$.

To examine the characteristics of the shape function, $b(r)$, $b'(r)$, $b(r)/r$, and the flaring-out component $-rb'(r)+b(r)$ is depicted in Fig. 6.1. Although all properties are fulfilled near the throat, conditions stipulated by $b'(r) < 1$, $b(r)/r < 1$, $\forall\ r > r_0$, and $b(r)/r \to 0$ for $r \to \infty$ are notably violated beyond a certain radial distance. Thus, it is apparent that the spacetime's asymptotic flatness diminishes after a certain distance due to the presence of massive gravitons. This can be interpreted as a consequence of the repulsive gravity effect, which is another distinctive feature of the dRGT massive gravity theory. A similar effect is observed in the black hole solution in massive gravity, where the asymptotic structure changes due to this effect [554]. It is worth noting that repulsive gravity behaviour is also observed in BHT massive gravity [553], as well as in other modified gravities involving exotic matter and energy [548–552].

Upon revisiting the discussion regarding non-asymptotic geometry, as $r \to \infty$, the ratio $b(r)/r$ does not approach '0'; instead, it tends towards '∞'. This behaviour arises from the inclusion of linear r and r^2 terms with γ and Λ respectively in Eq. (6.37), resulting in the absence of asymptotic flatness. It is obvious and can be mathematically proven that alternative selections of $f(R,T)$ in ultrastatic wormhole geometry also involve such terms with r and r^2, incorporating γ and Λ in the shape function. Comparable scenarios can be observed in other gravitational theories, including Einstein's

gravity coupled with massive gravitons (which will be discussed later in this chapter), and in $f(R)$ massive gravity. Therefore, it can be inferred that this characteristic is a common aspect of wormholes in dRGT massive gravity.

To ascertain the presence of the repulsive gravity effect in the wormhole solution and its potential impact on the asymptotic structure, it is essential to examine the photon deflection angle within the wormhole. The deflection angle becomes negative in a spacetime where repulsive gravity influences photons, as demonstrated in previous studies [554].

6.3.1 Repulsive behaviour of gravity

To examine the deflection angle of photons from null geodesics, initially a general spherically symmetric and static line element is introduced, as described by [14, 572]

$$ds^2 = -A(r)dt^2 + B(r)dr^2 + C(r)d\Omega^2 \,. \tag{6.38}$$

The geodesic equation, which establishes the relationship between the momenta one-forms of a freely falling body and the background geometry, is provided by [572]

$$\frac{dp_\beta}{d\lambda} = \frac{1}{2} g_{\nu\alpha,\beta} p^\nu p^\alpha \,, \tag{6.39}$$

where λ denotes the affine parameter. It is evident that if the components of $g_{\alpha\nu}$ do not vary with x^β for a fixed index β, then p_β remains constant. Thus, when considering solely the equatorial slice with $\theta = \pi/2$, the $g_{\alpha\beta}$ terms in Eq. (6.39) are independent of t, θ, ϕ, allowing determination of the corresponding killing vector fields $\delta^\mu_\alpha \partial_\nu$ with α as a cyclic coordinate. Consequently, the constants of motion p_t and p_ϕ can be set as $p_t = -E$ and $p_\phi = L$, where E and L denote the energy and angular momentum of the photon, respectively. Hence, the following expressions are obtained

$$\begin{aligned} p_t = \dot{t} = g^{t\nu} p_\nu = \frac{E}{A(r)} \,, \\ p_\phi = \dot{\phi} = g^{\phi\nu} p_\nu = \frac{L}{C(r)} \,, \end{aligned} \tag{6.40}$$

where the overdot denotes differentiation with respect to the affine parameter λ. Similarly, the equation for the radial null geodesic is easily derived as

$$\dot{r}^2 = \frac{1}{B(r)} \left(\frac{E^2}{A(r)} - \frac{L^2}{C(r)} \right) . \tag{6.41}$$

However, expressing the equation for the photon orbit in terms of the impact parameter $\mu = L/E$ yields:

$$\left(\frac{dr}{d\phi} \right)^2 = \frac{C(r)^2}{\mu^2 B(r)} \left[\frac{1}{A(r)} - \frac{\mu^2}{C(r)} \right] . \tag{6.42}$$

To calculate the deflection angle of a photon, a source can be considered with a photon radius r_s influencing the geometry. The photons can intersect the surface only if an

existing solution r_0 satisfies the condition $r_0 > r_s$ and $\dot{r}^2 = 0$, where r_0 represents the turning point. In this scenario, the impact parameter is given by

$$\mu = \frac{L}{E} = \pm\sqrt{\frac{C(r_0)}{A(r_0)}}\,. \tag{6.43}$$

Thus, it is evident that in the weak field limit, $\mu \approx \sqrt{C(r_0)}$. Consequently, if a photon originates from the polar limit defined by $\lim_{r\to\infty}\left(r, -\frac{\pi}{2} - \frac{\alpha}{2}\right)$, passes through the turning point at $(r_0, 0)$, and hits $\lim_{r\to\infty}\left(r, \frac{\pi}{2} + \frac{\alpha}{2}\right)$, then the photon deflection angle is identified as α, as a function of r_0 [547]. This angle can be calculated by Eq. (6.42) as follows:

$$\alpha(r_0) = -\pi + 2\int_{r_0}^{\infty} \frac{\sqrt{B(r)}dr}{\sqrt{C(r)}\left[\left(\frac{A(r_0)}{A(r)}\right)\left(\frac{C(r)}{C(r_0)}\right) - 1\right]^{1/2}}\,. \tag{6.44}$$

For the present choice of Morris-Thorne line element (6.23), this equation takes the form

$$\alpha(r_0) = -\pi + 2\int_{r_0}^{\infty} \frac{dr}{r\left[\left(1 - \frac{b(r)}{r}\right)\left(\frac{r^2}{r_0^2} - 1\right)\right]^{1/2}}\,. \tag{6.45}$$

The deflection angle of photons in massive gravity can now be demonstrated by numerically integrating the aforementioned equation, subject to the shape function specified in Eq. (6.37), as depicted in Fig 6.2.

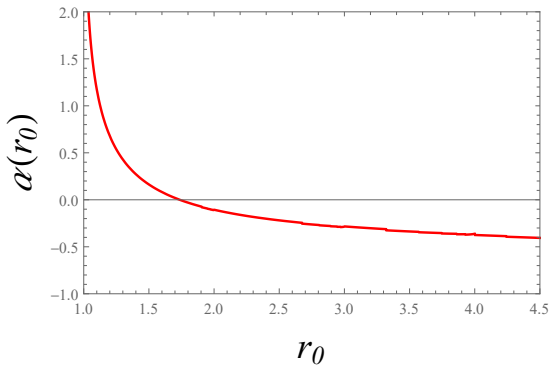

Figure 6.2: The deflection angle of photon in $f(R,T)$-massive gravity for $r_0 = 1, \sigma = -1, \gamma = 0.06, \Lambda = 0.07, \alpha = 1$, and $\beta = 2$. The angle is negative after a certain distance, representing the repulsive behaviour of gravity.

Remarkably, the deflection angle assumes a negative value beyond a certain threshold of r_0. This phenomenon can be attributed to the presence of repulsive gravity. Without considering the massive gravity parameters γ and Λ (i.e., in the absence of massive gravity), it can be verified that negative deflection angles do not occur [461]. Additionally, from Fig. 6.1, it is evident that inconsistencies in the spacetime structure, such as disturbance in asymptotic flatness, manifest beyond a radial distance where the repulsive gravity effect comes into play. Therefore, it can be inferred that the complexity of the asymptotic structure results from the repulsive nature of gravity.

However, the repulsive characteristic of anisotropic dark energy is inherent in massive gravitons. Consequently, their presence may physically induce the repulsive effect observed in dRGT massive gravity.

6.4 Wormhole in Einstein-massive gravity

To initiate the study of Einstein gravity within the framework of dRGT massive gravity, the action is given by

$$S = \int d^4x\sqrt{-g}\left(\frac{1}{16\pi}\left[R + m_g^2\mathcal{U}(g,\phi^a)\right] + \mathcal{L}_m\right). \tag{6.46}$$

This action incorporates the effects of both Einstein gravity and dRGT massive gravity, along with other relevant parameters outlined in section 6.2. By varying the action with respect to $g_{\mu\nu}$, the following field equation can be derived:

$$G_{\mu\nu} = 8\pi T_{\mu\nu} - m_g^2 X_{\mu\nu}\,. \tag{6.47}$$

The above outcomes can be straightforwardly obtained by setting $f(R,T) = R$, implying $f_R(R,T) = 1$, in the $f(R,T)$ massive gravity.

In Eq. (6.47), the EM tensor of Einstein's gravity adheres to the principle of energy conservation, while the collective EM tensor for the coupled perfect fluid-massive graviton system is expressed as

$$T_{\mu\nu}^{tot} = diag\left(-\rho^E - \rho^{(g)}, p_r^E + p_r^{(g)}, p_t^E + p_t^{(g)}, p_t^E + p_t^{(g)}\right), \tag{6.48}$$

where the superscript 'E' denotes the EM components for Einstein gravity. Consequently, one can express the conservation laws $\nabla^\mu T_{\mu\nu}^{tot} = 0$, $\nabla^\mu T_{\mu\nu} = 0$, and $\nabla^\mu T_{\mu\nu}^{(g)} = 0$ directly. In Einstein-massive gravity, constructing a wormhole may be feasible with non-exotic matter sources, leveraging the exotic nature of massive gravitons to manipulate the violation of energy conditions.

To derive the field equation calculations for the wormhole geometry, Eq. (6.24), (6.25), and (6.26) are substituted into Eq. (6.47) to get

$$\rho = \frac{b'}{8\pi r^2} + \left(\frac{2\gamma - \Lambda r}{8\pi r}\right), \tag{6.49}$$

$$p_r = -\frac{b}{8\pi r^3} + \left(1 - \frac{b}{r}\right)\frac{\Phi'}{4\pi r} - \left(\frac{2\gamma - \Lambda r}{8\pi r}\right), \tag{6.50}$$

$$p_t = \left(\frac{-rb' + b}{16\pi r^3}\right) + \left(\frac{-rb' + 2r - b}{16\pi r^2}\right)\Phi' + \frac{1}{8\pi}\left(1 - \frac{b}{r}\right)\left(\Phi'' + \Phi'^2\right) - \left(\frac{2\gamma - \Lambda r}{8\pi r}\right). \tag{6.51}$$

In this context, it is aimed to construct an anisotropic pressure solution within an ultrastatic wormhole geometry, for which the restriction is given by Φ = constant, implying $\Phi' = \Phi'' = 0$. Consequently, the equation of state for the solution, denoted as $p_t = \sigma p_r$, determines the shape function of the wormhole. Utilizing the boundary condition at the wormhole throat, i.e., $b(r_0) = r_0$, yields the final shape function as follows:

$$b(r) = r\left[\left(\frac{r}{r_0}\right)^{2\sigma} - \frac{4\gamma(1-\sigma)}{(1-2\sigma)}\left(r - r_0\left(\frac{r}{r_0}\right)^{2\sigma}\right) + \Lambda\left(r^2 - r_0^2\left(\frac{r}{r_0}\right)^{2\sigma}\right)\right]. \tag{6.52}$$

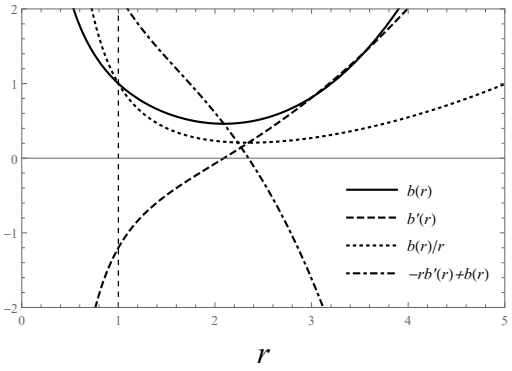

Figure 6.3: Nature of the shape function in Einstein-massive gravity according to the Morris-Thorne wormhole properties for $\sigma = -1, \gamma = 0.06$, and $\Lambda = 0.07$. The vertical dashed line represent the throat radius $r_0 = 1$.

The shape function bears strong resemblance to that obtained in $f(R,T)$ gravity. Visualizations of the shape function properties, including $b(r)$, $b'(r)$, $b(r)/r$, and $(-rb'(r) + b(r))$, are depicted in Fig. 6.3. These plots reveal a departure from asymptotic flatness beyond a certain radial distance, attributed to the presence of linear r and r^2 terms with γ and Λ respectively. However, when the expression is devoid of the massive gravity parameters (i.e., $\gamma = \Lambda = 0$), a shape function that asymptotically conforms well is retrieved.

Discussion on the repulsive effect of gravity in this context is indeed warranted. Thus, Eq. (6.45) is employed to plot the numerical solution of the deflection angle of photons in the dRGT extension of Einstein gravity. The presence of a negative deflection angle indicates the existence of repulsive gravity, with all other comprehensive discussions paralleling those in $f(R,T)$-massive gravity. This plot is illustrated in Fig. 6.4, and upon comparison with Fig. 6.3, it becomes apparent that the Morris-Thorne wormhole shape function properties are compromised beyond the radial distance where the deflection angle turns negative. Therefore, even in Einstein-massive gravity, the asymptotic flatness of the traversable wormhole is disturbed due to the repulsive effect of gravity, which can be attributed to the anisotropic dark energy behaviour of massive gravitons.

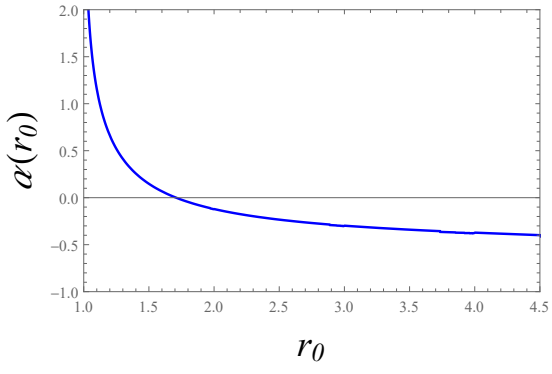

Figure 6.4: The deflection angle of photon in Einstein-massive gravity for $r_0 = 1, \sigma = -1, \gamma = 0.06, \Lambda = 0.07$. The angle is negative after a certain distance, representing the repulsive behaviour of gravity.

6.5 Energy Conditions

It is crucial to examine energy conditions in the context of traversable wormhole configurations to understand the matter content within the wormhole. As previously discussed, the throat of typical static Morris-Thorne wormholes requires exotic matter that violates the Null Energy Condition (NEC), to keep the wormhole throat open and traversable. Interestingly, in massive gravity theory, the massive graviton energy-momentum tensor can naturally exhibit features of energy condition violation, as the massive graviton density may be negative in certain regions where radial pressure is positive [573]. Thus, the existence of wormholes in massive gravity theory could be a natural consequence.

In this section, the energy conditions for wormhole configurations will be explored successively in $f(R,T)$-massive gravity and Einstein-massive gravity.
Energy conditions can be summarized in principal pressure forms as follows:

(i) NEC: $\rho + p_r \geq 0, \quad \rho + p_t \geq 0;$
(ii) WEC: $\rho \geq 0, \quad \rho + p_r \geq 0, \quad \rho + p_t \geq 0;$
(iii) SEC: $\rho + p_r \geq 0, \quad \rho + p_t \geq 0, \quad \rho + p_r + 2p_t \geq 0;$
(iv) DEC: $\rho \geq 0, \quad \rho - |p_r| \geq 0, \quad \rho - |p_t| \geq 0.$

Note that, standard mathematical techniques can be employed to compute ρ, $\rho + p_r$, $\rho + p_t$, $\rho - |p_r|$, $\rho - |p_t|$, and $\rho + p_r + 2p_t$ from equations (6.30), (6.31), and (6.32), while incorporating the shape function defined in Eq. (6.37). Utilizing these six terms enables the investigation of all four energy conditions for $f(R,T)$-massive gravity. The mathematical outcomes of these terms are graphically depicted in Fig. 6.5 for parameter choices $\alpha = 1$, $\beta = 2$, $\sigma = -1$, and $r_0 = 1$. Furthermore, a summary of the results obtained from the plots is provided in Table 6.1.

From the analysis presented in Fig. 6.5 and Table 6.1, it is evident that all energy conditions, including energy density, are upheld throughout the wormhole region, starting from $r = 0.87$ and $r = 0.83$, respectively, for $\gamma = 0.01$, $\Lambda = 0.7$ and $\gamma = -0.01$, $\Lambda = 0.7$. Furthermore, the differences in energy condition components are marginal for varying signs of γ. However, they exhibit a high sensitivity to the effective cosmological constant (Λ). Specifically, for $\gamma = 0.01$, $\Lambda = -0.7$, all components are entirely negative, indicating a violation of energy conditions. Moreover, for smaller values of γ and Λ, corresponding to less significant effects of massive gravity, energy conditions are violated at the wormhole throat but become satisfied beyond a certain radial distance.

It is worth noting that for the first two combinations of γ and Λ, that is $\gamma = 0.01$, $\Lambda = 0.7$ and $\gamma = -0.01$, $\Lambda = 0.7$, the construction of the wormhole is feasible with ordinary matter, meeting all energy conditions. This scenario has been extensively investigated in [559], affirming the possibility of constructing wormholes with ordinary matter in modified gravity theories. However, violation of the Null Energy Condition (NEC) is common at the wormhole throat to maintain traversability. Previous studies in $f(R,T)$ gravity [570, 571] have also explored wormhole models with non-exotic mat-

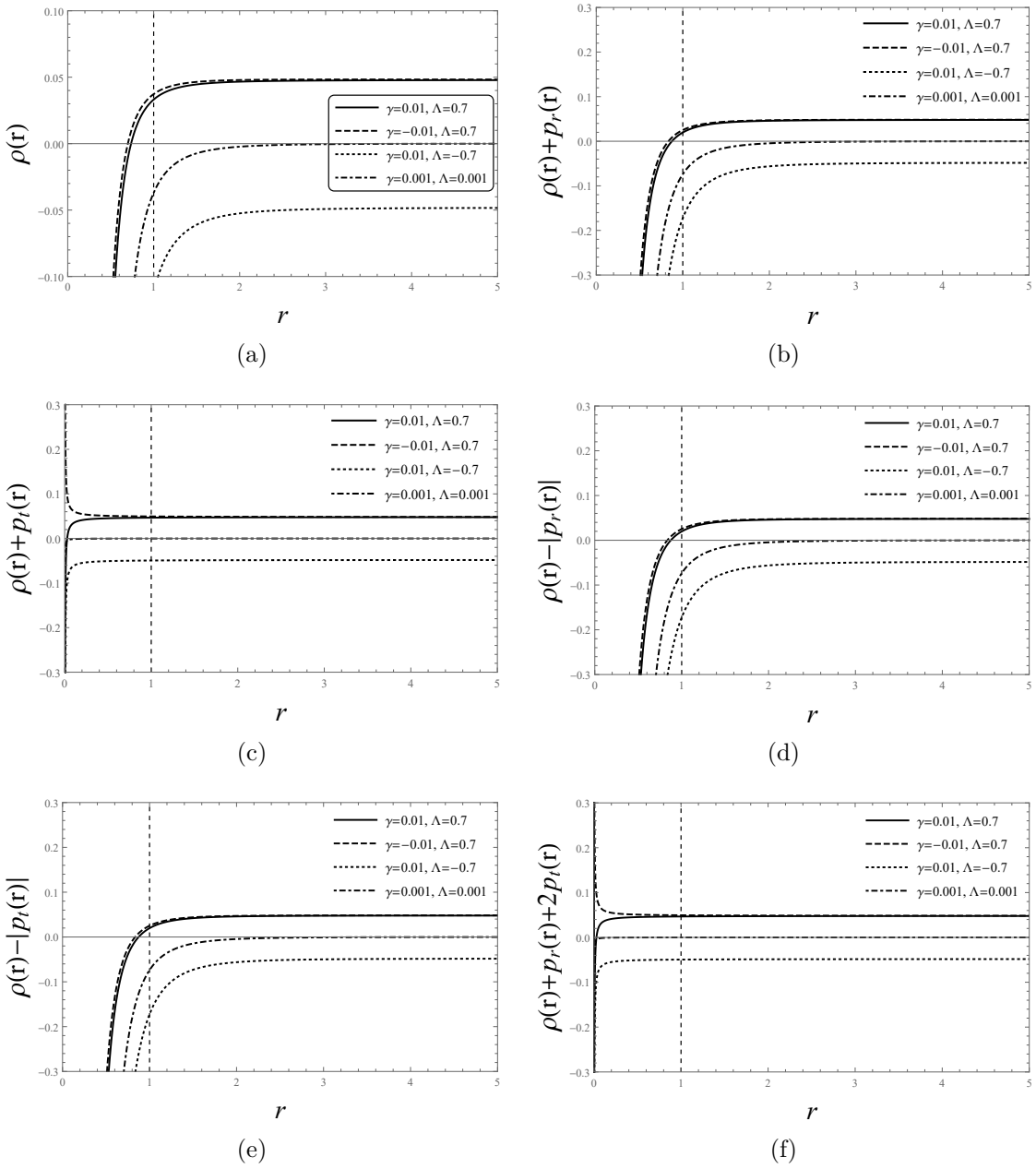

Figure 6.5: The variation of energy condition components, $\rho,\ \rho+p_r,\ \rho+p_t,\ \rho-|p_r|,\ \rho-|p_t|$, and $\rho+p_r+2p_t$, against radial coordinate r, for four different combinations of γ and Λ. The fixed parameters are $\alpha=1,\ \beta=2,\ \sigma=-1$, and the throat radius $r_0=1$. The vertical dashed line represents the throat radius.

ters, where the curvature matter source serves as the exotic matter, violating energy conditions. In the present context, the matter source of massive gravitons, acting as anisotropic dark energy, combined with the curvature matter source, results in the violation of energy condition components. Therefore, conventional matter can serve as the matter source, while the strong repulsive dark energy nature of massive gravitons

Terms	γ and Λ	Result
ρ	$\gamma = 0.01,\ \Lambda = 0.7$	≥ 0 for $r \in [\ 0.73, \infty)$
	$\gamma = -0.01,\ \Lambda = 0.7$	≥ 0 for $r \in [\ 0.69, \infty)$
	$\gamma = 0.01,\ \Lambda = -0.7$	Always < 0
	$\gamma = 0.001,\ \Lambda = 0.001$	≥ 0 for $r \in [\ 5.29, \infty)$
$\rho + p_r$	$\gamma = 0.01,\ \Lambda = 0.7$	≥ 0 for $r \in [\ 0.87, \infty)$
	$\gamma = -0.01,\ \Lambda = 0.7$	≥ 0 for $r \in [\ 0.83, \infty)$
	$\gamma = 0.01,\ \Lambda = -0.7$	Always < 0
	$\gamma = 0.001,\ \Lambda = 0.001$	≥ 0 for $r \in [\ 6.09, \infty)$
$\rho + p_t$	$\gamma = 0.01,\ \Lambda = 0.7$	≥ 0 for $r \in [\ 0.02, \infty)$
	$\gamma = -0.01,\ \Lambda = 0.7$	Always > 0
	$\gamma = 0.01,\ \Lambda = -0.7$	Always < 0
	$\gamma = 0.001,\ \Lambda = 0.001$	≥ 0 for $r \in [\ 2, \infty)$
$\rho - \lvert p_r \rvert$	$\gamma = 0.01,\ \Lambda = 0.7$	≥ 0 for $r \in [\ 0.87, \infty)$
	$\gamma = -0.01,\ \Lambda = 0.7$	≥ 0 for $r \in [\ 0.83, \infty)$
	$\gamma = 0.01,\ \Lambda = -0.7$	Always < 0
	$\gamma = 0.001,\ \Lambda = 0.001$	≥ 0 for $r \in [\ 6.09, \infty)$
$\rho - \lvert p_t \rvert$	$\gamma = 0.01,\ \Lambda = 0.7$	≥ 0 for $r \in [\ 0.87, \infty)$
	$\gamma = -0.01,\ \Lambda = 0.7$	≥ 0 for $r \in [\ 0.83, \infty)$
	$\gamma = 0.01,\ \Lambda = -0.7$	Always < 0
	$\gamma = 0.001,\ \Lambda = 0.001$	≥ 0 for $r \in [\ 6.09, \infty)$
$\rho + p_r + 2p_t$	$\gamma = 0.01,\ \Lambda = 0.7$	≥ 0 for $r \in [\ 0.02, \infty)$
	$\gamma = -0.01,\ \Lambda = 0.7$	Always > 0
	$\gamma = 0.01,\ \Lambda = -0.7$	Always < 0
	$\gamma = 0.001,\ \Lambda = 0.001$	≥ 0 for $r \in [\ 2, \infty)$

Table 6.1: Numerical outcomes regarding the potential zones where corresponding energy conditions are satisfied.

induces a repulsive gravity effect in spacetime, significantly affecting the asymptotic flatness of the geometry.

Conversely, the Einstein-massive gravity model exhibits very little deviation from our linear $f(R,T)$-massive gravity formulation. By setting $\alpha = 1$ and $\beta = 0$ in Eq. (6.30), (6.31), (6.32), and (6.37), one can effortlessly recover the EM components and the shape function for Einstein gravity. Mathematically, the EM components show only a loose dependency on β, and visually, the energy conditions display quite similar behaviour for $\alpha = 1$ and $\beta = 0$. For scenarios where $\gamma = 0.01,\ \Lambda = 0.7$, and $\gamma = -0.01,\ \Lambda = 0.7$, an ordinary matter wormhole is also present. However, it is solely the massive gravity sector that introduces the violations in energy conditions. Therefore, it is apparent that the discussions pertaining to the Einstein-massive gravity model closely parallel those of the $f(R,T)$ gravity.

6.6 Equilibrium Analysis

The equilibrium condition for the current study is described by the generalized Tolman–Oppenheimer–Volkov (TOV) equation, expressed as

$$\frac{dp_r}{dr} + \frac{\Phi'}{2}(\rho + p_r) + \frac{2}{r}(p_r - p_t) = 0\,, \tag{6.53}$$

which serves as a fundamental and elegant approach to examining the stability of static astrophysical solutions, including wormholes and compact objects. Further insights into this equation can be found in references such as [570, 574–577].

Alternatively, Eq. (6.53) can be formulated as

$$F_a + F_g + F_h = 0\,, \tag{6.54}$$

providing the equilibrium condition for the wormhole. Here,

$$\begin{aligned} F_a &= \frac{2}{r}(p_t - p_r)\,, \\ F_g &= -\frac{\Phi'}{2}(\rho + p_r)\,, \\ F_h &= -\frac{dp_r}{dr}\,. \end{aligned}$$

The above set of equations illustrates the balance of forces within the wormhole, where F_a represents the force from the anisotropic matter, F_g is the gravitational force, and F_h is the hydrostatic force. Notably, F_a generates from the modifications in the gravitational Lagrangian of the Einstein-Hilbert action. However, as indicated by Eq. (6.54), for the system to remain in equilibrium, the sum of these forces must equate to zero.

In Fig. 6.6, the behaviour of F_a, F_g, and F_h are plotted for specific parameter values that ensure the satisfaction of energy conditions. However, F_g is zero for the choice of ultrastatic geometry, such that Φ is constant, implying the gravitational force has no impact on the model. From the visualization, it is apparent that the other two forces are equal in magnitude but opposite in direction. This observation confirms the equilibrium of forces achieved through the combined effect of the three force terms, thereby affirming the stability of the system.

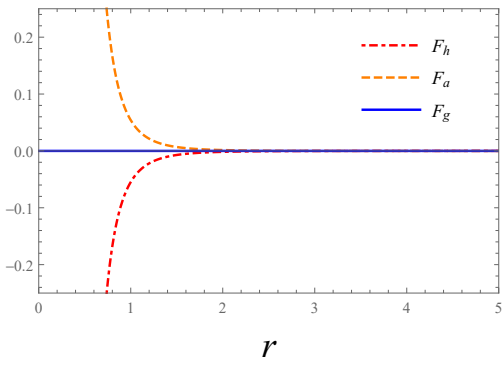

Figure 6.6: Plot demonstrating the nature of three forces for equilibrium analysis, including $F_g = 0$ for the ultrastatic wormhole. The plot is exhibited for $r_0 = 1, \sigma = -1, \gamma = 0.01, \Lambda = 0.7$ and $\alpha = 1, \beta = 2$.

6.7 Discussions

In this chapter, a static wormhole solution is presented within the context of dRGT massive gravity, which extends $f(R,T)$ gravity and Einstein gravity. It is worth noting that while energy conservation is violated in $f(R,T)$ gravity [122], one could alternatively consider the conservation of energy-momentum as proposed by [569]. Interestingly, the field equations remain similar, allowing for the investigation of wormhole solutions even with non-exotic matter.

The shape function derived from the anisotropic pressure solution in the model incorporates terms involving products of r and r^2 with the massive gravity parameters γ and Λ. This leads to severe issues in achieving asymptotically flat geometry in the spacetime beyond a certain radial distance. While one could potentially extend the region of asymptotically well-behaved spacetime by choosing smaller values of γ and Λ, achieving a globally complete asymptotic flat wormhole solution may require restricted choices of the shape function.

The examination of the repulsive effect of gravity in spacetime can be carried out through the observation of negative deflection angles of photons. It is found that in an extended spacetime description with massive gravity, the deflection angle becomes negative due to terms involving γ and Λ. Hence, the non-asymptotic flatness and the presence of repulsive gravity are generic features of dRGT massive gravity, with massive gravitons sourcing these effects in both black holes and wormholes.

Upon investigating the barotropic equation of state ($p_r = \omega\rho$) to derive the shape function, the following expression is obtained:

$$b(r) = r\left(\frac{r_0}{r}\right)^{1+1/\omega} + \frac{r(8\pi+\beta)(1+\omega)}{2\alpha(4\pi+\beta)} \times \left[-\frac{2\gamma}{1+2\omega}\left(r - r_0\left(\frac{r_0}{r}\right)^{1+1/\omega}\right) + \frac{\Lambda}{1+3\omega}\left(r^2 - r_0^2\left(\frac{r_0}{r}\right)^{1+1/\omega}\right)\right].$$

It is evident that this expression closely resembles the solution for anisotropic pressure, thus reproducing all the properties of the anisotropic solution. Consequently, dRGT-Einstein gravity also replicates all the effects and analyses present in the $f(R,T)$ model, albeit in a special limit.

The investigation surrounding wormhole solutions in massive gravity holds a significant interest, as the energy-momentum tensor stemming from the massive gravitons inherently violates null energy conditions. Additionally, the introduction of $f(R,T)$ modifications in massive gravity appears to be more suitable for constructing wormholes with well-behaved matter sources. In the current investigation, it is established that for various values of γ and Λ, there exists a large number of possibilities for ordinary matter wormholes that satisfy all energy conditions. In this scenario, the typical matter source of the wormhole consists of ordinary matter, while the matter source of massive gravitons coupled with the curvature term of $f(R,T)$ gravity serves as the geometric matter responsible for the negative energy density required to keep the wormhole throat open. However, in Einstein-massive gravity, it is solely the massive gravitons that serve as the source of the exotic component in non-exotic matter wormholes. It

is important to note here that the pronounced repulsive nature of massive gravitons gives rise to the repulsive effect of gravity, leading to non-asymptotic flatness in both $f(R,T)$ massive gravity and Einstein massive gravity scenarios.

Finally, the equilibrium analysis of the Tolman–Oppenheimer–Volkov (TOV) equation suggests that the wormhole remains stable under hydrostatic equilibrium conditions.

CHAPTER 7

EVOLVING WORMHOLE IN dRGT MASSIVE GRAVITY

7.1 Prelude

Wormholes serve as connectors between separate universes or distant locations within a single universe, necessitating the presence of exotic matter, a substance with negative energy density, for their construction of traversable variants. This concept finds support in quantum field theory, particularly evidenced by the Casimir effect [578]. Exploration into wormholes featuring negative energy densities within the framework of quantum gravity has been pursued through the application of the path integral formulation [579, 580]. Hochberg and Kephart have suggested that gravitational compression of the vacuum may lead to the formation of wormholes characterized by negative energy [581]. Consequently, an intriguing demonstration of exotic matter is observed in the generation of attractive forces between parallel metal plates within a vacuum [582].

From a theoretical standpoint, cosmology stands out as a particularly promising domain for the investigation of exotic fluids. It is widely acknowledged that the universe's acceleration is attributed to exotic matter satisfying the condition $\omega < -1/3$, with a corresponding equation of state $p = \omega\rho$. Phantom energy, characterized by $\omega < -1$, possesses unique attributes such as negative temperature and energy, contributing to the concept of the Big Rip, where its energy density evolves with the universe's expansion [38]. Thus, evolving wormhole configurations in different cosmological background have been extensively investigated in various contexts [385,387,388,395,583–592], where some of them are found to be consistent with the classical energy conditions.

In this chapter, the dynamic wormhole configuration has been explored within the framework of Einstein-massive gravity, incorporating considerations of traceless, barotropic and anisotropic pressure fluids. A thorough examination has been conducted on the limitations of throat radius imposed by the constants originating from the wormhole configuration. It is observed that the throat of the wormhole, positioned between two distant universes, experiences simultaneous expansion accompanied by

acceleration. Notably, in traceless, barotropic and anisotropic pressure fluids, there is a wide range of different parameter choices that may lead to wormhole configurations with non-exotic matter at the throat. Similar to the static wormholes in dRGT theory, the anisotropic dark energy nature of coupled massive gravitons serves as the exotic energy, while the matter source in GR behaves as ordinary.

Since the emergent universe scenario is of particular interest in this study, the chapter commences with a brief review in Section 7.2. Consequently, the formulation of the field equations pertaining to dRGT massive gravity is outlined in Section 7.3. This section also encompasses a detailed exploration of spacetime geometry and the derivation of the metric's field equations. The subsequent Section (7.4) entails the computation of evolving wormhole solutions within the contexts of traceless fluid, barotropic equation of state (EOS), and anisotropic pressure fluid. A comprehensive analysis of the energy conditions is presented in Section 7.5. Finally, the discourse culminates in Section 7.6 with a substantial discussion on the findings.

The natural units are consistently employed throughout the study, where $G = c = 1$.

7.2 Emergent universe: A review

Inflation stands as one of the most effective frameworks for elucidating the early universe's physics, addressing key concepts within Big Bang cosmology [593–595], with earlier contributions noted [62,596,597]. Notable among its accomplishments is the prediction of a nearly scale-invariant primordial power spectrum, subsequently confirmed with high precision through Cosmic Microwave Background (CMB) observations [598]. However, the success of inflation relies heavily on several assumptions, including a sufficiently prolonged period of quasi-exponential expansion and the validity of perturbation theory within this phase. Yet, these assumptions often introduce challenges for inflationary models, such as the fine-tuning issue associated with potential parameters. Additionally, concerns have been raised regarding the initial singularity problem inherited from Big Bang cosmology [599].

To address the primordial Big Bang singularity of standard cosmology, cosmologists have proposed alternative scenarios, such as the emergent universes [600–602], which emerges from the pursuit of inflationary models devoid of singularities within classical general relativity. An emergent universe depicts a model where a time-like singularity never occurs, exhibiting nearly static behaviour in the distant past (as $t \to -\infty$). Over time, the model transitions into an inflationary phase. This perspective aligns with a contemporary reinterpretation and expansion of the original Lemaître-Eddington universe concept.

The emergent universe hypothesis posits a scenario where a spatially closed universe, governed by General Relativity and characterized by a minimally coupled scalar field to gravity, originates from an initially past-eternal Einstein static condition with a finite initial dimension. This universe then transitions through a phase of super-inflation before progressing towards slow-roll inflation, ultimately leading to the conventional hot-Big Bang cosmological model. In 1967, Harrison originally explored a closed universe with only radiation, approaching an Einstein static model asymptot-

ically. After a significant interval, Ellis and collaborators developed closed universe models involving a scalar field ϕ with a specific self-interacting potential and possibly ordinary matter with $p = \omega\rho$, where $(-1/3 \leq \omega \leq 1)$ [601, 602]. However, they did not provide exact analytic solutions, although the asymptotic behaviour aligns with the emergent universe scenario. Additionally, Mukherjee *et al.* [603] derived solutions for the Starobinsky model resembling emergent universe features. Subsequently, they proposed a general prescription for an emergent model with an ad hoc equation of state, exhibiting exotic nature in certain instances [604].

In recent years, extensive research has delved into various aspects of this model, examining its stability, fine-tuning concerns, and both theoretical and observational feasibility (see [605–641]). One noteworthy alternative scenario for the early universe [642] involves String Gas cosmology, wherein an emergent universe arises during the Hagedorn phase of a thermal system consisting of superstrings [600, 643–646]. Another avenue explored is the Galilean Genesis model [647]. Researches have conducted phenomenological investigations into the causal generation of primordial field fluctuations within this framework, utilizing approaches such as Conformal Cosmology [648–653] and Pseudo-Conformal Cosmology [654, 655]. Subsequent studies have addressed the challenge of successfully translating scale-invariant primordial field fluctuations into curvature perturbations [656, 657]. Recently, conjectures like the Swampland hypothesis [658] and Trans-Planckian Censorship (TCC) [659] have imposed significant restrictions on potential inflationary models [660–663]. However, alternative cosmologies such as bouncing and emergent models remain consistent with these conjectures and are easily met. While a comprehensive understanding of the emergent phase is still lacking, there are promising avenues for exploration [664]. Furthermore, a modified iteration of the emergent universe theory suggests that the universe underwent a period of slow contraction [665–668] or slow expansion [626, 669–673]. Recent findings indicate that emergent-type universes, which initiate with a minimal Hubble rate, are generally favored over inflationary models within a landscape scenario, as outlined in [674, 675].

For the requirements of the emergent scenario, a spatially flat FRW metric is considered as

$$ds^2 = dt^2 - a^2(t)d\vec{x} \cdot d\vec{x}\,. \tag{7.1}$$

In the absence of alterations to General Relativity, the background dynamics in the context adhere to the following two equations of motion:

$$H^2 = \frac{\rho}{3M_p^2}\,, \qquad \dot{H} = -\frac{\rho + P}{2M_p^2}\,, \tag{7.2}$$

where $M_p \equiv 1/\sqrt{8\pi G}$ denotes the reduced Planck mass, and ρ and P respectively signify the energy density and pressure of the matter fields present in the universe. Consequently, in this considered framework, the Hubble parameter H is non-negative.

To avoid singularity, it is necessary for the spacetime to be geodesically complete [676], that is the trajectory of a null geodesic, governed by the equations:

$$\frac{dk^\nu}{d\lambda} + \Gamma^\nu_{\mu\rho}k^\mu k^\rho = 0\,, \qquad \text{and} \qquad g_{\mu\nu}k^\mu k^\nu = 0\,, \tag{7.3}$$

is possible for all admissible values of the affine parameter. Here, λ denotes the affine parameter and $k^\mu = \frac{dx^\mu}{d\lambda}$ represents the tangent vector to the geodesic. In the spatially flat FRW universe described by the line element (7.1), it can be demonstrated that

$$\frac{dk^0}{dt} + Hk^0 = 0\,. \tag{7.4}$$

By making use of particular choices of Hubble rate H, it is expected to obtain the equation of states for the matters dominating the emergent universe scenario. However, it is interesting to note that for different thermodynamic processes, the model can deviate from the above setup through variations in Eq. (7.2). For instance, readers may refer to [608, 613, 640, 641, 677].

7.3 The field equations

The de Rham-Gabadadze-Tolley (dRGT) massive gravity theory can be viewed as Einstein gravity coupled with a scalar field. Therefore, its action consists of the well-known Einstein-Hilbert action along with suitable nonlinear interaction terms, described as follows [157, 158]

$$S = \int d^4x\sqrt{-g}\left(\frac{1}{16\pi}\Big[R + m_g^2\mathcal{U}(g,\phi^a)\Big] + \mathcal{L}_m\right), \tag{7.5}$$

where the matter Lagrangian is denoted as $\mathcal{L}_m$, and g represents the determinant of the metric tensor $g_{\mu\nu}$. The self-interaction potential for the graviton, $\mathcal{U}$, introduces modifications to the usual gravitational sector through the graviton mass m_g. In four dimensions, this potential can be written as:

$$\mathcal{U} = \mathcal{U}_2 + \alpha_3\mathcal{U}_3 + \alpha_4\mathcal{U}_4\,, \tag{7.6}$$

where α_3 and α_4 are two dimensionless free parameters in the theory of massive gravity. The functional forms of the potentials $\mathcal{U}_j$ can be expressed in terms of the metric $g_{\mu\nu}$ and the Stückelberg scalar ϕ^a as:

$$\begin{aligned}
\mathcal{U}_2 &= [\mathcal{K}]^2 - [\mathcal{K}^2]\,,\\
\mathcal{U}_3 &= [\mathcal{K}]^3 - 3[\mathcal{K}][\mathcal{K}^2] + 2[\mathcal{K}^3]\,,\\
\mathcal{U}_4 &= [\mathcal{K}]^4 - 6[\mathcal{K}]^2[\mathcal{K}^2] + 8[\mathcal{K}][\mathcal{K}^3] + 3[\mathcal{K}^2]^2 - 6[\mathcal{K}^4]\,,
\end{aligned} \tag{7.7}$$

with

$$\mathcal{K}^\mu{}_\nu = \delta^\mu_\nu - \sqrt{g^{\mu\lambda}\partial_\lambda\phi^a\partial_\nu\phi^b\mathcal{F}_{ab}}\,. \tag{7.8}$$

In Eq. (7.7), $[\mathcal{K}]$ denotes the trace of K^μ_ν, where $(\mathcal{K}^i)^\mu_\nu = \mathcal{K}^\mu_{\rho_1}\mathcal{K}^{\rho_1}_{\rho_2}\ldots\mathcal{K}^{\rho_i}_\nu$. The interaction terms are identified as symmetric polynomials of $\mathcal{K}$. For a given order, the coefficients for each combination are chosen to ensure that these terms do not introduce higher derivative terms in the equations of motion. Notably, this definition of $\mathcal{K}$ is not unique, as an alternative action can be obtained with a different definition of $\mathcal{K}$.

The four scalar Stückelberg fields ϕ^a are introduced in the theory to restore general covariance. This field is analogous to the reference fiducial metric

$$\mathcal{F}_{ab} = diag(0, 0, c^2, c^2 \sin^2\theta)\,, \tag{7.9}$$

where c is a positive constant with the dimension of length. The reference metric's dependence solely on the spatial components ensures that general covariance is maintained in the t and r coordinates, but it is disrupted in the two angular dimensions. One can also consider a more comprehensive reference metric that does not maintain diffeomorphism invariance in the r-direction. For example, to preserve rotational symmetry on the sphere and general time reparametrization invariance, a natural choice could be $\mathcal{F}_{ab} = diag(0, 1, c^2, c^2 \sin^2\theta)$. Another way to break diffeomorphism invariance in the r-direction could involve a different form of $\mathcal{F}_{ab}$, where $\sin^2\theta\mathcal{F}_{\theta\theta} = \mathcal{F}_{\phi\phi} = F(r)$, with all other components set to zero. This implies that exploring various forms for the reference metric can lead to a range of new solutions, making massive gravity with this reference metric a compelling subject for researchers. However, this study does not aim to delve into such investigations.

Note that the unitary gauge is realized as, $\phi^a = x^\mu\delta^a_\mu$ [678], leading to the expression

$$\sqrt{g^{\mu\lambda}\partial_\lambda\phi^a\partial_\nu\phi^b\mathcal{F}_{ab}} = \sqrt{g^{\mu\lambda}\mathcal{F}_{\lambda\nu}}\,. \tag{7.10}$$

In this gauge, the tensor $g_{\mu\nu}$ signifies the observable metric linked to the five degrees of freedom of the massive graviton. It is crucial to recognize that since the Stückelberg scalars transform under coordinate transformations, fixing these scalars—such as by selecting the unitary gauge—means that any subsequent coordinate transformation will violate the gauge condition and lead to further modifications to the Stückelberg scalars.

Next, the effective energy-momentum tensor $X_{\mu\nu}$ of the massive gravitons is determined as

$$\begin{aligned} X^\mu_\nu = \mathcal{K}^\mu_\nu - [\mathcal{K}]\delta^\mu_\nu - \alpha\left[(\mathcal{K}^2)^\mu_\nu - [\mathcal{K}]\mathcal{K}^\mu_\nu + \frac{1}{2}\delta^\mu_\nu\,\mathcal{U}_2\right] \\ + 3\beta\left[(\mathcal{K}^3)^\mu_\nu - [\mathcal{K}](\mathcal{K}^2)^\mu_\nu + \frac{1}{2}\mathcal{K}^\mu_\nu\,\mathcal{U}_2 - \frac{1}{6}\delta^\mu_\nu\,\mathcal{U}_3\right]\,, \end{aligned} \tag{7.11}$$

where α and β are dimensionless constants introduced here to accommodate the parameters α_3 and α_4, as given by

$$\alpha = 1 + 3\alpha_3\,, \qquad \beta = \alpha_3 + 4\alpha_4\,. \tag{7.12}$$

Eq. (7.11) satisfies the conservation relation due to the Bianchi identities as $\nabla^\mu X_{\mu\nu} = 0$, where ∇^μ denotes the covariant derivative compatible with the metric $g_{\mu\nu}$. Consequently, the principal pressure form of the energy-momentum tensor for massive gravitons is defined as

$$\frac{m_g^2}{8\pi}X_{\mu\nu} = -(\rho^{(g)} + p_t^{(g)})u_\mu u_\nu - p_t^{(g)}g_{\mu\nu} - (p_r^{(g)} - p_t^{(g)})\chi_\mu\chi_\nu\,, \tag{7.13}$$

where u^μ is the timelike four-vector and χ^μ is the spacelike vector orthogonal to the timelike unit vector, satisfying $u_\mu u^\mu = -1$ and $\chi_\mu\chi^\mu = 1$. The quantities $\rho^{(g)}$, $p_r^{(g)}$, and

$p_t^{(g)}$ denote the total energy density, radial pressure, and transverse pressure for the massive gravitons, respectively.

Thus, the action is now ready to be varied with respect to the metric $g_{\mu\nu}$ to derive the field equation for dRGT-Einstein massive gravity, given by

$$G_{\mu\nu} = 8\pi T_{\mu\nu} - m_g^2 X_{\mu\nu}\,. \tag{7.14}$$

Now, considering the Lagrangian matter density $\mathcal{L}_m = \rho$, the coupling of a usual matter (sourced by Einstein sector, which can either be traceless, barotropic, or anisotropic) and the massive gravitons are introduced, such that the total matter source is defined by the exchange of energy and momentum between the two. The EM tensor for the Einstein gravity is written as

$$T_{\mu\nu} = (\rho + p_t)u_\mu u_\nu + p_t g_{\mu\nu} + (p_r - p_t)\chi_\mu \chi_\nu\,, \tag{7.15}$$

whereas the same for massive gravity is given by Eq. (7.13). Thus, the total matter sector is given by

$$T^{tot}_{\mu\nu} = diag\left(-\rho - \rho^{(g)}, p_r + p_r^{(g)}, p_t + p_t^{(g)}, p_t + p_t^{(g)}\right)\,. \tag{7.16}$$

In the realm of this particular investigation, one might explore the metric ansatz for the evolving dynamic wormhole [395] by considering

$$ds^2 = -e^{2\Phi(r)}dt^2 + a(t)^2\left[\frac{dr^2}{1-\frac{b(r)}{r}} + r^2 d\Omega^2\right]\,, \tag{7.17}$$

where $\Phi(r)$, $b(r)$, and $a(t)$ denote the redshift function, shape function, and cosmic scale factor, respectively, and $d\Omega^2 = d\theta^2 + \sin^2\theta d\phi^2$.

With all these components, it is straightforward to compute the density and pressure components $\rho^{(g)}(r,t)$ and $p^{(g)}_{r,\perp}(r,t)$ for massive gravitons. From equations (7.7), (7.11), (7.13), and (7.17), one gets

$$\rho^{(g)}(r,t) \equiv \frac{m_g^2}{8\pi}X^t{}_t = \frac{1}{8\pi}\left(\Lambda - \frac{2\gamma}{ar} - \frac{\epsilon}{a^2r^2}\right)\,, \tag{7.18}$$

$$p_r^{(g)}(r,t) \equiv -\frac{m_g^2}{8\pi}X^r{}_r = -\frac{1}{8\pi}\left(\Lambda - \frac{2\gamma}{ar} - \frac{\epsilon}{a^2r^2}\right)\,, \tag{7.19}$$

$$p^{(g)}_{\theta,\phi}(r,t) \equiv -\frac{m_g^2}{8\pi}X^{\theta,\phi}_{\theta,\phi} = -\frac{1}{8\pi}\left(\Lambda - \frac{\gamma}{ar}\right)\,. \tag{7.20}$$

Here, the effective cosmological constant Λ and the parameters γ and ϵ, which are linear combinations of the parameters α and β, are introduced. These are given by

$$\Lambda \equiv -3m_g^2(1+\alpha+\beta), \qquad \gamma \equiv -m_g^2 c(1+2\alpha+3\beta)\,, \qquad \epsilon \equiv m_g^2 c^2(\alpha+3\beta)\,. \tag{7.21}$$

Therefore, by setting $m_g = 0$, one retrieves the usual solutions found in Einstein's GR. For $c = 0$, where $\gamma = \epsilon = 0$, the solution can be categorized based on the

values of α and β. If $1+\alpha+\beta<0$, it leads to the de Sitter solution, whereas if $1+\alpha+\beta>0$, it results in the Anti-de Sitter solution. As will be discussed in Section 7.4, the term $\gamma a/r$ is a distinguishing feature of this solution, setting it apart from other solutions. However, this term also introduces unavoidable challenges in the evolving wormhole solution. The constant potential ϵ corresponds to the global monopole term, which naturally arises from the graviton mass. A global monopole solution typically originates from a topological defect in high-energy physics during the early universe, caused by gauge-symmetry breaking [679, 680]. Different combinations of α and β can yield various solutions. To simplify the theory, particular parameter relations are sometimes chosen so that γ or ϵ from Eq. (7.21) can be neglected. For example, choosing $\alpha=-3\beta$ neglects ϵ [681]. Additionally, $\beta=\alpha^2/3$ leads to the Schwarzschild–de Sitter solution [682].

Next, the fundamental requirements to assure the navigability of the wormhole structure (7.17) involve the subsequent conditions:

1. Wormhole construction involves connecting two flat regions via a throat, where the throat radius is determined by a global minimum defined by $r=r_0$ such that $b(r_0)=r_0$. As a result, the radial coordinate ranges from $r\in[\,r_0,\infty)$.

2. To prevent horizons and singularities, it is crucial for the redshift function $\Phi(r)$ to remain finite throughout, enabling $e^{\Phi(r)}>0$ for $r>r_0$. The ultrastatic wormhole, with $\Phi(r)=0$, is particularly important, indicating $e^{\Phi(r)}=1$.

3. The flaring-out condition $-rb'(r)+b(r)>0$ needs to be met at or near the throat at $r=r_0$.

4. Lastly, asymptotic flatness demands $\Phi(r)\to 0$ and $b(r)/r\to 0$ as $r\to\infty$.

Interested readers can find more detailed discussions on the traversability conditions in Morris-Thorne type wormholes in [321].

Utilizing the orthonormal frame, the metric signature, represented by $g_{\hat{\mu}\hat{\nu}}=\text{diag}\,(-1,1,1,1)$, defines corresponding basis vectors as follows:

$$\begin{aligned}
\mathbf{e}_{\hat{0}} &= e^{-\Phi}\mathbf{e}_t\,,\\
\mathbf{e}_{\hat{1}} &= \frac{\mathbf{e}_r\sqrt{1-b/r}}{a}\,,\\
\mathbf{e}_{\hat{2}} &= \frac{\mathbf{e}_\theta}{ar}\,,\\
\mathbf{e}_{\hat{3}} &= \frac{\mathbf{e}_\phi}{ar\sin\theta}\,.
\end{aligned} \tag{7.22}$$

With this setup, one can now calculate the components of the Einstein tensor for the spacetime described by (7.17):

$$G_{00}=\frac{b'}{r^2a^2}-3H^2e^{-2\Phi}\,, \tag{7.23}$$

$$G_{11} = -\frac{b}{r^3a^2} + \frac{2\Phi'}{ra^2}\left(1-\frac{b}{r}\right) - e^{-2\Phi}\left(2\dot{H}+3H^2\right), \tag{7.24}$$

$$G_{22} = G_{33} = \frac{1}{a^2}\left(1-\frac{b}{r}\right)\left(\Phi''+\Phi'^2\right) + \frac{1}{2r^3a^2}\left(-rb'+b\right) - \frac{\Phi'}{2r^2a^2}\left(rb'+b-2r\right) - e^{-2\Phi}\left(2\dot{H}+3H^2\right). \tag{7.25}$$

where the prime and overdot in the expressions denote derivatives with respect to r and t, and the Hubble parameter is $H(a) = \dot{a}(t)/a(t)$. It can be observed that the energy-momentum components of Einstein gravity, as expressed by Eq. (7.15), adheres to the principle of energy conservation, specifically satisfying $\nabla^\mu T_{\mu\nu} = 0$. Consequently, the computation of the total EM tensor, encompassing the coupled perfect fluid-massive graviton system outlined in Eq. (7.16), also upholds $\nabla^\mu T^{tot}_{\mu\nu} = 0$. Hence, it follows evidently that $\nabla^\mu T^{(g)}_{\mu\nu} = 0$. Thus, by referring to Eq. (7.14) and the components of the Einstein tensor, the field equations can be expressed as:

$$\rho = \frac{b'}{8\pi r^2a^2} + \frac{3H^2}{8\pi}e^{-2\Phi} - \frac{1}{8\pi}\left(\Lambda - \frac{2\gamma}{ar} - \frac{\epsilon}{a^2r^2}\right), \tag{7.26}$$

$$p_r = -\frac{b}{8\pi r^3a^2} + \left(1-\frac{b}{r}\right)\frac{\Phi'}{4\pi ra^2} - \frac{e^{-2\Phi}}{8\pi}\left(2\dot{H}+3H^2\right) + \frac{1}{8\pi}\left(\Lambda - \frac{2\gamma}{ar} - \frac{\epsilon}{a^2r^2}\right), \tag{7.27}$$

$$p_t = \frac{1}{8\pi a^2}\left(1-\frac{b}{r}\right)\left(\Phi''+\Phi'^2\right) + \left(\frac{-rb'+b}{16\pi r^3a^2}\right) - \left(\frac{rb'+b-2r}{16\pi r^2a^2}\right)\Phi' - \frac{e^{-2\Phi}}{8\pi}\left(2\dot{H}+3H^2\right) + \frac{1}{8\pi}\left(\Lambda - \frac{\gamma}{ar}\right). \tag{7.28}$$

To develop an evolving wormhole solution, a simplified approach restricts the choices of $\Phi(r)$, $b(r)$, and $a(t)$, focusing on the corresponding dynamics. Yet, this method may overlook the influence of massive gravity parameters on the solutions. An alternative approach introduces specific constraints on the energy density, radial pressures and transverse pressures, such as traceless, barotropic or anisotropic fluids' equation of state. This study explores various fluid solutions applicable to a specific type of wormhole, namely the ultrastatic wormhole, wherein the field equations are modified as follows:

$$\rho = \frac{b'}{8\pi r^2a^2} + \frac{3H^2}{8\pi} - \frac{1}{8\pi}\left(\Lambda - \frac{2\gamma}{ar} - \frac{\epsilon}{a^2r^2}\right), \tag{7.29}$$

$$p_r = -\frac{b}{8\pi r^3a^2} - \frac{2\dot{H}+3H^2}{8\pi} + \frac{1}{8\pi}\left(\Lambda - \frac{2\gamma}{ar} - \frac{\epsilon}{a^2r^2}\right), \tag{7.30}$$

$$p_t = \left(\frac{-rb'+b}{16\pi r^3a^2}\right) - \frac{2\dot{H}+3H^2}{8\pi} + \frac{1}{8\pi}\left(\Lambda - \frac{\gamma}{ar}\right). \tag{7.31}$$

Thus, everything is prepared to explore wormhole solutions and engage in the analysis of their dynamics.

7.4 Wormhole Solution

In this segment, three specific selections of the pressure components are examined for solution computation: (i) Fluid with tracelessness, (ii) application of a barotropic Equation of State (EOS), and (iii) Anisotropic fluid. It is notable that, by examining the field equations (7.30) and (7.31), one can discern that the isotropic fluid solution ($p_t = p_r$) possesses certain inherent limitations due to its lack of incorporation of the cosmic scale factor $a(t)$. Consequently, this solution is set aside; however, its limitations are succinctly deliberated in the *Discussions* (Sec. 7.6).

7.4.1 Traceless fluid $(-\rho + p_r + 2p_t = 0)$

For the selection of a matter fluid with zero trace, it leads to the condition $T = 0$, implying $-\rho + p_r + 2p_t = 0$. This condition yields the following expression:

$$\frac{b'(r)}{r^2} + 3a(t)\ddot{a}(t) + 3\dot{a}(t)^2 - 2\Lambda a(t)^2 + \frac{\epsilon}{r^2} + \frac{3\gamma a(t)}{r} = 0\,, \tag{7.32}$$

where Λ and ϵ represent the effective cosmological constant, and the global monopole potential term respectively. Additionally, γ and ϵ together define the deviation from Schwarzschild de Sitter and Anti-de Sitter solution. In black hole solutions of massive gravity, $\gamma < 0$ behaves like black holes surrounded by a quintessence field in the absence of the Λ and ϵ terms. Subsequently, in the absence of γ, black holes are identified in the D bound and the Bekenstein bound [190]. However, in wormhole configurations, γ is found to have no particular physical effect. Further, it is noteworthy that the term consisting of γ in (7.32) contains the ultimate challenge in variable separation. Therefore, the only way out is to neglect γ using the imposed constraint on α and β. This is, however, not utterly disturbing as explained in the previous section with proper references.

Thus, by considering $\alpha = -(1 + 3\beta)/2$, such that $\gamma = 0$, Eq. (7.32) takes the following expressions with a separation constant c_1:

$$\frac{b'(r)}{r^2} + \frac{\epsilon}{r^2} = c_1\,, \tag{7.33}$$

$$3a(t)\ddot{a}(t) + 3\dot{a}(t)^2 - 2\Lambda a(t)^2 = -c_1\,. \tag{7.34}$$

The determination of the shape function $b(r)$ is facilitated by enforcing the throat condition $b(r = r_0) = r_0$, yielding the expression:

$$b(r) = r_0 + \frac{c_1}{3}\left(r^3 - r_0^3\right) - \epsilon(r - r_0)\,. \tag{7.35}$$

The scale factor can subsequently be obtained as:

$$a(t)^2 = \frac{c_1}{2\Lambda} + A_1 e^{2\sqrt{\Lambda/3}t} + B_1 e^{-2\sqrt{\Lambda/3}t}\,, \tag{7.36}$$

where A_1 and B_1 represent arbitrary integration constants. Note that if $B_1 = 0$, the universe's evolution originates from an emergent phase in the infinite past, denoted by

$a(t) \to a_0(=\sqrt{c_1/2\Lambda})$ and $H \to 0$ as $t \to -\infty$. Hence, the wormhole configuration described above emerges from an emergent phase. Given the dependence of Λ on the mass of the massive gravitons, it is plausible to speculate that the current theory of massive gravity could circumvent the big-bang singularity.

For the validation of the flaring-out condition in the current wormhole setup, it is determined that the radial parameter 'r' is constrained as follows:

$$r < r_0 \left[\frac{1}{2}\left(\frac{3(1+\epsilon)}{c_1 r_0^2} - 1\right)\right]^{1/3} = r_1(\text{say})\,. \tag{7.37}$$

The given constraint on r imposes two limitations on the throat radius r_0, i.e.,

(i) $\frac{3(1+\epsilon)}{c_1 r_0^2} - 1 > 0 \qquad$ i.e. $r_0^2 < \frac{3(1+\epsilon)}{c_1}$,

(ii) $\frac{1}{2}\left(\frac{3(1+\epsilon)}{c_1 r_0^2} - 1\right) > 1 \qquad$ i.e. $r_0^2 < \frac{(1+\epsilon)}{c_1}$,

such that

$$r_0^2 < \frac{(1+\epsilon)}{c_1}\,. \tag{7.38}$$

Thus, by selecting a large positive value for the separation constant c_1, it becomes feasible to reduce the throat radius to a small value. Additionally, the current wormhole configuration is confined within a finite region: $r_0 \leq r < r_1$.

7.4.2 Barotropic EOS ($p_r = \omega\rho$)

When considering the Equation of State (EOS) within barotropic matter, the relationship between radial pressure and energy density is expressed as $p_r = \omega\rho$, where ω represents the equation of state parameter. Substituting Eq. (7.29) and (7.30) into this equation yields:

$$\begin{aligned}&\frac{r\omega b'(r) + b(r)}{r^3} + 2a(t)\ddot{a}(t) + (1+3\omega)\dot{a}(t)^2 \\ &- (1+\omega)\Lambda a(t)^2 + (1+\omega)\frac{\epsilon}{r^2} + 2(1+\omega)\frac{\gamma a(t)}{r} = 0\,.\end{aligned} \tag{7.39}$$

Similar to the traceless fluid scenario, this equation also lacks separability. Interestingly, under the same assumption, $\gamma = 0$, it can be decomposed into functions dependent on r and t as follows:

$$\frac{r\omega b'(r) + b(r)}{r^3} + (1+\omega)\frac{\epsilon}{r^2} = c_2\,, \tag{7.40}$$

$$2a(t)\ddot{a}(t) + (1+3\omega)\dot{a}(t)^2 - (1+\omega)\Lambda a(t)^2 = -c_2\,, \tag{7.41}$$

where c_2 represents the separation constant. In solving the initial differential equation (7.40), the expression for the shape function is given by

$$b(r) = \begin{cases} r_0\left(\frac{r}{r_0}\right)^3 - \epsilon\left[r - r_0\left(\frac{r}{r_0}\right)^3\right] - 3c_2 r^3 \ln\left(\frac{r}{r_0}\right), & \text{for } \omega = -\frac{1}{3}. \\ r_0\left(\frac{r_0}{r}\right)^{1/\omega} - \epsilon\left[r - r_0\left(\frac{r_0}{r}\right)^{1/\omega}\right] + \frac{c_2}{1+3\omega}\left[r^3 - r_0^3\left(\frac{r_0}{r}\right)^{1/\omega}\right], & \text{for } \omega \neq -\frac{1}{3}. \end{cases} \tag{7.42}$$

Furthermore, the scale factor $a(t)$ can be derived from the second-order non-linear differential equation (7.41) as:

$$a(t) = \begin{cases} \sqrt{\frac{3A_2}{\Lambda} - \frac{9c_2^2}{16\Lambda^2}}\ \mathrm{Sinh}\left[2\sqrt{\frac{\Lambda}{3}}(t-t_0)\right] + \frac{3c_2}{4\Lambda}, & \text{for } \omega = \frac{1}{3}. \\ \sqrt{\frac{3c_2}{2(\Lambda+3B_2)}}\ \mathrm{Sinh}\left[\sqrt{\frac{\Lambda}{3}+B_2}\,(t-t_0)\right], & \text{for } \omega = -1. \end{cases} \tag{7.43}$$

where t_0, A_2, and B_2 denote integration constants, and the integral representation of t in terms of the scale factor a for $\omega = -\frac{1}{3}$ is given as follows:

$$(t - t_0) = \int \frac{da}{\sqrt{\frac{\Lambda}{3}a^2 - c_2 \ln(a) + a_0}}\,. \tag{7.44}$$

The relationship between the scale factor $a(t)$ and t as given by Eq. (7.44), is illustrated in Fig. 7.1. To ensure compliance with the flaring-out condition, constraints on the throat radius are summarized in Table 7.1.

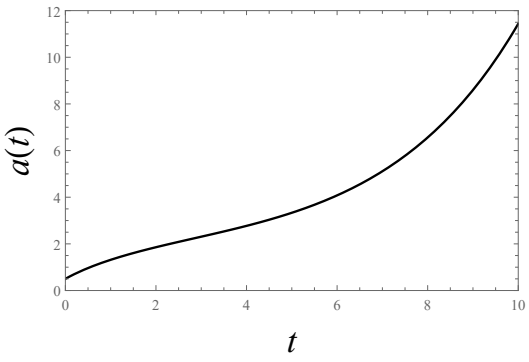

Figure 7.1: Variation of scale factor $a(t)$ against the cosmic time t for the barotropic fluid with $\omega = -\frac{1}{3}$. The relevant parameters are considered as $\Lambda = 0.3$, $c_2 = 1$, and $a_0 = 0.5$.

7.4.3 Anisotropic pressure ($p_t = \sigma p_r,\ \sigma \neq 1$)

When the fluid under consideration exhibits anisotropic properties, considering p_r and p_t from equations (7.30) and (7.31) yields the following differential equation:

$$\frac{-rb'(r) + (1+2\sigma)b(r)}{2r^3} - (1-\sigma)\left(2a(t)\ddot{a}(t) + \dot{a}(t)^2 - \Lambda a(t)^2\right) + \frac{\sigma\epsilon}{r^2} - (1-2\sigma)\frac{\gamma a(t)}{r} = 0\,. \tag{7.49}$$

For the separability of the shape function $b(r)$ and the scale factor $a(t)$, setting $\gamma = 0$ results in the differential equations for 'b' and 'a' taking the form:

$$\frac{-rb'(r) + (1+2\sigma)b(r)}{2r^3} + \frac{\sigma\epsilon}{r^2} = c_3\,, \tag{7.50}$$

$$2a(t)\ddot{a}(t) + \dot{a}(t)^2 - \Lambda a(t)^2 = \bar{c}_3\,, \tag{7.51}$$

Case I	$\omega = -\frac{1}{3}$
Flaring-out condition	$$r > r_0 \exp\left(\frac{(1+\epsilon)}{3c_2 r_0^2} - \frac{1}{2}\right). \quad (7.45)$$
Region of wormhole extension and restriction on the throat radius	The wormhole configuration is infinitely extended as $r_0 \leq r < \infty$, with $$r_0^2 > \frac{2(1+\epsilon)}{3c_2}. \quad (7.46)$$
Case II	$\omega = \frac{1}{3}$
Flaring-out condition	$$r < r_0 \left[2\left(\frac{2(1+\epsilon)}{c_2 r_0^2} - 1\right)\right]^{1/6}. \quad (7.47)$$
Region of wormhole extension and restriction on the throat radius	The wormhole configuration is finitely extended as $$r_0 \leq r < r_0 \left[2\left(\frac{2(1+\epsilon)}{c_2 r_0^2} - 1\right)\right]^{1/6}, \quad (7.48)$$ with $$r_0^2 < \frac{4(1+\epsilon)}{3c_2}.$$
Case III	$\omega = -1$
Flaring-out condition and region of wormhole extension	The flaring-out condition is satisfied for all $r \geq r_0$, and the wormhole configuration is infinitely extended as $r_0 \leq r < \infty$.

Table 7.1: Restrictions imposed by the flaring-out condition for different state parameters in barotropic fluid.

having c_3 the constant of separation, where the assumption $\bar{c}_3 = \frac{c_3}{1-\sigma}$ is made simultaneously.

Upon imposing the throat condition $b(r_0) = r_0$, the solution to (7.50) yields the shape function given by

$$b(r) = r\left(\frac{r}{r_0}\right)^{2\sigma} - \epsilon\left[r - r_0\left(\frac{r}{r_0}\right)^{1+2\sigma}\right] - \bar{c}_3\left[r^3 - r_0^3\left(\frac{r}{r_0}\right)^{1+2\sigma}\right]. \quad (7.52)$$

Similarly, solving (7.51) for the cosmic scale factor leads to its representation in terms

of elliptic integrals:

$$(t - t_0) = \int \frac{da}{\sqrt{\frac{\Lambda}{3}a^2 + \frac{A_3}{a} + \bar{c}_3}}\,. \tag{7.53}$$

Employing a numerical approach, the evolution of this scale factor can be obtained with respect to cosmic time t, as depicted in Figure 7.2.

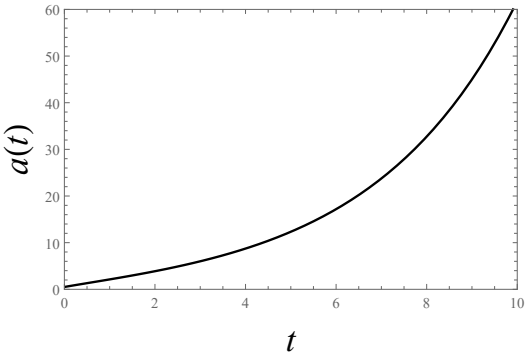

Figure 7.2: Variation of scale factor $a(t)$ against the cosmic time t for anisotropic fluid. The relevant parameters are considered as $\sigma = \frac{1}{2}$, $\Lambda = 0.3$, $c_3 = 1$, and $a_0 = 0.5$.

In the context of verifying the flaring-out condition within the wormhole configuration, it is observed that the radial parameter 'r' is constrained as follows:

$$r < r_0 \left[\sigma\left(1 - \frac{(1+\epsilon)}{\bar{c}_3 r_0^2}\right)\right]^{1/2(1-\sigma)} = r_2 \text{ (say)}\,. \tag{7.54}$$

Consequently, for the current wormhole model, the expression enclosed in the square bracket must remain greater than unity. This condition imposes a limitation on the throat radius, expressed as

(i) $1 - \frac{(1+\epsilon)}{\bar{c}_3 r_0^2} > 0$ i.e. $r_0^2 > \frac{1+\epsilon}{\bar{c}_3}$,

(ii) $\sigma\left(1 - \frac{(1+\epsilon)}{\bar{c}_3 r_0^2}\right) > 1$ i.e. $r_0^2 > -\frac{(1+\epsilon)\sigma}{c_3}$.

Hence, in the current scenario, the wormhole's geometric structure is finitely extended as $r_0 \leq r < r_2$, subject to the specified constraint on the throat radius corresponding to the given limitations on the separation constant.

Lastly, a graphical depiction of $\left(1 - \frac{b(r)}{r}\right)$ plotted against the radial coordinate r for the three aforementioned types of wormholes is presented, as illustrated in Fig. 7.3. One may visualize that with proper choices of parameters, the wormhole configurations mostly agree with the hyperbolic FRW universe at large radial parameters. Consequently, these evolving wormhole solutions are supported by the accelerated expansion, in which both of the universes on either side of the throat are simultaneously accelerated. This observation can be verified in traceless and barotropic fluid systems respectively by the exponential and hyperbolic functions of Eq. (7.36) and (7.43).

However, note that in barotropic fluid with ($\omega = 1/3, c_2 = 0.0001$), the solution does not agree with the hyperbolic FRW universe. On the other hand, a large dependence on the sign and values of the separation constants is identified, highlighting the additional importance of these parameters.

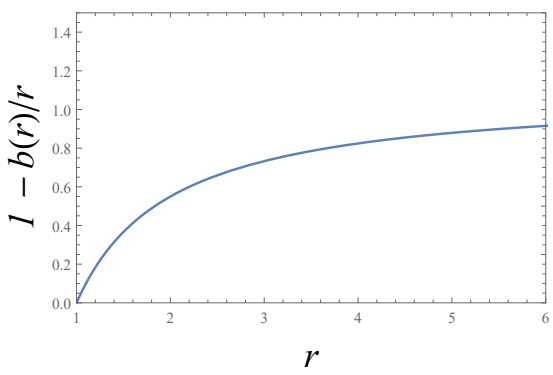

(a) Traceless fluid with $c_1 = 0.0001$

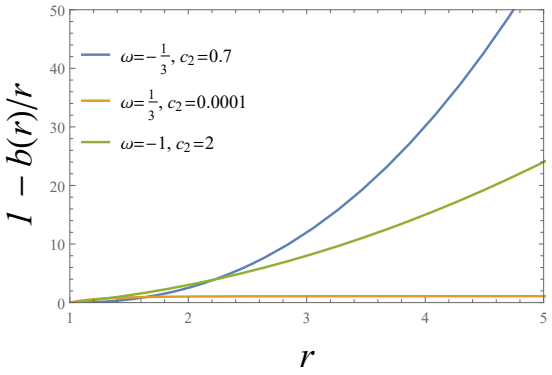

(b) Barotropic fluid

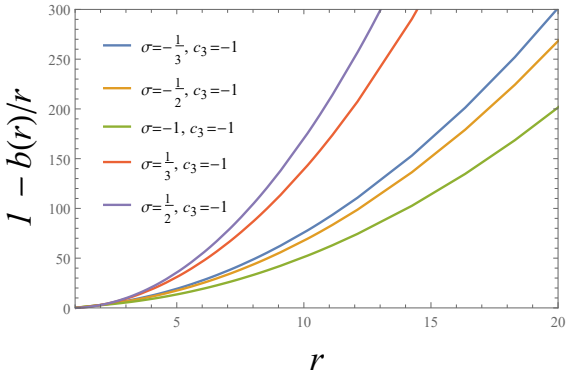

(c) Anisotropic fluid

Figure 7.3: Variation of $(1 - b(r)/r)$ against the radial coordinate r for three types of solutions. The legends in (b) and (c) denote the choice of constants and EOS parameters. The throat radius and ϵ are fixed at $r_0 = 1,\ \epsilon = 0.1$ in each plot.

7.5 Energy Conditions

One of the intriguing and somewhat distinctive aspects of forming traversable wormholes involves the necessity of exotic matter that violates classical energy principles. This exotic matter is essential for maintaining the wormhole throat open and ensuring its traversability. As discussed earlier, this characteristic has been extensively explored in the evolution of traversable wormholes and Morris-Thorne type wormholes within various versions of modified theories. Notably, some of these theories accommodate matter that adheres to energy conditions in different ways. Even when conventional matter meets these conditions, the presence of coupled matter is required to serve as exotic energy, enabling traversability. In [559], this concept is thoroughly examined concerning geometrical matter.

Furthermore, the dRGT massive gravity theory emerges as another significant contender, wherein the potential existence of non-exotic matter at the wormhole throat is intuitively investigated in the previous chapter. It is suggested that massive gravitons might function as exotic dark energy, allowing coupled matter such as perfect fluids in

Einstein gravity to satisfy the NEC, WEC, SEC, and DEC. According to the definitions in Chapter 2, NEC, WEC, SEC and DEC are written in the principal pressure forms as

(I) NEC : $\rho + p_r \geq 0, \quad \rho + p_t \geq 0;$

(II) WEC : $\rho \geq 0, \quad \rho + p_r \geq 0, \quad \rho + p_t \geq 0;$

(III) SEC : $\rho + p_r \geq 0, \quad \rho + p_t \geq 0, \quad \rho + p_r + 2p_t \geq 0;$

(IV) DEC : $\rho \geq 0, \quad \rho - |p_r| \geq 0, \quad \rho - |p_t| \geq 0.$

Now, in this section, the energy conditions for evolving wormhole solutions are investigated thoroughly within the framework of Einstein-massive gravity. The discussion has been divided into three parts for three different fluid solutions.

• **Traceless fluid:**

According to the principal pressure terms in energy conditions, the expressions for $\rho(r,t)$, $(\rho(r,t) + p_r(r,t))$, $(\rho(r,t) + p_t(r,t))$, $(\rho(r,t) - |p_r(r,t)|)$, $(\rho(r,t) - |p_t(r,t)|)$, and $(\rho(r,t) + p_r(r,t) + 2p_t(r,t))$ components are computed by substituting equations (7.35), (7.36) into (7.29), (7.30) and (7.31) for traceless fluid configuration.

Therefore, a comprehensive analysis of the energy conditions has been conducted for this model with fixed values of the throat radius $r_0 = 1$, effective cosmological constant $\Lambda = 0.3$, and $c_1 = 1$. Calculations have been performed for various combinations of three parameters, namely ϵ, A_1, and B_1, with observations summarized in Table 7.2. It can be observed that the energy conditions are significantly influenced by A_1 and B_1. For $A_1 = -1, B_1 = 1$, the components exhibit singularity at a specific point in time. However, for $\epsilon = -1$, $A_1 = 1$, $B_1 = -1$, the energy conditions are fully satisfied across the entire range of r and t, as visualized in the 3D plot shown in Fig. 7.4.

ϵ	A_1 **and** B_1	**Energy condition**
$\epsilon = +1$	$A_1 = 1,\ B_1 = 1$	completely violated.
	$A_1 = 1,\ B_1 = -1$	violated for a certain range in t.
	$A_1 = -1,\ B_1 = 1$	satisfied for a certain time interval with the presence of singularity.
	$A_1 = -1,\ B_1 = -1$	completely violated.
$\epsilon = -1$	$A_1 = 1,\ B_1 = 1$	completely violated.
	$A_1 = 1,\ B_1 = -1$	completely satisfied for the whole range.
	$A_1 = -1,\ B_1 = 1$	completely satisfied with the presence of singularity.
	$A_1 = -1,\ B_1 = -1$	completely violated.

Table 7.2: Results for the energy conditions in a traceless fluid solution with the throat radius fixed at $r_0 = 1$, an effective cosmological constant of $\Lambda = 0.3$, and $c_1 = 1$.

• **Barotropic fluid with $\omega = \frac{1}{3}$:**

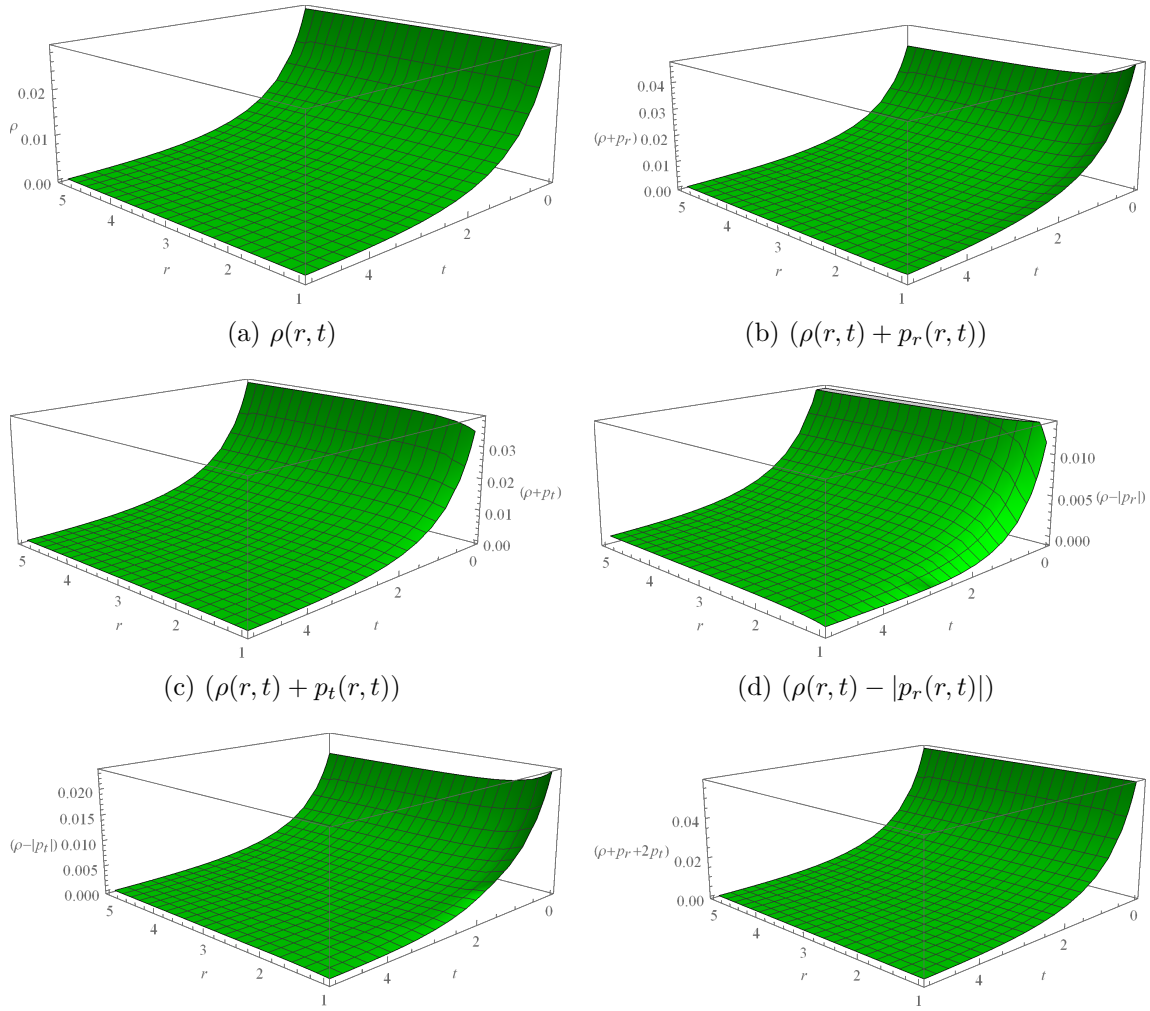

(a) $\rho(r,t)$ (b) $(\rho(r,t)+p_r(r,t))$

(c) $(\rho(r,t)+p_t(r,t))$ (d) $(\rho(r,t)-|p_r(r,t)|)$

(e) $(\rho(r,t)-|p_t(r,t)|)$ (f) $(\rho(r,t)+p_r(r,t)+2p_t(r,t))$

Figure 7.4: Nature of energy condition components for traceless fluid against the radial parameter r and cosmic time t. The parameters are fixed at $r_0 = 1$, $\Lambda = 0.3$, $c_1 = 1$, $A_1 = 1$, $B_1 = -1$ and $\epsilon = -1$.

Now, consider the scenario where $\omega = 1/3$ in the context of a barotropic fluid to examine the corresponding energy conditions. As in the previous case, the shape function (7.42) and the scale factor (7.43) are substituted into Eqs. (7.29), (7.30), and (7.31) to derive the components of the energy conditions: $\rho(r,t)$, $(\rho(r,t)+p_r(r,t))$, $(\rho(r,t)+p_t(r,t))$, $(\rho(r,t)-|p_r(r,t)|)$, $(\rho(r,t)-|p_t(r,t)|)$, and $(\rho(r,t)+p_r(r,t)+2p_t(r,t))$.

An extensive analysis of the energy conditions is carried out by varying the parameters c_2, A_2, and ϵ while keeping a fixed set of values: $r_0 = 1$, $\Lambda = 0.3$, $t_0 = 0$, and $\omega = 1/3$. The findings are summarized in Table 7.3, where it is noted that $A_2 = 1$ and $c_2 = -1$ lead to singularities in the energy condition components. Conversely, for negative values of A_2, the components exhibit complex values, thereby violating the energy conditions. However, with $\epsilon = -1$, $A_2 = 1$, and $c_2 = 1$, all energy conditions are fully satisfied. This situation is illustrated in a 3D plot shown in Fig. 7.5.

ϵ	A_2 **and** c_2	**Energy condition**
$\epsilon = +1$	$A_2 = 1,\ c_2 = 1$	completely violated at the throat.
	$A_2 = 1,\ c_2 = -1$	satisfied for a certain time interval with the presence of singularity.
	$A_2 = -1,\ c_2 = 1$	completely violated.
	$A_2 = -1,\ c_2 = -1$	completely violated.
$\epsilon = -1$	$A_2 = 1,\ c_2 = 1$	completely satisfied.
	$A_2 = 1,\ c_2 = -1$	only DEC is violated for a small time interval with the presence of singularity.
	$A_2 = -1,\ c_2 = 1$	completely violated.
	$A_2 = -1,\ c_2 = -1$	completely violated.

Table 7.3: Results for the energy conditions in a barotropic fluid solution with the throat radius fixed at $r_0 = 1$, an effective cosmological constant of $\Lambda = 0.3$, the state parameter $\omega = 1/3$ and $t_0 = 0$.

• **Anisotropic fluid:**

Similar to the previous two solutions, energy conditions for the anisotropic fluid are extensively analyzed for fixed values of the throat radius $r_0 = 1$ and cosmological constant $\Lambda = 0.3$. The variation in ϵ, σ, and c_3 values shows noticeable deviations in the energy condition components, as listed in Table 7.4. It is observed that, regardless of the sign of ϵ, $\sigma = 1/3$ and $c_3 = 1$ show energy condition violation at the wormhole throat, whereas for $\sigma = -1/3$ and $c_3 = 1$, only the DEC is slightly violated at the throat. Apart from that, when c_3 is negative (i.e., $c_3 = -1$) with $\sigma = \pm 1/3$, all the energy conditions are completely satisfied throughout the spacetime.

ϵ	σ **and** c_3	**Energy condition**
$\epsilon = +0.1$	$\sigma = 1/3,\ c_3 = 1$	only violated at the throat.
	$\sigma = 1/3,\ c_3 = -1$	completely satisfied.
	$\sigma = -1/3,\ c_3 = 1$	only DEC is violated for a small time interval at the throat.
	$\sigma = -1/3,\ c_3 = -1$	completely satisfied.
$\epsilon = -0.1$	$\sigma = 1/3,\ c_3 = 1$	only violated at the throat.
	$\sigma = 1/3,\ c_3 = -1$	completely satisfied.
	$\sigma = -1/3,\ c_3 = 1$	only DEC is violated for a small time interval at the throat.
	$\sigma = -1/3,\ c_3 = -1$	completely satisfied.

Table 7.4: Results for the energy conditions in an anisotropic fluid solution with the throat radius fixed at $r_0 = 1$ and an effective cosmological constant $\Lambda = 0.3$.

From the above discussions, it can be inferred that there are numerous possibilities for evolving wormholes with non-exotic matter within the framework of dRGT massive gravity theory. As already demonstrated in Chapter 6, the construction of traversable wormholes in dRGT theory involves massive gravitons acting as anisotropic dark en-

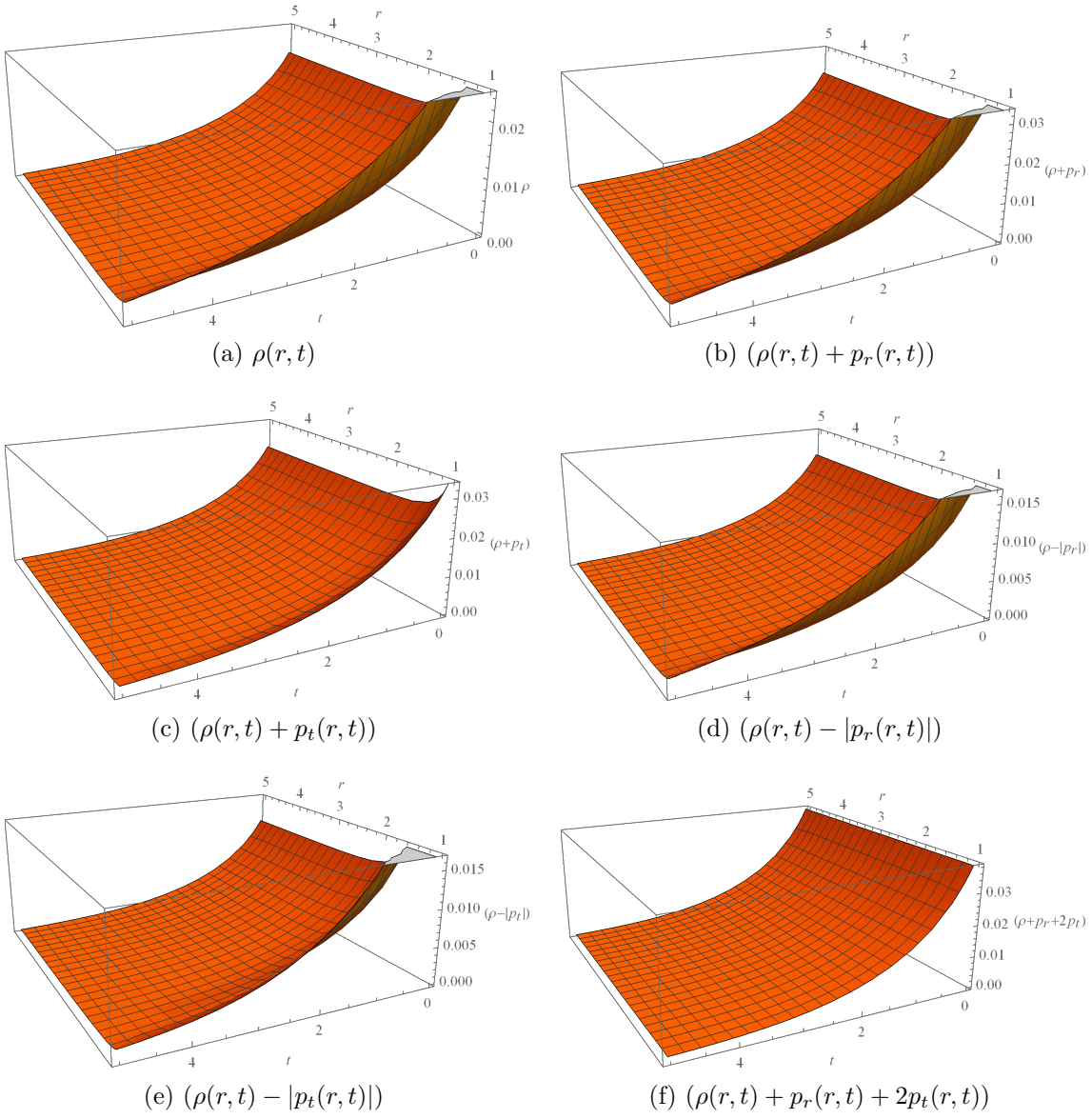

(a) $\rho(r,t)$ (b) $(\rho(r,t)+p_r(r,t))$

(c) $(\rho(r,t)+p_t(r,t))$ (d) $(\rho(r,t)-|p_r(r,t)|)$

(e) $(\rho(r,t)-|p_t(r,t)|)$ (f) $(\rho(r,t)+p_r(r,t)+2p_t(r,t))$

Figure 7.5: Nature of energy condition components for barotropic fluid against the radial parameter r and cosmic time t. The parameters are fixed at $r_0 = 1$, $\Lambda = 0.3$, $\omega = 1/3$, $t_0 = 0$, $A_2 = 1$, $c_2 = 1$ and $\epsilon = -1$.

ergy. This phenomenon results in the violation of energy conditions, permitting the coupled matter to remain ordinary. Consequently, under certain stringent constraints on the parameter choices, this coupled matter can adhere to all classical energy conditions, enabling the construction of wormholes with ordinary matter at the throat.

7.6 Discussions

In this investigation, the method of smoothly blending spherically inhomogeneous wormhole metrics has been employed within the cosmological context of dRGT massive gravity, which interacts with Einstein gravity. The model emerges from a combination of two fluid systems: one being a perfect fluid governed by GR, while the other consists of massive gravitons exhibiting spatially anisotropic characteristics akin to dark energy. A notable characteristic of the model is the existence of non-zero effective cosmological constant (Λ) and global monopole potential (ϵ) originating from the mass of the massive gravitons. Of significance is the energy density accountable for the existence and sustenance of the wormhole, which is distinguished by its non-uniform and anisotropic nature. This energy-matter content may manifest as a traceless fluid, an ideal barotropic fluid, or any anisotropic cosmic fluid conforming to the requisites of homogeneity and anisotropy.

Across all three scenarios: traceless, barotropic, and anisotropic pressure fluids, it is crucial that a straightforward approximation on the parameters of massive gravity, namely $\gamma = 0$, permits the easy separation of the wormhole shape function and scale factor. Remarkably, this approximation does not significantly alter other parameters. Referring to Eq. (7.21), it is obtained that $\alpha = -\frac{1+3\beta}{2}$ for $\gamma = 0$, yielding $\Lambda = -\frac{3}{2}m_g^2(1-\beta)$, and $\epsilon = -m_g^2c^2\left(\frac{1-3\beta}{2}\right)$. Hence, a restriction on the massive gravity parameters are derived. Subsequently, it is identified that the deviation of the wormhole shape function and scale factor from GR are imposed by additional terms consisting of ϵ and Λ, respectively, in the extension to massive gravity.

Note that the development of wormhole models outlined in this study is underpinned by the accelerated expansion occurring on both sides of the wormhole throat. However, some of these models diverge from the hyperbolic FRW universe models depicted in Fig. 7.3. Moreover, an intriguing observation arises concerning traceless fluid, wherein the scale factor exhibits an emergent scenario evolution. This suggests that the corresponding wormhole configuration has originated from an emergent universe in the past, aligning with findings in [677].

In Section 7.4, wormhole solutions for traceless, barotropic, and anisotropic fluids are derived and assessed the validity of these solutions with respect to their flaring-out conditions. It was noted that while some wormhole solutions extend infinitely, others are confined within finite regions. As discussed in Chapter 6, the static traversable wormholes violate the asymptotic condition in dRGT massive gravity due to the repulsive gravitational effect exerted by massive gravitons. This repulsion significantly distorts curvature, disrupting flatness, and potentially inducing effects stemming from accelerated expansion.

Except for three types of fluids' solution, the isotropic fluid ($p_t = p_r$) solution does not explicitly rely on the scale parameter $a(t)$. Nonetheless, even when incorporating the inflation mechanism within the framework by assuming a reasonable choice of $a(t)$ with $\dot{a}(t)/a(t) = H(t) \neq 0$, there exists a plethora of options for $a(t)$. However, the potential solution for the shape function, namely in the form: $b(r) = r^3/r_0^2$, does not correspond to a well-defined asymptotic structure due to the violation of the flaring-out

condition ($-rb'(r) + b(r) = -2r^3/r_0^2 < 0$) throughout space. Nevertheless, there may still be a meaningful physical interpretation. Opting for a suitable scale factor such as $a(t) = a_0 e^{H_0 t}$ yields the metric in the form:

$$ds^2 = -dt^2 + a_0^2 e^{2H_0 t}\left[\frac{dr^2}{1-\frac{r^2}{r_0^2}} + r^2 d\Omega^2\right].$$

The spatial structure of the metric signifies an exponentially expanding 3-sphere, thus representing an empty closed universe with $\frac{1}{r_0^2} > 0$.

In the domain of massive gravity theory, a notable phenomenon is the behaviour of the energy-momentum tensor of massive gravitons. This tensor exhibits characteristics of anisotropic dark energy, leading to violations of energy conditions. When exploring evolving wormholes, the interplay between perfect fluid and massive gravitons, reveals intriguing dynamics. In all three types of fluids' solution, a wide range of parameter choices generate wormhole configurations with non-exotic matter at the throat. It is however, also possible that for some of the choices energy condition components at the throat transition from positive to negative values over cosmological time, signifying the evolution from non-exotic to exotic matter.

A crucial observation is that distant from the throat, the geometries of evolving wormholes resemble those of a flat FRW universe. If the throat lies beyond an observer's cosmological horizon, causal connection to it is severed, leading the observer to perceive the universe as isotropic and homogeneous. This scenario presents a challenge for observers to discern whether they reside in a space with constant curvature or within a wormhole spacetime.

CHAPTER 8

CONCLUDING REMARK

The thesis comprises eight chapters, commencing with an introduction and brief literature review in the initial two chapters, followed by the presentation of research works in the next five chapters. Finally, the present chapter intends to conclude the thesis with a brief summary and future prospects arising from the overall discussions.

The first chapter delves into a concise overview of Einstein's General Relativity and its expansion through the emergence of modified gravity theories. It particularly scrutinizes modifications such as $f(R)$ and $f(R,T)$ gravity, as well as the recently developed dRGT massive gravity. The second chapter introduces the theoretical aspect of time travel within general relativity, exploring closed timelike curves (CTCs) and wormholes. Following the review of CTCs in the first part of the chapter, a summary of spacetime geometries containing CTCs is provided. Similarly, the second part offers a historical overview of wormhole research, followed by discussions of well-known metrics like the Morris-Thorne wormhole, rotating Teo wormhole, and cosmological wormholes.

Chapter 3 analyzes the formation and dynamics of CTCs within the interior van Stockum spacetime, with special attention to the characteristics of particles, primarily in terms of their angular momentum, as they traverse these orbits. The chapter concludes by generalizing the obtained results to general axisymmetric, rotating spacetime metrics. It is found that zero angular momentum particles are completely forbidden to exist in CTCs and CTGs of the interior van Stockum and consequently, in any general axisymmetric spacetimes, thus, allowing only non-zero angular momentum particles for the motion. The range of backward time-jump and the minimum amount of energy required by a particle to traverse the CTGs are also explored in this context. Interestingly, a number of observations to characterize the interior dust cylinder provide the presence of an infinitely long black cylinder, separate from the exterior spacetime, among others.

Chapter 4 extends the results of Chapter 3 with extended discussions and new findings in Kerr-Newman geometry. It explores the CTCs within the naked singularity

(NS) and black hole (BH), both extremal and non-extremal, of the metric with given limits. It is found that for the neutral particles and particles with identical (polarity) charge to the source, the spacetime only allows positive angular momentum particles to traverse the CTCs, restricting zero and negative angular momentum particles in both the NS and BH. However, for the particles with opposite charge to the source, the spacetime is dominated by the Coulomb attraction which draws all the particles into CTCs. Additionally, the study of geodesic confinement showed that the central singularity is always covered by a complete empty region that restricts particles at a considerable distance, limiting their interaction with the singularity. The radius of this surface has been explored with an accurate expression.

In Chapter 5, closed timelike geodesic (CTG) orbits within different geodesic trajectories of test particles on the wormhole surface are examined, connecting CTCs and wormholes in terms of particle dynamics. The geodesic orbits are visualized by plotting them on the wormhole embedding geometry, resulting in the emergence of bound and escape orbits. Here, the bound orbits mostly represent interacting trajectories that may cause causality to be violated.

Chapter 6 extensively investigates the static Morris-Thorne wormhole solution in dRGT massive gravity, highlighting the intriguing outcome of the repulsive gravity effect on the geometry. The chapter starts with the wormhole solution in coupled dRGT-$f(R,T)$ massive gravity, then extends them to Einstein-massive gravity with a special limit on $f(R,T)$. The analysis of the shape function properties, and consequently, the negative deflection angle of photons, indicates the presence of repulsive gravity, which may have originated from the massive gravitons. This study shows that the effect, however, disturbs the asymptotic flatness of the overall geometry, but the wormhole remains stable under hydrostatic equilibrium. Subsequently, in this chapter, studying the components of the energy condition holds considerable significance, particularly because for many choices of the massive gravity parameters, the throat of the wormhole is threaded by non-exotic matter, satisfying all classical energy conditions.

Chapter 7 delves into the evolving cosmological wormhole solution within massive gravity, also generalizing the results from Chapter 6. In this study, wormhole solutions are obtained, particularly in Einstein-massive gravity, for traceless, barotropic, and anisotropic fluids. A detailed analysis of the flaring-out conditions and the extension of the wormholes is carried out with precise expressions, providing finitely extended wormholes in some cases, whereas other cases give infinitely extended wormhole solutions. Subsequently, the investigation of the energy conditions is formulated along with 3D plots to describe the traversability conditions. It is found that a wide range of parameter selections produce non-exotic matter wormholes, confirming the viability of evolving wormholes with ordinary matter at the throat in dRGT massive gravity theory.

In conclusion, this thesis comprehensively explores the intricate interplay between particle characteristics, closed timelike curves, and wormholes, shedding light on funda-

mental aspects of spacetime geometries. Although, phenomenologically closed timelike curves and wormholes are interesting in the context of quantum gravity, they have a wide range of future prospects.

While wormholes remain purely speculative within the realm of theoretical physics, advancements in our understanding of exotic matter, negative energy may provide avenues for quantum theory of gravity. Research efforts could focus on developing theoretical frameworks that incorporate quantum effects to stabilize wormholes and prevent their collapse. This could involve investigating exotic matter that counteract the gravitational forces pulling the wormhole shut, as well as exploring quantum fluctuations that might influence the wormhole's geometry.

Furthermore, experimental studies aiming to detect signatures of wormholes or phenomena associated with their existence could be pursued. Advanced astrophysical observations, such as accretion disk formation in wormhole shadows, gravitational wave detectors or high-energy particle experiments, may offer insights into potential observational manifestations of wormholes or related phenomena.

Moreover, interdisciplinary collaborations between theoretical physicists, cosmologists, and experts in quantum gravity could lead to novel insights and methodologies for studying wormholes. By integrating concepts from various fields of physics, researchers may uncover new approaches for understanding the fundamental nature of space-time and the potential existence of traversable wormholes.

Overall, the future of wormhole research holds the promise of unraveling one of the most intriguing mysteries of the universe, offering potential insights into the fabric of space-time and the fundamental laws governing our cosmos.

REFERENCES

[1] A. Einstein, "The foundation of the general theory of relativity.," Annalen Phys. **49** (1916) no.7, 769-822

[2] S. W. Hawking and G. F. R. Ellis, "The Large Scale Structure of Space-Time," Cambridge University Press, 1973, doi:10.1017/9781009253161

[3] R. V. Eötvös , "Uber die anziehung der erde auf versehiedene substanzen," *Mathematische und Naturwissenschaftliche Berichte aus Ungarn* **8**, 65 (1890).

[4] L. Southerns and J. J. Thomson, "A determination of the ratio of mass to weight for a radioactive substance," *Proceedings of the Royal Society of London. Series A, Containing Papers of a Mathematical and Physical Character* **84** no. 571, 325–344 (1910).

[5] H. H. Potter and O. W. Richardson, "Some experiments on the proportionality of mass and weight,"*Proceedings of the Royal Society of London. Series A, Containing Papers of a Mathematical and Physical Character* **104** no. 728, 588–610 (1923).

[6] P. G. Roll, R. Krotkov and R. H. Dicke, "The Equivalence of inertial and passive gravitational mass," Annals Phys. **26** (1964), 442-517

[7] I. I. Shapiro, C. C. Counselman and R. W. King, "Verification of the Principle of Equivalence for Massive Bodies," Phys. Rev. Lett. **36** (1976), 555-558

[8] T. M. Niebauer, M. P. Mchugh and J. E. Faller, "Galilean Test for the Fifth Force," Phys. Rev. Lett. **59** (1987), 609-612

[9] E. G. Adelberger, C. W. Stubbs, B. R. Heckel, Y. Su, H. E. Swanson, G. Smith, J. H. Gundlach and W. F. Rogers, "Testing the equivalence principle in the field of the earth: Particle physics at masses below 1-microEV?," Phys. Rev. D **42** (1990), 3267-3292

[10] S. Baessler, B. R. Heckel, E. G. Adelberger, J. H. Gundlach, U. Schmidt and H. E. Swanson, "Improved Test of the Equivalence Principle for Gravitational Self-Energy," Phys. Rev. Lett. **83** (1999), 3585

[11] P. Touboul, G. Métris, M. Rodrigues, Y. André, Q. Baghi, J. Bergé, D. Boulanger, S. Bremer, P. Carle and R. Chhun, *et al.* "MICROSCOPE Mission: First Results of a Space Test of the Equivalence Principle," Phys. Rev. Lett. **119** (2017) no.23, 231101

[12] S. M. Carroll, "Spacetime and Geometry: An Introduction to General Relativity," Cambridge University Press, 2019, doi:10.1017/9781108770385

[13] R. d'Inverno, "Introducing Einstein's relativity," *Clarendon Press*, (1992).

[14] C. W. Misner, K. S. Thorne and J. A. Wheeler, "Gravitation," W. H. Freeman, 1973, ISBN 978-0-7167-0344-0, 978-0-691-17779-3

[15] J. B. Hartle, "Gravity: An introduction to Einstein's general relativity," *Addison-Wesley*, (2003).

[16] A. Bakopoulos and P. Kanti, Gen. Rel. Grav. **46** (2014), 1742

[17] A. Bakopoulos, "Gravitoelectromagnetism: Basic principles, novel approaches and their application to Electromagnetism," *Master thesis* (2016) [arXiv:1610.08357 [gr-qc]].

[18] A. Bakopoulos and P. Kanti, "Novel Ansatzes and Scalar Quantities in Gravito-Electromagnetism," Gen. Rel. Grav. **49** (2017) no.3, 44

[19] I. H. Stairs, "Testing general relativity with pulsar timing," Living Rev. Rel. **6** (2003), 5

[20] J. M. Weisberg, D. J. Nice and J. H. Taylor, "Timing Measurements of the Relativistic Binary Pulsar PSR B1913+16," Astrophys. J. **722** (2010), 1030-1034

[21] M. Kramer, I. H. Stairs, R. N. Manchester, M. A. McLaughlin, A. G. Lyne, R. D. Ferdman, M. Burgay, D. R. Lorimer, A. Possenti and N. D'Amico, *et al.* "Tests of general relativity from timing the double pulsar," Science **314** (2006), 97-102

[22] J. Antoniadis, P. C. C. Freire, N. Wex, T. M. Tauris, R. S. Lynch, M. H. van Kerkwijk, M. Kramer, C. Bassa, V. S. Dhillon and T. Driebe, *et al.* "A Massive Pulsar in a Compact Relativistic Binary," Science **340** (2013), 6131

[23] B. P. Abbott *et al.* [LIGO Scientific and Virgo], "Observation of Gravitational Waves from a Binary Black Hole Merger," Phys. Rev. Lett. **116** (2016) no.6, 061102

[24] B. P. Abbott *et al.* [LIGO Scientific and Virgo], "GW170817: Observation of Gravitational Waves from a Binary Neutron Star Inspiral," Phys. Rev. Lett. **119** (2017) no.16, 161101

[25] K. Akiyama *et al.* [Event Horizon Telescope], "First M87 Event Horizon Telescope Results. I. The Shadow of the Supermassive Black Hole," Astrophys. J. Lett. **875** (2019), L1

[26] K. Akiyama *et al.* [Event Horizon Telescope], "First Sagittarius A* Event Horizon Telescope Results. I. The Shadow of the Supermassive Black Hole in the Center of the Milky Way," Astrophys. J. Lett. **930** (2022) no.2, L12

[27] S. Perlmutter *et al.* [Supernova Cosmology Project], "Measurements of Ω and Λ from 42 high redshift supernovae," Astrophys. J. **517** (1999), 565-586

[28] A. G. Riess *et al.* [Supernova Search Team], "Observational evidence from supernovae for an accelerating universe and a cosmological constant," Astron. J. **116** (1998), 1009-1038

[29] S. Perlmutter, M. S. Turner and M. J. White, "Constraining dark energy with SNe Ia and large scale structure," Phys. Rev. Lett. **83** (1999), 670-673

[30] A. G. Riess *et al.* [Supernova Search Team], "The farthest known supernova: support for an accelerating universe and a glimpse of the epoch of deceleration," Astrophys. J. **560** (2001), 49-71

[31] C. L. Bennett *et al.* [WMAP], "First year Wilkinson Microwave Anisotropy Probe (WMAP) observations: Preliminary maps and basic results," Astrophys. J. Suppl. **148** (2003), 1-27

[32] G. Hinshaw *et al.* [WMAP], "First year Wilkinson Microwave Anisotropy Probe (WMAP) observations: The Angular power spectrum," Astrophys. J. Suppl. **148** (2003), 135

[33] A. G. Riess *et al.* [Supernova Search Team], "Type Ia supernova discoveries at z $>$ 1 from the Hubble Space Telescope: Evidence for past deceleration and constraints on dark energy evolution," Astrophys. J. **607** (2004), 665-687

[34] E. J. Copeland, M. Sami and S. Tsujikawa, "Dynamics of dark energy," Int. J. Mod. Phys. D **15** (2006), 1753-1936

[35] L. M. Wang, R. R. Caldwell, J. P. Ostriker and P. J. Steinhardt, "Cosmic concordance and quintessence," Astrophys. J. **530** (2000), 17-35

[36] M. S. Turner, "Dark energy and the new cosmology," [arXiv:astro-ph/0108103 [astro-ph]].

[37] R. R. Caldwell, "A Phantom menace?," Phys. Lett. B **545** (2002), 23-29

[38] R. R. Caldwell, M. Kamionkowski and N. N. Weinberg, "Phantom energy and cosmic doomsday," Phys. Rev. Lett. **91** (2003), 071301

[39] R. P. Woodard, "How Far Are We from the Quantum Theory of Gravity?," Rept. Prog. Phys. **72** (2009), 126002

[40] J. Binney, S. Tremaine, Galactic Dynamics, Princeton University Press (1987)

[41] M. Persic, P. Salucci and F. Stel, "The Universal rotation curve of spiral galaxies: 1. The Dark matter connection," Mon. Not. Roy. Astron. Soc. **281** (1996), 27

[42] A. Borriello and P. Salucci, "The Dark matter distribution in disk galaxies," Mon. Not. Roy. Astron. Soc. **323** (2001), 285

[43] P. Salucci, A. Lapi, C. Tonini, G. Gentile, I. Yegorova and U. Klein, "The Universal Rotation Curve of Spiral Galaxies. 2. The Dark Matter Distribution out to the Virial Radius," Mon. Not. Roy. Astron. Soc. **378** (2007), 41-47

[44] F. S. N. Lobo, "The Dark side of gravity: Modified theories of gravity," (2008) [arXiv:0807.1640 [gr-qc]].

[45] Paulo Crawford, "Einstein's 'Zurich Notebook' and the Genesis of General Relativity", Boletim da SPM, Nmero especial Mira Fernandes, pp. 223-245.

[46] A. Pais "Subtle is the Lord..." The Science and the life of Albert Einstein, *Cambridge University Press*, (1982).

[47] H. Weyl, Space Time Matter, *Dover Publications*, (1922).

[48] A. S. Eddington, The Mathematical Theory of Relativity, *Cambridge University Press, Cambridge*, (1923).

[49] H. Weyl, "Zur Gravitationstheorie," Annalen Phys. **359** (1917) no.18, 117-145

[50] E. Schrödinger, "Space-Time Structure," Cambridge University Press (1963)

[51] E. Cartan, "Sur les variétés à connexion affine et la théorie de la relativité généralisée. (première partie)," Annales Sci. Ecole Norm. Sup. **40** (1923), 325-412, Annales Sci. Ecole Norm. Sup. **41** (1924), 1-25, Annales Sci. Ecole Norm. Sup. **42** (1925), 17-88
English translation: A. Magnon, A. Ashtekar, "On manifolds with an affine connection and the theory of general relativity," Napoli: Bibliopolis (1986)

[52] H. A. Buchdahl, "Non-Linear Lagrangians and Cosmological Theory," Mon. Not. Roy. Astron. Soc. **150** (1970) no.1, 1-8

[53] J. D. Barrow and A. C. Ottewill, "The Stability of General Relativistic Cosmological Theory," J. Phys. A **16** (1983), 2757

[54] S. Capozziello, V. F. Cardone and A. Troisi, "Dark energy and dark matter as curvature effects," JCAP **08** (2006), 001

[55] S. Capozziello, V. F. Cardone and A. Troisi, "Low surface brightness galaxies rotation curves in the low energy limit of r**n gravity: no need for dark matter?," Mon. Not. Roy. Astron. Soc. **375** (2007), 1423-1440

[56] A. Borowiec, W. Godlowski and M. Szydlowski, "Dark matter and dark energy as a effects of Modified Gravity," eConf **C0602061** (2006) 09, Int. J. Geom. Meth. Mod. Phys. **4** (2007) 183-196

[57] C. F. Martins and P. Salucci, "Analysis of Rotation Curves in the framework of R**n gravity," Mon. Not. Roy. Astron. Soc. **381** (2007), 1103-1108

[58] C. G. Boehmer, T. Harko and F. S. N. Lobo, "Dark matter as a geometric effect in f(R) gravity," Astropart. Phys. **29** (2008), 386-392

[59] O. Bertolami, C. G. Boehmer, T. Harko and F. S. N. Lobo, "Extra force in f(R) modified theories of gravity," Phys. Rev. D **75** (2007), 104016

[60] O. Bertolami and J. Paramos, "Do f(R) theories matter?," Phys. Rev. D **77** (2008), 084018

[61] T. P. Sotiriou and V. Faraoni, "f(R) Theories Of Gravity," Rev. Mod. Phys. **82** (2010), 451-497

[62] A. A. Starobinsky, "A New Type of Isotropic Cosmological Models Without Singularity," Phys. Lett. B **91** (1980), 99-102

[63] S. M. Carroll, V. Duvvuri, M. Trodden and M. S. Turner, "Is cosmic speed - up due to new gravitational physics?," Phys. Rev. D **70** (2004), 043528

[64] A. De Felice and S. Tsujikawa, "f(R) theories," Living Rev. Rel. **13** (2010), 3

[65] L. Amendola, D. Polarski and S. Tsujikawa, "Are f(R) dark energy models cosmologically viable ?," Phys. Rev. Lett. **98** (2007), 131302

[66] S. Capozziello, S. Nojiri, S. D. Odintsov and A. Troisi, "Cosmological viability of f(R)-gravity as an ideal fluid and its compatibility with a matter dominated phase," Phys. Lett. B **639** (2006), 135-143

[67] S. Nojiri and S. D. Odintsov, "Modified f(R) gravity consistent with realistic cosmology: From matter dominated epoch to dark energy universe," Phys. Rev. D **74** (2006), 086005

[68] M. Amarzguioui, O. Elgaroy, D. F. Mota and T. Multamaki, "Cosmological constraints on f(r) gravity theories within the palatini approach," Astron. Astrophys. **454** (2006), 707-714

[69] L. Amendola, R. Gannouji, D. Polarski and S. Tsujikawa, "Conditions for the cosmological viability of f(R) dark energy models," Phys. Rev. D **75** (2007), 083504

[70] T. Chiba, "1/R gravity and scalar - tensor gravity," Phys. Lett. B **575** (2003), 1-3

[71] A. L. Erickcek, T. L. Smith and M. Kamionkowski, "Solar System tests do rule out 1/R gravity," Phys. Rev. D **74** (2006), 121501

[72] T. Chiba, T. L. Smith and A. L. Erickcek, "Solar System constraints to general f(R) gravity," Phys. Rev. D **75** (2007), 124014

[73] S. Nojiri and S. D. Odintsov, "Modified non-local-F(R) gravity as the key for the inflation and dark energy," Phys. Lett. B **659** (2008), 821-826

[74] G. J. Olmo, "Limit to general relativity in f(R) theories of gravity," Phys. Rev. D **75** (2007), 023511

[75] W. Hu and I. Sawicki, "Models of f(R) Cosmic Acceleration that Evade Solar-System Tests," Phys. Rev. D **76** (2007), 064004

[76] S. Nojiri and S. D. Odintsov, "Modified gravity with negative and positive powers of the curvature: Unification of the inflation and of the cosmic acceleration," Phys. Rev. D **68** (2003), 123512

[77] V. Faraoni, "Solar System experiments do not yet veto modified gravity models," Phys. Rev. D **74** (2006), 023529

[78] T. Faulkner, M. Tegmark, E. F. Bunn and Y. Mao, "Constraining f(R) Gravity as a Scalar Tensor Theory," Phys. Rev. D **76** (2007), 063505

[79] P. J. Zhang, "The behavior of f(R) gravity in the solar system, galaxies and clusters," Phys. Rev. D **76** (2007), 024007

[80] S. Capozziello and S. Tsujikawa, "Solar system and equivalence principle constraints on f(R) gravity by chameleon approach," Phys. Rev. D **77** (2008), 107501

[81] M. Ferraris, M. Francaviglia and I. Volovich, "The Universality of vacuum Einstein equations with cosmological constant," Class. Quant. Grav. **11** (1994), 1505-1517

[82] D. N. Vollick, "1/R Curvature corrections as the source of the cosmological acceleration," Phys. Rev. D **68** (2003), 063510

[83] E. E. Flanagan, "Higher order gravity theories and scalar tensor theories," Class. Quant. Grav. **21** (2003), 417-426

[84] X. H. Meng and P. Wang, "Palatini formation of modified gravity with ln R terms," Phys. Lett. B **584** (2004), 1-7

[85] B. Li and M. C. Chu, "CMB and Matter Power Spectra of Early f(R) Cosmology in Palatini Formalism," Phys. Rev. D **74** (2006), 104010

[86] N. J. Poplawski, "Interacting dark energy in f(R) gravity," Phys. Rev. D **74** (2006), 084032

[87] B. Li, K. C. Chan and M. C. Chu, "Constraints on f(R) Cosmology in the Palatini Formalism," Phys. Rev. D **76** (2007), 024002

[88] B. Li, J. D. Barrow and D. F. Mota, "The Cosmology of Ricci-Tensor-Squared gravity in the Palatini variational approach," Phys. Rev. D **76** (2007), 104047

[89] A. Iglesias, N. Kaloper, A. Padilla and M. Park, "How (Not) to Palatini," Phys. Rev. D **76** (2007), 104001

[90] T. P. Sotiriou and S. Liberati, "Metric-affine f(R) theories of gravity," Annals Phys. **322** (2007), 935-966

[91] T. Multamaki and I. Vilja, "Spherically symmetric solutions of modified field equations in f(R) theories of gravity," Phys. Rev. D **74** (2006), 064022

[92] A. de la Cruz-Dombriz, A. Dobado and A. L. Maroto, "Black Holes in f(R) theories," Phys. Rev. D **80** (2009), 124011 [erratum: Phys. Rev. D **83** (2011), 029903]

[93] S. H. Hendi and D. Momeni, "Black hole solutions in F(R) gravity with conformal anomaly," Eur. Phys. J. C **71** (2011), 1823

[94] G. G. L. Nashed, "New rotating AdS/dS black holes in $f(R)$ gravity," Phys. Lett. B **815** (2021), 136133

[95] G. L. L. Nashed and S. Nojiri, "Rotating black hole in f(R) theory," JCAP **11** (2021) no.11, 007

[96] G. G. L. Nashed and S. Nojiri, "Specific neutral and charged black holes in f(R) gravitational theory," Phys. Rev. D **104** (2021) no.12, 124054

[97] G. G. L. Nashed, "Uniqueness of non-trivial spherically symmetric black hole solution in special classes of F (R) gravitational theory," Phys. Lett. B **812** (2021), 136012

[98] Z. Y. Tang, B. Wang and E. Papantonopoulos, "Exact charged black hole solutions in D-dimensions in $f(R)$ gravity," Eur. Phys. J. C **81** (2021) no.4, 346

[99] S. C. Jaryal and A. Chatterjee, "Gravitationally collapsing stars in $f(R)$ gravity," Eur. Phys. J. C **81** (2021) no.4, 273

[100] Z. Y. Tang, B. Wang, T. Karakasis and E. Papantonopoulos, "Curvature scalarization of black holes in f(R) gravity," Phys. Rev. D **104** (2021) no.6, 064017

[101] T. Karakasis, E. Papantonopoulos, Z. Y. Tang and B. Wang, "Black holes of (2+1)-dimensional $f(R)$ gravity coupled to a scalar field," Phys. Rev. D **103** (2021) no.6, 064063

[102] T. Karakasis, E. Papantonopoulos, Z. Y. Tang and B. Wang, "Exact black hole solutions with a conformally coupled scalar field and dynamic Ricci curvature in f(R) gravity theories," Eur. Phys. J. C **81** (2021) no.10, 897

[103] E. Elizalde, G. G. L. Nashed, S. Nojiri and S. D. Odintsov, "Spherically symmetric black holes with electric and magnetic charge in extended gravity: physical properties, causal structure, and stability analysis in Einstein's and Jordan's frames," Eur. Phys. J. C **80** (2020) no.2, 109

[104] P. Cañate, "A no-hair theorem for black holes in $f(R)$ gravity," Class. Quant. Grav. **35** (2018) no.2, 025018

[105] P. Cañate, L. G. Jaime and M. Salgado, "Spherically symmetric black holes in $f(R)$ gravity: Is geometric scalar hair supported ?," Class. Quant. Grav. **33** (2016) no.15, 155005

[106] W. X. Feng, C. Q. Geng, W. F. Kao and L. W. Luo, "Equation of State of Neutron Stars with Junction Conditions in the Starobinsky Model," Int. J. Mod. Phys. D **27** (2017) no.01, 1750186

[107] M. Aparicio Resco, Á. de la Cruz-Dombriz, F. J. Llanes Estrada and V. Zapatero Castrillo, "On neutron stars in $f(R)$ theories: Small radii, large masses and large energy emitted in a merger," Phys. Dark Univ. **13** (2016), 147-161

[108] S. Capozziello, M. De Laurentis, R. Farinelli and S. D. Odintsov, "Mass-radius relation for neutron stars in f(R) gravity," Phys. Rev. D **93** (2016) no.2, 023501

[109] K. V. Staykov, D. Popchev, D. D. Doneva and S. S. Yazadjiev, "Static and slowly rotating neutron stars in scalar–tensor theory with self-interacting massive scalar field," Eur. Phys. J. C **78** (2018) no.7, 586

[110] S. S. Yazadjiev, D. D. Doneva and K. D. Kokkotas, "Rapidly rotating neutron stars in R-squared gravity," Phys. Rev. D **91** (2015) no.8, 084018

[111] S. S. Yazadjiev, D. D. Doneva, K. D. Kokkotas and K. V. Staykov, "Non-perturbative and self-consistent models of neutron stars in R-squared gravity," JCAP **06** (2014), 003

[112] A. Ganguly, R. Gannouji, R. Goswami and S. Ray, "Neutron stars in the Starobinsky model," Phys. Rev. D **89** (2014) no.6, 064019

[113] A. V. Astashenok, S. Capozziello and S. D. Odintsov, "Further stable neutron star models from f(R) gravity," JCAP **12** (2013), 040

[114] A. S. Arapoglu, C. Deliduman and K. Y. Eksi, "Constraints on Perturbative f(R) Gravity via Neutron Stars," JCAP **07** (2011), 020

[115] A. Cooney, S. DeDeo and D. Psaltis, "Neutron Stars in f(R) Gravity with Perturbative Constraints," Phys. Rev. D **82** (2010), 064033

[116] F. S. N. Lobo and M. A. Oliveira, "Wormhole geometries in f(R) modified theories of gravity," Phys. Rev. D **80** (2009), 104012

[117] P. Pavlovic and M. Sossich, "Wormholes in viable $f(R)$ modified theories of gravity and Weak Energy Condition," Eur. Phys. J. C **75** (2015), 117

[118] H. Golchin and M. R. Mehdizadeh, "Quasi-cosmological Traversable Wormholes in $f(R)$ Gravity," Eur. Phys. J. C **79** (2019) no.9, 777

[119] E. F. Eiroa and G. Figueroa Aguirre, "Thin-shell wormholes with charge in F(R) gravity," Eur. Phys. J. C **76** (2016) no.3, 132

[120] N. Godani and G. C. Samanta, "Traversable Wormholes in $R + \alpha R^n$ Gravity," Eur. Phys. J. C **80** (2020) no.1, 30

[121] A. D. Dolgov and M. Kawasaki, "Can modified gravity explain accelerated cosmic expansion?," Phys. Lett. B **573** (2003), 1-4

[122] T. Harko, F. S. N. Lobo, S. Nojiri and S. D. Odintsov, "$f(R,T)$ gravity," Phys. Rev. D **84** (2011), 024020

[123] M. Sharif and M. Zubair, "Thermodynamics in f(R,T) Theory of Gravity," JCAP **03** (2012), 028 [erratum: JCAP **05** (2012), E01]

[124] P. Rudra, "Does $f(R,T)$ gravity admit a stationary scenario between dark energy and dark matter in its framework?," Eur. Phys. J. Plus **130** (2015) no.4, 66

[125] H. Shabani and M. Farhoudi, "f(R,T) Cosmological Models in Phase Space," Phys. Rev. D **88** (2013), 044048

[126] F. G. Alvarenga, A. de la Cruz-Dombriz, M. J. S. Houndjo, M. E. Rodrigues and D. Sáez-Gómez, "Dynamics of scalar perturbations in $f(R,T)$ gravity," Phys. Rev. D **87** (2013) no.10, 103526 [erratum: Phys. Rev. D **87** (2013) no.12, 129905]

[127] A. Das, S. Ghosh, B. K. Guha, S. Das, F. Rahaman and S. Ray, "Gravastars in f(R,T) gravity," Phys. Rev. D **95** (2017) no.12, 124011

[128] R. Zaregonbadi, M. Farhoudi and N. Riazi, "Dark Matter From f(R,T) Gravity," Phys. Rev. D **94** (2016), 084052

[129] M. Sharif and A. Siddiqa, "Propagation of polar gravitational waves in $f(R,T)$ scenario," Gen. Rel. Grav. **51** (2019) no.6, 74

[130] P. Rudra and K. Giri, "Observational constraint in $f(R,T)$ gravity from the cosmic chronometers and some standard distance measurement parameters," Nucl. Phys. B **967** (2021), 115428

[131] P. Rudra, "A time-dependent spacetime in f(R,T) gravity: Gravitational collapse," Int. J. Mod. Phys. D **31** (2022) no.13, 2250095

[132] P. H. R. S. Moraes, R. A. C. Correa and R. V. Lobato, "Analytical general solutions for static wormholes in $f(R,T)$ gravity," JCAP **07** (2017), 029

[133] P. Sahoo, A. Kirschner and P. K. Sahoo, "Phantom fluid wormhole in $f(R,T)$ gravity," Mod. Phys. Lett. A **34** (2019) no.37, 1950303

[134] E. Elizalde and M. Khurshudyan, "Wormhole models in $f(R,T)$ gravity," Int. J. Mod. Phys. D **28** (2019) no.15, 1950172

[135] P. H. R. S. Moraes and P. K. Sahoo, "Modelling wormholes in $f(R,T)$ gravity," Phys. Rev. D **96** (2017) no.4, 044038

[136] Z. Yousaf, M. Ilyas and M. Zaeem-ul-Haq Bhatti, "Static spherical wormhole models in $f(R,T)$ gravity," Eur. Phys. J. Plus **132** (2017) no.6, 268

[137] E. Elizalde and M. Khurshudyan, "Wormhole formation in $f(R,T)$ gravity: Varying Chaplygin gas and barotropic fluid," Phys. Rev. D **98** (2018) no.12, 123525

[138] M. Sharif and I. Nawazish, "Viable wormhole solutions and Noether symmetry in f(R,T) gravity," Annals Phys. **400** (2019), 37-63

[139] D. Deb, F. Rahaman, S. Ray and B. K. Guha, "Strange stars in $f(R,T)$ gravity," JCAP **03** (2018), 044

[140] G. A. Carvalho, R. V. Lobato, P. H. R. S. Moraes, J. D. V. Arbañil, R. M. Marinho, E. Otoniel and M. Malheiro, "Stellar equilibrium configurations of white dwarfs in the f(R, T) gravity," Eur. Phys. J. C **77** (2017) no.12, 871

[141] T. M. Ordines and E. D. Carlson, "Limits on $f(R,T)$ gravity from Earth's atmosphere," Phys. Rev. D **99** (2019) no.10, 104052

[142] S. N. Gupta, "Gravitation and Electromagnetism," Phys. Rev. **96** (1954), 1683-1685

[143] S. Weinberg, "Photons and Gravitons in Perturbation Theory: Derivation of Maxwell's and Einstein's Equations," Phys. Rev. B **138** (1965) 988–1002

[144] S. Deser, "Selfinteraction and gauge invariance," Gen. Rel. Grav. **1** (1970), 9-18

[145] R. P. Feynman, F. B. Morinigo and W. G. Wagner, Feynman Lectures on Gravitation (Addison Wesley, Reading, MA, 1995)

[146] D. G. Boulware and S. Deser, "Classical General Relativity Derived from Quantum Gravity," Annals Phys. **89** (1975), 193

[147] M. Fierz and W. Pauli, "On relativistic wave equations for particles of arbitrary spin in an electromagnetic field," Proc. Roy. Soc. Lond. A **173** (1939), 211-232

[148] H. van Dam and M. J. G. Veltman, "Massive and massless Yang-Mills and gravitational fields," Nucl. Phys. B **22** (1970), 397-411

[149] V. I. Zakharov, "Linearized gravitation theory and the graviton mass," JETP Lett. **12** (1970), 312

[150] A. I. Vainshtein, "To the problem of nonvanishing gravitation mass," Phys. Lett. B **39** (1972), 393-394

[151] E. Babichev and C. Deffayet, "An introduction to the Vainshtein mechanism," Class. Quant. Grav. **30** (2013), 184001

[152] D. G. Boulware and S. Deser, "Can gravitation have a finite range?," Phys. Rev. D **6** (1972), 3368-3382

[153] G. R. Dvali, G. Gabadadze and M. Porrati, "Metastable gravitons and infinite volume extra dimensions," Phys. Lett. B **484** (2000), 112-118

[154] G. R. Dvali, G. Gabadadze and M. Porrati, "4-D gravity on a brane in 5-D Minkowski space," Phys. Lett. B **485** (2000), 208-214

[155] G. R. Dvali and G. Gabadadze, "Gravity on a brane in infinite volume extra space," Phys. Rev. D **63** (2001), 065007

[156] E. A. Bergshoeff, O. Hohm and P. K. Townsend, "Massive Gravity in Three Dimensions," Phys. Rev. Lett. **102** (2009), 201301

[157] C. de Rham and G. Gabadadze, "Generalization of the Fierz-Pauli Action," Phys. Rev. D **82** (2010), 044020

[158] C. de Rham, G. Gabadadze and A. J. Tolley, "Resummation of Massive Gravity," Phys. Rev. Lett. **106** (2011), 231101

[159] C. de Rham, "Massive Gravity," Living Rev. Rel. **17** (2014), 7

[160] W. Siegel, "Hidden gravity in open string field theory," Phys. Rev. D **49** (1994), 4144-4153

[161] N. Arkani-Hamed, H. Georgi and M. D. Schwartz, "Effective field theory for massive gravitons and gravity in theory space," Annals Phys. **305** (2003), 96-118

[162] P. Creminelli, A. Nicolis, M. Papucci and E. Trincherini, "Ghosts in massive gravity," JHEP **09** (2005), 003

[163] C. Deffayet and J. W. Rombouts, "Ghosts, strong coupling and accidental symmetries in massive gravity," Phys. Rev. D **72** (2005), 044003

[164] A. E. Gumrukcuoglu, C. Lin and S. Mukohyama, "Open FRW universes and self-acceleration from nonlinear massive gravity," JCAP **11** (2011), 030

[165] A. E. Gumrukcuoglu, C. Lin and S. Mukohyama, "Cosmological perturbations of self-accelerating universe in nonlinear massive gravity," JCAP **03** (2012), 006

[166] T. M. Nieuwenhuizen, "Exact Schwarzschild-de Sitter black holes in a family of massive gravity models," Phys. Rev. D **84** (2011), 024038

[167] S. G. Ghosh, L. Tannukij and P. Wongjun, "A class of black holes in dRGT massive gravity and their thermodynamical properties," Eur. Phys. J. C **76** (2016) no.3, 119

[168] L. Tannukij, P. Wongjun and S. G. Ghosh, "Black String in dRGT Massive Gravity," Eur. Phys. J. C **77** (2017) no.12, 846

[169] S. G. Ghosh, R. Kumar, L. Tannukij and P. Wongjun, "Rotating black strings in de Rham-Gabadadze-Tolley massive gravity," Phys. Rev. D **101** (2020) no.10, 104042

[170] P. Burikham, S. Ponglertsakul and L. Tannukij, "Charged scalar perturbations on charged black holes in de Rham-Gabadadze-Tolley massive gravity," Phys. Rev. D **96** (2017) no.12, 124001

[171] S. Ponglertsakul, P. Burikham and L. Tannukij, "Quasinormal modes of black strings in de Rham–Gabadadze–Tolley massive gravity," Eur. Phys. J. C **78** (2018) no.7, 584

[172] P. Boonserm, T. Ngampitipan and P. Wongjun, "Greybody factor for black holes in dRGT massive gravity," Eur. Phys. J. C **78** (2018) no.6, 492

[173] P. Boonserm, T. Ngampitipan and P. Wongjun, "Greybody factor for black string in dRGT massive gravity," Eur. Phys. J. C **79** (2019) no.4, 330

[174] Y. Ma, Y. Zhang, L. Zhang, L. Wu, Y. Huang and Y. Pan, "Thermodynamic properties of higher-dimensional dS black holes in dRGT massive gravity," Eur. Phys. J. C **80** (2020) no.3, 213

[175] S. H. Hendi, H. Zarei, M. Faizal, B. Pourhassan and Z. Armanfard, "Black string in massive gravity," Nucl. Phys. B **965** (2021), 115362

[176] B. Wu, C. Wang, Z. M. Xu and W. L. Yang, "Ruppeiner geometry and thermodynamic phase transition of the black hole in massive gravity," Eur. Phys. J. C **81** (2021) no.7, 626

[177] S. Kanzi, S. H. Mazharimousavi and İ. Sakallı, "Greybody factors of black holes in dRGT massive gravity coupled with nonlinear electrodynamics," Annals Phys. **422** (2020), 168301

[178] P. Li, Y. Huang, C. J. Feng and X. Z. Li, "Superradiant instabilities for a charged black hole in de Rham-Gabadadze-Tolley theory," Phys. Rev. D **102** (2020) no.2, 024063

[179] G. Geçim, "Quantum gravity correction to the thermodynamic quantities of the charged dRGT black hole," Turk. J. Phys. **44** (2020) no.6, 564-578

[180] S. H. Hendi and M. Momennia, "Quasinormal modes of black holes in dRGT massive gravity under electromagnetic perturbations," Iran. J. Phys. Res. **21** (2021) no.1, 213-218

[181] P. Boonserm, C. H. Chen, T. Ngampitipan and P. Wongjun, "Greybody factor for massive fermion emitted by a black hole in de Rham-Gabadadze-Tolley massive gravity theory," Phys. Rev. D **104** (2021) no.8, 084054

[182] S. A. H. Mansoori, L. Li, M. Rafiee and M. Baggioli, "What's inside a hairy black hole in massive gravity?," JHEP **10** (2021), 098

[183] P. Sriling, R. Nakarachinda and P. Wongjun, "Thermodynamics of black string from Rényi entropy in de Rham–Gabadadze–Tolley massive gravity theory," Class. Quant. Grav. **39** (2022) no.18, 185006

[184] R. P. Singh, B. K. Singh, R. K. Gupta and S. Sachan, "Thermodynamic properties of Bardeen black holes in dRGT massive gravity," doi:10.1139/cjp-2021-0092 [arXiv:2201.05309 [hep-th]].

[185] S. Kazempour, Y. C. Zou and A. R. Akbarieh, "Analysis of accretion disk around a black hole in dRGT massive gravity," Eur. Phys. J. C **82** (2022) no.3, 190

[186] P. Chunaksorn, E. Hirunsirisawat, R. Nakarachinda, L. Tannukij and P. Wongjun, "Thermodynamics of asymptotically de Sitter black hole in dRGT massive gravity from Rényi entropy," Eur. Phys. J. C **82** (2022) no.12, 1174

[187] T. K. Safir, C. L. A. Rizwan and D. Vaid, "Ruppeiner geometry, $P - V$ criticality and interacting microstructures of black holes in dRGT massive gravity," Int. J. Mod. Phys. A **37** (2022) no.25, 2250158

[188] M. A. Haddou, "Quasi-normal modes of near-extremal black holes in dRGT massive gravity using Physics-Informed Neural Networks (PINNs)," [arXiv:2303.02395 [gr-qc]].

[189] C. Fairoos and T. Sharqui, "Topological nature of black hole solutions in dRGT massive gravity," Int. J. Mod. Phys. A **38** (2023) no.25, 2350133

[190] H. Hadi, A. R. Akbarieh and P. S. Ilkhchi, "Massive gravity solution of black holes and entropy bounds," Eur. Phys. J. Plus **138** (2023) no.4, 330

[191] P. Boonserm, S. Phalungsongsathit, K. Sansuk and P. Wongjun, "Greybody factors for massive scalar field emitted from black holes in dRGT massive gravity," Eur. Phys. J. C **83** (2023) no.7, 657

[192] T. K. Safir, A. N. Kumara, S. Punacha, C. L. Ahmed Rizwan, C. Fairoos and D. Vaid, "Dynamic phase transition of black holes in massive gravity," Annals Phys. **458** (2023), 169480

[193] A. R. Akbarieh, P. S. Ilkhchi, Y. Izadi and M. Khoshrangbaf, "Black holes in R2-dRGT massive gravity," Int. J. Geom. Meth. Mod. Phys. **20** (2023) no.11, 2350196

[194] X. R. Chen, B. Wu and Z. M. Xu, "Thermodynamics of black holes in massive gravity with holography," Phys. Dark Univ. **42** (2023), 101317

[195] A. Malik, A. Mehmood and M. Umair Shahzad, "Thermodynamic topological classification of higher dimensional and massive gravity black holes," Annals Phys. **463** (2024), 169617

[196] K. Jafarzade, B. Eslam Panah and M. E. Rodrigues, "Thermodynamics and optical properties of phantom AdS black holes in massive gravity," Class. Quant. Grav. **41** (2024) no.6, 065007

[197] M. S. Hou, H. Xu and Y. C. Ong, "Hawking Evaporation of Black Holes in Massive Gravity," Eur. Phys. J. C **80** (2020) no.11, 1090

[198] S. H. Hendi, K. Jafarzade and B. Eslam Panah, "Black holes in dRGT massive gravity with the signature of EHT observations of M87*," JCAP **02** (2023), 022

[199] S. Panpanich and P. Burikham, "Fitting rotation curves of galaxies by de Rham-Gabadadze-Tolley massive gravity," Phys. Rev. D **98** (2018) no.6, 064008

[200] B. Afshar, N. Riazi and H. Moradpour, "A note on inflation in dRGT massive gravity," Eur. Phys. J. C **82** (2022) no.5, 430

[201] S. M. Aslmarand, A. R. Akbarieh, Y. Izadi, S. Kazempour and L. Shao, "Cosmological aspects of cubic Galileon massive gravity," Phys. Rev. D **104** (2021) no.8, 083543

[202] S. Kazempour and A. R. Akbarieh, "Cosmology in Brans–Dicke–de Rham–Gabadadze–Tolley massive gravity," Phys. Rev. D **105** (2022) no.12, 123515

[203] S. Kazempour, A. R. Akbarieh, H. Motavalli and L. Shao, "Cosmology of Dirac-Born-Infeld-de Rham-Gabadadze-Tolley massive gravity," Phys. Rev. D **106** (2022) no.2, 023508

[204] T. Tangphati, A. Chatrabhuti, D. Samart and P. Channuie, "Thin-shell wormholes in de Rham-Gabadadze-Tolley massive gravity," Eur. Phys. J. C **80** (2020) no.8, 722

[205] Z. Amirabi, "3+1-Dimensional GR versus dRGT massive gravity: a thin-shell wormholes comparison," Eur. Phys. J. Plus **135** (2020) no.1, 9

[206] T. Tangphati, A. Chatrabhuti, D. Samart and P. Channuie, "Traversable wormholes in $f(R)$-massive gravity," Phys. Rev. D **102** (2020) no.8, 084026

[207] N. Kamma, P. Wongjun, R. Nakarachinda and B. Gumjudpai, "Traversable wormholes in massive gravity theory," J. Phys. Conf. Ser. **1719** (2021) no.1, 012018

[208] Z. Y. Nie, Y. P. Hu and H. Zeng, "The holographic p + ip solution failed to win the competition in dRGT massive gravity," Eur. Phys. J. C **80** (2020) no.11, 1015

[209] L. A. Johnson, C. R. T. Jones and S. Paranjape, "Constraints on a Massive Double-Copy and Applications to Massive Gravity," JHEP **02** (2021), 148

[210] M. Kenna-Allison, A. E. Gumrukcuoglu and K. Koyama, "Cosmic acceleration and growth of structure in massive gravity," Phys. Rev. D **102** (2020) no.10, 103524

[211] M. Mousavi and K. Atazadeh, "Cosmological future singularities in massive gravity and massive bigravity," Phys. Dark Univ. **35** (2022), 100942

[212] L. Engelbrecht, C. R. T. Jones and S. Paranjape, "Supersymmetric Massive Gravity," JHEP **10** (2022), 130

[213] N. Ondo and V. Shyam, "The role of dRGT mass terms in cutoff holography and the Randall–Sundrum II scenario," [arXiv:2206.04005 [hep-th]].

[214] B. Bellazzini, G. Isabella, S. Ricossa and F. Riva, "Massive gravity is not positive," Phys. Rev. D **109** (2024) no.2, 024051

[215] M. Beigmohammadi and K. Karami, "Generalized second law of thermodynamics in massive gravity," Eur. Phys. J. C **84** (2024) no.1, 40

[216] T. Flöss, D. Roest and T. Westerdijk, "Non-linear Electrodynamics from Massive Gravity," [arXiv:2308.04349 [hep-th]].

[217] S. F. Hassan, R. A. Rosen and A. Schmidt-May, "Ghost-free Massive Gravity with a General Reference Metric," JHEP **02** (2012), 026

[218] S. F. Hassan and R. A. Rosen, "Bimetric Gravity from Ghost-free Massive Gravity," JHEP **02** (2012), 126

[219] A. Falkowski and G. Isabella, "Matter coupling in massive gravity," JHEP **04** (2020), 014

[220] K. Hinterbichler and R. A. Rosen, "Interacting Spin-2 Fields," JHEP **07** (2012), 047

[221] A. Momeni, J. Rumbutis and A. J. Tolley, "Massive Gravity from Double Copy," JHEP **12** (2020), 030

[222] O. Bertolami and F. S. N. Lobo, "Time and Causation," NeuroQuantol. **7** (2009), 1-15 [arXiv:0902.0559 [gr-qc]].

[223] C. Rovelli (Transcription: P. Frisoni), "Introduction to Loop Quantum Gravity: Rovelli's lectures on LQG," [arXiv:2305.12215 [gr-qc]].

[224] M. Visser, "Lorentzian wormholes: From Einstein to Hawking," AIP Press (1995).

[225] P. J. Nahin, "Time Machines: Time Travel in Physics, Metaphysics and Science Fiction," Springer-Verlag and AIP Press, New York (1999)

[226] S. W. Kim and K. S. Thorne, "Do vacuum fluctuations prevent the creation of closed timelike curves?," Phys. Rev. D **43** (1991), 3929-3947

[227] D. Deutsch, "Quantum mechanics near closed timelike lines," Phys. Rev. D **44** (1991), 3197-3217

[228] S. V. Krasnikov, "On the quantum stability of the time machine," Phys. Rev. D **54** (1996), 7322-7327

[229] J. Friedman, M. S. Morris, I. D. Novikov, F. Echeverria, G. Klinkhammer, K. S. Thorne and U. Yurtsever, "Cauchy problem in space-times with closed timelike curves," Phys. Rev. D **42** (1990), 1915-1930

[230] V. Prasad, R. Srinivasan and S. Gutti, "Chronology protection problem in modified Kerr-Newman spacetimes," Phys. Rev. D **99** (2019) no.2, 024023

[231] M. Bojowald, R. Goswami, R. Maartens and P. Singh, "A Black hole mass threshold from non-singular quantum gravitational collapse," Phys. Rev. Lett. **95** (2005), 091302

[232] M. R. Mbonye and D. Kazanas, "A Non-singular black hole model as a possible end-product of gravitational collapse," Phys. Rev. D **72** (2005), 024016

[233] S. Hossenfelder, L. Modesto and I. Premont-Schwarz, "A Model for non-singular black hole collapse and evaporation," Phys. Rev. D **81** (2010), 044036

[234] G. Martín-Vázquez and C. Sabín, "Closed timelike curves and chronology protection in quantum and classical simulators," Class. Quant. Grav. **37** (2020) no.4, 045013

[235] K. Godel, "An Example of a New Type of Cosmological Solutions of Einstein's Field Equations of Gravitation," Rev. Mod. Phys. **21** (1949), 447-450

[236] W. J. van Stockum, "The gravitational feild of a distribution of particles rotating about an axis of symmetry," Proc. Roy. Soc. Edinburgh **57** (1937), 135-154

[237] R. P. Kerr, "Gravitational field of a spinning mass as an example of algebraically special metrics," Phys. Rev. Lett. **11** (1963), 237-238

[238] F. J. Tipler, "Rotating cylinders and the possibility of global causality violation," Phys. Rev. D **9** (1974), 2203-2206

[239] W. B. Bonnor, "A rotating dust cloud in general relativity," J. Phys. A: Math. Gen. **10** (1977), 1673-1677

[240] J. R. Gott, III, "Closed timelike curves produced by pairs of moving cosmic strings: Exact solutions," Phys. Rev. Lett. **66** (1991), 1126-1129

[241] R. M. Wald, "General Relativity," Chicago University Press, 1984

[242] F. S. N. Lobo, "Nature of time and causality in physics," [arXiv:0710.0428 [gr-qc]].

[243] S. Chandrasekhar and J. P. Wright, "The Geodesics in Gödel's Universe," Proc. Natl. Acad. Sci. USA **47** (1961), 341–347.

[244] H. Stein, "On the Paradoxical Time-Structures of Gödel," Philos. Sci. **37** (1970), 589–601.

[245] M. Novello and M. J. Reboucas, "Rotating universe with successive causal and non-causal regions," Phys. Rev. D **19** (1979), 2850

[246] J. Pfarr, "Time travel in Gödel's space," Gen. Rel. Grav. **13** (1981), 1073-1091.

[247] D. B. Malament, "Minimal acceleration requirements for "time travel" in Gödel space-time," J. Math. Phys. **26** (1985), 774-777.

[248] D. B. Malament, "A note about closed timelike curves in Gödel space-time," J. Math. Phys. **28** (1987), 2427-2430.

[249] M. Novello, I. D. Soares and J. Tiomno, "Geodesic Motion and Confinement in Godel's Universe," Phys. Rev. D **27** (1983), 779-788

[250] H. Ishihara and S. Matsuno, "Gödel-type solutions in Einstein–Maxwell–scalar field theories," PTEP **2022** (2022) no.1, 013E02

[251] T. P. Kling, F. Ahmed and M. Lalumiere, "Wave Fronts in a Causality-Violating Gödel-Type Metric," Adv. High Energy Phys. **2020** (2020), 8713756

[252] D. Bini, A. Geralico, R. T. Jantzen and W. Plastino, "Gödel spacetime, planar geodesics and the Möbius map," Gen. Rel. Grav. **52** (2020) no.8, 73

[253] B. C. Nolan, "Causality violation without time-travel: closed lightlike paths in Gödel's universe," Class. Quant. Grav. **37** (2020) no.8, 085007

[254] D. Bini, A. Geralico, R. T. Jantzen and W. Plastino, "Gödel spacetime: Planar geodesics and gyroscope precession," Phys. Rev. D **100** (2019) no.8, 084051

[255] W. J. Geng, S. L. Li, H. Lü and H. Wei, "Gödel metrics with chronology protection in Horndeski gravities," Phys. Lett. B **780** (2018), 196-199

[256] T. Kling, K. Roebuck and E. Grotzke, "Null Geodesics and Wave Front Singularities in the Godel Space-time," Grav. **50** (2018), 7

[257] S. L. Li, X. H. Feng, H. Wei and H. Lu, "Gödel universe from string theory," Eur. Phys. J. C **77** (2017) no.5, 289

[258] S. Khodabakhshi and A. Shojai, "Induced rotation from de Sitter–Gödel–de Sitter phase transition," Phys. Rev. D **92** (2015) no.12, 123541

[259] B. R. Steadman, "Letter: Causality Violation on van Stockum Geodesics," Gen. Rel. Grav. **35** (2003), 1721–1726.

[260] R. Opher, N. O. Santos and A. Wang, "Geodesic motion and confinement in van Stockum space–time," J. Math. Phys. **37** (1996), 1982–1990

[261] P. Collas and D. Klein, "Causality violating geodesics in Bonnor's rotating dust metric," Gen. Rel. Grav. **36** (2004), 2549

[262] O. Grøn and S. Johannesen, "Closed timelike geodesics in a gas of cosmic strings," New J. Phys. **10** (2008), 103025

[263] S. W. Hawking, "The Chronology protection conjecture," Phys. Rev. D **46** (1992), 603-611

[264] A. Ori, "Rapidly moving cosmic strings and chronology protection," Phys. Rev. D **44** (1991), 2214-2215

[265] C. Cutler, "Global structure of Gott's two - string space-time," Phys. Rev. D **45** (1992), 487-494

[266] J. D. E. Grant, "Cosmic strings and chronology protection," Phys. Rev. D **47** (1993), 2388-2394

[267] D. Laurence, "Isometries between Gott's two-string spacetime and Grant's generalization of Misner space," Phys. Rev. D **50** (1994), 4957

[268] S. Deser, R. Jackiw and G. 't Hooft, "Physical cosmic strings do not generate closed timelike curves," Phys. Rev. Lett. **68** (1992), 267-269

[269] S. Deser and R. Jackiw, "Time travel?," Comments Nucl. Part. Phys. **20** (1992) no.6, 337-354 [arXiv:hep-th/9206094 [hep-th]].

[270] S. Deser, "Physical obstacles to time travel," Class. Quant. Grav. **10** (1993), S67-S73

[271] S. M. Carroll, E. Farhi and A. H. Guth, "An Obstacle to building a time machine," Phys. Rev. Lett. **68** (1992), 263-266 [erratum: Phys. Rev. Lett. **68** (1992), 3368]

[272] S. M. Carroll, E. Farhi, A. H. Guth and K. D. Olum, "Energy momentum restrictions on the creation of Gott time machines," Phys. Rev. D **50** (1994), 6190-6206

[273] B. Jensen and A. Ottewill, "Renormalized Electromagnetic Stress Tensor in Schwarzschild Space-time," Phys. Rev. D **39** (1989), 1130

[274] E. T. Newman, R. Couch, K. Chinnapared, A. Exton, A. Prakash and R. Torrence, "Metric of a Rotating, Charged Mass," J. Math. Phys. **6** (1965), 918-919

[275] B. Carter, "Complete Analytic Extension of the Symmetry Axis of Kerr's Solution of Einstein's Equations," Phys. Rev. **141** (1966), 1242-1247

[276] B. Carter, "Global structure of the Kerr family of gravitational fields," Phys. Rev. **174** (1968), 1559-1571

[277] M. Calvani, F. de Felice, B. Muchotrzeb and F. Salmistraro, "Time machine and geodesic motion in Kerr metric," Gen. Rel. Grav. **9** (1978), 155-163

[278] F. J. Tipler, "Existence of Closed Timelike Geodesics in Lorentz Spaces," Proc. Am. Math. Soc. **79** (1979), 1

[279] G. J. Galloway, "Closed Timelike Geodesics," Trans. Am. Math. Soc. **285** (1984), 1

[280] M. Guediri, "On the Nonexistence of Closed Timelike Geodesics in Flat Lorentz 2-Step Nilmanifolds," Trans. Am. Math. Soc. **355** (2002), no. 2, 775-786

[281] R. J. Gleiser, M. Gurses, A. Karasu and O. Sarioglu, "Closed timelike curves and geodesics of Godel-type metrics," Class. Quant. Grav. **23** (2006), 2653-2664

[282] M. Sánchez, "On causality and closed geodesics of compact Lorentzian manifolds and static spacetimes," Differential Geometry and its Applications **24** (2006), 21–32

[283] M. Guediri, "Closed Timelike Geodesics in Compact Spacetimes," Trans. Am. Math. Soc. **359** (2007), no. 6, 007, 2663-2673

[284] M. Sanchez, "On the geometry of static space-times," Nonlinear Analysis **63** (2005), e455-e463

[285] C. Rovelli, "Can we travel to the past? Irreversible physics along closed timelike curves," [arXiv:1912.04702 [gr-qc]].

[286] L. G. Bishop, F. Costa and T. C. Ralph, "Time-travelling billiard-ball clocks: a quantum model," Phys. Rev. A **103** (2021) no.4, 042223

[287] F. Ahmed, "Axially Symmetric Type N Space-Time with Causality Violating Curves and the von Zeipel Cylinder," Grav. Cosmol. **26** (2020) no.3, 265-272

[288] J. P. Luminet, "Closed Timelike Curves, Singularities and Causality: A Survey from Gödel to Chronological Protection," Universe **7** (2021) no.1, 12

[289] B. B. Hazarika, "Axially symmetric Petrov type II general space–time and closed timelike curves," Int. J. Mod. Phys. A **36** (2021) no.03, 2150017 [erratum: Int. J. Mod. Phys. A **36** (2021) no.30, 2192005]

[290] F. Ahmed, "Type III Spacetime with Closed Timelike Curves," [arXiv:2105.08523 [gr-qc]].

[291] Y. Duan, F. Liu, Y. Wang and Y. C. Ong, "On the Counter-Rotation of Closed Timelike Curves," Universe **8** (2022) no.1, 28

[292] S. Gutti, S. Kulkarni, V. Prasad and S. Suresh, "Ecosystem for Closed Timelike Curves: An Energy Conditions Perspective," [arXiv:2108.04117 [gr-qc]].

[293] C. Vairogs, V. Katariya and M. M. Wilde, "Quantum state discrimination circuits inspired by Deutschian closed timelike curves," Phys. Rev. A **105** (2022) no.5, 052434

[294] C. Barceló, J. E. Sánchez, G. García-Moreno and G. Jannes, "Chronology protection implementation in analogue gravity," Eur. Phys. J. C **82** (2022) no.4, 299

[295] S. Krasnikov, "A Causality Preserving Evolution of a Pair of Strings †," Universe **8** (2022) no.12, 640

[296] S. Gutti, S. Kulkarni and V. Prasad, "Closed timelike curves and energy conditions in regular spacetimes," Eur. Phys. J. C **82** (2022) no.12, 1136

[297] C. Baladrón and A. Khrennikov, "Simulation of Closed Timelike Curves in a Darwinian Approach to Quantum Mechanics," Universe **9** (2023) no.2, 64

[298] Z. Zhao and L. Modesto, "Quantum avoidance of Gödel's closed timelike curves," Eur. Phys. J. C **83** (2023) no.6, 517

[299] G. Sanzeni, "Non existence of closed null geodesics in Kerr spacetimes," [arXiv:2308.09631 [math.DG]].

[300] D. Astesiano, D. Bini, A. Geralico and M. L. Ruggiero, "Particle motion in a rotating dust spacetime: the Bonnor solution," [arXiv:2310.04157 [gr-qc]].

[301] H. K. Nguyen and F. S. N. Lobo, "Closed Timelike Curves Induced by a Buchdahl-inspired Vacuum Spacetime in R^2 Gravity," Universe **9** (2023), 467

[302] L. Flamm, "Beitrage zur Einsteinschen Gravitationstheorie," Phys. Z. **17** (1916), 448.

[303] A. Einstein and N. Rosen, "The Particle Problem in the General Theory of Relativity," Phys. Rev. **48** (1935), 73-77

[304] J. A. Wheeler, "Geons," Phys. Rev. **97** (1955), 511-536

[305] J. A. Wheeler, "Geometrodynamics," (Academic Press, New York, 1962).

[306] S. W. Hawking, "Wormholes in Space-Time," Phys. Rev. D **37** (1988), 904-910

[307] R. P. Geroch, "Topology in general relativity," J. Math. Phys. **8** (1967), 782-786

[308] C. W. Misner and J. A. Wheeler, "Classical physics as geometry: Gravitation, electromagnetism, unquantized charge, and mass as properties of curved empty space," Annals Phys. **2** (1957), 525-603

[309] F. J. Ernst, "Variational Calculations in Geon Theory," Phys. Rev. **105** (1957), 1662-1664

[310] F. J. Ernst, "Linear and Toroidal Geons," Phys. Rev. **105** (1957), 1665-1670

[311] D. R. Brill and J. B. Hartle, "Method of the Self-Consistent Field in General Relativity and its Application to the Gravitational Geon," Phys. Rev. **135** (1964), B271-B278

[312] A. Komar, "Bootstrap Gravitational Geons," Phys. Rev. **137** (1965), B462-B466

[313] C. H. Brans, "Singularities in bootstrap gravitational geons," Phys. Rev. **140** (1965), B1174-B1176;

[314] D. J. Kaup, "Klein-Gordon Geon," Phys. Rev. **172** (1968), 1331-1342

[315] M. Lunetta, I. Wolk and A. F. D. F. Teixeira, "Pure Massless Scalar Geon," Phys. Rev. D **21** (1980), 3281-3283

[316] P. R. Anderson and D. R. Brill, "Gravitational geons revisited," Phys. Rev. D **56** (1997), 4824-4833

[317] T. Diemer and M. J. Hadley, "Charge and the topology of space-time," Class. Quant. Grav. **16** (1999), 3567-3577

[318] C. W. Misner, "Wormhole Initial Conditions," Phys. Rev. **118** (1960), 1110-1111

[319] R. W. Fuller and J. A. Wheeler, "Causality and Multiply Connected Space-Time," Phys. Rev. **128** (1962), 919-929

[320] J. C. Graves and D. R. Brill, "Oscillatory Character of Reissner-Nordstrom Metric for an Ideal Charged Wormhole," Phys. Rev. **120** (1960), 1507-1513

[321] M. S. Morris and K. S. Thorne, "Wormholes in space-time and their use for interstellar travel: A tool for teaching general relativity," Am. J. Phys. **56** (1988), 395-412

[322] M. S. Morris, K. S. Thorne and U. Yurtsever, "Wormholes, Time Machines, and the Weak Energy Condition," Phys. Rev. Lett. **61** (1988), 1446-1449

[323] B. K. Harrison, K. S. Thorne, M. Wakano and J. A. Wheeler, "Gravitational Theory and Gravitational Collapse," (University of Chicago Press, Chicago, 1965).

[324] Y. B. Zel'dovich and I. D. Novikov, "Relativistic Astrophysics, Vol. I: Stars and Relativity," (University of Chicago Press, Chicago, 1971).

[325] G. Klinkhammer, "Averaged energy conditions for free scalar fields in flat space-times," Phys. Rev. D **43** (1991), 2542-2548

[326] F. J. Tipler, "Energy conditions and spacetime singularities," Phys. Rev. D **17** (1978), 2521-2528

[327] T. A. Roman, "Quantum Stress Energy Tensors and the Weak Energy Condition," Phys. Rev. D **33** (1986), 3526-3533

[328] L. H. Ford, "Constraints on negative energy fluxes," Phys. Rev. D **43** (1991), 3972-3978

[329] L. H. Ford, "Quantum Coherence Effects and the Second Law of Thermodynamics," Proc. Roy. Soc. Lond. A **364** (1978), 227-236

[330] L. H. Ford and T. A. Roman, "Averaged energy conditions and quantum inequalities," Phys. Rev. D **51** (1995), 4277-4286

[331] L. H. Ford and T. A. Roman, "Quantum field theory constrains traversable wormhole geometries," Phys. Rev. D **53** (1996), 5496-5507

[332] L. H. Ford and T. A. Roman, "The Quantum interest conjecture," Phys. Rev. D **60** (1999), 104018

[333] M. J. Pfenning and L. H. Ford, "Quantum inequalities on the energy density in static Robertson-Walker space-times," Phys. Rev. D **55** (1997), 4813-4821

[334] P. K. F. Kuhfittig, "Static and dynamic traversable wormhole geometries satisfying the Ford-Roman constraints," Phys. Rev. D **66** (2002), 024015

[335] F. Lobo and P. Crawford, "Constraints on wormhole geometries," The 9th Marcel Grossmann Meeting (MG9), Proceedings, Rome, Italy, 2000, edited by Vahe G. Gurzadyan, Robert Jantzen and Remo Ruffini (World Scientific, Singapore, 2002), 855-856.

[336] T. A. Roman, "Some thoughts on energy conditions and wormholes," [arXiv:gr-qc/0409090 [gr-qc]].

[337] M. Visser, "Jerk and the cosmological equation of state," Class. Quant. Grav. **21** (2004), 2603-2616

[338] C. Barcelo and M. Visser, "Twilight for the energy conditions?," Int. J. Mod. Phys. D **11** (2002), 1553-1560

[339] D. Hochberg, A. Popov and S. V. Sushkov, "Selfconsistent wormhole solutions of semiclassical gravity," Phys. Rev. Lett. **78** (1997), 2050-2053

[340] S. V. Sushkov, "A selfconsistent semiclassical solution with a throat in the theory of gravity," Phys. Lett. A **164** (1992), 33-37.

[341] C. Barcelo and M. Visser, "Traversable wormholes from massless conformally coupled scalar fields," Phys. Lett. B **466** (1999), 127-134

[342] A. A. Popov and S. V. Sushkov, "Vacuum polarization of a scalar field in wormhole space-times," Phys. Rev. D **63** (2001), 044017

[343] A. A. Popov, "Stress energy of a quantized scalar field in static wormhole space-times," Phys. Rev. D **64** (2001), 104005

[344] N. R. Khusnutdinov and S. V. Sushkov, "Ground state energy in a wormhole spacetime," Phys. Rev. D **65** (2002), 084028

[345] A. R. Khabibullin, N. R. Khusnutdinov and S. V. Sushkov, "Casimir effect in a wormhole spacetime," Class. Quant. Grav. **23** (2006), 627-634

[346] N. R. Khusnutdinov, "Semiclassical wormholes," Phys. Rev. D **67** (2003), 124020

[347] R. Garattini, "Self sustained traversable wormholes?," Class. Quant. Grav. **22** (2005), 1105-1118

[348] R. Garattini and F. S. N. Lobo, "Self sustained phantom wormholes in semi-classical gravity," Class. Quant. Grav. **24** (2007), 2401-2413

[349] H. G. Ellis, "Ether flow through a drainhole - a particle model in general relativity," J. Math. Phys. **14** (1973), 104-118

[350] H. G. Ellis, "The evolving, flowless drain hole: a nongravitating particle model in general relativity theory," Gen. Rel. Grav. **10** (1979), 105-123

[351] K. A. Bronnikov, "Scalar-tensor theory and scalar charge," Acta Phys. Polon. B **4** (1973), 251-266

[352] T. Kodama, "General Relativistic Nonlinear Field: A Kink Solution in a Generalized Geometry," Phys. Rev. D **18** (1978), 3529-3534

[353] G. Clement, "Einstein-Yang-Mills-Higgs solitons," Gen. Rel. Grav. **13** (1981), 763-770

[354] G. Clément, "The Ellis geometry," Am. J. Phys. **57** (1989), 967.

[355] E. G. Harris, "Wormhole connecting two Reissner-Nordstrom universes," Am. J. Phys. **61** (1993), 1140-1144

[356] C. Barcelo and M. Visser, "Scalar fields, energy conditions, and traversable wormholes," Class. Quant. Grav. **17** (2000), 3843-3864

[357] M. Visser, "Traversable wormholes: Some simple examples," Phys. Rev. D **39** (1989), 3182-3184

[358] M. Visser, "Traversable wormholes from surgically modified Schwarzschild space-times," Nucl. Phys. B **328** (1989), 203-212

[359] M. Visser, "Traversable wormholes: The Roman ring," Phys. Rev. D **55** (1997), 5212-5214

[360] M. Visser and D. Hochberg, "Generic wormhole throats," The Internal Structure of Black Holes and Spacetime Singularities, Institute of Physics, Bristol, edited by L.M. Burko and A. Ori, Annals Israel Phys. Soc. **13** (1997), 249

[361] N. Dadhich, S. Kar, S. Mukherji and M. Visser, "R = 0 space-times and selfdual Lorentzian wormholes," Phys. Rev. D **65** (2002), 064004

[362] V. P. Frolov and I. Novikov, "Wormhole as a device for study black hole's interior," Phys. Rev. D **48** (1993), 1607-1615

[363] D. Hochberg and T. W. Kephart, "Wormhole cosmology and the horizon problem," Phys. Rev. Lett. **70** (1993), 2665-2668

[364] G. Clement, "Flat wormholes from straight cosmic strings," J. Math. Phys. **38** (1997), 5807-5819

[365] R. O. Aros and N. Zamorano, "A Wormhole at the core of an infinite cosmic string," Phys. Rev. D **56** (1997), 6607-6614

[366] F. Schein, P. C. Aichelburg and W. Israel, "String supported wormhole space-times and causality violations," Phys. Rev. D **54** (1996), 3800-3805

[367] F. Schein and P. C. Aichelburg, "Traversable wormholes in geometries of charged shells," Phys. Rev. Lett. **77** (1996), 4130-4133

[368] E. Teo, "Rotating traversable wormholes," Phys. Rev. D **58** (1998), 024014

[369] P. K. F. Kuhfittig, "Axially symmetric rotating traversable wormholes," Phys. Rev. D **67** (2003), 064015

[370] S. A. Hayward, "Wormholes supported by pure ghost radiation," Phys. Rev. D **65** (2002), 124016

[371] S. A. Hayward and H. Koyama, "How to make a traversable wormhole from a Schwarzschild black hole," Phys. Rev. D **70** (2004), 101502

[372] H. Koyama and S. A. Hayward, "Construction and enlargement of traversable wormholes from Schwarzschild black holes," Phys. Rev. D **70** (2004), 084001

[373] P. F. Gonzalez-Diaz, "Ring holes and closed timelike curves," Phys. Rev. D **54** (1996), 6122-6131

[374] P. F. Gonzalez-Diaz, "Wormholes and ringholes in a dark - energy universe," Phys. Rev. D **68** (2003), 084016

[375] D. N. Vollick, "Maintaining a wormhole with a scalar field," Phys. Rev. D **56** (1997), 4724-4728

[376] S. W. Kim and S. P. Kim, "The Traversable wormhole with classical scalar fields," Phys. Rev. D **58** (1998), 087703

[377] S. W. Kim and H. Lee, "Exact solutions of a charged wormhole," Phys. Rev. D **63** (2001), 064014

[378] F. Parisio, "Wormholes: Controlling exotic matter with a magnetic field," Phys. Rev. D **63** (2001), 087502

[379] L. A. Gergely, "Wormholes, naked singularities and universes of ghost radiation," Phys. Rev. D **65** (2002), 127503

[380] K. A. Bronnikov and S. Grinyok, "Charged wormholes with nonminimally coupled scalar fields, existence and stability," [arXiv:gr-qc/0205131 [gr-qc]].

[381] K. A. Bronnikov, "Regular magnetic black holes and monopoles from nonlinear electrodynamics," Phys. Rev. D **63** (2001), 044005

[382] A. V. B. Arellano and F. S. N. Lobo, "Evolving wormhole geometries within nonlinear electrodynamics," Class. Quant. Grav. **23** (2006), 5811-5824

[383] A. V. B. Arellano and F. S. N. Lobo, "Non-existence of static, spherically symmetric and stationary, axisymmetric traversable wormholes coupled to nonlinear electrodynamics," Class. Quant. Grav. **23** (2006), 7229-7244

[384] C. G. Boehmer, T. Harko and F. S. N. Lobo, "Conformally symmetric traversable wormholes," Phys. Rev. D **76** (2007), 084014

[385] D. Hochberg and M. Visser, "The Null energy condition in dynamic wormholes," Phys. Rev. Lett. **81** (1998), 746-749

[386] D. Hochberg and M. Visser, "Dynamic wormholes, anti-trapped surfaces, and energy conditions," Phys. Rev. D **58** (1998), 044021

[387] S. Kar, "Evolving wormholes and the weak energy condition," Phys. Rev. D **49** (1994), 862-865

[388] S. Kar and D. Sahdev, "Evolving Lorentzian wormholes," Phys. Rev. D **53** (1996), 722-730

[389] S. W. Kim, "The Cosmological model with traversable wormhole," Phys. Rev. D **53** (1996), 6889-6892

[390] M. Visser, S. Kar and N. Dadhich, "Traversable wormholes with arbitrarily small energy condition violations," Phys. Rev. Lett. **90** (2003), 201102

[391] S. Kar, N. Dadhich and M. Visser, "Quantifying energy condition violations in traversable wormholes," Pramana **63** (2004), 859-864

[392] M. Visser, "Quantum wormholes," Phys. Rev. D **43** (1991), 402-409

[393] S. W. Kim, "Schwarzschild-de Sitter type wormhole," Phys. Lett. A **166** (1992), 13-16

[394] F. S. N. Lobo and P. Crawford, "Linearized stability analysis of thin shell wormholes with a cosmological constant," Class. Quant. Grav. **21** (2004), 391-404

[395] T. A. Roman, "Inflating Lorentzian wormholes," Phys. Rev. D **47** (1993), 1370-1379

[396] M. S. R. Delgaty and R. B. Mann, "Traversable wormholes in (2+1)-dimensions and (3+1)-dimensions with a cosmological constant," Int. J. Mod. Phys. D **4** (1995), 231-246

[397] J. P. S. Lemos, F. S. N. Lobo and S. Quinet de Oliveira, "Morris-Thorne wormholes with a cosmological constant," Phys. Rev. D **68** (2003), 064004

[398] F. S. N. Lobo, "Surface stresses on a thin shell surrounding a traversable wormhole," Class. Quant. Grav. **21** (2004), 4811-4832

[399] F. S. N. Lobo, "Energy conditions, traversable wormholes and dust shells," Gen. Rel. Grav. **37** (2005), 2023-2038

[400] J. P. S. Lemos and F. S. N. Lobo, "Plane symmetric traversable wormholes in an Anti-de Sitter background," Phys. Rev. D **69** (2004), 104007

[401] A. DeBenedictis and A. Das, "On a general class of wormhole geometries," Class. Quant. Grav. **18** (2001), 1187-1204

[402] A. DeBenedictis and A. Das, "Higher dimensional wormhole geometries with compact dimensions," Nucl. Phys. B **653** (2003), 279-304

[403] M. Visser, "Quantum Mechanical Stabilization of Minkowski Signature Wormholes," Phys. Lett. B **242** (1990), 24-28

[404] S. w. Kim, H. j. Lee, S. K. Kim and J. M. Yang, "(2+1)-dimensional Schwarzschild-de Sitter wormhole," Phys. Lett. A **183** (1993), 359-362

[405] G. P. Perry and R. B. Mann, "Traversible wormholes in (2+1)-dimensions," Gen. Rel. Grav. **24** (1992), 305-321

[406] E. Poisson and M. Visser, "Thin shell wormholes: Linearization stability," Phys. Rev. D **52** (1995), 7318-7321

[407] E. F. Eiroa and G. E. Romero, "Linearized stability of charged thin shell wormholes," Gen. Rel. Grav. **36** (2004), 651-659

[408] M. Ishak and K. Lake, "Stability of transparent spherically symmetric thin shells and wormholes," Phys. Rev. D **65** (2002), 044011

[409] C. Armendariz-Picon, "On a class of stable, traversable Lorentzian wormholes in classical general relativity," Phys. Rev. D **65** (2002), 104010

[410] H. a. Shinkai and S. A. Hayward, "Fate of the first traversible wormhole: Black hole collapse or inflationary expansion," Phys. Rev. D **66** (2002), 044005

[411] A. Chodos and S. L. Detweiler, "Spherically Symmetric Solutions in Five-dimensional General Relativity," Gen. Rel. Grav. **14** (1982), 879

[412] G. Clement, "A Class of Wormhole Solutions to Higher Dimensional General Relativity," Gen. Rel. Grav. **16** (1984), 131

[413] J. W. Moffat and T. Svoboda, "Traversible wormholes and the negative stress energy problem in the nonsymmetric gravitational theory," Phys. Rev. D **44** (1991), 429-432

[414] A. G. Agnese and M. La Camera, "Wormholes in the Brans-Dicke theory of gravitation," Phys. Rev. D **51** (1995), 2011-2013

[415] L. A. Anchordoqui, S. E. Perez Bergliaffa and D. F. Torres, "Brans-Dicke wormholes in nonvacuum space-time," Phys. Rev. D **55** (1997), 5226-5229

[416] K. K. Nandi, B. Bhattacharjee, S. M. K. Alam and J. Evans, "Brans-Dicke wormholes in the Jordan and Einstein frames," Phys. Rev. D **57** (1998), 823-828

[417] P. E. Bloomfield, "Comment on Brans-Dicke wormholes in the Jordan and Einstein frames," Phys. Rev. D **59** (1999), 088501

[418] K. K. Nandi, "Reply to Comment on 'Brans-Dicke wormholes in the Jordan and Einstein frames'," Phys. Rev. D **59** (1999), 088502

[419] K. K. Nandi, A. Islam and J. Evans, "Brans wormholes," Phys. Rev. D **55** (1997), 2497-2500

[420] F. He and S. W. Kim, "New Brans-Dicke wormholes," Phys. Rev. D **65** (2002), 084022

[421] S. You-Gen, G. Han-Ying, T. Zhen-Qiang and D. Hao-Gang, "Wormholes in the Kaluza-Klein theory," Phys. Rev. D **44** (1991), 1330-1331

[422] B. Bhawal and S. Kar, "Lorentzian wormholes in Einstein-Gauss-Bonnet theory," Phys. Rev. D **46** (1992), 2464-2468

[423] H. Koyama, S. A. Hayward and S. W. Kim, "Construction and enlargement of dilatonic wormholes by impulsive radiation," Phys. Rev. D **67** (2003), 084008

[424] L. A. Anchordoqui and S. E. Perez Bergliaffa, "Wormhole-surgery and cosmology on the brane: The World is not enough," Phys. Rev. D **62** (2000), 067502

[425] C. Barcelo and M. Visser, "Brane surgery: Energy conditions, traversable wormholes, and voids," Nucl. Phys. B **584** (2000), 415-435

[426] K. A. Bronnikov and S. W. Kim, "Possible wormholes in a brane world," Phys. Rev. D **67** (2003), 064027

[427] F. S. N. Lobo, "A General class of braneworld wormholes," Phys. Rev. D **75** (2007), 064027

[428] M. La Camera, "Wormhole solutions in the Randall-Sundrum scenario," Phys. Lett. B **573** (2003), 27-32

[429] B. Mishra, A. S. Agrawal, S. K. Tripathy and S. Ray, "Traversable wormhole models in f(R) gravity," Int. J. Mod. Phys. A **37** (2022) no.05, 2250010

[430] N. Furey and A. DeBenedictis, "Wormhole throats in R**m gravity," Class. Quant. Grav. **22** (2005), 313-322

[431] R. Dick, "On the Newtonian limit in gravity models with inverse powers of R," Gen. Rel. Grav. **36** (2004), 217-224

[432] K. Ghoroku and T. Soma, "Lorentzian wormholes in higher derivative gravity and the weak energy condition," Phys. Rev. D **46** (1992), 1507-1516

[433] V. P. Frolov and I. D. Novikov, "Physical Effects in Wormholes and Time Machine," Phys. Rev. D **42** (1990), 1057-1065

[434] J. L. Friedman and M. S. Morris, "The Cauchy problem for the scalar wave equation is well defined on a class of space-times with closed timelike curves," Phys. Rev. Lett. **66** (1991), 401-404

[435] G. Klinkhammer, "Vacuum polarization of scalar and spinor fields near closed null geodesics," Phys. Rev. D **46** (1992), 3388-3394

[436] S. W. Kim, "Particle creation for the time travel through the wormhole," Phys. Rev. D **46** (1992), 2428-2434

[437] M. Lyutikov, "Vacuum polarization at the chronology horizon of the Roman space-time," Phys. Rev. D **49** (1994), 4041-4048

[438] W. A. Hiscock and D. A. Konkowski, "Quantum vacuum energy in Taub-NUT-type cosmologies," Phys. Rev. D **26** (1982), 1225-1230

[439] L. X. Li and J. R. Gott, III, "A selfconsistent vacuum for Misner space and the chronology protection conjecture," Phys. Rev. Lett. **80** (1998), 2980

[440] W. A. Hiscock, "Quantized fields and chronology protection," [arXiv:gr-qc/0009061 [gr-qc]].

[441] M. Visser, "The Quantum physics of chronology protection," [arXiv:gr-qc/0204022 [gr-qc]].

[442] K. S. Thorne, "Closed timelike curves," Proceedings of the 13th Conference on General Relativity and Gravitation, edited by R. J. Gleiser *et al.* (Institute of Physics Publishing, Bristol, 1993), p. 295.

[443] F. S. N. Lobo, "Phantom energy traversable wormholes," Phys. Rev. D **71** (2005), 084011

[444] F. S. N. Lobo, "Stability of phantom wormholes," Phys. Rev. D **71** (2005), 124022

[445] S. V. Sushkov, "Wormholes supported by a phantom energy," Phys. Rev. D **71** (2005), 043520

[446] O. B. Zaslavskii, "Exactly solvable model of wormhole supported by phantom energy," Phys. Rev. D **72** (2005), 061303

[447] P. K. F. Kuhfittig, "Seeking exactly solvable models of traversable wormholes supported by phantom energy," Class. Quant. Grav. **23** (2006), 5853-5860

[448] F. S. N. Lobo, "Chaplygin traversable wormholes," Phys. Rev. D **73** (2006), 064028

[449] F. S. N. Lobo, "Van der Waals quintessence stars," Phys. Rev. D **75** (2007), 024023

[450] P. F. Gonzalez-Diaz, "Achronal cosmic future," Phys. Rev. Lett. **93** (2004), 071301

[451] P. F. Gonzalez-Diaz and J. A. Jimenez-Madrid, "Phantom inflation and the 'big trip'," Phys. Lett. B **596** (2004), 16-25

[452] P. F. Gonzalez-Diaz, "K-essential phantom energy: Doomsday around the corner?," Phys. Lett. B **586** (2004), 1-4

[453] P. F. Gonzalez-Diaz, "You need not be afraid of phantom energy," Phys. Rev. D **68** (2003), 021303

[454] J. G. Cramer, R. L. Forward, M. S. Morris, M. Visser, G. Benford and G. A. Landis, "Natural wormholes as gravitational lenses," Phys. Rev. D **51** (1995), 3117-3120

[455] D. F. Torres, G. E. Romero and L. A. Anchordoqui, "Wormholes, gamma-ray bursts and the amount of negative mass in the universe," Mod. Phys. Lett. A **13** (1998), 1575-1582

[456] M. Safonova, D. F. Torres and G. E. Romero, "Microlensing by natural wormholes: Theory and simulations," Phys. Rev. D **65** (2002), 023001

[457] M. Safonova, D. F. Torres and G. E. Romero, "Macrolensing signatures of large scale violations of the weak energy condition," Mod. Phys. Lett. A **16** (2001), 153-162

[458] S. A. Hayward, "Black holes and traversible wormholes: A Synthesis," 11th Workshop on General Relativity and Gravitation (JGRG11), Tokyo, Japan, 9-12 Jan 2002 [arXiv:gr-qc/0203051 [gr-qc]].

[459] G. J. Olmo, D. Rubiera-Garcia and A. Sanchez-Puente, "Geodesic completeness in a wormhole spacetime with horizons," Phys. Rev. D **92** (2015) no.4, 044047

[460] C. Chakraborty and P. Pradhan, "Behavior of a test gyroscope moving towards a rotating traversable wormhole," JCAP **03** (2017), 035

[461] A. Mishra and S. Chakraborty, "On the trajectories of null and timelike geodesics in different wormhole geometries," Eur. Phys. J. C **78** (2018) no.5, 374

[462] P. Taylor, "Propagation of Test Particles and Scalar Fields on a Class of Wormhole Space-Times," Phys. Rev. D **90** (2014) no.2, 024057 [erratum: Phys. Rev. D **95** (2017) no.10, 109904]

[463] M. Cataldo, L. Liempi and P. Rodríguez, "Traversable Schwarzschild-like wormholes," Eur. Phys. J. C **77** (2017) no.11, 748

[464] F. Willenborg, S. Grunau, B. Kleihaus and J. Kunz, "Geodesic motion around traversable wormholes supported by a massless conformally-coupled scalar field," Phys. Rev. D **97** (2018) no.12, 124002

[465] M. Amir, K. Jusufi, A. Banerjee and S. Hansraj, "Shadow images of Kerr-like wormholes," Class. Quant. Grav. **36** (2019) no.21, 215007

[466] M. Amir, A. Banerjee and S. D. Maharaj, "Shadow of charged wormholes in Einstein–Maxwell–dilaton theory," Annals Phys. **400** (2019), 198-207

[467] M. Wielgus, J. Horak, F. Vincent and M. Abramowicz, "Reflection-asymmetric wormholes and their double shadows," Phys. Rev. D **102** (2020) no.8, 084044

[468] R. Shaikh, P. Banerjee, S. Paul and T. Sarkar, "A novel gravitational lensing feature by wormholes," Phys. Lett. B **789** (2019), 270-275 [erratum: Phys. Lett. B **791** (2019), 422-423]

[469] R. Shaikh, P. Banerjee, S. Paul and T. Sarkar, "Strong gravitational lensing by wormholes," JCAP **07** (2019), 028 [erratum: JCAP **12** (2023), E01]

[470] N. Tsukamoto, "Gravitational lensing by two photon spheres in a black-bounce spacetime in strong deflection limits," Phys. Rev. D **104** (2021) no.6, 064022

[471] G. Gyulchev, P. Nedkova, V. Tinchev and S. Yazadjiev, "On the shadow of rotating traversable wormholes," Eur. Phys. J. C **78** (2018) no.7, 544

[472] R. Shaikh, "Shadows of rotating wormholes," Phys. Rev. D **98** (2018) no.2, 024044

[473] A. Abdujabbarov, B. Juraev, B. Ahmedov and Z. Stuchlík, "Shadow of rotating wormhole in plasma environment," Astrophys. Space Sci. **361** (2016) no.7, 226

[474] O. Sarbach and T. Zannias, "The propagation of particles and fields in wormhole geometries," AIP Conf. Proc. **1473** (2012) no.1, 223-232

[475] P. G. Nedkova, V. K. Tinchev and S. S. Yazadjiev, "Shadow of a rotating traversable wormhole," Phys. Rev. D **88** (2013) no.12, 124019

[476] M. Azreg-Aïnou, "Confined-exotic-matter wormholes with no gluing effects—Imaging supermassive wormholes and black holes," JCAP **07** (2015), 037

[477] T. Ohgami and N. Sakai, "Wormhole shadows," Phys. Rev. D **91** (2015) no.12, 124020

[478] T. Ohgami and N. Sakai, "Wormhole shadows in rotating dust," Phys. Rev. D **94** (2016) no.6, 064071

[479] F. H. Vincent, M. Wielgus, M. A. Abramowicz, E. Gourgoulhon, J. P. Lasota, T. Paumard and G. Perrin, "Geometric modeling of M87* as a Kerr black hole or a non-Kerr compact object," Astron. Astrophys. **646** (2021), A37

[480] F. Rahaman, K. N. Singh, R. Shaikh, T. Manna and S. Aktar, "Shadows of Lorentzian traversable wormholes," Class. Quant. Grav. **38** (2021) no.21, 215007

[481] E. Berti, E. Barausse, V. Cardoso, L. Gualtieri, P. Pani, U. Sperhake, L. C. Stein, N. Wex, K. Yagi and T. Baker, *et al.* "Testing General Relativity with Present and Future Astrophysical Observations," Class. Quant. Grav. **32** (2015), 243001

[482] Y. Gong, S. Hou, D. Liang and E. Papantonopoulos, "Gravitational waves in Einstein-æther and generalized TeVeS theory after GW170817," Phys. Rev. D **97** (2018) no.8, 084040

[483] S. Hou and Z. H. Zhu, "Gravitational memory effects and Bondi-Metzner-Sachs symmetries in scalar-tensor theories," JHEP **01** (2021), 083

[484] Z. Mark, A. Zimmerman, S. M. Du and Y. Chen, "A recipe for echoes from exotic compact objects," Phys. Rev. D **96** (2017) no.8, 084002

[485] V. Cardoso, E. Franzin and P. Pani, "Is the gravitational-wave ringdown a probe of the event horizon?," Phys. Rev. Lett. **116** (2016) no.17, 171101 [erratum: Phys. Rev. Lett. **117** (2016) no.8, 089902]

[486] V. Cardoso, S. Hopper, C. F. B. Macedo, C. Palenzuela and P. Pani, "Gravitational-wave signatures of exotic compact objects and of quantum corrections at the horizon scale," Phys. Rev. D **94** (2016) no.8, 084031

[487] P. Bueno, P. A. Cano, F. Goelen, T. Hertog and B. Vercnocke, "Echoes of Kerr-like wormholes," Phys. Rev. D **97** (2018) no.2, 024040

[488] J. T. Gálvez Ghersi, A. V. Frolov and D. A. Dobre, "Echoes from the scattering of wavepackets on wormholes," Class. Quant. Grav. **36** (2019) no.13, 135006

[489] J. B. Dent, W. E. Gabella, K. Holley-Bockelmann and T. W. Kephart, "Gravitational waves from a black hole orbiting in a wormhole geometry," Phys. Rev. D **104** (2021) no.4, 044030

[490] H. Liu, P. Liu, Y. Liu, B. Wang and J. P. Wu, "Echoes from phantom wormholes," Phys. Rev. D **103** (2021) no.2, 024006

[491] S. s. Bao, S. Hou and H. Zhang, "Searching for wormholes with gravitational wave scattering," Eur. Phys. J. C **83** (2023) no.2, 127

[492] D. C. Dai and D. Stojkovic, "Observing a Wormhole," Phys. Rev. D **100** (2019) no.8, 083513

[493] J. H. Simonetti, M. J. Kavic, D. Minic, D. Stojkovic and D. C. Dai, "Sensitive searches for wormholes," Phys. Rev. D **104** (2021) no.8, L081502

[494] A. Almheiri, D. Marolf, J. Polchinski and J. Sully, "Black Holes: Complementarity or Firewalls?," JHEP **02** (2013), 062

[495] A. Almheiri, D. Marolf, J. Polchinski, D. Stanford and J. Sully, "An Apologia for Firewalls," JHEP **09** (2013), 018

[496] A. Einstein, B. Podolsky and N. Rosen, "Can quantum mechanical description of physical reality be considered complete?," Phys. Rev. **47** (1935), 777-780

[497] J. Maldacena and L. Susskind, "Cool horizons for entangled black holes," Fortsch. Phys. **61** (2013), 781-811

[498] P. Gao, D. L. Jafferis and A. C. Wall, "Traversable Wormholes via a Double Trace Deformation," JHEP **12** (2017), 151

[499] J. Maldacena, A. Milekhin and F. Popov, "Traversable wormholes in four dimensions," Class. Quant. Grav. **40** (2023) no.15, 155016

[500] Z. Fu, B. Grado-White and D. Marolf, "Traversable Asymptotically Flat Wormholes with Short Transit Times," Class. Quant. Grav. **36** (2019) no.24, 245018

[501] Z. Fu, B. Grado-White and D. Marolf, "A perturbative perspective on self-supporting wormholes," Class. Quant. Grav. **36** (2019) no.4, 045006 [erratum: Class. Quant. Grav. **36** (2019) no.24, 249501]

[502] J. Maldacena, D. Stanford and Z. Yang, "Diving into traversable wormholes," Fortsch. Phys. **65** (2017) no.5, 1700034

[503] J. Maldacena and A. Milekhin, "Humanly traversable wormholes," Phys. Rev. D **103** (2021) no.6, 066007

[504] D. Jafferis, A. Zlokapa, J. D. Lykken, D. K. Kolchmeyer, S. I. Davis, N. Lauk, H. Neven and M. Spiropulu, "Traversable wormhole dynamics on a quantum processor," Nature **612** (2022) no.7938, 51-55

[505] S. Sachdev and J. Ye, "Gapless spin fluid ground state in a random, quantum Heisenberg magnet," Phys. Rev. Lett. **70** (1993), 3339

[506] A. Kitaev, "A simple model of quantum holography," KITP strings seminar and Entanglement 2015 program (2015). http://online.kitp.ucsb.edu/online/entangled15/

[507] Ä. Baumeler, F. Costa, T. C. Ralph, S. Wolf and M. Zych, "Reversible time travel with freedom of choice," Class. Quant. Grav. **36** (2019) no.22, 224002

[508] G. Tobar and F. Costa, "Reversible dynamics with closed time-like curves and freedom of choice," Class. Quant. Grav. **37** (2020) no.20, 205011

[509] P. Collas and D. Klein, "Frame dragging anomalies for rotating bodies," Gen. Rel. Grav. **36** (2004), 1197

[510] H. Andreka, I. Nemeti and C. Wuthrich, "A Twist in the geometry of rotating black holes: Seeking the cause of acausality," Gen. Rel. Grav. **40** (2008), 1809-1823

[511] The Laser Interferometer Gravitational-Wave Observatory (LIGO), http://www.ligo.org

[512] The Event Horizon Telescope (EHT), http://www.eventhorizontelescope.org

[513] The Advanced Telescope for High ENergy Astrophysics (ATHENA), http://www.the-athena-x-rayobservatory.eu

[514] The Square Kilometre Array (SKA), http://www.skatelescope.org

[515] The Evolved Laser Interferometer Space Antenna (eLISA), http://www.elisascience.org

[516] H. Reissner, "Über die Eigengravitation des elektrischen Feldes nach der Einsteinschen Theorie," Annalen Phys. **355** (1916) no.9, 106-120

[517] G. Nordström, "On the Energy of the Gravitation field in Einstein's Theory," Proc. K. Ned. Akad. Wet. **20** (1918) no.2, 1238-1245.

[518] J. R. Wilson, Ann. N.Y. Acad. Sci. **262**, 123 (1975).

[519] T. Damour, R. Hanni, R. Ruffini, and J. Wilson, Phys. Rev. D **17**, 1518 (1978).

[520] R. Ruffini, G. Vereshchagin and S. S. Xue, "Electron-positron pairs in physics and astrophysics: from heavy nuclei to black holes," Phys. Rept. **487** (2010), 1-140

[521] T. Adamo and E. T. Newman, "The Kerr-Newman metric: A Review," Scholarpedia **9** (2014), 31791

[522] M. Johnston and R. Ruffini, "Generalized Wilkins effect and selected orbits in a Kerr-Newman geometry," Phys. Rev. D **10** (1974), 2324-2329

[523] M. Calvani and R. Turolla, "Complete Description of Photon Trajectories in the Kerr-Newman Space-time," J. Phys. A **14** (1981), 1931-1942

[524] E. Hackmann and H. Xu, "Charged particle motion in Kerr-Newmann space-times," Phys. Rev. D **87** (2013) no.12, 124030

[525] S. Soroushfar, R. Saffari, S. Kazempour, S. Grunau and J. Kunz, "Detailed study of geodesics in the Kerr-Newman-(A)dS spacetime and the rotating charged black hole spacetime in $f(R)$ gravity," Phys. Rev. D **94** (2016) no.2, 024052

[526] Z. Stuchlik and S. Hledik, "Equatorial photon motion in the Kerr-Newman spacetimes with a non-zero cosmological constant," Class. Quant. Grav. **17** (2000), 4541-4576

[527] C. Y. Liu, D. S. Lee and C. Y. Lin, "Geodesic motion of neutral particles around a Kerr–Newman black hole," Class. Quant. Grav. **34** (2017) no.23, 235008

[528] C. Y. Wang, D. S. Lee and C. Y. Lin, "Null and timelike geodesics in the Kerr-Newman black hole exterior," Phys. Rev. D **106** (2022) no.8, 084048

[529] Y. W. Hsiao, D. S. Lee and C. Y. Lin, "Equatorial light bending around Kerr-Newman black holes," Phys. Rev. D **101** (2020) no.6, 064070

[530] P. Slaný and Z. Stuchlík, "Equatorial circular orbits in Kerr–Newman–de Sitter space-times," Eur. Phys. J. C **80** (2020) no.6, 587

[531] G. V. Kraniotis, "Gravitational redshift/blueshift of light emitted by geodesic test particles, frame-dragging and pericentre-shift effects, in the Kerr–Newman–de Sitter and Kerr–Newman black hole geometries," Eur. Phys. J. C **81** (2021) no.2, 147

[532] D. V. Gal'tsov and K. V. Kobialko, "Completing characterization of photon orbits in Kerr and Kerr-Newman metrics," Phys. Rev. D **99** (2019) no.8, 084043

[533] A. Garnier, "Motion equations in a Kerr–Newman–de Sitter spacetime: some methods of integration and application to black holes shadowing in Scilab," Class. Quant. Grav. **40** (2023) no.13, 135011

[534] D. Kapec and A. Lupsasca, "Particle motion near high-spin black holes," Class. Quant. Grav. **37** (2020) no.1, 015006

[535] S. W. Wei, B. M. Gu, Y. Q. Wang and Y. X. Liu, "Photon emission of extremal Kerr–Newman black holes," Eur. Phys. J. C **77** (2017) no.2, 128

[536] C. M. Chen, S. P. Kim, J. R. Sun and F. Y. Tang, "Pair Production in Near Extremal Kerr-Newman Black Holes," Phys. Rev. D **95** (2017) no.4, 044043

[537] X. B. Xu, N. Bai and Y. H. Gao, "On neutral scalar radiation by a massive orbiting star in extremal Kerr-Newman black hole," Fortsch. Phys. **63** (2015), 323-330

[538] P. T. Chruściel, M. Maliborski and N. Yunes, "Structure of the singular ring in Kerr-like metrics," Phys. Rev. D **101** (2020) no.10, 104048

[539] P. T. Chrusciel, C. R. Olz and S. J. Szybka, "Space-time diagrammatics," Phys. Rev. D **86** (2012), 124041

[540] D. Pugliese, H. Quevedo and R. Ruffini, "Equatorial circular orbits of neutral test particles in the Kerr-Newman spacetime," Phys. Rev. D **88** (2013) no.2, 024042

[541] G. Clément, D. Gal'tsov and M. Guenouche, "Rehabilitating space-times with NUTs," Phys. Lett. B **750** (2015), 591-594

[542] G. Clément, D. Gal'tsov and M. Guenouche, "NUT wormholes," Phys. Rev. D **93** (2016) no.2, 024048

[543] G. Clément and D. Gal'tsov, "Rotating traversable wormholes in Einstein-Maxwell theory," Phys. Lett. B **838** (2023), 137677

[544] F. de Felice, "Repulsive Phenomena and Energy Emission in the Field of a Naked Singularity," Astron. Astrophys. **34** (1974), 15

[545] D. Pugliese, H. Quevedo and R. Ruffini, "Circular motion of neutral test particles in Reissner-Nordström spacetime," Phys. Rev. D **83** (2011), 024021

[546] G. C. Samanta, N. Godani and K. Bamba, "Traversable wormholes with exponential shape function in modified gravity and general relativity: A comparative study," Int. J. Mod. Phys. D **29** (2020) no.09, 2050068

[547] A. Bhattacharya and A. A. Potapov, "Bending of light in Ellis wormhole geometry," Mod. Phys. Lett. A **25** (2010), 2399-2409

[548] T. Kitamura, K. Nakajima and H. Asada, "Demagnifying gravitational lenses toward hunting a clue of exotic matter and energy," Phys. Rev. D **87** (2013) no.2, 027501

[549] K. Izumi, C. Hagiwara, K. Nakajima, T. Kitamura and H. Asada, "Gravitational lensing shear by an exotic lens object with negative convergence or negative mass," Phys. Rev. D **88** (2013), 024049

[550] T. Kitamura, K. Izumi, K. Nakajima, C. Hagiwara and H. Asada, "Microlensed image centroid motions by an exotic lens object with negative convergence or negative mass," Phys. Rev. D **89** (2014) no.8, 084020

[551] K. Nakajima, K. Izumi and H. Asada, "Negative time delay of light by a gravitational concave lens," Phys. Rev. D **90** (2014) no.8, 084026

[552] R. Shaikh and S. Kar, "Gravitational lensing by scalar-tensor wormholes and the energy conditions," Phys. Rev. D **96** (2017) no.4, 044037

[553] K. Nakashi, S. Kobayashi, S. Ueda and H. Saida, "Null Geodesics and Repulsive Behavior of Gravity in (2+1)-dimensional Massive Gravity," PTEP **2019** no.7, 073E02

[554] S. Panpanich, S. Ponglertsakul and L. Tannukij, "Particle motions and Gravitational Lensing in de Rham-Gabadadze-Tolley Massive Gravity Theory," Phys. Rev. D **100** (2019) no.4, 044031

[555] T. Muller, "Exact geometric optics in a Morris-Thorne wormhole spacetime," Phys. Rev. D **77** (2008), 044043

[556] K. A. Bronnikov and J. P. S. Lemos, "Cylindrical wormholes," Phys. Rev. D **79** (2009), 104019

[557] K. A. Bronnikov and V. G. Krechet, "Rotating cylindrical wormholes and energy conditions," Int. J. Mod. Phys. A **31** (2016) no.02n03, 1641022

[558] K. A. Bronnikov and V. G. Krechet, "Potentially observable cylindrical wormholes without exotic matter in general relativity," Phys. Rev. D **99** (2019) no.8, 084051

[559] D. Roy, A. Dutta and S. Chakraborty, "Does violation of cosmic no-hair conjecture guarantee the existence of wormhole?," EPL **140** (2022) no.1, 19002

[560] H. Fukutaka, K. Tanaka and K. Ghoroku, "Wormhole Solutions in Higher Derivative Gravity," Phys. Lett. B **222** (1989), 191-194

[561] D. Hochberg, "Lorentzian wormholes in higher order gravity theories," Phys. Lett. B **251** (1990), 349-354

[562] K. A. Bronnikov and E. Elizalde, "Spherical systems in models of nonlocally corrected gravity," Phys. Rev. D **81** (2010), 044032

[563] P. Kanti, B. Kleihaus and J. Kunz, "Wormholes in Dilatonic Einstein-Gauss-Bonnet Theory," Phys. Rev. Lett. **107** (2011), 271101

[564] P. Kanti, B. Kleihaus and J. Kunz, "Stable Lorentzian Wormholes in Dilatonic Einstein-Gauss-Bonnet Theory," Phys. Rev. D **85** (2012), 044007

[565] T. Harko, F. S. N. Lobo, M. K. Mak and S. V. Sushkov, "Modified-gravity wormholes without exotic matter," Phys. Rev. D **87** (2013) no.6, 067504

[566] P. H. R. S. Moraes and P. K. Sahoo, "Nonexotic matter wormholes in a trace of the energy-momentum tensor squared gravity," Phys. Rev. D **97** (2018) no.2, 024007

[567] N. Godani and G. C. Samanta, "Traversable wormholes supported by non-exotic matter in general relativity," New Astron. **84** (2021), 101534

[568] R. Sengupta, S. Ghosh, M. Kalam and S. Ray, "Traversable wormhole on the brane with non-exotic matter: a broader view," Class. Quant. Grav. **39** (2022) no.10, 105004

[569] S. Chakraborty, "An alternative $f(R,T)$ gravity theory and the dark energy problem," Gen. Rel. Grav. **45** (2013), 2039-2052

[570] A. Banerjee, M. K. Jasim and S. G. Ghosh, "Wormholes in f(R,T) gravity satisfying the null energy condition with isotropic pressure," Annals Phys. **433** (2021), 168575

[571] M. Ilyas and A. R. Athar, "Some specific wormhole solutions in f(R, T) gravity," Phys. Scripta **97** (2022) no.4, 045003

[572] B. F. Schutz, "A First Course in General Relativity," Cambridge University Press, 1985, ISBN 978-0-511-98418-1

[573] S. V. Sushkov and M. S. Volkov, "Giant wormholes in ghost-free bigravity theory," JCAP **06** (2015), 017

[574] R. C. Tolman, "Static solutions of Einstein's field equations for spheres of fluid," Phys. Rev. **55** (1939), 364-373

[575] J. R. Oppenheimer and G. M. Volkoff, "On massive neutron cores," Phys. Rev. **55** (1939), 374-381

[576] A. Jawad and S. Rani, "Lorentz Distributed Noncommutative Wormhole Solutions in Extended Teleparallel Gravity," Eur. Phys. J. C **75** (2015) no.4, 173

[577] O. Sokoliuk and A. Baransky, "On the existence and stability of traversable wormhole solutions in modified theories of gravity," Eur. Phys. J. C **81** (2021) no.8, 781

[578] H. B. G. Casimir, "On the attraction between two perfectly conducting plates," Indag. Math. **10** (1948) no.4, 261-263

[579] A. Hebecker, T. Mikhail and P. Soler, "Euclidean wormholes, baby universes, and their impact on particle physics and cosmology," Front. Astron. Space Sci. **5** (2018), 35

[580] T. G. Mertens and G. J. Turiaci, "Solvable models of quantum black holes: a review on Jackiw–Teitelboim gravity," Living Rev. Rel. **26** (2023) no.1, 4

[581] D. Hochberg and T. W. Kephart, "Lorentzian wormholes from the gravitationally squeezed vacuum," Phys. Lett. B **268** (1991), 377-383

[582] S. Avino, E. Calloni, S. Caprara, M. De Laurentis, R. De Rosa, T. Di Girolamo, L. Errico, G. Gagliardi, M. Grilli and V. Mangano, *et al.* "Progress in a Vacuum Weight Search Experiment," MDPI Physics **2** (2020) no.1, 1-13

[583] K. Sato, M. Sasaki, H. Kodama and K. i. Maeda, "Creation of Wormholes by First Order Phase Transition of a Vacuum in the Early Universe," Prog. Theor. Phys. **65** (1981), 1443

[584] M. R. Bordbar and N. Riazi, "Time-dependent wormhole in an inhomogeneous spherically symmetric space time with a cosmological constant," Astrophys. Space Sci. **331** (2011), 315-320

[585] M. Heydari-Fard and M. Heydari-Fard, "Inhomogeneous exact solution in brane gravity and its applications," Gen. Rel. Grav. **49** (2017) no.2, 21

[586] M. Cataldo, P. Labrana, S. del Campo, J. Crisostomo and P. Salgado, "Evolving Lorentzian wormholes supported by phantom matter with constant state parameters," Phys. Rev. D **78** (2008), 104006

[587] M. Cataldo, S. del Campo, P. Minning and P. Salgado, "Evolving Lorentzian wormholes supported by phantom matter and cosmological constant," Phys. Rev. D **79** (2009), 024005

[588] M. Cataldo, P. Meza and P. Minning, "N-dimensional static and evolving Lorentzian wormholes with cosmological constant," Phys. Rev. D **83** (2011), 044050

[589] M. Cataldo and S. del Campo, "Two-fluid evolving Lorentzian wormholes," Phys. Rev. D **85** (2012), 104010

[590] M. Cataldo, F. Aróstica and S. Bahamonde, "(N+1)-dimensional Lorentzian evolving wormholes supported by polytropic matter," Eur. Phys. J. C **73** (2013) no.8, 2517

[591] M. Kord Zangeneh, F. S. N. Lobo and H. Moradpour, "Evolving traversable wormholes satisfying the energy conditions in the presence of pole dark energy," Phys. Dark Univ. **31** (2021), 100779

[592] S. Pan and S. Chakraborty, "Dynamic wormholes with particle creation mechanism," Eur. Phys. J. C **75** (2015) no.1, 21

[593] A. H. Guth, "The Inflationary Universe: A Possible Solution to the Horizon and Flatness Problems," Phys. Rev. D **23** (1981), 347-356

[594] A. D. Linde, "A New Inflationary Universe Scenario: A Possible Solution of the Horizon, Flatness, Homogeneity, Isotropy and Primordial Monopole Problems," Phys. Lett. B **108** (1982), 389-393

[595] A. Albrecht and P. J. Steinhardt, "Cosmology for Grand Unified Theories with Radiatively Induced Symmetry Breaking," Phys. Rev. Lett. **48** (1982), 1220-1223

[596] L. Z. Fang, "Entropy Generation in the Early Universe by Dissipative Processes Near the Higgs' Phase Transitions," Phys. Lett. B **95** (1980), 154-156

[597] K. Sato, "First-order phase transition of a vacuum and the expansion of the Universe," Mon. Not. Roy. Astron. Soc. **195** (1981) no.3, 467-479

[598] E. Komatsu *et al.* [WMAP], "Seven-Year Wilkinson Microwave Anisotropy Probe (WMAP) Observations: Cosmological Interpretation," Astrophys. J. Suppl. **192** (2011), 18

[599] A. Borde and A. Vilenkin, "Eternal inflation and the initial singularity," Phys. Rev. Lett. **72** (1994), 3305-3309

[600] R. H. Brandenberger and C. Vafa, "Superstrings in the Early Universe," Nucl. Phys. B **316** (1989), 391-410

[601] G. F. R. Ellis and R. Maartens, "The emergent universe: Inflationary cosmology with no singularity," Class. Quant. Grav. **21** (2004), 223-232

[602] G. F. R. Ellis, J. Murugan and C. G. Tsagas, "The Emergent universe: An Explicit construction," Class. Quant. Grav. **21** (2004) no.1, 233-250

[603] S. Mukherjee, B. C. Paul, S. D. Maharaj and A. Beesham, "Emergent universe in Starobinsky model," [arXiv:gr-qc/0505103 [gr-qc]].

[604] S. Mukherjee, B. C. Paul, N. K. Dadhich, S. D. Maharaj and A. Beesham, "Emergent Universe with Exotic Matter," Class. Quant. Grav. **23** (2006), 6927-6934

[605] D. J. Mulryne, R. Tavakol, J. E. Lidsey and G. F. R. Ellis, "An Emergent Universe from a loop," Phys. Rev. D **71** (2005), 123512

[606] G. W. Gibbons, "The Entropy and Stability of the Universe," Nucl. Phys. B **292** (1987), 784-792

[607] J. D. Barrow, G. F. R. Ellis, R. Maartens and C. G. Tsagas, "On the stability of the Einstein static universe," Class. Quant. Grav. **20** (2003), L155-L164

[608] A. Banerjee, T. Bandyopadhyay and S. Chakraborty, "Emergent Universe in Brane World Scenario," Grav. Cosmol. **13** (2007), 290-292

[609] C. G. Boehmer, L. Hollenstein and F. S. N. Lobo, "Stability of the Einstein static universe in f(R) gravity," Phys. Rev. D **76** (2007), 084005

[610] L. Parisi, M. Bruni, R. Maartens and K. Vandersloot, "The Einstein static universe in Loop Quantum Cosmology," Class. Quant. Grav. **24** (2007), 6243-6254

[611] S. del Campo, R. Herrera and P. Labrana, "Emergent universe in a Jordan-Brans-Dicke theory," JCAP **11** (2007), 030

[612] U. Debnath, "Emergent Universe and Phantom Tachyon Model," Class. Quant. Grav. **25** (2008), 205019

[613] A. Banerjee, T. Bandyopadhyay and S. Chakraborty, "Emergent Universe in Brane World Scenario with Schwarzschild-de Sitter Bulk," Gen. Rel. Grav. **40** (2008), 1603-1607

[614] A. Beesham, S. V. Chervon and S. D. Maharaj, "An Emergent universe supported by a nonlinear sigma model," Class. Quant. Grav. **26** (2009), 075017

[615] S. del Campo, R. Herrera and P. Labrana, "On the Stability of Jordan-Brans-Dicke Static Universe," JCAP **07** (2009), 006

[616] B. C. Paul and S. Ghose, "Emergent Universe Scenario in the Einstein-Gauss-Bonnet Gravity with Dilaton," Gen. Rel. Grav. **42** (2010), 795-812

[617] B. C. Paul, P. Thakur and S. Ghose, "Constraints on Exotic Matter for An Emergent Universe," Mon. Not. Roy. Astron. Soc. **407** (2010), 415

[618] K. Zhang, P. Wu and H. W. Yu, "The Stability of Einstein static universe in the DGP braneworld," Phys. Lett. B **690** (2010), 229-232

[619] B. C. Paul, S. Ghose and P. Thakur, "Emergent Universe from A Composition of Matter, Exotic Matter and Dark Energy," Mon. Not. Roy. Astron. Soc. **413** (2011), 686

[620] S. Chattopadhyay and U. Debnath, "Emergent universe in chameleon, f(R) and f(T) gravity theories," Int. J. Mod. Phys. D **20** (2011), 1135-1152

[621] S. del Campo, E. I. Guendelman, A. B. Kaganovich, R. Herrera and P. Labrana, "Emergent Universe from Scale Invariant Two Measures Theory," Phys. Lett. B **699** (2011), 211-216

[622] S. del Campo, E. I. Guendelman, R. Herrera and P. Labrana, "Emerging Universe from Scale Invariance," JCAP **06** (2010), 026

[623] P. Labrana, "Emergent Universe by Tunneling," Phys. Rev. D **86** (2012), 083524

[624] Y. F. Cai, M. Li and X. Zhang, "Emergent Universe Scenario via Quintom Matter," Phys. Lett. B **718** (2012), 248-254

[625] P. Rudra, "Emergent Universe With Exotic Matter In Loop Quantum Cosmology, DGP Brane World and Kaluza-Klein Cosmology," Mod. Phys. Lett. A **27** (2012), 1250189

[626] Z. G. Liu and Y. S. Piao, "A Galileon Design of Slow Expansion: Emergent universe," Phys. Lett. B **718** (2013), 734-739

[627] A. Aguirre and J. Kehayias, "Quantum Instability of the Emergent Universe," Phys. Rev. D **88** (2013), 103504

[628] Y. F. Cai, Y. Wan and X. Zhang, "Cosmology of the Spinor Emergent Universe and Scale-invariant Perturbations," Phys. Lett. B **731** (2014), 217-226

[629] K. Atazadeh, Y. Heydarzade and F. Darabi, "Einstein Static Universe in Braneworld Scenario," Phys. Lett. B **732** (2014), 223-227

[630] K. Zhang, P. Wu and H. Yu, "Emergent universe in spatially flat cosmological model," JCAP **01** (2014), 048

[631] S. Bag, V. Sahni, Y. Shtanov and S. Unnikrishnan, "Emergent Cosmology Revisited," JCAP **07** (2014), 034

[632] Q. Huang, P. Wu and H. Yu, "Emergent scenario in the Einstein-Cartan theory," Phys. Rev. D **91** (2015) no.10, 103502

[633] C. G. Böhmer, N. Tamanini and M. Wright, "Einstein static universe in scalar-fluid theories," Phys. Rev. D **92** (2015) no.12, 124067

[634] P. Labraña, "Emergent universe scenario and the low CMB multipoles," Phys. Rev. D **91** (2015) no.8, 083534

[635] M. Khodadi, Y. Heydarzade, F. Darabi and E. N. Saridakis, "Emergent universe in Hořava-Lifshitz-like F(R) gravity," Phys. Rev. D **93** (2016) no.12, 124019

[636] K. Zhang, P. Wu, H. Yu and L. W. Luo, "Stability of Einstein static state universe in the spatially flat branemodels," Phys. Lett. B **758** (2016), 37-41

[637] C. Ríos, P. Labraña and A. Cid, "The Emergent Universe and the Anomalies in the Cosmic Microwave Background," J. Phys. Conf. Ser. **720** (2016), 012008

[638] K. Martineau and A. Barrau, "Primordial power spectra from an emergent universe: basic results and clarifications," Universe **4** (2018) no.12, 149

[639] P. Labrana and H. Cossio, "Emergent Universe by Tunneling in a Jordan-Brans-Dicke Theory," Eur. Phys. J. C **79** (2019) no.4, 303

[640] S. Chakraborty, "Is Emergent Universe a Consequence of Particle Creation Process?," Phys. Lett. B **732** (2014), 81-84

[641] S. Bhattacharya and S. Chakraborty, "A model of the emergent Universe in inhomogeneous spacetime," Class. Quant. Grav. **33** (2016) no.3, 035013

[642] R. H. Brandenberger, "Introduction to Early Universe Cosmology," PoS **ICFI2010** (2010), 001

[643] T. Battefeld and S. Watson, "String gas cosmology," Rev. Mod. Phys. **78** (2006), 435-454

[644] A. Nayeri, R. H. Brandenberger and C. Vafa, "Producing a scale-invariant spectrum of perturbations in a Hagedorn phase of string cosmology," Phys. Rev. Lett. **97** (2006), 021302

[645] R. H. Brandenberger, "String Gas Cosmology," [arXiv:0808.0746 [hep-th]].

[646] R. H. Brandenberger, "String Gas Cosmology: Progress and Problems," Class. Quant. Grav. **28** (2011), 204005

[647] P. Creminelli, A. Nicolis and E. Trincherini, "Galilean Genesis: An Alternative to inflation," JCAP **11** (2010), 021

[648] V. A. Rubakov, "Harrison-Zeldovich spectrum from conformal invariance," JCAP **09** (2009), 030

[649] M. Osipov and V. Rubakov, "Scalar tilt from broken conformal invariance," JETP Lett. **93** (2011), 52-55

[650] M. Libanov and V. Rubakov, "Cosmological density perturbations from conformal scalar field: infrared properties and statistical anisotropy," JCAP **11** (2010), 045

[651] M. Libanov, S. Mironov and V. Rubakov, "Properties of scalar perturbations generated by conformal scalar field," Prog. Theor. Phys. Suppl. **190** (2011), 120-134

[652] M. Libanov, S. Mironov and V. Rubakov, "Non-Gaussianity of scalar perturbations generated by conformal mechanisms," Phys. Rev. D **84** (2011), 083502

[653] M. V. Libanov and V. A. Rubakov, "Comparison of dynamical and spectator models of a (pseudo)conformal universe," Theor. Math. Phys. **173** (2012), 1457-1465

[654] K. Hinterbichler and J. Khoury, "The Pseudo-Conformal Universe: Scale Invariance from Spontaneous Breaking of Conformal Symmetry," JCAP **04** (2012), 023

[655] K. Hinterbichler, A. Joyce and J. Khoury, "Non-linear Realizations of Conformal Symmetry and Effective Field Theory for the Pseudo-Conformal Universe," JCAP **06** (2012), 043

[656] L. Perreault Levasseur, R. Brandenberger and A. C. Davis, "Defrosting in an Emergent Galileon Cosmology," Phys. Rev. D **84** (2011), 103512

[657] Y. Wang and R. Brandenberger, "Scale-Invariant Fluctuations from Galilean Genesis," JCAP **10** (2012), 021

[658] G. Obied, H. Ooguri, L. Spodyneiko and C. Vafa, "De Sitter Space and the Swampland," [arXiv:1806.08362 [hep-th]].

[659] A. Bedroya and C. Vafa, "Trans-Planckian Censorship and the Swampland," JHEP **09** (2020), 123

[660] S. K. Garg and C. Krishnan, "Bounds on Slow Roll and the de Sitter Swampland," JHEP **11** (2019), 075

[661] P. Agrawal, G. Obied, P. J. Steinhardt and C. Vafa, "On the Cosmological Implications of the String Swampland," Phys. Lett. B **784** (2018), 271-276

[662] R. H. Brandenberger and J. Martin, "Trans-Planckian Issues for Inflationary Cosmology," Class. Quant. Grav. **30** (2013), 113001

[663] A. Bedroya, R. Brandenberger, M. Loverde and C. Vafa, "Trans-Planckian Censorship and Inflationary Cosmology," Phys. Rev. D **101** (2020) no.10, 103502

[664] R. Brandenberger, "Trans-Planckian Censorship Conjecture and Early Universe Cosmology," LHEP **2021** (2021), 198

[665] J. Khoury, B. A. Ovrut, P. J. Steinhardt and N. Turok, "The Ekpyrotic universe: Colliding branes and the origin of the hot big bang," Phys. Rev. D **64** (2001), 123522

[666] J. Khoury and P. J. Steinhardt, "Adiabatic Ekpyrosis: Scale-Invariant Curvature Perturbations from a Single Scalar Field in a Contracting Universe," Phys. Rev. Lett. **104** (2010), 091301

[667] J. Khoury and G. E. J. Miller, "Towards a Cosmological Dual to Inflation," Phys. Rev. D **84** (2011), 023511

[668] A. Joyce and J. Khoury, "Scale Invariance via a Phase of Slow Expansion," Phys. Rev. D **84** (2011), 023508

[669] Y. S. Piao and E. Zhou, "Nearly scale invariant spectrum of adiabatic fluctuations may be from a very slowly expanding phase of the universe," Phys. Rev. D **68** (2003), 083515

[670] Y. S. Piao and Y. Z. Zhang, "Phantom inflation and primordial perturbation spectrum," Phys. Rev. D **70** (2004), 063513

[671] Y. S. Piao, "Primordial perturbations during a slow expansion," Phys. Rev. D **76** (2007), 083505

[672] Y. S. Piao, "Adiabatic Spectra During Slowly Evolving," Phys. Lett. B **701** (2011), 526-529

[673] Z. G. Liu, J. Zhang and Y. S. Piao, "A Galileon Design of Slow Expansion," Phys. Rev. D **84** (2011), 063508

[674] J. L. Lehners, "Eternal Inflation With Non-Inflationary Pocket Universes," Phys. Rev. D **86** (2012), 043518

[675] M. C. Johnson and J. L. Lehners, "Cycles in the Multiverse," Phys. Rev. D **85** (2012), 103509

[676] A. Borde, A. H. Guth and A. Vilenkin, "Inflationary space-times are incompletein past directions," Phys. Rev. Lett. **90** (2003), 151301

[677] S. Chakraborty and S. Bhattacharya, "Cosmic evolution with a general Gaussian type scale factor," Int. J. Mod. Phys. D **27** (2018) no.14, 1847019

[678] D. Vegh, "Holography without translational symmetry," [arXiv:1301.0537 [hep-th]].

[679] Q. Huang, J. Chen and Y. Wang, "Spinning Particle in Gravitational Field of Black Hole Involving Global Monopole," Int. J. Theor. Phys. **54** (2015) no.2, 459-471

[680] T. Tamaki and N. Sakai, "Properties of global monopoles with an event horizon," Phys. Rev. D **69** (2004), 044018

[681] L. Berezhiani, G. Chkareuli, C. de Rham, G. Gabadadze and A. J. Tolley, "On Black Holes in Massive Gravity," Phys. Rev. D **85** (2012), 044024

[682] H. Kodama and I. Arraut, "Stability of the Schwarzschild–de Sitter black hole in the dRGT massive gravity theory," PTEP **2014** (2014), 023E02